Silurian and Devonian source rocks and crude oils from the western part of Libya:

organic geochemistry, palynology and carbon isotope stratigraphy

Mohamed M. A. Elkelani

Utrecht Studies in Earth Sciences 71

LPP Contributions Series No. 42

Utrecht 2014

Utrecht Studies in Earth Sciences 71

Members of the dissertation committee

Prof. dr. Jack J. Middelburg	Utrecht University, The Netherlands
Prof. dr. Henk Brinkhuis	Royal NIOZ & Utrecht University, The Netherlands
Prof. dr. Appy Sluijs	Utrecht University, The Netherlands
Prof. dr. Thomas Wagner	University of Newcastle, School of Civil Engineering and Geosciences, United Kindom
Dr. Erik W. Tegelaar	Shell Global Solutions B.V., Rijswijk, The Netherlands

ISSN 2211-4335

LPP Contributions Series No. 42
ISBN 978-90-6266-380-4

Contact:
Mohamed M.A. Elkelani
M.A.Elkelani@uu.nl
elkelanily@yahoo.com

Cartography and figures:
Communication & Marketing (8750), Faculty of Geosciences, Utrecht University

Printed in the Netherlands by WPS, Zutphen.

Silurian and Devonian source rocks and crude oils from the western part of Libya:

organic geochemistry, palynology and carbon isotope stratigraphy

Organische geochemie, palynologie en koostofisotopenstratigrafie
van aardoliemoedergesteenten uit het Siluur en Devoon van westelijk Libië
en daaruit gevormde aardolie

(met een samenvatting in het Nederlands)

PROEFSCHRIFT

ter verkrijging van de graad van doctor aan de Universiteit Utrecht
op gezag van de rector magnificus, prof. dr. G.J. van der Zwaan,
ingevolge het besluit van het college voor promoties in het openbaar te verdedigen op

woensdag 28 januari 2015 des middags te 12.45 uur

door

Mohamed M.A. Elkelani

geboren op 10 december 1965 te Tripoli, Libië

Promotoren:

Prof. dr. G. J. Reichart
Prof. dr. ir. J. S. Sinninghe Damsté

Co-promotor:

Dr. ir. K. G. J. Nierop

This Research was funded by Shell Exploration & Production Libya GmbH
Libyan Petroleum Institute (LPI), Tripoli, Libya
National Oil Corporation (NOC), Tripoli, Libya

الى:

أبي وأمي وزجتي واخوتي وأخواتي

وأبنائي: ريحان ورغد وأنس ورنيم

الى روح أختي " موده " تغمدها الله بواسع رحمته

Dedicated to:
My father and my mother, my wife and my children: Raihan, Ragad, Anas, and Raneem. This work is dedicated to the soul of my sister "Mawada" who has traveled without saying Good-bye.

Contents

1 General introduction and synopsis

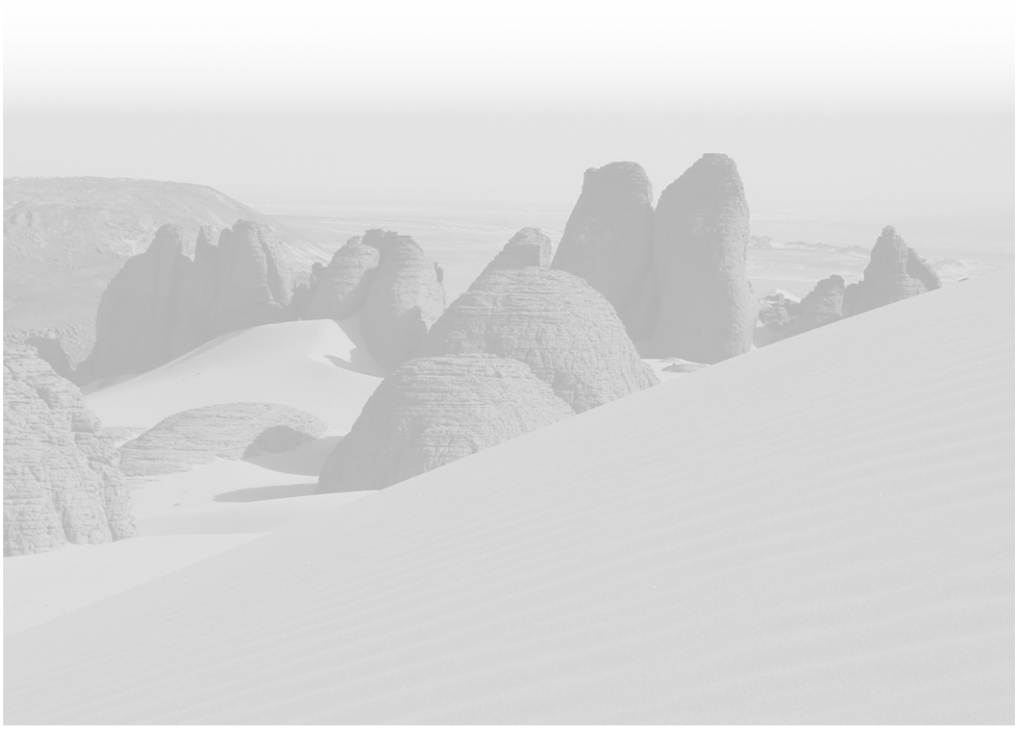

1. The Middle Palaeozoic

The source rocks for most North African petroleum reservoirs, which together form one of the largest sources of petroleum globally, were deposited during the Middle Palaeozoic era. The Palaeozoic, ranging from 542 to 251 Ma, covers about 290 Myr, which exceeds the combined duration of the Mesozoic and Cenozoic eras. During this long time interval Earth experienced a large range of different environmental, paleogeography and climate conditions. Most of the Palaeozoic, from the Cambrian to the Carboniferous, has commonly been regarded as a global greenhouse period with high atmospheric pCO_2 (Pages *et al.*, 2006; Berner, 1994), interrupted by major but relatively short-lived ice ages in the Late Ordovician, in the Late Devonian and in the Early Carboniferous (Loydell *et al.*, 2009). The Middle Palaeozoic, comprising the Silurian and the Devonian, is characterized by a generally warm climate sandwiched between the Ordovician and Late Devonian ice ages. These climatic changes probably profoundly affected sedimentation, hence the geological record spanning this interval, both through changes in sea level and by affecting oceanic circulation.

The Palaeozoic is characterized by substantial episodes of black shale (i.e., rocks with a total organic carbon content exceeding 1% by weight) deposition, hence representing a common sediment type for that time interval. In many localities geological sections spanning this time interval consist of intercalated carbonates and shales. These regular changes between carbonate and shales probably reflect shallowing/deepening of the depositional environment due to sea-level fluctuations, related to either local tectonics or global changes. Interest in the organic-rich deposits of the Palaeozoic primarily reflects the economic importance of the hydrocarbons potentially generated from them (Wignall, 1991). Still, these black shales also attracted much attention from scientists due to their association with sea-level change and mass extinctions (Loydell, 2009).

Black shales potentially provide important records for reconstructing past changes in climate and ocean circulation. Overall processes involved in black shale formation can typically be considered to be the product of increased biological productivity and/or enhanced organic matter preservation (Tyson, 1995). However, as climate and paleogeography in the Palaeozoic differed considerably from today, it is necessary to independently determine the processes responsible for the deposition of the Palaeozoic black shales in North Africa.

1.1. The Silurian succession in North Africa

During Palaeozoic times, the Saharan platform was part of the northern passive margin of the Gondwana supercontinent. The tectonic setting of this craton was remarkably calm from Cambrian to Devonian times, while deformation progressively increased during Upper Devonian and Carboniferous times, announcing the late Carboniferous Hercynian compression.

The glaciations at the end of the Ordovician-Silurian have been studied extensively because of the associated major extinction event, and also because it was characterized by widespread graptolitic black shale deposition (Lüning *et al.*, 2000; Armstrong *et al.*, 2005). The late Ordovician glaciations lasted only a relatively short period (approximately 1.0 Myr), superimposed on an otherwise warm episode of Earth's climate (Brenchley *et*

al., 1994; Kump *et al.*, 1999). Baltica, and to some extent, Laurentia, occupied tropical and subtropical latitudes, their geological record is at that time dominated by carbonate deposits (Berner and Kothavala, 2001). In contrast, the area that now comprises Libya drifted across the South Pole and was regularly covered by an extensive ice cap (Fig.1).

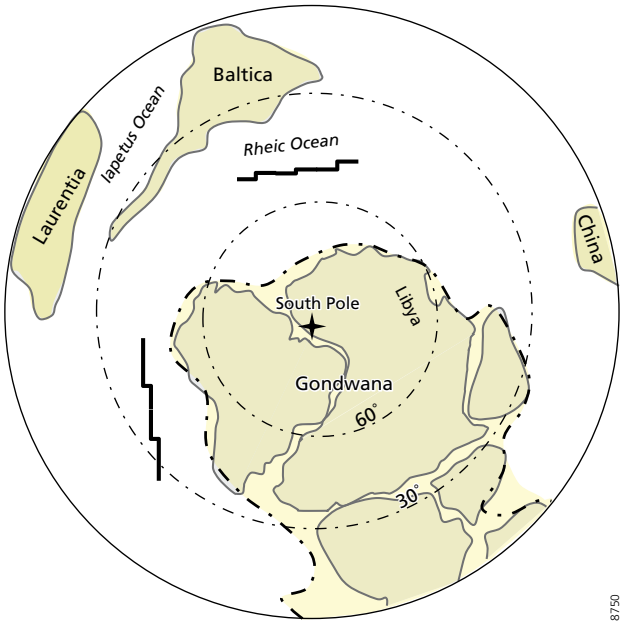

Fig. 1. Late Ordovician paleogeographical reconstruction for the Southern hemisphere at the end of the Ordovician with the location of Libya, Ghadamis and Murzuq Basin indicated (modified after Ghienne and Deynoux, 1998; Scotese and Mckerrow, 1991).

The early Silurian period was a time of global sea-level rise resulting from the melting of the ice cap that, amongst others, covered the massifs of Hoggar and Tibisti and was characterized by extensive deposition of black shales on the North African Gondwanan margin from Rhuddanian to early Wenlock times. In Libya, the Silurian sequence has been divided lithologically into two major units: Tanezzuft and Akakus. These two formations represent the entire Early to Late Silurian succession in western Libya. On the other hand, the basal Tanezzuft is generally interpreted as being the major local source rock for the petroleum found in that area, the upper part of Tanezzuft and the Akakus formation provide potential reservoir rocks.

In North Africa and Arabia, the organic rich shale often occurs at or near the base of the Silurian shale unit. This black shale has been termed "hot" shale based on its high natural radioactivity (> 150 API) and this term is used extensively in the Palaeozoic of North Africa and Arabia (Lüning *et al.*, 2000). In Libya, the Silurian succession comprises well-laminated mainly light and dark grey shales, which lie above a sharp lithology boundary with the sandstones of the Memouniat Formation. Locally this sandstone is well developed as a separate unit, especially near the top of the sequence. In parts other

of areas, such as the Nafusah Uplift and near the Al Qarqaf Arch, the Silurian sequence is missing due to late Hercynian erosion. In the western part of Libya these organic-rich shales form the basal part of the Tanezzuft Formation, which sourced most of the hydrocarbons in the Ghadamis and Murzuq basins discovered there to date.

The Ghadamis Basin extends between Libya, Algeria, and Tunisia, with the depocenter close to the triple junction between the countries (Boote *et al.*, 1998). It covers an area of 250,000 km^2, with the Al Qarqaf Arch defining the southern edge of this basin and the northeastern margin being the Nufusa Arch (Fig. 2). South of the Ghadamis Basin, the Murzuq Basin is triangular in shape, with one of its points oriented southward (Bellini *et al.*, 1980). The southern half of the basin extends to north Niger and is locally called the Jadu Basin. It covers an area of over 350,000 km^2. The basin is bounded to the north by the Al Qarqaf uplift, to the east by the Tibesti Massif and to the west by the Tihemboka Arch.

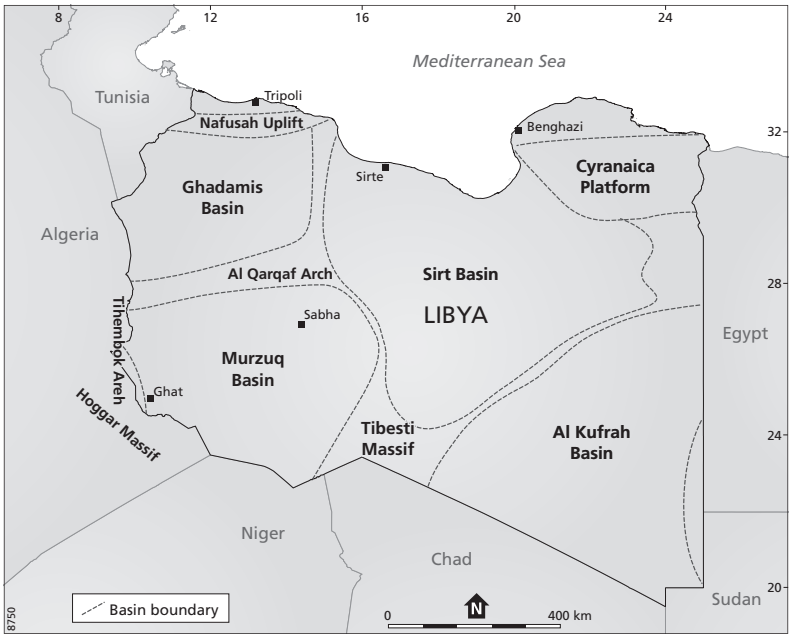

Fig. 2. Map of study area showing location of the Ghadamis and Murzuq Basins.

1.2. Devonian succession

During the Devonian, many of the Early Palaeozoic oceans were closing as Laurasia and Baltica collided into the newly formed continent of Laurussia (Fig. 3). The North African margin was at that time bordering the seaway separating Laurussia from the southern supercontinent of Gondwana (Bond & Wignall, 2005). The Devonian was a time of widespread formation of black shales and Late Devonian organic-rich sediments have

attracted special consideration, as they coincide with mass-extinction pulses and global signals of marine anoxia (Wignall, 2005).

In Ghadamis Basin, the middle to Upper Devonian in Murzuq is represented by a condensed section with a sandier facies and several local erosional unconformities. The major Late Devonian unconformity associated with the early Hercynian also marks an overall change in Paleozoic facies types in the Murzuq Basin. Whereas the older record shows recurring shale deposition, open-marine shales dominate the sediments of the Upper Devonian and Lower and Middle Carboniferous. The widespread inversion and erosion during the mid-Devonian apparently affected the central Murzuq Basin, and the Awaynat Wanin Formation was deposited on the eroded surface. However, this formation is absent from the western margin of the basin. The name Awaynat Wanin was introduced by Lelubre (1946), based on exposures on the western flanks of the Al Qarqaf uplift (Boote *et al.*, 1998).

Frasnian black shales have been deposited in many parts of North Africa and hence potentially form an important hydrocarbon source rock in this region. Time-equivalent Frasnian organic-rich deposits in Europe occur, for example, in the Rhenish Massif/Harz Mountains (Germany) and the Montagne Noire (France). The organically richest and thickest Frasnian black shales are deposited in central North Africa (Western Libya and Algeria).

Outcrops of the Silurian and Devonian shales occur in a belt surrounding the Murzuq Basin in SW Libya (Fig. 4A). The presence or absence of the "hot" shales in the outcrop around the basin has not yet been studied systematically. On the western flank of the Murzuq Basin, graptolite ages (Fig. 4B) collected during geological mapping give a first indication that the "hot" shale may pinch out toward the north, and is possibly also absent from Jebel Al Qarqaf (Lüning *et al.* 2000).

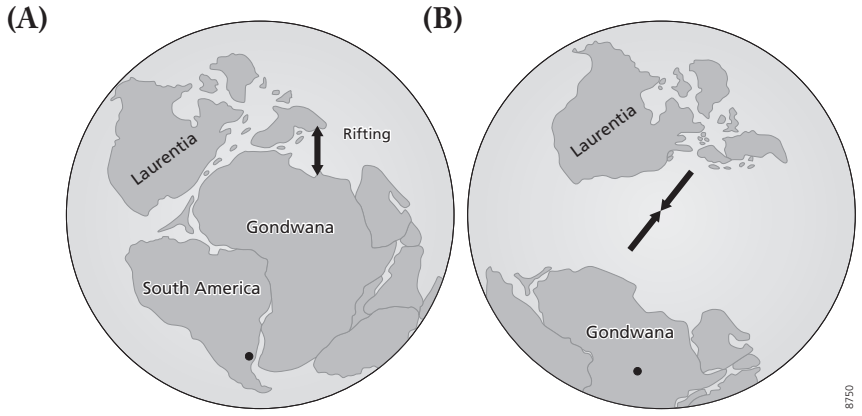

Fig. 3. Early Devonian to Late Devonian paleogeographic reconstruction (after Van der Voo, 1988). (A) Early Devonian showing short-lived approach of Gondwana toward Laurentia, (B). Late Devonian southward drift of Gondwana. The black circle indicates the South Pole.

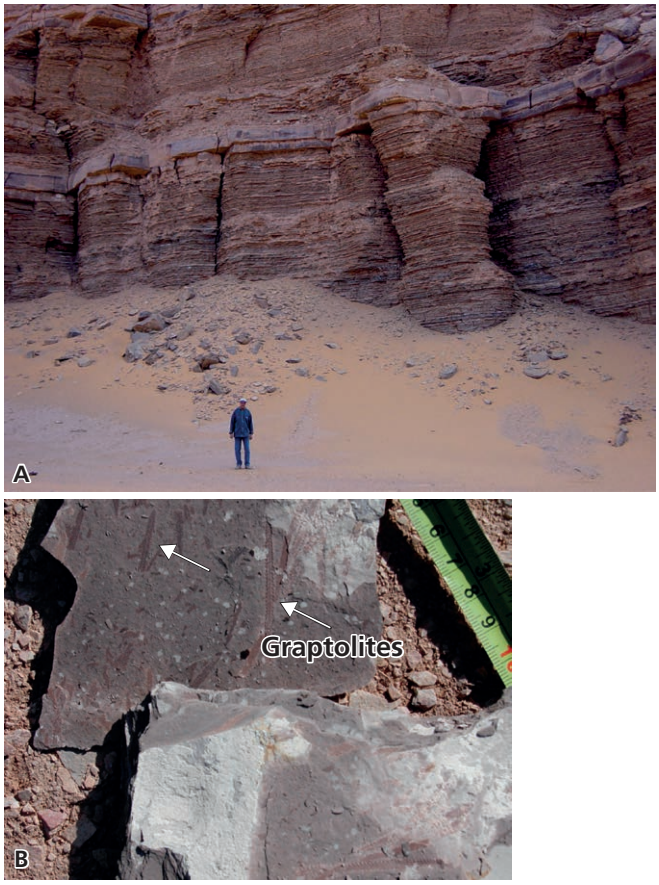

Fig. 4. (A) Devonian outcrops in the western part of Libya, near Al Qarqaf Arch, (B) Silurian graptolites.

1.3. Al Qarqaf Arch

The Al Qarqaf uplift complex extends in a NE-SW direction and separates Ghadamis Basin from Murzuq Basin to the south. The Silurian section is thinner or totally eroded over Al Qarqaf arch area, but increases in thickness away from the arch area (Boote et al., 1998). This implies that the Al Qarqaf uplift played a major role in determining the paleo relief when the Silurian successions were deposited and hence predates these deposits. The Al Qarqaf arch started from Late Cambrian-Early Ordovician and separated the two basins in Late Devonian (Fig. 5), whereas the two basins still remained somewhat connected in the area of the Atshan Saddle (Belhaj, 2000).

2. Deposition of the organic-rich "hot" shale

The distribution of organic-rich Silurian "hot" shales is patchy with coeval deposits onlapping onto paleogeographic highs (Lüning *et al.*, 2000, 2005). Around larger regional paleohighs, shales are replaced by sandstones, which formed during the transgressive reworking of older rocks. The "hot" shale unit is absent from paleohighs that were dominated by higher-energy, marine to terrestrial sandstone-siltstone being deposited or characterized by non-deposition (Armstrong *et al.*, 2005). After the Rhuddanian, sea level rise resulted in an increased connectivity between the previously separated water bodies on the continental shelf. This sea level rise also increased the water depth of the layer beneath the thermocline, making this layer less susceptible to oxygen depletion. The "hot" shale unit is overlain by organically lean gray-green shales with gamma-ray background values ranging between 90 and 100 API. The Silurian shales are generally organically lean, except for those deposited in the lower Llandoverian (Rhuddanian) and Upper Llandoverian and/or lower Wenlockian when several additional anoxic phases occurred (Lüning *et al.*, 2000).

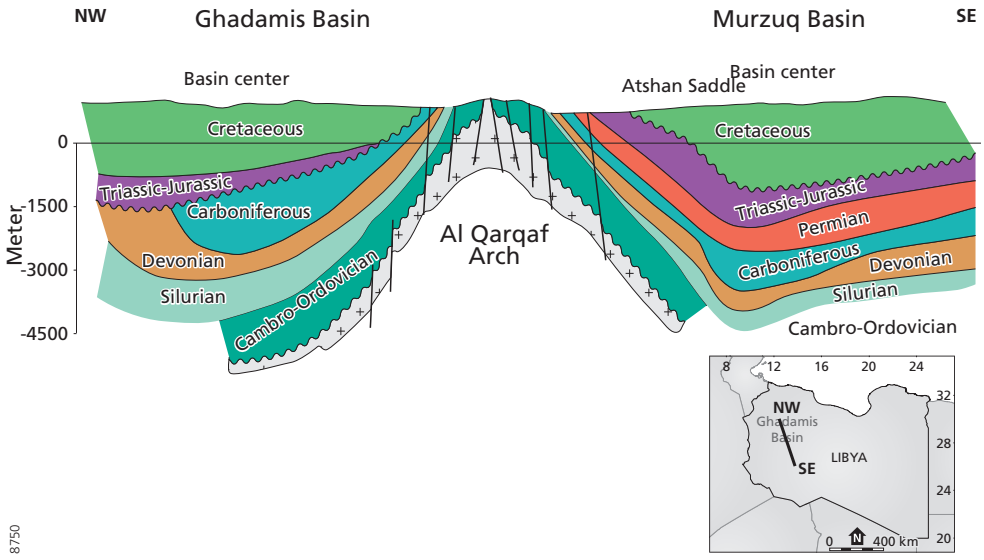

Fig. 5. Schematic NW-SE cross-section through Al Qaqaf Arch and Ghadamis and Murzuq basin and shwoing structural development from Lower Paleozoic to present (modified and redrawing after Boote *et al.*, 1998).

3. Libyan petroleum reservoirs

The chemistry of organic matter contained within a sedimentary rock changes over time reflecting its temperature and burial history. This change or thermal maturity is measured and can be combined with organic matter quality to predict the potential of

a source rock to have produced hydrocarbons. The principal source rocks in Ghadamis and Murzuq Basins are the Silurian Tanezzuft "hot" shales. True vitrinite is not found in rocks of Silurian age, as land-plants did not exist yet. Thus some authors have proposed to using reflectivity measurements on zooclasts such as graptolites and chitinozoans, and the results can be referred to a thermal alternation index (TAI) (Tyson, 1995). Alternatively, others proposed the use of biomarker organic compound ratios calibrated to true vitrinite reflectance (Radke *et al.*, 1983, 1986). Maturity studies indicate considerable variation in the maturity of the Early Silurian Tanezzuft formation source rock in Libyan Ghadamis and Murzuq Basins (Hallett, 2002). In the western part of Libya, the Libyan oil varies greatly in character, from low-sulfur to light oils and waxy oils. These variations are probably due to the nature of the source rock and subsequent maturation history (Boote *et al.*, 1998; Hallett, 2002).

Clearly, the Silurian source rocks are mature and extensive enough to generate the commercially interesting quantities of oil and gas/condensate mixtures recovered from the Ghadamis and Murzuq Basins. Most oil and gas fields and discoveries within the study area are believed to have received hydrocarbons primarily from mature Silurian source rocks (Boote *et al.*, 1998). However, appreciable contributions from mature Devonian source rocks are also possible; it has been suggested that multiple sources from the Palaeozoic contributed hydrocarbons to different trap locations (Belhaj, 2000).

4. Biomarkers and palynomorphs

Biomarkers (chemical fossils) are sedimentary organic compounds whose carbon skeleton suggest an unambiguous link with biological products, and were synthesized by biota present at the time of deposition of the sediment (Eglinton *et al.*, 1964). Lipids derived from organisms contributing organic matter to depositional environments can be preserved in the sedimentary record where they can act as biological markers for both organisms and environmental conditions (e.g. Farrimond *et al.*, 2003). Molecules preserved in the Silurian and Devonian source rocks of Ghadamis and Murzuq Basins could potentially provide valuable information on the environmental conditions during deposition. However, thermal maturity of source rocks (and crude oils) can be an important factor influencing the biomarker composition. Still, even when thermally altered, biomarkers can sometimes still be of help for reconstructing the paleoenvironment. In case of strong thermal or biological alteration when most information in free biomarkers is lost, asphaltenes and kerogens may have preserved biomarkers incorporated within their complex structures (e.g. Hartgers *et al.*, 1993; Hartgers *et al.*, 1994; Sinninghe Damsté *et al.*, 1998).

Most carbon isotopic studies rely on the analyses of bulk $\delta^{13}C_{TOC}$, which may be influenced by relative changes in composition of the organic matter as well. For instance, sugar moieties are known to be isotopically enriched compared to lipids and relative changes in their concentrations during early diagenesis could potentially affect bulk $\delta^{13}C_{TOC}$ values (e.g. Van Dongen *et al.*, 2002). Compound specific isotope analyses on selected molecules such as, for example, the *n*-alkanes ($\delta^{13}C_{n\text{-alkanes}}$), avoid the effect of selective preservation and/or mixing between different organic matter sources on bulk

organic carbon isotope records (Schouten *et al.*, 1998). Hence, this technique allows a more robust incorporation of stable carbon isotopes in the integrated stratigraphy.

The stratigraphy of the organic-rich sequences from the North African Paleozoic largely relies on the biostratigraphy of organic remains (Le Hérissé, 2000). For the Silurian and Devonian biostratigraphic age-control, especially for drill cores in which it is difficult to establish reliable ranges for larger fossil groups, is mainly provided by acritarchs and chitinozoans. During the Devonian miospores can also be used for age-control. The palynomorph assemblages, including other important groups such as the prasinophytes, also provide valuable information about the depositional environment.

5. Scope and framework of the thesis

The primary goal of this thesis is to reconstruct the depositional environment on the North Africa margin during the Silurian and Devonian in the western part of Libya. Onset and limits, both in time and spatially, of the deposition of the so-called "hot" shales are probably not the same across the North African Margin. The timing of these forms an important question, highly relevant to hydrocarbon exploration. Investigating differences in "hot" shale deposition between separate sedimentary basins requires good age control and adequate means for correlation. Although, such questions are often addressed by investigating outcrop samples, the Tanezzuft and Awaynat Wanin outcrops are heavily weathered and oxidized and, therefore, no longer suitable for organic biostratigraphic and geochemical studies. For that reason, this thesis concentrates on records drilled from the sub-surface. Within these drill holes, organic matter preservation is excellent, although biomarkers might be affected by thermal maturation.

The main objectives of this thesis are related to the following questions:

1. Is it possible to develop a biostratigraphy for the Silurian and Devonian based on palyno-morphs, in particular using acritarchs, chitinzoans and miospores?
2. How did environmental change control sedimentary organic matter preservation during the deposition of the Silurian and Devonian successions?
3. What is the maturity of the Silurian and Devonian source rocks and how did this impact the biomarker distribution?
4. Is it possible to make oil to source rock correlations in thermally highly mature settings?

In order to answer these primary questions a series of sub-questions needed to be addressed:

i What was the true amplitude of the different carbon isotopic excursions, measured on bulk organic carbon?
ii Is it possible to correlate the different observed carbon isotopic excursions locally and possibly globally?
iii What controlled differences in organic matter deposition through time between the different sub-basins?

These objectives require a multi-disciplinary approach, combining organic geochemistry and palynology, which is presented in the subsequent chapters.

In **Chapter 2** a biostratigraphic framework is established for three cores from two basins (Murzuq and Ghadamis) along the African continental margin. Bulk and compound specific carbon isotopic records have been analyzed for correlating the different cores. Compound specific carbon analyses allowed for unraveling local and global isotopic signals. Four major carbon isotope positive excursions have been identified. The "hot" shale interval in the Ghadamis Basin is characterized by two distinct isotopic excursions, whereas other excursions occurred in the lean shales. In the Murzuq Basin no carbon isotopic excursion is observed within the "hot" shale. "Hot" shale deposition is hence diachronous between the two basins, with deposition starting earlier in Ghadamis Basin and also continuing longer. Most of the observed positive carbon isotope excursions in Ghadamis Basin occur close to known important bioevents and can be correlated to carbon isotopic events known from other areas.

The Devonian formations in the western part of Libya have not been extensively studied and the facies distribution is largely unknown (e.g. Loboziak *et al*., 1992; Mergl & Massa, 2000). Although many wells have been drilled in the Murzuq Basin, studies focusing on the Middle to Late Devonian black shale succession are scant. In **Chapter 3**, the first carbon isotope signals for the Middle-Late Devonian black shale sequence from the Awaynat Wanin Formation in the Murzuq Basin in western Libya are presented. The $\delta^{13}C_{org}$ record is discussed in the light of a new biostratigraphic framework and compared with events known from other locations. The black shale is characterized by high TOC and sulfur contents. The abundant presence of marine amorphous organic matter (AOM) together with prasinophytes algae in this black shale in the Murzuq Basin is in line with geochemical indications of a restricted depositional environment. The onset of Frasnian black shale sedimentation is probably associated with the earliest Frasnian eustatic sea level rise, as it concurs with a major positive $\delta^{13}C_{org}$ carbon isotope excursion of about 3‰. This positive excursion appears to be linked to the coeval deposition of organic-rich black shales in Morocco, Algeria, Germany, Poland and South China.

In **Chapter 4,** the organic composition of the "hot" and lean shales in the Ghadamis and Murzuq basins is analyzed to assess maturity and paleoenvironmental deposition. These Silurian sediments comprise source rocks of high maturity; those from Murzuq Basin are also partially biodegraded. Hydrocarbon biomarkers extracted from these shales are strongly biased by these processes and do not provide much information on original composition. Therefore, the molecular composition of asphaltenes and kerogens was investigated by pyrolysis-gas chromatography/mass spectrometry. The presence of specific aromatic pyrolysis products derived from carotenoids derived from phototrophic anaerobes showed that euxinic conditions extended into the photic zone, enhancing organic carbon preservation during periods of enhanced water column stratification.

Thermal maturity is an important parameter for assessing petroleum evolution in sedimentary basins. In **Chapter 5,** two-dimensional gas chromatography, coupled with time of flight mass spectrometry (GGxGC-ToF-MS) was applied to identify diamondoids in source rock extracts and crude oils from the western part of Libya (Ghadamis Basin). Combining diamondoids and more traditional biomarkers allows a more refined assessment of maturity and potential inter-calibration in a setting characterized by high -maturity source rocks. The estimated maturity shows considerable variability between the northern and southern part of the Ghadamis Basin, ranging from early mature to late mature for oil generation. While the source rock extracts contain

both adamantane and diamantane, the crude oil contains adamantane only. This probably implies that the crude oils were expulsed before diamantane formed in the source rock. Comparing the relative distribution of diamondoids between the crude oils shows two groups with similar composition. The crude oils from the northern part of the basin more closely resemble the diamondoid composition of the local source rock extracts, whereas the composition of the crude oils from the south suggests that at least part of the oil recovered here originates from another source.

2 Stable carbon isotope and palynological records from the Silurian "hot" shale in Libya

Mohamed A.Elkelani [1], Gert-Jan Reichart [1,2], Jaap.S. Sinninghe Damsté [1,2], Bas van de Schootbrugge [3], Zwier Smeenk[3]

[1] *Utrecht University, Geochemistry, Faculty of Geosciences, Department of Earth Science, Budapestlaan 4, 3584 CD Utrecht, The Netherlands.*

[2] *NIOZ Royal Netherlands institute for Sea Research, P.O. Box 59, 1790 AB, Den Burg,The Netherlands*

[3] *Utrecht University, Marine Palynology and Paleoceanography, Laboratory of Palaeobotany and Palynology, Faculty of Geosciences, Department of Earth Sciences, Budapestlaan 4, 3584 CD,Utrecht, The Netherlands*

Abstract

Organic-rich ("hot") shales in the North African/Arabian region from the late Ordovician/early Silurian (443 Ma) are the source of almost all Palaeozoic oils in North Africa and the Middle East. Although of evident economic importance, the stratigraphy and depositional environment of these "hot" shales is not always clear. Large regional differences are observed in "hot" shale thickness; moreover, at some locations the "hot" shale seems to consist of multiple layers. To investigate the main Libyan "hot" shale, three boreholes (core and cutting samples) covering the Tanezzuft and Akakus Formation from the Ghadamis basin, and the Tanezzuft and Awaynat Wanin formations from the Murzuq basins in western Libya, were studied for their palynological composition, organic carbon content and their bulk carbon isotopic composition ($\delta^{13}C_{TOC}$). To avoid effects of selective preservation and mixing between different sources on bulk organic carbon isotope records, we performed compound specific carbon isotope analyses on *n*-alkanes ($\delta^{13}C_{n\text{-alkanes}}$). An informal acritarch stratigraphy was constructed based on known ranges of key marker taxa and on the basis of changes in the palynomorph assemblages. Based on this stratigraphy, the Ghadamis and Murzuq sediments studied cover the late Ordovician to Devonian periods. The marine acritarch flora is accompanied by common terrestrial miospores and cryptospores, suggesting a proximal position and significant admixing of land-derived material into the marine setting. The lowermost Tanezzuft Formation ("hot" shale) is characterized by low abundances of acritarchs in the palynological assemblages and a high abundance of prasinophytes, coinciding with high stable carbon isotope values. The sediment is dominated by what was probably originally well-preserved AOM, which is typical for laminated black shales with (Type II) oil-prone kerogen, deposited in a distal stratified-shelf sea basin with dysoxic-anoxic depositional conditions. The Tanezzuft Formation represents a progressive transgression, first drowning the deepest parts of palaeodepressions, and later extending to palaeohighs and margins. The $\delta^{13}C_{TOC}$ record shows a significant positive excursion during the onset of the "hot" shale deposition in the Ghadamis Basin with a rapid onset and a gradual recovery. Based on the bulk organic carbon-stable isotope record from the Ghadamis basin, two positive excursions have been identified within the "hot" shale interval. The first excursion coincides with the early to late Aeronian, the second excursion coincing with the early Sheinwoodian. For the Aeronian, excursion no time-equivalent event has yet been recognized elsewhere. Alternatively, this event mainly reflects local changes in carbon cycling within the lean shale. A third positive carbon isotope excursion was observed, which seems correlated to the late Homerian double-peaked excursion. In the Murzuq Basin, a fourth excursion is observed that corresponds to the Silurian-Devonian boundary isotopic excursion, also known as the "Klonk" event.

Key words: *Palynomorphs, Palynofacies, Carbon isotopes, Gondwana, Silurian, Hot shale*

1 Introduction

The long-held paradigm of a Silurian Period characterized by equable climate conditions and limited global change has recently been challenged. The challenge is based on new geochemical and palaeontological findings that document several major changes in fauna, climate and carbon cycling. These changes started in the latest Ordovician period (Brenchley *et al.*, 1994; Copper & Keller, 2001; Calner *et al.*, 2006), when ice caps on Gondwana disintegrated. The late Ordovician glaciations lasted only a relatively short period (approximately 1.0 my) and were superimposed on a greenhouse episode characterized by atmospheric CO_2 concentration estimated to have been 15-20 times higher than preindustrial levels (Brenchley *et al.*, 1994; Kump *et al.*, 1999; Berner & Kothavala, 2001). The glaciations at the end of the Ordovician have been studied extensively because of the associated major extinction event, and also because of the widespread organic-rich graptolitic black shale deposition following this event in the Early Silurian on the northern Gondwana margin (Lüning *et al.*, 2000; Armstrong *et al.*, 2005). Several distinct positive carbon excursions in both organic and inorganic carbon have been identified during the Early and late Silurian, and point to distinct pertubations of the carbon cycle, often associated with faunal extinctions and lithological changes (Munnecke *et al.*, 2003). These excursions have been recognized in records from both high- (Gondwana) and low-latitude (Laurentia & Baltica) locations (Fig. 1), Three positive carbon isotope excursions have been reported during LIandovery (Early Silurian) and Wenlock and Ludlow (both Late Silurian) in Tunisia (Vecoli *et al.*, 2009), Sweden (Munnecke *et al.*, 2003), Norway (Kaljo & Martma, 2006), New York State and Ontario (Brand *et al.*, 2006), Wales (Loydell & Fryda, 2007b), Nevada (Saltzman, 2001), Australia (Andrew *et al.*, 1994; (Samtleben *et al.*, 1996; Munnecke *et al.*, 2003), Britain and on Gotland (Corfield *et al.*,1992; Azmy *et al.*, 1998; Samtleben *et al.*, 2000).

During the early Silurian, widespread organic matter rich deposition occurred along the northern margin of Gondwana, which today extends from Iran via Jordan, Syria and Saudi Arabia along the northern African margin into Morocco. This early Silurian organic-rich "hot" shale is the most important Palaeozoic hydrocarbon source rock in North Africa and Arabia (Belhaj, 1996; Lüning *et al.*, 2000). The term "hot" shale refers to the high level of natural radioactivity in certain shale units due to an increase in authigenic uranium, and as such can be recognized readily in well logs due to their high gamma-ray values up to 400 API (American Petroleum Institute unit) (Lüning et al., 2000; Armstrong et al., 2005). High gamma ray values have also been recorded in the Qusaiba "hot" shale of Saudi Arabia (Aoudeh & Al-Hajri 1995), in the lower and middle Rhuddanian "hot" shale of Jordan (Butcher, 2009) and in the Rhuddanian of Tunisia (Vecoli et al., 2009). The "hot" shale unit is overlain by organically lean gray-green shales with gamma-ray background values ranging typically between 90-150 API (Luning *et al.*, 2000; Loydell *et al.*, 2009). In the western part of Libya, these organic rich shales form the basal part of the Tanezzuft Formation, which sourced most of the hydrocarbon discovered there to date (Lüning *et al.*, 2000). Similarly, on the Arabian Peninsula the time equivalent Qusaiba Member also played a major role in petroleum generation (Le Hérissé, 2000; Al-Hajri, 1991). The high economical significance of these formations makes studying the conditions associated with their deposition highly relevant.

Because of the interest from the oil industry, the Palaeozoic strata in western Libya, and specifically the Tanezzuft source rock, has been subject to intense sedimentological and stratigraphic studies (Klitzsch, 1969, 1970; Bellini & Massa, 1980; Belhaj, 1996; Lüning *et al.*, 2000). Still, because of the petroleum-related focus of these studies, many aspects of the depositional environment and the relation to the global record of the Silurian successions in Libya remain largely unknown.

Here we establish a biostratigraphic framework for three cores, from two basins (Murzuq and Ghadamis) along the African continental margin, correlating the lower Silurian of Libya to the global record. The sediments do not contain appreciable carbonates; bulk and compound specific carbon isotopic records were analyzed for both stratigraphical and reconstruction purposes. Compound specific carbon analyses allow for unraveling local and global isotopic signals. At present no correlation exists between the global stable carbon isotopic records and Libya. The high organic carbon content of the early Silurian "hot" shale, and the large regional extent of these deposits, suggests that these deposits may have played a major role in the isotopic shifts themselves due to the large-scale burial of isotopically light organic matter. Comparing the Libyan $\delta^{13}C$ record

Fig. 1. Late Ordovician palaeogeographical reconstruction map of the Southern hemisphere at the end of the Ordovician indicating Libya (Ghadamis and Murzuq Basins) and the locations of which carbon isotope excursions were compared in this study, 1- Tunisia (Vecoli *et al.*, 2009); 2- Baltica (Kaljo *et al.*, 1998) and Dob's Linn, Scotland (Underwood *et al.*, 1997); 3- Laurentia (Saltzman, 2001); 4- China (Wang *et al.*, 1993) (modified after Ghienne, 1998; Scotese and Mckerrow, 1991).

with the global record thus enables us to unravel local contributions to this global-scale process.

2. Geological Setting

Palaeogeographically, North Africa was located at the margin of Gondwana. Late Ordovician Gondwana was positioned at high latitudes, gradually moving northward to mid-palaeolatitudes (Fig. 1). The high-latitudes in combination with an overall cold climate resulted in the onset of severe glaciations and the rapid build-up of an ice-cap. At that time, the area that now comprises Libya drifted across the South Pole and was regularly covered by an extensive ice cap. Baltica, and partially Laurentia, occupied tropical and subtropical latitudes; their geological record is at that time dominated by carbonate deposits (Berner & Kothavala, 2001). The first major marine transgression covering the greater part of the North Africa craton started in the early Silurian as a result of the melting of the ice cap.

The records constructed here are based on cores and cuttings obtained from drilling in the Murzuq and Ghadamis basins (Fig. 2). The Ghadamis Basin comprises parts of Libya, Algeria, and Tunisia, with its depo-center close to the triple junction between the countries (Belhaj, 2000; Boote *et al.*, 1998). It covers an area of 250,000 km^2, with the Al Qarqaf Arch defining the southern edge of this basin and the northeastern margin being the Djeffara-Nufusa Arch. The Amguid Spur and El Biod Arch mark the western extent of the basin.

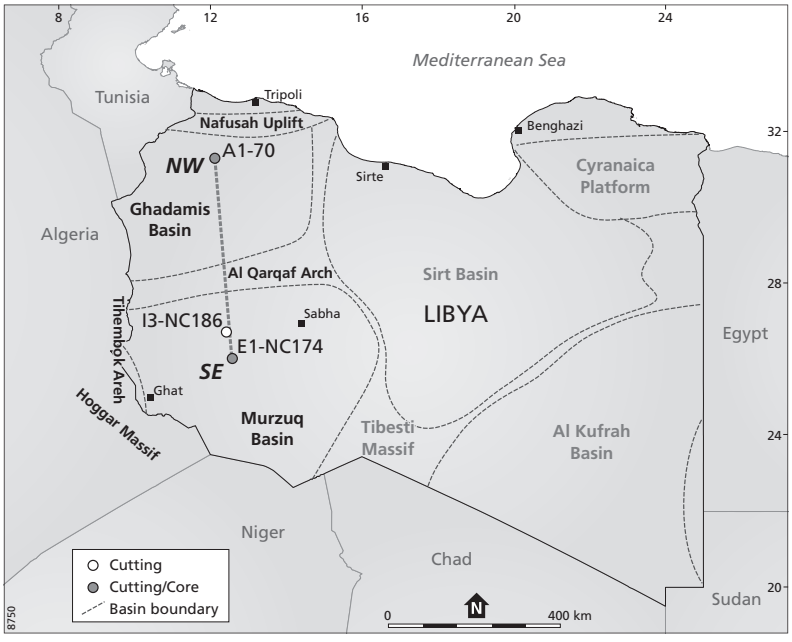

Fig. 2. Geographic map showing well locations of Ghadamis and Murzuq Basins.

South of the Ghadamis Basin, the Murzuq Basin is triangular in shape, with one of its points oriented southward (Bellini & Massa, 1980). The southern half of the basin extends to north Niger and is locally called the Jadu Basin. It covers an area of over 350,000 km^2. The basin is bounded to the north by the Al Qarqaf uplift, to the east by the Tibesti massif and to the west by the Tihemboka Arch (Fig. 2).

In these basins, the Palaeozoic strata are mainly represented by a succession, consisting of alternating shales, silt and sand stones, which reaches a cumulative preserved thickness of more than 6100 m in the northwestern part of the Ghadamis basin. The Ghadamis and Murzuq Basins were not always completely separated from each other. During the Silurian, the basins were probably partly connected in the area of the Atshan Saddle (Klitzsch, 1968). From late Cambrian-Early Ordovician times onward, the Al Qarqaf Arch was uplifted, ultimately separating the two basins during the Late Devonian.

The Ghadamis and Murzuq basins are considered intra-cratonic sag basins. The margins of these basins are structures uplifted during the Hercynian and Alpine Orogenies (Klitzsch, 1970; Selley, 1997). The Silurian sequence reaches a thickness of more than 600 m in the central part of the Ghadamis Basin and similar thickness in the western part of the Murzuq Basin. The Silurian shows large spatial differences in thickness as it is completely eroded in the northern parts of Ghadamis Basin and the northeastern part of the Murzuq Basin. The Silurian sequence has been divided lithologically into two major units: Tanezzuft and Akakus. While the basal Tanezzuft is generally interpreted as being the major local source rock, the upper part of Tanezzuft and the Akakus formation provides the reservoir rock (Figs. 3 and 4). On top of the Akakus formation the Tadrart

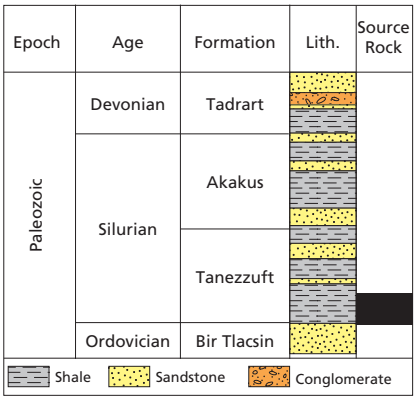

Figure 3. Generalized stratigraphic column of the Ghadamis Basin (modified after NOC, 2000).

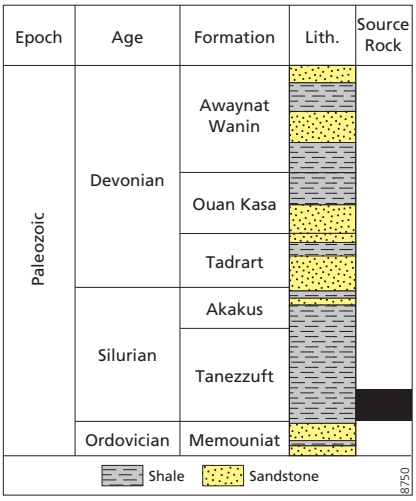

Figure 4. Generalized stratigraphic column of the Murzuq Basin (modified after NOC, 2000).

formation is deposited, concordantly albeit with a hiatus (Belhaj, 1996) (Figs. 3 and 4). Still, the overall stratigraphic column is not well-defined for the Libyan Silurian.

Deposition of the Tanezzuft shale has been linked to melting of the continental ice sheets during the early Silurian (Klitzsch, 1970), based on the overall sedimentology. The base of the sequence consists of shales, which gradually shift to silty shales. The Silurian in these basins is represented by sand-rich sediments belonging to the Akakus Formation. This implies a transgression followed by a regression (Belhaj, 1996; Lüning *et al*., 2000). Still, although the formations are similar in the two basins, they are probably deposited across these basins diachronically, not simultaneously (Bellini & Massa, 1980; Belhaj, 1996; Lüning *et al*., 2000). Independent constraints on the ages of the successions are hence needed to unravel the depositional history across both basins.

3. Materials and methods

3.1. Sampling and lithology description

Core, cuttings samples and wireline log data (gamma-ray data have been obtained from the well log of the A1-70 borehole, by Arabian Gulf Oil Company, I3-NC186 by Repsol Oil Company and E1-NC174 boreholes, by LASMO Grand Maghreb Ltd) (Fig. 2). Sub samples were collected by targeting the shales intercalated within the sequences.

The A1-70 borehole in the Ghadamis Basin was drilled by Shell in 1959, spanning from the base of the Tanezzuft Fm. to the top of the Akakus Fm. (Fig. 3). The investigated section is from a depth between 3118 m and 2728 m and has been analyzed together with cuttings from the intervals between the cored sections. Two samples were collected from just below the "hot" shale, which forms the base of the Tanezzuft, between 3118 m and 3112 m. The lithology consists of irregularly alternating fine-grained sandstones and siltstones. The interval between 3103 m and 3050 m consists of mainly organic-rich black to dark grey shale. This shale is correlated to distinctly elevated gamma ray values in the wireline log, and thus corresponds to the "hot" shales definition (Lüning et al., 2000). The interval between 3050 m and 2775 m consist of dark grey silty shales. Finally, the interval between 2775 m and 2719 m consists of alternating fine-grained sandstones and siltstones.

Two boreholes from Murzuq Basin were sampled: I3-NC186 and E1-NC174 (Fig 2). The Repsol Oil Company drilled the I3-NC186 borehole in 2006. Only cutting samples could be obtained and larger pieces were carefully handpicked in an attempt to minimize the effect of caving. The sub-sampled section ranges from 1420 m to 1125 m depth, and only contains the Tanezzuft formation. The interval between 1420 m and 1396 m consists of organic-rich black shale ("hot" shale), followed by an interval between 1396 m and 1125 m, consisting of alternating dark gray shales, siltstones and sandstones (Fig. 4). The E1-NC174 borehole was drilled in 1997 by LASMO Grand Maghreb Ltd. Both core and cutting samples were available for this study. Although core samples are preferred for biostratigraphy purposes, this was not always possible; cutting samples were added to increase resolution. In core E1-174 the interval studied is from 2221 m to 1844 m depth. The cored interval extends from 2221 m to 2195 m. The Early Silurian "hot" shales in the E1-NC174 borehole consist of homogenous dark black, hard shales and contain abundant

graptolites from 2221 m to 2195 m. The interval from 2179 m to 1921 m consists of dark grey shales and siltstones. Finally, the interval between 1905 m and 1844 m consists of an alternation of shale, siltstones and fine-grained sandstones.

3.2. Methods

All samples were analyzed for total organic carbon (TOC %), stable carbon isotopic composition of the total organic carbon ($\delta^{13}C_{TOC}$), whereas palynology was performed on selected samples only. For the A1-70 borehole, compound specific carbon isotopic analysis was performed on selected samples.

3.2.1. Palynology

For palynological analysis, 41 samples were selected, with sample intervals varying according to the material available, 12 samples from A1-70 borehole, 7 samples from I3-NC186 and 22 samples from the E1-NC174 borehole. About 15 gram of shale from each sample was treated using standard palynological techniques (e.g. Brinkhuis *et al.*, 2003). In short, samples were disaggregated with a pestle and mortar (to pieces about 5mm in diameter) and then subjected to 20% hydrochloric acid (HCl) treatment to dissolve carbonate. Samples were then allowed to stand until any reaction had stopped. After three washes with distilled water, the samples were treated with 40% hydrofluoric acid (HF) to remove any silicate material and were then allowed to stand for at least 24 hours, followed again by three washes with distilled water. No oxidation was performed on the organic residue. The size of the palynomorphs ranged from about 5 µm to > 200 µm. A 250 µm mesh sieve was used to remove oversized organic material, whereas sieving with a 10 µm mesh allowed the collection of the fraction containing palynomorphs. Because of the large amount of mineral residue that still occurred in the samples after sieving, $ZnCl_2$ was applied to separate the lighter organic material from the heavier mineral particles like pyrite. Subsequently a small aliquot of the residue was mounted on a slide, embedded with glycerine jelly, covered, sealed with paraffin wax and studied using transmitted light microscopy. For A1-70 palynofacies were quantified by counting to a minimum of 200 palynomorphs per sample and standardizing relative abundances for the different palynomorph groups (palynomorphs, AOM, and phytoclasts).

3.2.2. TOC and carbon isotope analysis

Samples were decalcified using 0.5 g of finely powdered material, which was allowed to react with 12 ml 1M HCl for 24 h. After decalcification residues were washed with demineralized water, centrifuged and decanted three times to remove acid-soluble components. By carefully weighing samples before and after decalcification weight loss was monitored. Subsequently Total Organic Carbon (TOC) was determined using an elemental analyzer (Fisons NA 1500 NCS) and corrected by compensating for the weight loss during decalcification to obtain the original sedimentary values.

Stable carbon isotope analysis of the organic matter was performed on 40-300 µg of the decalcified residues using an isotope ratio mass spectrometer (Thermofinnigan Delta Plus) coupled online to an elemental analyzer (Fisons NA 1500 NCS). Graphite

Quartzite (GQ) was used as an internal standard and nicotinamide as a control; results normalized relative to Vienna Pee Dee Belemnite (VPDB) using international standards. Precision and accuracy of the analyses was better than 0.1‰, based on the control and duplicates.

3.2.3. Extraction and biomarker work-up

Powdered rock (15-20 g of 12 selected core and cutting samples) were extracted with an azeotropic solvent mixture of 200 ml of DCM/MeOH (9/1: v/v) using a Soxhlet unit for 24 h. Extracts were transferred to a round bottom flask to remove the anti-bumping granules, and subsequently dried using a rotary evaporator until a few drops of solvent were left. These extracts were then transferred to a pre-weighed small vial and reduced to dryness under a stream of nitrogen. Vials with extracts were weighed again to allow quantification. When required elemental sulfur was removed from the extracts using activated copper, the extracts were dried again under a stream of nitrogen and the weights were recorder before and after. The extracts were separated into non-polar and polar fractions using short column chromatography on activated alumina by eluting with *n*-hexane, and MeOH/DCM (1:1, v/v) as eluents, respectively. The hydrocarbon fractions were directly analyzed by gas chromatography (GC).

Hydrocarbon fractions were treated by urea-adduction to remove the branched and cyclic compounds (including the unresolved complex mixture (UCM). The hydrocarbon fractions were dissolved in hexane, and 200 µl of urea were dissolved in MeOH (10%). Then 200 µl of acetone were added and shaken. After 30 min at 20 °C, solvents were evaporated under a nitrogen stream, and remaining urea crystals were washed with hexane to remove cyclic and branched hydrocarbons. Crystals were then dissolved in 500 µl of water (ultra-pure) and 500 µl of MeOH. The wash solvents, containing adduct straight chain components (*n*-alkane) were extracted from this solvent mixture using hexane and then dried under nitrogen. They were subsequently dissolved in hexane prior to gas chromatography (GC), GC/mass spectrometry (GC/MS) and GC-Isotope Ratio Mass Spectrometry (GC-IRMS) analyses.

3.2.4. Instrumental analytical methods

The adducted hydrocarbons were dissolved in hexane to a concentration of 1 mg/ml. The fractions were run on an FID for organic compounds: an HP6890 series II gas chromatograph equipped with CP-Sil 5 CB column (25 long m, 0.32mm in diameter, film thickness 0.12µm). Helium was used as carrier gas, kept at constant pressure (100 kPa). Samples were injected on-column. The oven temperature was programmed from 70 to 130°C at 30 °C/min, from 130 to 320 °C at 4 °C/min and kept at 320 °C for 20 min. The data was collected on a Lab Agilent chemstation data acquisition system. Each fraction was also analyzed and identified by GC/MS (Thermo Trace GC Ultra). A fused silica column (30 m x0.32 mm i.d., film thickness 0.1µm, coated with CP Sil-5CB was used with helium as a carrier gas) set at constant flow. Samples were injected on-column using the same temperature program as used for the GC-FID analyses.

Carbon isotopic compositions of individual n-alkanes were determined using Gas Chromatography Isotope-Ratio Mass Spectrometry (GC-IRMS, ThermoFisher Delta

V), at Utrecht University, using the same column and temperature program as for the GC analyses. Carbon isotope ratios for individual alkanes were calculated against a gas standard measured at the beginning and end of each run and verified using a co-injected internal standard. Carbon isotopic compositions are reported relative to VPDB‰ and based on duplicate analyses where possible.

4. Results

4.1 Palynology and palynofacies

We investigated 41 palynological (both core and cutting) samples, obtained from both the grey and dark black shales sections, as these are generally more suitable for palynological studies. The presence/absence of various acritarch, chitinozoan and spore species were determined in the different boreholes, as well as the relative abundance of the different palynological groups. Acritarch, chitinozoan and spore species identified are plotted in a composite stratigraphic range chart for the wells A1-70, I3-NC186 and E1-NC174 (Figs. 5-8, Plates I-VIII). Although graptolites potentially could provide the best constrained bio-events for the Silurian, such events are not well studied in Libya and, therefore, not easy to transfer to the cored record. Hence, based on a detailed taxonomic evaluation of the various groups of palynomorphs an informal palynological zonation has been constructed and applied in this study. Ages were assigned based on known ranges of key marker taxa and overall palynomorph assemblages. Previous studies on the palynomorphs of Libya have been referenced, together with studies addressing palynology of neighboring North African countries.

The restricted stratigraphic distributions of most species encountered are in close agreement with what is known from other areas globally. The acritarch, spore, and chitinozoan species are taxonomically well-established, and allow for detailed age determination of both the Ghadamis and Murzuq Basins sections. Age assignment and constraints are primarily based on chitinozoan biostratigraphy. Although the acritarch taxa have much longer ranges, their occurrences are overall in good agreement with the primarily chitinozoan and spore based age models.

4.1.1 A1-70 borehole (Ghadamis Basin)

Within the studied interval we recognized acritarchs and prasinophytes (organic-walled marine microphytoplankton), chitinozoans (marine microplankton), miospores (sporomorphs spores), zooclasts (organic fragments of animals, mostly arthropod exoskeletons, graptolites and scolecodonts), amorphous organic matter (AOM), and phytoclasts (organic fragments of plant material).

Down core occurrences of principal stratigraphic marker taxa in A1-70 are plotted in Fig. 5. More than 50 acritarch species were identified in A1-70. The preservation of the various types of organic-walled microfossils was variable, ranging from very good to well-preserved, based on the colors of vesicle walls, which ranged from light to medium dark and brownish (Plates I, II, III, and IV). Overall no evidence for reworked acritarchs was observed, based on color and general appearance. All samples yielded abundant

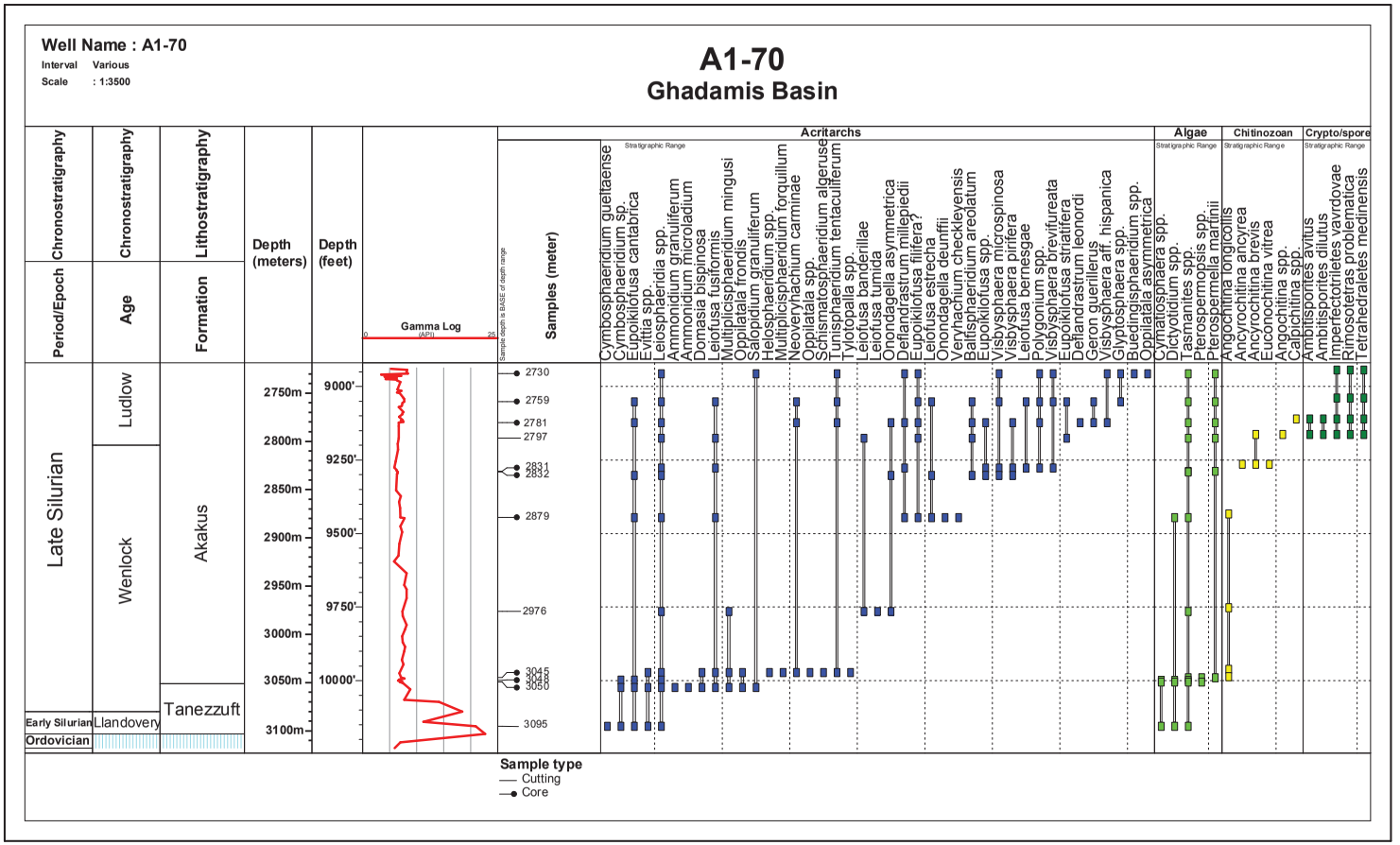

Fig. 5. Palynological range chart of A1-70 borehole (Ghadamis Basin).

palynomorphs, amorphous organic matter, and phytoclasts, in variable and relative abundance and diversity (Fig. 6).

Starting from a depth of 3103 m to 3095 m, at the base of the Tanezzuft formation, palynofacies type and palynomorph assemblages abruptly change, together with a change in lithology from dark black shale to sandstone (Fig. 5 and 6). Within the black shale section of the core AOM dominates the assemblage (71-79%), masking the other components. The AOM appears well aggregated and yellow-brown in color when using ultraviolet light excitation. The slides also regularly seem to contain very fine pyrite particles, often occurring in framboidal aggregates (Plate IV, 7). The interval (3103 m to 3095 m) contains eight species, of which 3 can be considered Early Silurian marker species: *Tunisphaeridium tentaculaferum, Cymbosphaeridium* cf. *cariniosum* and *Eupoikilofusa* sp. Prasinophytes are abundant within this interval, being represented by *Tasmanites* (large, perforate thick-walled palynomorphs produced by marine prasinophyte algae), *Leiosphaeridia* (thick-walled smooth spherical bodies, typically brightly fluorescent) and *Cymatiosphaera* sp. (Fig. 5, Plates I and II). Within the Tanezzuft and lower Akakus Formation, AOM is, relatively well-preserved, based on general appearance and color, (Plate IV). Sporomorphs are generally rare or absent within this interval. In the Tanezzuft and lower Akakus Formations, in addition to AOM, graptolite zooclasts form an important part of the organic matter (Plate IV, 3). Above the "hot" shale we observed a gradual decrease and ultimately complete absence of graptolite zooclasts in the upper Akakus Formation (2976 m to 2730 m).

Most of the record above the "hot" shale (between 3095 m and 2832 m) is rich in acritarchs, with well-preserved assemblages dominated by *Ammonidium microcladum, Ammonidium granuliferum, Domasia bispinosa, Helosphaeridium* sp., *Salopidium granuliferum, Tunisphaeridium tentaculaferum, Oppilatala frondis, Tylotopalla* sp., *Onondagella asymmetrica*, and *Leiofusa* sp.. The prasinophyte assemblage is more diverse in the lower part overlying the "hot" shale, due to the inception of *Pterospermopsis martinii, Pterospermella* sp., *Dictyotidium* sp., *Cymatiosphaera* sp., *Tasmanites, Leiosphaeridia,* and *Quadraditum fantasticum*. The interval from 3095 m to 3045 m contains abundant *Ammonidium microcladum, Tylotopalla* sp. and rarely *Quadraditum fantasticum*.

The upper part of the studied interval, between 2832 m 2730 m, shows a marked change in the palynomorph composition and palynofacies. An abundance of palynomorphs, spores and cryptospores with chitinozoa, scolecodont, cuticles and tracheid-like fragments increases (Fig. 6). The amount of AOM is limited and overall does not show features related to enhanced OM preservation. In contrast, within the same interval, acritarchs are well-preserved and include some long-ranging taxa (Late Ordovician-Silurian) such as *Baltisphaeridium areolatum granulosum,* but also some taxa characteristic of middle-late Silurian age, such as species of *Visbysphaera gotlandica, Buedingisphaeridium* cf. *pyramidale, Tunisphaeridium tentaculaferum, Glyptosphaera speciosa, Veryhachium trispinosum, Leiofusa* sp., *Polygonium* sp. Other marker taxa with more restricted stratigraphic ranges have been recorded such as *Deflandrastrum* cf. *leonardi, Deflandrastrum millepiedi, Deflandrastrum authierae,* (Fig. 6, Plates I, II).

The palynomorph composition and palynofacies show a distinct overall change at 2797 m. At this depth abundances of palynomorphs increase, while the relative amount of AOM is reduced (Plate III). From this depth onward we observe the abundant occurrence of land-derived organic debris and palynomorphs (a.o. spores).

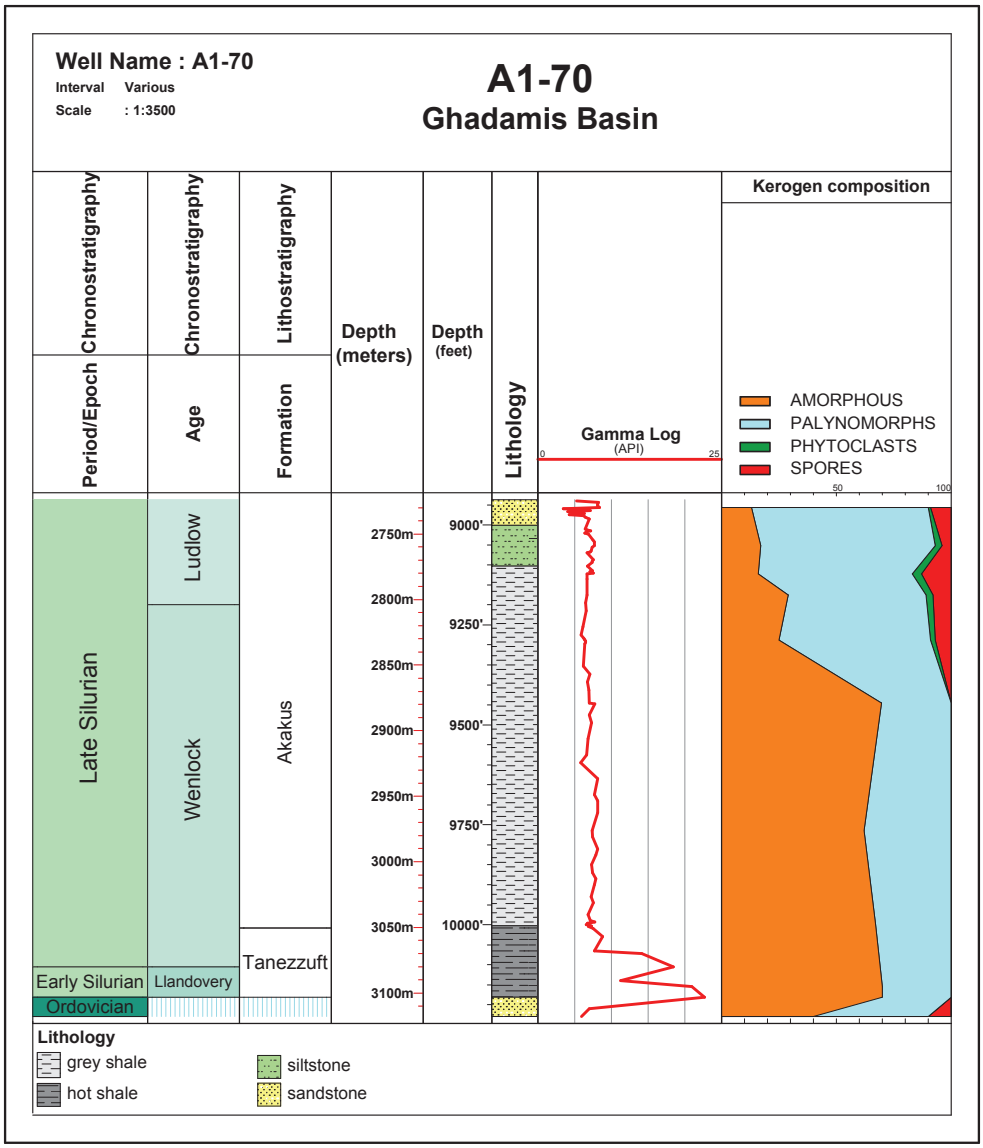

Fig. 6. Stratigraphic variation of palynofacies types of A1-70 borehole (Ghadamis Basin).

Based on these data an age model was constructed for this borehole. Chitinozoans are absent from the base of the section, and subsequently are rare in the stratigraphic interval between 3103 m and 2879 m, being represented only by *Angochitina longicollis*. The known stratigraphic range for this species is from Telychian time to the lower Ludlow (Verniers et al., 1995). The interval between 2831 m and 2781 m contains more chitinozoan species, such as *Ancyrochitina ancyrea, Ancyrochitina brevis, Euconochitina vitrea*, and *Calpichitina* sp., which together indicates a Ludlow to early Pridoli age (Fig. 5, Plate III). These chitinozoan ages are based on the synthetic chitinozoan range chart for the Silurian

compiled by Paris *et al*. (1995), containing data from the global Silurian chitinozoan zonation. Other marker taxa from acritarchs with more restricted stratigraphic ranges have been recorded such as *Deflandrastrum* cf. *leonardi*, *Deflandrastrum millepiedi*, and *Deflandrastrum authierae*, (Plates I, II). These taxa are restricted to the Late Ludlow, in NW Spain (Cramer, 1966: Al-Ameri, 1983) and Libya (Combaz, 1962; Tappan, 1980), thus suggesting a Late Ludlow age for this section. These species are very similar in morphology and size, as illustrated by Richardson's, 1988 study of the Akakus Formation of the Ghadamis Basin. The presence of *Tunisphaeridium tentaculaferum* supports an Aeronian age, either by comparison with the acritarch succession established in the Llandovery type area (Hill & Dorning, 1984), or correlation with the assemblage biozone of Hill & Molyneux (1988) from northeast Libya.

Several cryptospore, miospores and trilete spores are present, such as *Ambitisporites avitus, Ambitisporites dilutus, Imperfectotriletes vavrdovae, Rimosotetras problematica,* and *Tetrahedraletes medinensis.* Occurrences of these taxa are in line with late Ludlow times (Paris *et al*., 1995). Overall, the miospore assemblages are dominated by cryptospores, with trilete spores being rare. The first appearance of the oldest trilete spores is known to be diachronous from latest Ordovician to Llandovery. The oldest trilete spores are Hirnantian in age from Turkey (Steemans *et al.,* 1996), Rhuddanian in age from Saudi Arabia (Steemans *et al.,* 2000) and upper Aeronian from Libya (Richardson, 1988). Hence the trilete spores stratigraphy from Libya confirms the diachronous nature of the early spore record.

4.1.2. E1-NC174 borehole (Murzuq Basin)

The depth ranges of the principal taxa observed in this borehole are displayed in Fig. 7. Plates V, VI, VII, and VIII show typical examples of palynomorphs observed from this drill core, consisting of acritarchs, prasinophytes, chitinozoa and miospores.

The lower-most sample is already within the dark-black, organic-rich shale at the base of the Tanezzuft Formation (Fig. 7). The interval between 2221 m and 2179 m is dominated by AOM, with palynomorphs being rare or probably mostly obscured by the large amount of AOM. In the "hot" shale section of the Tanezzuft Formation the AOM is relatively well-preserved (Plate VII, 10). Although overwhelmed by the AOM, prasinophytes including *Pterospermella* sp., *Tasmanites*, *Dictyotidium dictyotum, and Leiosphaeridia* sp. (Plate VII) are also present.

Acritarch diversity declines from the base of the "hot" shale toward the top, which might partially be due to the lower number of specimens observed (Fig. 7). Still, a similar decline in diversity was recorded by Loydell *et al*., (2009) in the "hot" shale in the BG-14 core from Jordan. Vecoli *et al*. (2009) recorded only two acritarchs genera (*Veryhachium* and *Evittia*) within the "hot" shale of the Tt1 borehole in the Ghadamis Basin in southern Tunisia. Le Hérissé's study (2000) did not record any acritarchs in the "hot" shale of the Mukassir-1 well from Saudi Arabia. The interval from 2179 m until the top of the sequence yielded rich assemblages of acritarchs (Fig. 7; Plates V, VI) dominated by *Buedingiisphaeridium* cf. *pyramidale, Tunisphaeridium tentaculiferum, Eupoikilofusa* sp., *Oppilatala* sp., *Tylotopalla* sp., *Baiomenisus camurus* and *Beromia rexroadii.*

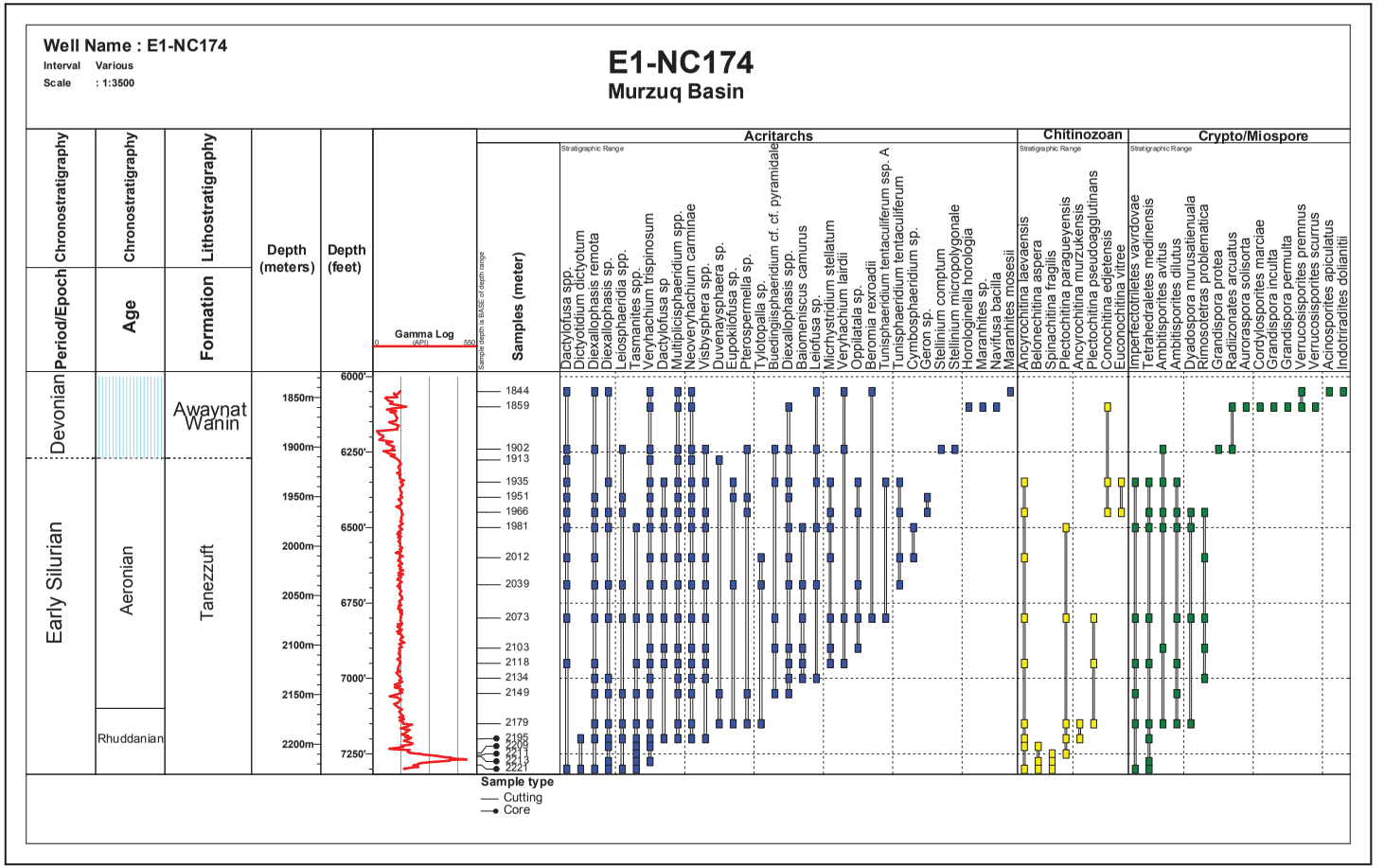

Fig. 7. Palynological range chart of E1-NC174 borehole (Murzuq Basin).

Graptolite zooclasts were dominant between 2221 m. and 2209 m. (Plate VII, 9), followed by a decrease and subsequent complete absence of graptolites from 2134 m toward the top of the studied sequence.

The upper part of the record, from 1905 m up to the top shows increasing abundances of palynomorphs, whereas AOM is absent. We also observed the abundant occurrence of land-derived organic debris and palynomorphs, such as miospores, and we still observed marine palynomorphs such as acritarchs (Plate VIII).

Based on these data an age model was constructed for this borehole. Recently, Loydell (2012) and Butcher (2013) provided the first detailed graptolite and chitinozoan biostratigraphy for the "hot" shale from North Africa, based on core E1-NC174. These studies showed that the "hot" shale is of mid-Rhuddanian age, occurring within the *Neodiplograptus africanus* and *Neodiplograptus fezzanensis* graptolite biozones. This implies that the "hot" shale is the stratigraphic equivalent of that in core BG-14 from Jordan studied by Lüning *et al*, (2005) and Loydell *et al.,* (2009). Unfortunately, this biostratigraphy is focused on the "hot" shale interval. In order to also correlate the upper part of the record, we have extended this stratigraphy toward the upper part of Tanezzuft Formation and the Akakus and Tadrart formations.

Chitinozoans occur in generally low but constant abundances throughout the stratigraphic interval between the base of the section and 2195 m. In this interval the species observed were recognized by Paris and Al-Hajri (1995) as indicating a latest Rhuddanian to middle Aeronian age (Butcher, 2013). Of the taxa observed in E1-NC174, only two are cosmopolitan, *Belonechitina postrobusta* and *Conochitina elongate,* with the remaining taxa not having been recorded outside of northern and western Gondwana (Butcher, 2013). The first chitinozoan biozone documented for the Llandovery of central Saudi Arabia, i.e. *Spinachitina fragilis*, is assigned to the earliest-Rhuddanian period. This age assignment is also supported by the occurrence of *S. fragilis* in northeast Saharan strata, assigned to earliest Rhuddanian (Butcher, 2013). This confirms the Rhuddanian age for the base of the section.

From the acritarchs species recognized *Beromia rexroadii* (Plate V Fig. 2) has some biostratigraphical potential, as it was recorded previously only from the Lower Silurian, Llandovery in North America (Wood, 1996). The wide geographic distribution and apparent short stratigraphic range of this acritarch suggests it may be a significant index fossil for correlating Upper Llandovery strata (Aeronian-Telychian boundary). The *Beromia rexroadii* species occurs within a diverse and abundant acritarch assemblage. The species is also recorded from the Brabant Massif in Belgium in a core dated late Aeronian to Telychian (Wauthoz, 2005). These ages are in line with the observed ranges here. *Dactylofusa* sp. and *Baiomeniscus camurus* are well represented in the samples between 2195 m and 1981 m. Both these species were first described from the Mapplewood shale of central New York, and assigned to the Middle Silurian by Loeblich (1970). Nevertheless, the Mapplewood Shale is now regarded as late Aeronian to early Wenlock (Wood, 1996), but these species are particularly abundant from late Aeronian to earliest-Telychian. This implies an Aeronian to earliest Telychian age for the middle part of the Tanezzuft formation.

Several cryptospore, miospores and trilete spores are present, similar to core A1-70 from the Ghadamis Basin. Especially in the upper part of the record, the species composition in the Murzuq and Ghadamis basins is identical. The upper part of the

record is characterized by the abundant occurrence of land-derived organic debris and Devonian miospores and acritarchs occurring between 1905 m up to 1844 m. This interval is overwhelmed by trilete and monolete spores. Selected characteristic miospores are *Radiizonates arcuatus*, *Aurorspora solisorta*, *Cordylosporites marciae*, and *Acinosporites apiculatus.* Acritarchs present are mainly of the veryhachid subgroup and may contain index acritarchs of *Horologinella horologia*, *Stellinium comptum*, *Stellinium micropolygonale,* and *Navifusa bacilla.* Miospores and acritarchs together indicate Middle to Late Devonian age (Melo & Loboziak 2003; Streel *et al*., 1988, 1990). The samples representing the interval towards the top of the Tanezzuft probably represent sediments that caved and were contaminated during drilling.

4.1.3. I3-NC186 borehole (Murzuq Basin)

More than 45 acritarch species were observed in samples studied from I3-NC186. All samples yielded palynomorphs, in variable abundance and diversity. Palynomorphs consisted of acritarchs, prasinophytes, chitinozoans, miospores, cryptospores, and zooclasts (mostly graptolites, scolecodonts) and AOM (Fig. 8 and Plates I, II, III, IV). The preservation of the various types of organic-walled microfossils was variable, ranging from very good (light yellow colours of vesicle walls) to medium preservation (brownish colors). The lower part of the record, the "hot" shale interval of the Tanezzuft Formation, is relatively enriched in AOM, with low abundances of other palynomorphs being observed. The AOM decreases toward the upper part of the Tanezzuft Formation, above the "hot" shale.

The palynomorph assemblages from the "hot" shale contain sixteen acritarch species, dominated by *Cymbosphaeridium* sp.*, Evittia* sp*, Eupoikilofusa* sp.*, Eupoikilofusa striatifera,* and also contain species such as *Evittia* sp.*, Leiofusa estrecha, Multiplicisphaeridium irregulare, Veryhachium wenlockianum, Neoveryhachium* sp.*, Tunisphaeridium caudatum,* and *Visbysphaera microspinosa*. Sporomorphs are generally rare, or absent within this interval. Within the "hot" shale interval prasinophytes are abundant, represented by *Tasmanites, Leiosphaeridia* and *Cymatiosphaera* sp.*, Cymatiosphaera* cf. *densisepta,* and *Dictyotidium dictyotum.* Graptolite zooclasts are dominant within the same interval.

The section between the "hot" shale and the upper part of the Tannezuft Formation is missing. Above the missing section, from 1353 m to 1262 m, a rich palynomorphs assemblage is observed. Acritarchs are well preserved and dominated by the species, *Domasia trispinosa, Helosphaeridium, Tunisphaeridium tentaculaferum, Oppilatala ramusculosa, Oppilatala eoplanktonica,* and *Geron gracilis.* In this interval, the prasinophyte assemblage is also more diverse, due to the inception of species such as *Pterospermella* sp., *Dictyotidium* sp.*, Cymatiosphaera* sp.*, Tasmanites,* and *Leiosphaeridia.* The top part of the studied sequence, from 1262 m to 1137 m, is characterized by the presence of *Ammonidium microcladum, Tylotopalla* sp., *Tylotopalla caelamenicutis* and *Schismatosphaeridium* sp. Based on these data an age model was constructed for this borehole. Chitinozoan assemblages are described here from the base of the section toward the top, based on the synthetic chitinozoan range chart from the global Silurian chitinozoan zonation for the Silurian (Hill *et al*., 1985; Paris e*t al*., 1995; Butcher, 2013). Of the still-observed species, *Lagenochitina* sp. (which is an index species for the Rhuddanian) is associated with *Conohitina edjelensis*. *Angochitina macclurei,* and

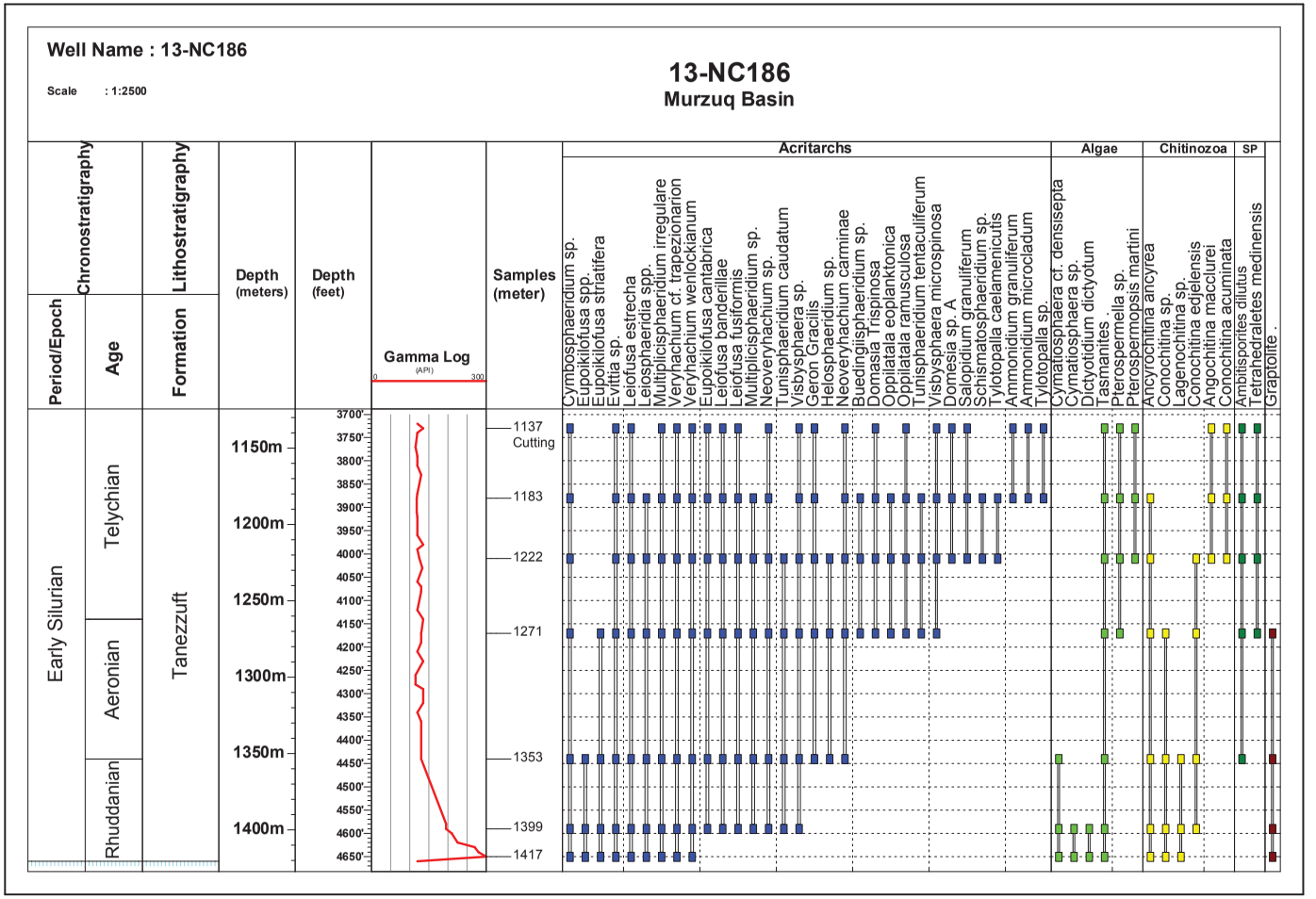

Fig. 8. Palynological range chart of I3-NC186 borehole (Murzuq Basin).

Conochitina acuminata, are present between 1222 m and 1137 m and indicate Late Telychian to early Wenlock times (Paris & Al-Hajri, 1995).

The spore and cryptospore assemblages permit linking these strata to the Middle to Late Llandovery time interval (Paris *et al.*, 1995). The spore assemblages are dominated by cryptospores, with trilete spores being very rare. The relative proportion of cryptospores decreases through the Llandovery.

Based on the discussion above on chitinozoan biostratigraphy, it appears that the studied sections from the E1-NC174 and I3-NC186 boreholes in Murzuq Basin record an assemblage of earliest Silurian age and earliest to late Silurian in the A1-70 borehole in Ghadamis Basin. The acritarchs, miospores and cryptospores assemblages seem to be no older than earliest Rhuddanian. A great similarity exists between North Gondwana and Saudi Arabian chitinozoan assemblages from the Middle Llandovery.

4.2. TOC, $\delta^{13}C_{TOC}$ and biomarker analysis

4.2.1. A1-70 borehole (Ghadamis Basin)

Within the section studied here, total organic carbon contents (TOC %) varies between 0.1 and 22.3% (Figs. 9A and B). These TOC values show a clear correlation to the gamma-ray intensity measurements from the well log. Based on gamma-ray intensity, organic carbon contents and lithology of the studied section is here are subdivided into three units. The lowermost unit (3118 m to 3112 m) is characterized by relatively low TOC values (average 1.4%), low gamma ray intensities and alternating silt and sandstones Fig. 9B). These rocks are probably part of the Ordovician Bir Tlacsin Formation (Fig. 3). The second unit (3112 m to 3048 m) is characterized by high radioactivity of over 250 API (American Petroleum Institute units) and consists of laminated, dark grey-to-black shales. The maximum TOC value measured in this interval is 22.3% (average 6.9%). The third unit (3048 m to 2743 m) is defined by, again, relatively low TOC values (average 0.7%), and a "cool" gamma – ray signature (Fig. 9A and B). This section consists of shale and siltstones, with the uppermost part consisting of sandstone.

$\delta^{13}C_{TOC}$ values in the studied section range from -31.4‰ to -25.8‰ (Fig. 9C). A clear excursion toward less negative values is observed coinciding with the second unit. Amplitude of this excursion is about 3‰, returning to stable values of about -31‰ in upper unit between 3031 m and 2832 m. In the upper part of the sequence, a rapid increase in $\delta^{13}C_{TOC}$ values is again observed of about 2 to 3‰, with values showing much scatter near the top of the section. The variation in $\delta^{13}C_{TOC}$ values is partly in line with the subdivision based on TOC except for the top, where stable TOC values are accompanied with scatter in $\delta^{13}C_{TOC}$.

Selected samples from the A1-70 borehole were also analyzed for hydrocarbon biomarkers. Typical distributions of *n*-alkanes for the "hot" versus lean shales are shown in Fig. 10. All intervals show *n*-alkane distributions with maximum relative abundances of the *n*-C_{17} to C_{21} *n*-alkanes. In general, the *n*-alkanes range from *n*-C_{15} to C_{30}, with the "hot" shale showing higher relative abundances of the shorter *n*-alkanes. As the hydrocarbon fractions were still not suitable for compound-specific stable carbon isotope analysis, these fractions were further purified using urea adduction (Fig. 10). The stable carbon isotopic composition of individual short-chain *n*-alkanes (*n*-C_{17} to *n*-C_{21}) show

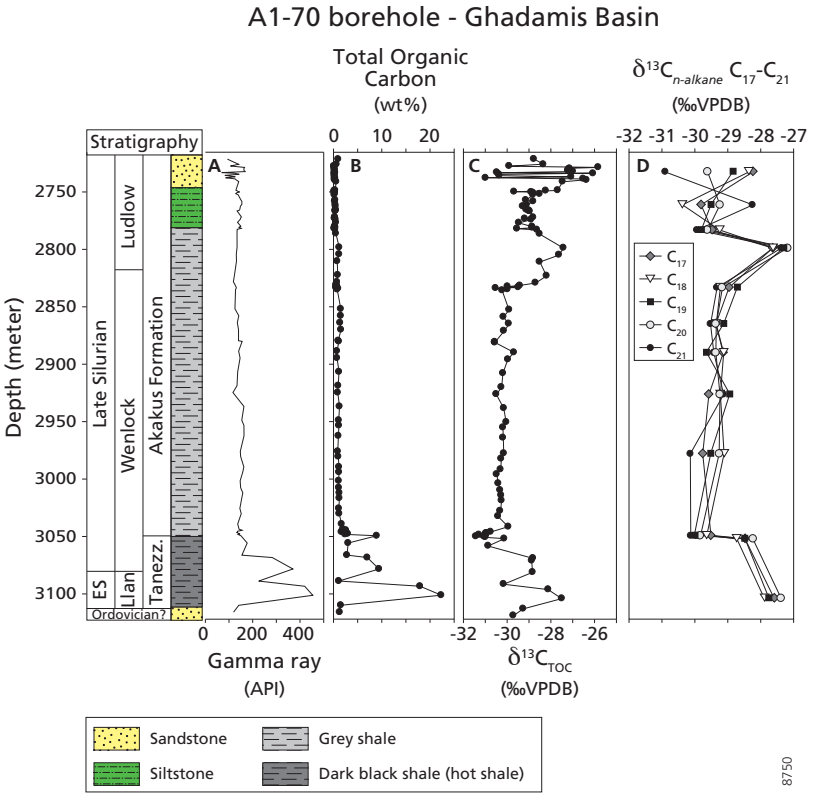

Fig. 9. Stratigraphic variation of (A) Gamma ray with correlations to (B) TOC and (C) $\delta^{13}C_{TOC}$, (D) short-chain *n*-alkane (C_{17}-C_{21}) from the A1-70 borehole (Ghadamis Basin). Abbreviation ES- Early Silurian; Lland- Llandovery; Tanf- Tanezzuft Formation.

generally similar $\delta^{13}C$ values, and they are in the same range as the bulk $\delta^{13}C_{TOC}$ values, between -30.8‰ and -27.5‰ (Figs. 9C and D). The trends observed in the $\delta^{13}C_{TOC}$ are mimicked by the short-chain *n*-alkanes $\delta^{13}C$ signal across the Tanezzuft and Akakus formations. Only at the top of the Akakus Formation values for the individual *n*-alkanes deviate from the $\delta^{13}C_{TOC}$ and shows more scatter.

4.2.2. E1-NC174 borehole (Murzuq Basin)

The early Silurian organic-rich shale in the E1-NC174 borehole can be easily identified by the high gamma-ray radioactivity (> 450 API). It ranges from 190 and 495 API at 2221 m to 2195 m respectively, with a thickness of ca. 27 m (Fig. 11A and B). Total organic carbon content (TOC %) varies between 0.3 and 12.0%. The "hot" shale unit is overlain by organically lean gray shales, with low gamma ray (background) values (API <150). The "hot" shale samples between 2221 m and 2195 m are organic matter-rich and have TOC contents between 2.4 and 12.0 % (Lüning *et al.*, 2003). A return to relatively

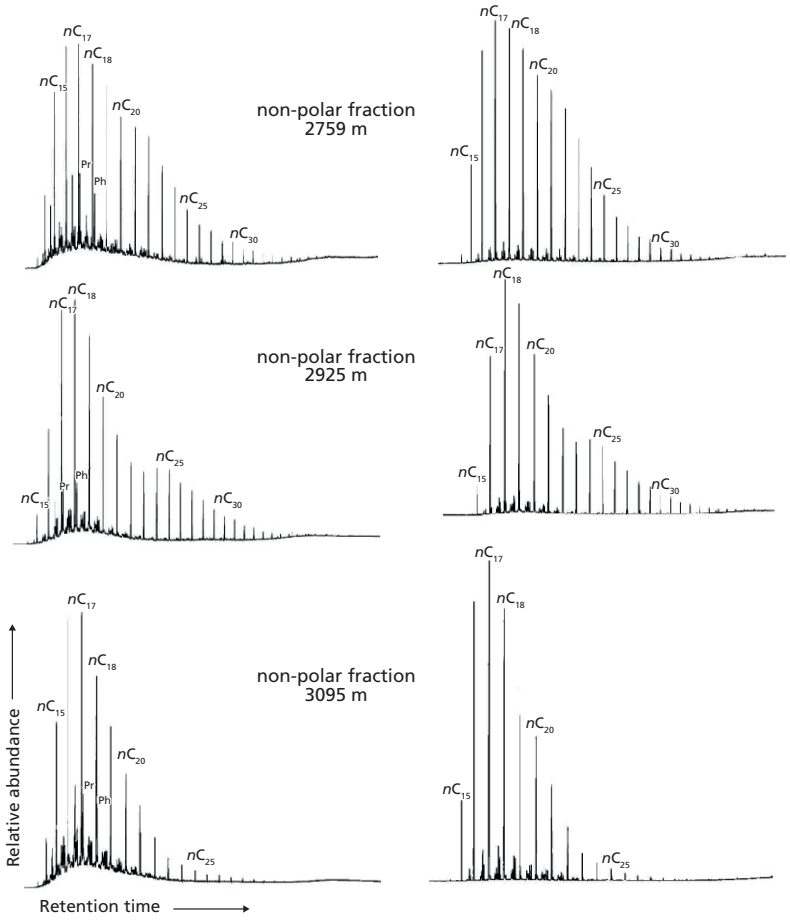

Fig. 10. Gas chromatograms of non-polar hydrocarbon fractions (left) and *n*-alkanes after urea adduction of rock extracts from A1-70 borehole (Ghadamis Basin).

low TOC values (average 0.5 %) is observed in the overlying grey shale interval (from 2179 m to 1844 m depths).

The $\delta^{13}C_{TOC}$ curve is plotted in Fig. 11C. $\delta^{13}C_{TOC}$ values range between -30.2‰ at 2221 m and -24.9 ‰ at 1921 m. In the Murzuq basin the most negative $\delta^{13}C_{TOC}$ value is observed at the base of the "hot" shale (the interval below the "hot" shale was not analyzed), with values of about -30.0 ‰. These values are followed by a rapid 1‰ shift to more positive values. Within the "hot" shale, values remain relatively stable at -29‰, followed by a gradual increase. In the middle part of the Tanezzuft Formation, values remain stable again at about -28 ‰ (Fig. 11C). In the upper part of the Tanezuft Formation, carbon isotopic values decrease again gradually toward the Awaynat Wanin Formation, showing an overall 3.3‰ positive shift.

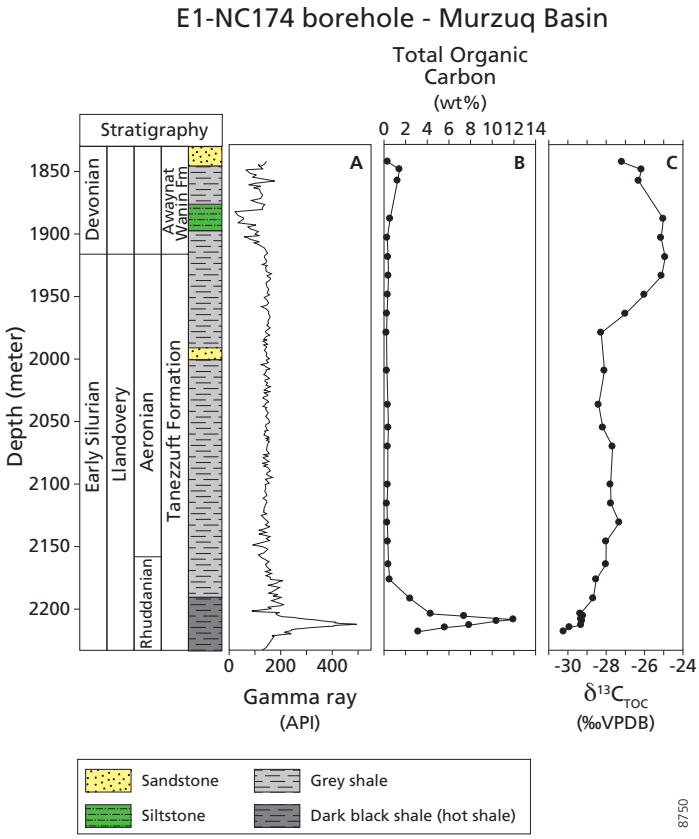

Fig. 11. Stratigraphic variation of (A) Gamma ray correlated to (B) TOC and (C) $\delta^{13}C_{TOC}$ from E1-NC174 borehole (Murzuq Basin).

4.2.3. I3-NC186 (Murzuq Basin)

The studied section can be subdivided into two distinct units based on gamma-ray intensity, lithology and TOC. The lower unit, consisting of laminated dark grey to black shale, contains up to 15.0 weight % TOC and has a high natural radioactivity (API >250) (Figs. 12A and B). This is again the so-called "hot" shale, which here reaches a thickness of about 22 m. The second unit shows a return to relatively low TOC values (average 0.5%) and low gamma – ray intensities (API <150) and consists of silty shales.

The $\delta^{13}C_{TOC}$ in the studied section show is relatively stable at values between -28.1‰ and -29.4‰ throughout the Tanezzuft Formation (Fig. 12C).

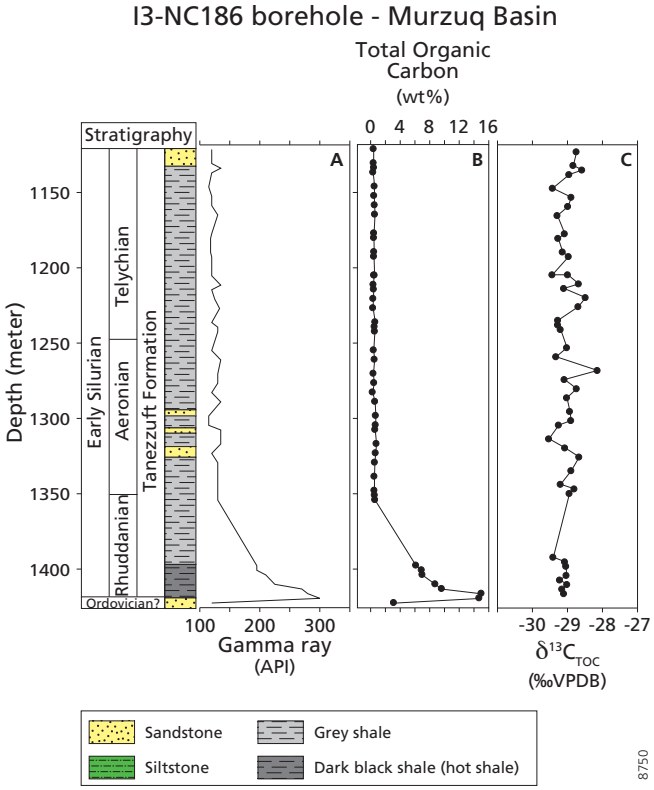

Fig. 12. Stratigraphic variation of (A) Gamma ray correlated to (B) TOC and (C) $\delta^{13}C_{TOC}$ from I3-NC186 borehole (Murzuq Basin).

5. Discussion

5.1. Regional (event) stratigraphy and setting

Palynological data and biostratigraphy for the A1-70 borehole in the northern part of the Ghadamis basin shows that the Llandovery/Wenlock (Tanezzuft Formation) is locally represented by a relatively thin sedimentary sequence (± 55 m), while the Wenlock/Ludlow (Akakus Formation) corresponds to a much thicker sedimentary column (> 322 m). The base of the Akakus Formation consists of outer shelf sediments (shales), showing a coarsening upward into fine sandstones.

Our palynological data of the E1-NC174 and I3-NC186 boreholes showed that the black shales in the Murzuq basin are exclusively of Rhuddanian age, and the entire Tanezzuft Formation was deposited during the Early Silurian (until Aeronian or Telychian). Hence, both boreholes from the Murzuq Basin (Fig. 13A) show that the Tanezzuft Formation (Llandoverian) in this basin consists of a much thicker sedimentary column of 293 m and 317 m respectively (compared to 30 m in Ghadamis basin). In both

records studied from the Murzuq basin, the Akakus Formation is lacking and Devonian strata directly overlie the Tanezzuft. Hence, the Wenlock is absent in the records studied from the Murzuq basin. Both Wenlock and Ludlow probably eroded as a consequence of the Caledonian orogeny, during the Late Silurian and/or Early Devonian (Fig. 13A and C), or were never deposited due to a lack of accommodation space. Either way, this unconformity is linked to a major phase of uplift, previously inferred for the entire North African Margin during the Upper Silurian and Lower Devonian (Klitsch, 1969). This implies that the sedimentation rate at Murzuq basin was much higher compared to Ghadamis basin (Fig.13B). Sedimentation resulted in a complete infill of the Murzuq Basin at times that "hot" shale deposition in Ghadamis Basin was still continuing (Fig.13C). Ultimately also in the Ghadamis basin, the facies shifted from the anoxicaly deposited "hot" shale to the silty sand Akakus Formation. Finally, the Ghadamis Basin also filled up rapidly.

Comparing the $\delta^{13}C_{TOC}$ records from the Ghadamis and Murzuq basins might suggest that the deposition of the "hot" shale started earlier in the Ghadamis basin as compared to the Murzuq basin. The isotopic excursion at 3103m observed in the Ghadamis basin reflects, based on the age model, the Early Silurian (Aeronian) isotope excursion (cf. Vecoli *et al.*, 2009). The fact that this excursion is recorded both in bulk organic carbon and in specific *n*-alkanes (Fig. 10) shows that this is a true signal, and not caused by changes in the overall composition of organic carbon (cf. Sinninghe Damsté and Köster, 1998). This positive excursion in $\delta^{13}C_{TOC}$ is missing in the Murzuq basin records, which suggests a diachronous onset of the "hot" shale. That is in line with the highly irregular pre-Silurian surface (Lüning *et al.*, 2000). Flooding related to the early Silurian transgression would result in initial black shales being deposited only in the lowest parts of the paleodepressions (Fig. 13B). Alternatively, the stable isotopic excursion observed in Ghadamis basin at the base of the Tanezzuft is expanded in the Murzuq basin. This is in line with the overall values in the Murzuq basin Tanezzuft (ca. -28‰), which are close to the values during the excursion in Ghadamis basin. This would imply that sedimentation rates differed considerably between the two basins, also during the earliest Silurian.

5.2. Causes for high TOC in Northern Africa during the Early Silurian

The palynofacies of the Early Silurian sediments at the base of the "hot" shale interval show high abundances of AOM, coinciding with high TOC values. In general, AOM is degraded when exposed to oxic conditions (Tyson, 1995). Increased TOC values also coincide with more fluorescent AOM (Plate IV, 7 and 7b), which suggests enhanced preservation of the organic matter, possibly related to dysoxic conditions. Also the laminations of the "hot" shale imply deposition under dysoxic to anoxic conditions. Hence, bottom water anoxia potentially contributed to the formation of the "hot" shale by enhancing organic matter preservation.

However, the very high TOC values (> weight 20%) observed within the "hot" shale require exceptional depositional conditions. Other factors must have contributed to generate the observed high TOC values of the sediments deposited during the Rhuddanian (Murzuq and Ghadamis) and Wenlock (Ghadamis only). These factors include enhanced sea surface productivity and a more efficient transfer of organic matter

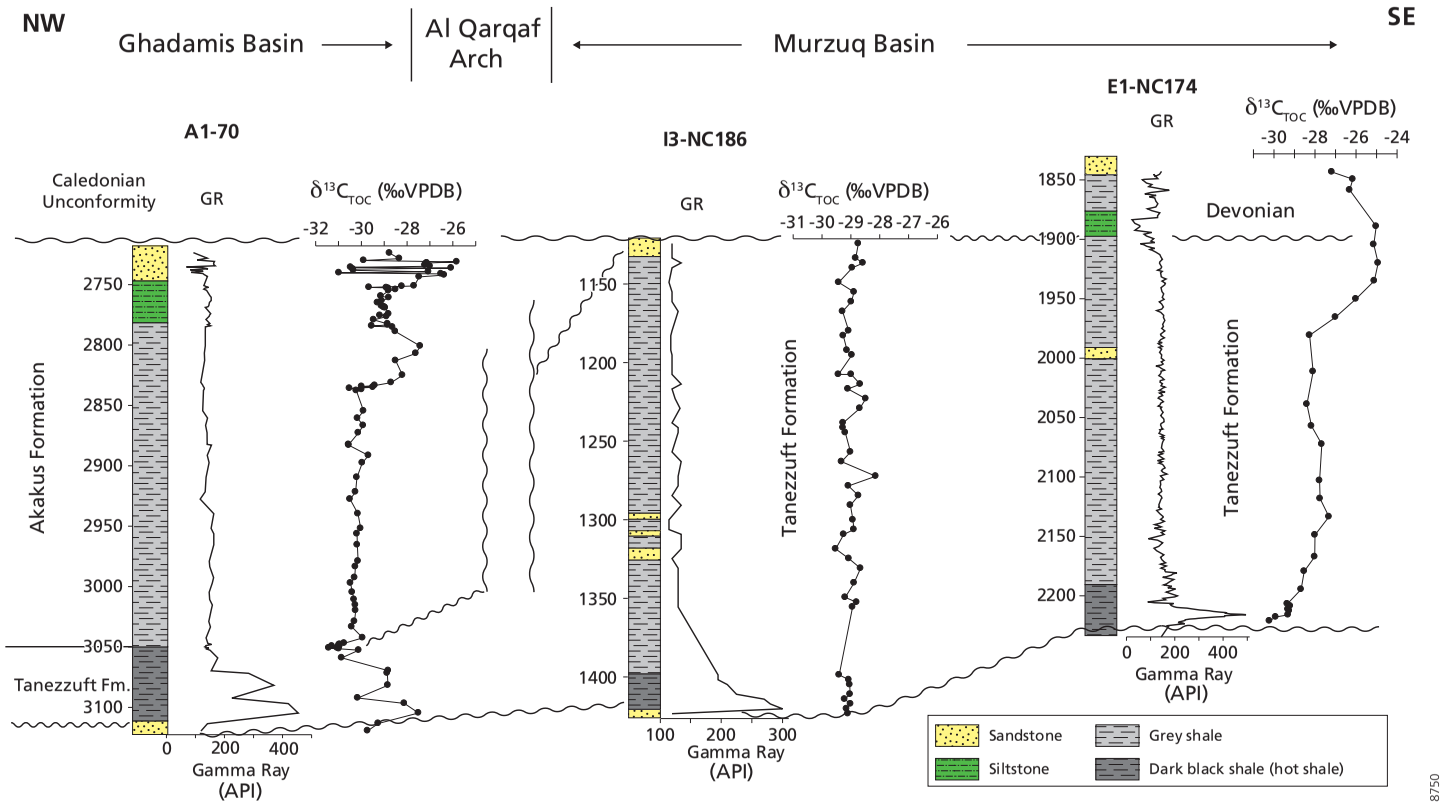
NW
Ghadamis Basin
Al Qarqaf Arch
Murzuq Basin
SE
A1-70
I3-NC186
E1-NC174
Caledonian Unconformity
GR
δ13CTOC (‰VPDB)
-32 -30 -28 -26
-31 -30 -29 -28 -27 -26
-30 -28 -26 -24
Devonian
Akakus Formation
Tanezzuft Fm.
Tanezzuft Formation
2750
2800
2850
2900
2950
3000
3050
3100
1150
1200
1250
1300
1350
1400
1850
1900
1950
2000
2050
2100
2150
2200
0 200 400
100 200 300
Gamma Ray (API)
Sandstone
Siltstone
Grey shale
Dark black shale (hot shale)
8750

Fig . 13 (A)

Fig . 13(B)

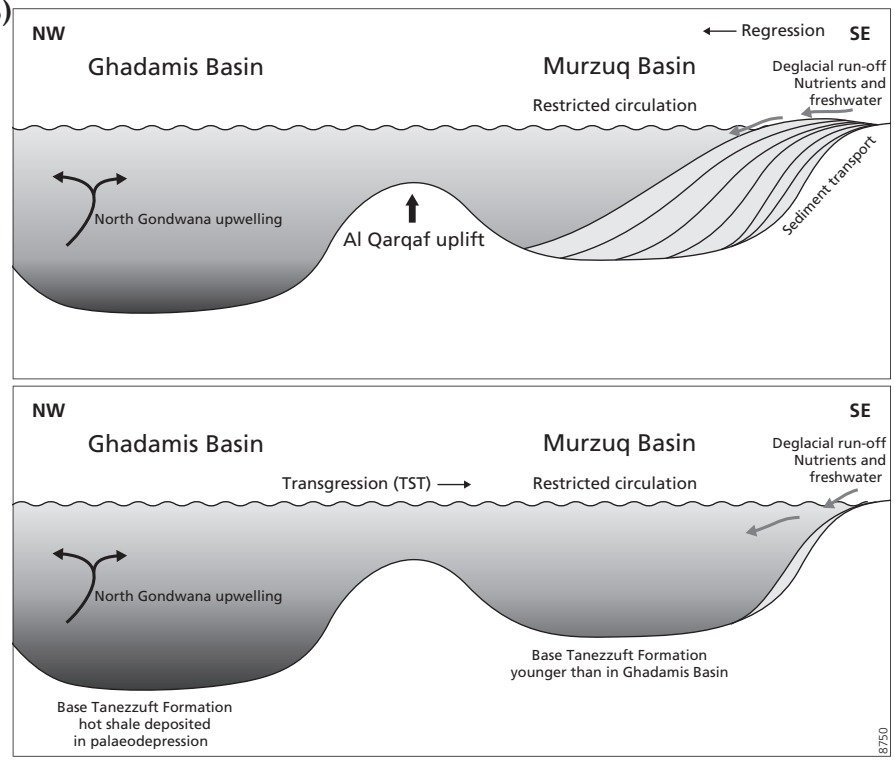

Fig . 13(C)

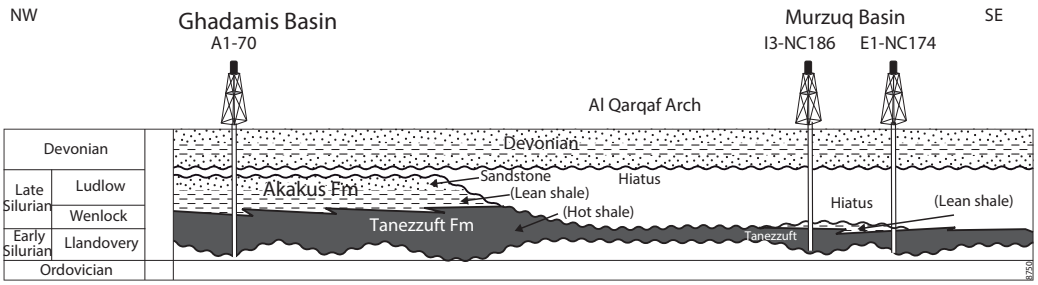

Fig. 13. **(A)** Correlation between A1-70 (Ghadamis Basin), I3-NC186 and E1-NC174 boreholes (Murzuq Basin), the Llandovery is thicker in the Murzuq Basin and thinner to the north of Ghadamis Basin, while the Ludlow is much thicker in the north of the Ghadamis and absent from Murzuq Basin, **(B)**. The Silurian transgression introduced marine shales onto the irregular Ordovician post-glacial surface. The initial sediment deposited during the Rhuddanian stage was black anaerobic shale with high gamma-ray levels, which forms excellent source rocks. The extended period of black shale deposition occurred regionally from Rhuddanian to early Wenlock times in the A1-70 borehole **(C)**. As the transgression spread, the localized depressions were flooded by open marine shale with a much lower organic content.

through the water column (Tyson, 1993). Changes in sea surface productivity are evident in both the Murzuq and Ghadamis basins. A low diversity of the acritarch assemblages is associated with an increase in the abundance of prasinophytes in the Early Silurian ("hot" shale) Tanezzuft Formation. At the same time chitinozoan abundance decreases. The highest abundance of thick-walled prasinophytes (*Tasmanites*-type algae) is observed in the lowermost part of the Tanezzuft. High abundances of prasinophyceae indicate enhanced surface water productivity (Combaz., 1966; Revill *et al*., 1994; Tyson., 1995). Extensive black shale deposition and anoxic conditions were thus most likely accompanied by enhanced surface water productivity. The presence of prasinophytes is generally correlated with dysoxic-anoxic conditions (Tyson, 1995). Prasinophytes algae dominate the marine palynomorph assemblage when the production of other groups is suppressed, and accordingly they have been described as "disaster taxa" in connection with black shales at the Permian-Triassic and Triassic-Jurassic boundaries (van de Schootbrugge *et al*., 2007; Richoz *et al*., 2012). The success of prasinophyte algae during times of widespread anoxic conditions is also related to their holoplanktonic life cycle, whereby the vegetative cysts (phycomata) remain in the oxygenated photic zone (van de Schootbrugge *et al*., 2013).

The unusual high TOC values imply that during "hot" shale deposition sedimentation rates must have been low, as inputs of (detrital) material would have diluted the organic matter. Today even the highest productive areas in the ocean, with enhanced preservation of organic matter because of bottom water anoxia (e.g. Peru Margin, Arabian Sea, and Black Sea), seldom show TOC values over 10% because of dilution with inorganic sedimentary components (Van der Weijden *et al*., 1999; Calvert & Pedersen, 1992; Calvert & Pedersen, 1993). Previously Armstrong *et al*. (2005), Lüning *et al*. (2005) and Loydell *et al*. (2009) discussed the marked increases in TOC seen in southern Jordan during the Early Silurian. They proposed that anoxic conditions related to the development of a pronounced halocline resulted from melt water input during deglaciation. An increased supply of meltwater-derived nutrients would, at the same time, have enhanced productivity. It is, however, difficult to reconcile the rather short time span involved with a deglaciation with the extended deposition of "hot" shale in Ghadamis Basin, about 17 My (Gradstein *et al*., 2004). The melting of an ice cap, even when covering a super continent, would not likely take more than a couple of hundreds of thousands of years (e.g. Zachos *et al*., 2001). In addition, enhanced melt water flow from the African continent would most likely have resulted in more detrital material being transported to the margins, which would have diluted the OC. Still, a meltwater spike might have triggered stratification, with the ocean system being unable to return to a well-ventilated state.

One of the most conspicuous features of the "hot" shale is that it is characterized by higher gamma-ray values, such as observed in the record studied here. These higher gamma-ray values are related to elevated uranium concentrations, as authigenic uranium precipitates in the sediments during anoxic bottom water conditions (Lüning *et al*., 2003). The high values observed here in both Murzuq and Ghadamis basins are in line with a relatively low sedimentation rate.

5.3. Carbon isotope events

Stable carbon isotopes are widely used both as chemostratigraphic tools as well as sources of information for reconstructing the paleo-environment. Several distinct positive $\delta^{13}C$

excursions allowed detailed stratigraphical correlations to be made between Lower Palaeozoic successions. The excursions themselves are thought to be caused by widespread increased organic matter burial or, possibly, enhanced weathering of terrestrial carbonates (Kump et al. 1999). The lower part of the "hot" shale interval in Ghadamis Basin shows two isotopic excursions, albeit they are separated by only one interval with lower $\delta^{13}C$ values (Fig. 10). The first ~ 2.0‰ positive shift occurs during the early Aeronian (middle LIandovery). This excursion was previously also recognized in Dob's Linn, Scotland, Cornwallis Island of Arctic Canada, and Argiles Principales Formation in Tunisia (Melchin & Holmden, 2006; Vecoli et al., 2009). The second excursion occurred during the early Sheinwoodian (LIandovery/Wenlock boundary or earliest Wenlock) and shows a ± 1.5‰ positive shift. This second excursion is one of the best-studied Silurian isotopic events, also known as the "Ireviken Event" (Munnecke *et al.*, 2003; Loydell, 2007; Jeppsson, 1990, 1997). This event (Fig. 14) appears to be global in character and has been observed in areas, such as the Baltic region (Kaljo *et al.*, 1997; Munnecke *et al.*, 2003) and North America (Saltzman, 2001; Cramer *et al.*, 2006).

The increasing number of publications treating the early Wenlock carbon isotope excursion shows the global character of the carbon cycle change, although the relative impact differs. The highest amplitude of the $\delta^{13}C$ peak reaches 6.6‰ in Norway (carbonate; Kaljo and Martma, 2006), followed by values at about 5.5‰ in New York State and Ontario (carbonate; Cramer *et al.*, 2006), about 5‰ in Sweden (carbonate; Gotland; Munnecke *et al.*, 2003) and about 3‰ in Tunisia and Wales (TOC; Vecoli *et al.*, 2009; Loydell and Frýda, 2007). Differences in amplitude of the carbon isotopic excursion between organic carbon and carbonate imply a change in fractionation between DIC and primary producers. In our records, the observed amplitude (± 2‰) is relatively modest; however, this is based on comparing the bulk and compound specific analyses, not influenced by changes in organic matter composition. Hence, changes in productivity and local recycling of CO_2 by, for instance, upwelling related productivity or strong stratification with productivity mainly occurring below the mixed layer, might have affected the amplitude of the carbon isotopic excursion.

The upper part of the Ghadamis basin record shows a large positive excursion in $\delta^{13}C_{TOC}$ coinciding with the Wenlock-Ludlow transition, whereas TOC values remain low and stable. Since this interval corresponds to the Wenlock-Ludlow boundary, this excursion seems time equivalent to the late Homerian double-peaked excursion, known from the Baltic (Martma et al., 2005; Kaljo and Martma, 2006). Also this excursion is not affected by differences in composition of TOC as the $\delta^{13}C$ record of *n*-alkanes (Fig. 10) shows a similar excursion, although the resolution of the latter does not allow resolving the double peak observed in the bulk carbon isotopic record. The amplitude of this excursion observed here (± 3 ‰) is similar to that observed elsewhere (e.g. Munecke *et al.*, 2003). The bulk carbon isotopic record also suggests some rapid changes in the top of the record, but these changes are not reflected by the $\delta^{13}C$ values of the *n*-alkanes. This implies that the observed changes are probably due to compositional differences rather than true isotopic trends.

Overall, in the Murzuq basin, the stable carbon isotope records show much less variability than that of the Ghadamis basin. Still, in the central part of the Murzuq basin (E1-NC174, Fig. 11C) a gradual change is observed in the carbon isotopic record during the Rhuddanian to Aeronian transition (middle Llandovery). Since no change

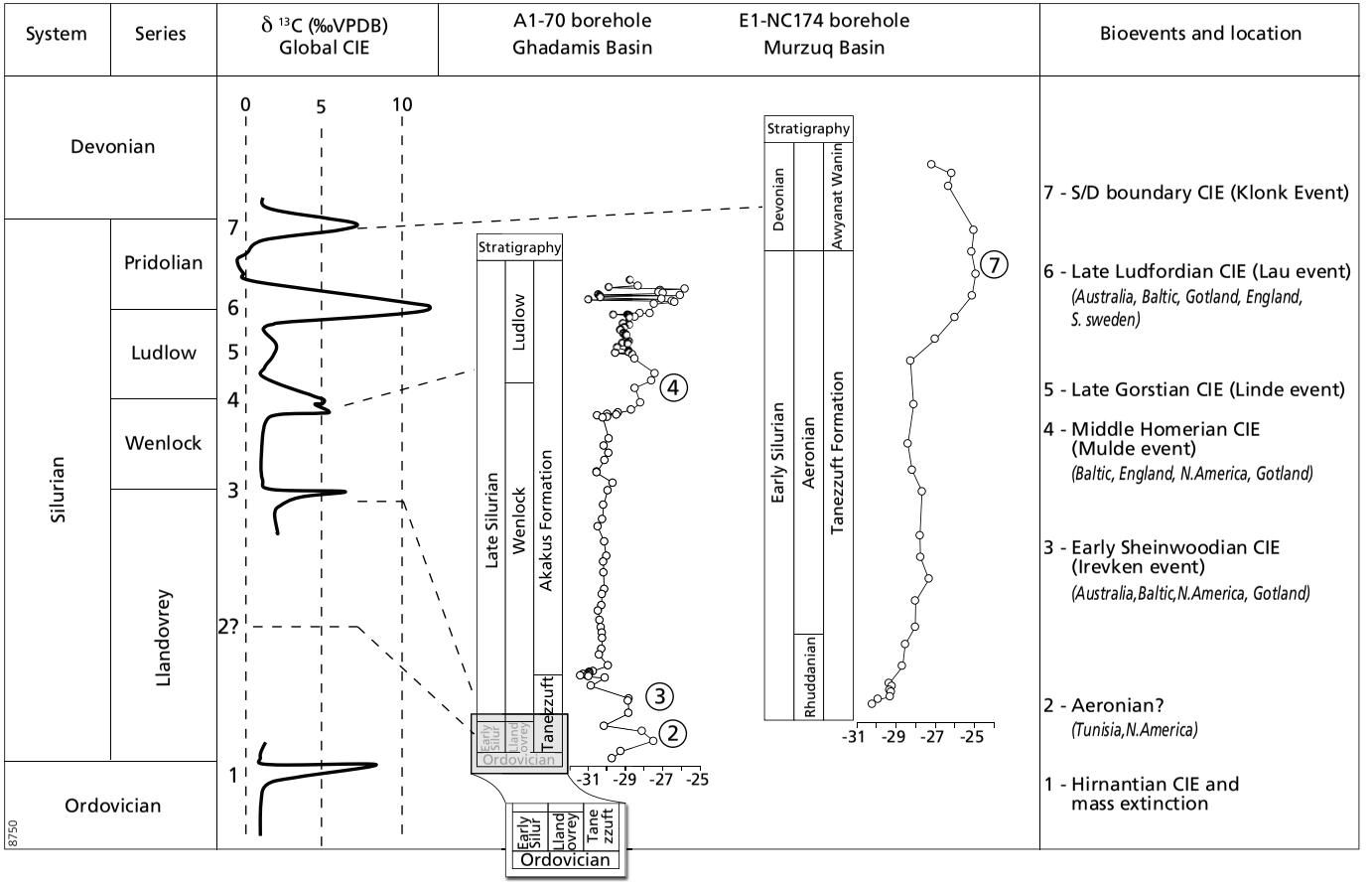

Fig. 14. Correlation of Silurian and Devonian $\delta^{13}C_{TOC}$ shifts from Ghadamis and Murzuq Basins (this study) and the major global positive carbon isotope excursions (CIE) of the late Ordovician, Silurian and Devonian and their relationship to biotic events (modified after Andrew et al., 1994; Underwood et al., 1997; Munnecke et al., 2003; Saltzman et al., 2000).

was observed over the same interval at the other Murzuq record, this likely reflects local or compositional effects. The Murzuq basin record containing the Silurian-Devonian boundary does show a large change in $\delta^{13}C_{org}$ toward more positive values in the upper part. From this boundary, the Klonk event is well-known from carbonate and shale sequences from many low-latitude settings (Munnecke *et al.*, 2003; Cramer & Saltzman, 2007). The observed amplitude of this event observed here (± 3.5 ‰) is more or less in line with records from other areas. Although the event in the Murzuq basin seems too old, this might be due to caving, as this record is based on cuttings. Maximum values compare well with the known age of the Klonk event.

By the end of the Silurian, a series of evolutionary innovations led to the initiation of early land plant-dominated terrestrial ecosystems (Kenrick & Crane, 1997; Edwards & Wellman, 2001). Absolute abundance of terrestrial miospores closely mirrors the $\delta^{13}C_{TOC}$ trend, which is in line with this explanation. The Murzuq record shows a marked difference in palynofloras with abundant and diverse land-derived miospore and cryptospores. Lecuyer and Paris (1997) showed a significant difference, up to 4‰, between the carbon isotopic ratios of land plant-derived woody fragments and marine algae from the Devonian age. Since we lack compound specific data for this section, our record miospores might contribute to the observed 3.5 ‰ positive shift.

The positive $\delta^{13}C$ excursion of the S-D boundary Klonk event was first reported from Europe (Buggisch & Joachimski, 2006) and Australia (Andrew *et al.*, 1994). In addition to these reports from Gondwana, Saltzman (2002) extensively described the highest peak $\delta^{13}C_{carb}$ values near the S-D boundary from three Laurentian carbonate successions (Central Nevada, Oklahoma and West Virginia). Although in Europe and in North America a 5.0‰ excursion was observed in carbonate-based records, the general appearance of the excursion is very similar. A slow increase in isotopic values is followed by a more stable phase, resulting in a more "hump"-like appearance. Malkowski *et al.* (2009) speculated that expanding vegetation in the vast lowland areas played a major role in creating this excursion. Enhanced fixation of isotopically light carbon in newly produced plant material would help in shifting isotopic values on geological time scales. Such a cause is in line with the here-observed synchronous shift in palynofacies and stable carbon isotopes.

The potential causes of the different Silurian positive carbon isotope excursions have been the subject of much debate (Kaljo *et al.*, 1995; Munnecke *et al.*, 2003; Saltzman, 2001; Melchin & Holmden 2006; Loydell, 2007; Stanley, 2010). Several of the excursions documented in this study can be correlated to the global record and likely involve changes in carbon sequestration, partitioning between the terrestrial and marine realms, and efficiency of the carbon pump. In addition, one local carbon isotopic excursion was observed during the Aeronian in the Ghadamis basin. In a review of carbon isotope excursions, Armstrong *et al.*, (2009) proposed that local stratification and phytoplankton blooms might have played a role in the Rhuddanian positive $\delta^{13}C_{TOC}$ excursion in Jordan. This seems likely for the earliest Silurian. However, the Aeronian conditions were much different and more open marine conditions likely prevailed. Alternatively, the event observed here during the Aeronian was in fact global, but was heretofore missed in isotopic records. The large amount of carbon stored (being the main Paleozoic source rock from North Africa and the Middle East) would argue for a global spike. In summary,

almost all positive carbon isotope excursions occur close to important bioevents; three of them are correlated to the global carbon isotopic curve: (Fig. 14).

a. Aeronian (middle LIandovery) occurred during the early phases of the massive black shale deposition, but this is only observed in North Africa and North America (Fig. 14, number 2).
b. Early Sheinwoodian (basal Wenlock-Ireviken Event) occurred during the later phases of a long, massive black shale deposition (Fig. 14, number 3).
c. Late Homerian (basal Ludlow-Mulde Event) carbon isotope positive excursion. Extensive black shale does not occur in association with this event (Fig. 14, number 4).
d. Silurian-Devonian (S-D) boundary (Klonk Event) carbon isotope positive excursion (Fig. 14, number 7).

6. Conclusions

An informal acritarch and chitinozoan biostratigraphy showed that the section containing the "hot" and lean shales from the Ghadamis and Murzuq sediments studied here cover late Ordovician to Devonian times. The "hot" shale contains well-preserved AOM, which is typical for laminated black shales deposited under dysoxic-anoxic depositional conditions. The base of the Tanezzuft Formation represents a transgression, with the oldest sediments being deposited in the palaeodepressions. Two positive carbon isotope excursions have been identified within the "hot" shale interval in Ghadamis basin, which are missing from the Murzuq records. The first excursion is early to late Aeronian and should have been reflected in the Murzuq as well, based on the stratigraphic correlation. The mismatch between the two records suggests strong differences in sedimentary regime. The second excursion has an early Sheinwoodian age, which is not present at Murzuq. Also, in the upper part of the section studied here, an isotopic excursion was observed within the lean shale, the so-called late Homerian double-peaked excursion. The Silurian-Devonian boundary isotopic excursion, known as the "Klonk" event, was observed in the Murzuq record only. Differences between the Ghadamis and Murzuq basins can be explained in different time spans captured by the records and an overall shift of organic matter-rich facies accumulation from the central part of the basin to the margins in response to ongoing sea level change and basin in fill.

Plate description and captions

Plate I. Prasinophytes and Acritarchs taxa from A1-70 and I3-NC186 borehole (Scale bar equals 10 μm. Well name and reference are followed by sample depth and slide number.

Fig.1. *Leiosphaeridia* sp. (Eisenack., *et al*, 1956; Downie and Sarjeant., 1963, 3095 m, 3048 m, 2831 m, slide n.12D, 9D*, 6D, X100.*

Fig.2. *Tasmanites* sp. (Newton., 1875) A1-70, 3095 m, 2879 m,2831 m, slide no. 12A, 7B, 5D, X100)

Fig.3. *Pterospermella foveolata* (Al-Ameri., 1986: Hill *et al*. 1985) A1-70, 3050 m, 3045 m, slide no, 11B, 9A, X100

Fig.4. *Dictyotidium faviformis* (Eisenack, 1955).3095 m, slide 12D, X100

Fig.5. *Dictyotidium dictyotum* (Eisenack, 1955; Le Hérissé., 1989; Massiak et al., 2003). 2759 m, slide no. 2B, X100

Fig.6. *Cymatiosphaera* sp. (O. Wetzel, 1933 emend, by Deflandre 1954, 3095 m, 3045 m, 2831 m, slide. 12D, 9A, 5B, 100X.

Fig.7. *Buedingiisphaeridium cf. Pyramidale* (Lister, 1970) A1-70, 2831 m, slide 6D, X100

Fig.8. *Domasia trispinosa* (Dowbie., 1960; Hill., 1974) (I3-NC186,1222 m,1183 m,1137 m, slide1A,2C,3A, X100)

Fig.9. *Domasia bispinosa* (Le Hérissé., 1989)(A1-70, 3050 m,3048 m, 3045 m, slide 11A,10B,9A,X100)

Fig.10. *Onondagella asymmetrica* (Denuff., 1954; emended by Cramer., 1966) (A1-70, 2976 m,2781 m, slide 8D, 3A,X100)

Fig.11. *Deflandrastrum authierae* (Combaz., 1962; Richardson and loannides., 1973)(2781 m, 2759 m, slide 2A,3A,X100)

Fig.12. *Deflandrastrum leonardi* (Combaz., 1962; Richardson and loannides., 1973) (2781 m, 2796 m, slide 3A, 4A,X100)

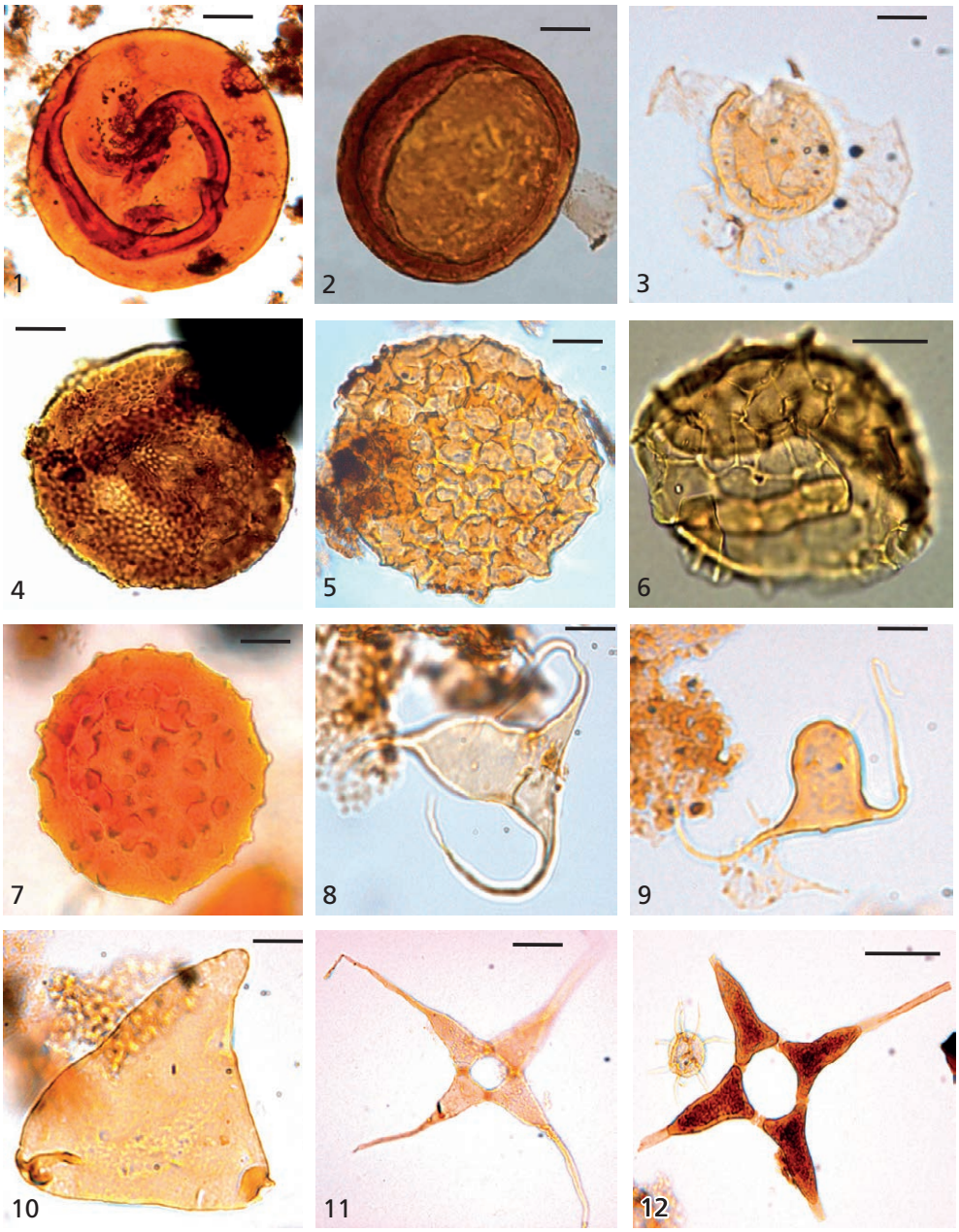

Plate. I (caption on page 54)

Plate II. Acritarchs (Scale bar 10µm)

Fig.1. *Ammonidium microcladum* (Downie., 1963; Le Hérissé., 2000) A1-70, 3050 m, slide no. 11B, X100.

Fig.2. *Ammonidium granuliferum* (Downie., 1963) I3-NC186, 1183 m, 1137 m, slide no. 2A, 1B, X100.

Fig.3. *Glyptosphaera speciosa*. (Kiryanov, 1978) A1-70, 2759 m, 2730 m, slide no, 2B, 1A, X100.

Fig.4. *Oppilatala insolita* (Loeblich and Wicander., 1976) 3050 m, 3045 m, slide no. 11A, 9A, X100.

Fig.5. *Eupoikilofusa* sp. (Cramer. 1970) A1-70, 2832 m, 2781 m, slide no. 6A, 3A, X40.

Fig.6. *Tunisphaeridium tentaculaferum* (Deunf and Evitt 1968) A1-70, 3045 m, 2781 m, 2730 m, slide no. 9A, 3B, 1A, X100.

Fig.7. *Salopidium granuliferum* A1-70, 3095 m, 3050 m, slide no, 12A, 11B, X100.

Fig.8. *Veryhachium trispinosum* (Eisenack, 1938a; Hill et al., 1985) A1-70, 2879 m, slide no.7A, X100.

Fig.9. *Polygonium* sp. A1-70, 2832 m, 2781 m, 2730 m, slide no. 6B, 3A, 1A, X100.

Fig.10. *Leiofusa* sp. (Cramer, 1964) A1-70, 2832 m, 2781 m, slide no. 6B, 3B, X100.

Fig.11. *Geron guerillerus* (Cramer, 1967a; Le Hérissé, 2000) A1-70, 2781 m, 2759 m, slide no. 3A, 2B, X100.

Fig.12. *Visbysphaera pirifera* (Eisenack, 1954; Richardson *et al*., 1973) A1-70, 2781 m, 2730 m, slide no. 3A, 1B, X100.

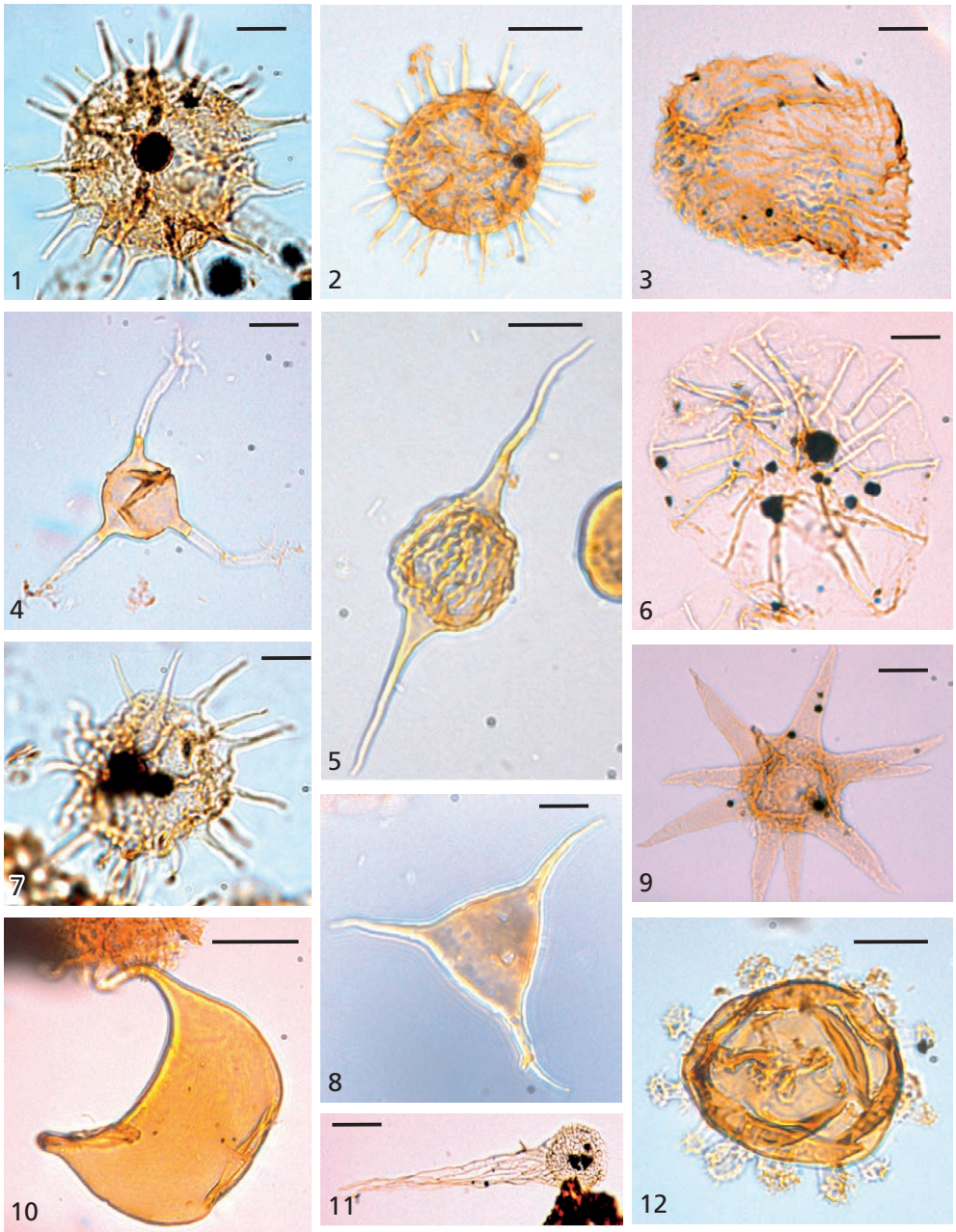

Plate. II (caption on page 56)

Plate III. Chitinozoa, Miospores and cryptospore (scale bar 60 *μm* and 40μm)

Fig.1. *Calpihitina* sp.*A* (Wilson and Hedlund, 1964; Paris., 1981) A1-70, 2781m, 2831 m, slide no. 5A, 3B, X40

Fig.2. *Angochitina* sp. (Eisenack, 1931) A1-70, 2797 m, slide no 4B, X40.

Fig.3. *Ancyrochitina prinmativa* (Eisenack, 1955a) 2759 m, 2730 m, slide no. 2A, 1B, X40

Fig.4. *Ancyrochitina brevis* (Al-Ameri, 1989) A1-70, 2831 m, 2797 m, slide no. 5A, 4A, X40

Fig.5. *Ancyochitina* spp. (Eisenack, 1955a) A1-70, 2781 m, slide no. 3A, X40

Fig.6. *Euconochitina vitrea* (Taugourdeau, 1962; Hill *et al*., 1985; Paris, 1988) A1-70, 2831 m, slide no. 5A, x40.

Fig.7. *Ancyrochitina ancyrea* (Eisenack, 1931; Jaglin and Paris., 2002) A1-70, 2831 m, slide no.5B, X40, I3-NC186, 1417 m, 1353 m, 1183 m, slide no.7A, 5B, 2A, X40.

Fig.8. *Ambitisporites avitus* (Hoffmister 1959; Steemans et al., 2000) A1-70, 2797 m, 2781 m, slide no. 4A, 3B, X100.

Fig.9. *Ambitisporites dilutes* (Hoffmister 1959) A1-70, 2797 m, 2781 m, slide no. 4B, 3B, X100. I3-NC186, 1353 m, 1222 m, 1137 m, Slide no. 5A, 3A, 1B, X100.

Fig.10. *Tetrahedraletes medinensis* (Wellman and Richardson 1993) A1-70, 2797 m, 2781 m, 2730 m, slide no. 4A, 3B, 1A, X100, I3-NC186, 1271 m, 1222 m, 1137t, slide no. 4A, 3A, 1B, X100.

Fig.11. *Rimosotetras problematica* (Burgess, 1991; Steemans *et al.*, 2007) A1-70, 2781 m, 2730 m, slide no. 4A, 3B, 1A, X100

Fig.12. *Tetrahedraletes medinensis* (Wellman and Richardson 1993) I3-NC186, 1271 m, 1222 m, 1137 m, slide no. 4A, 3A, 1A, X100.

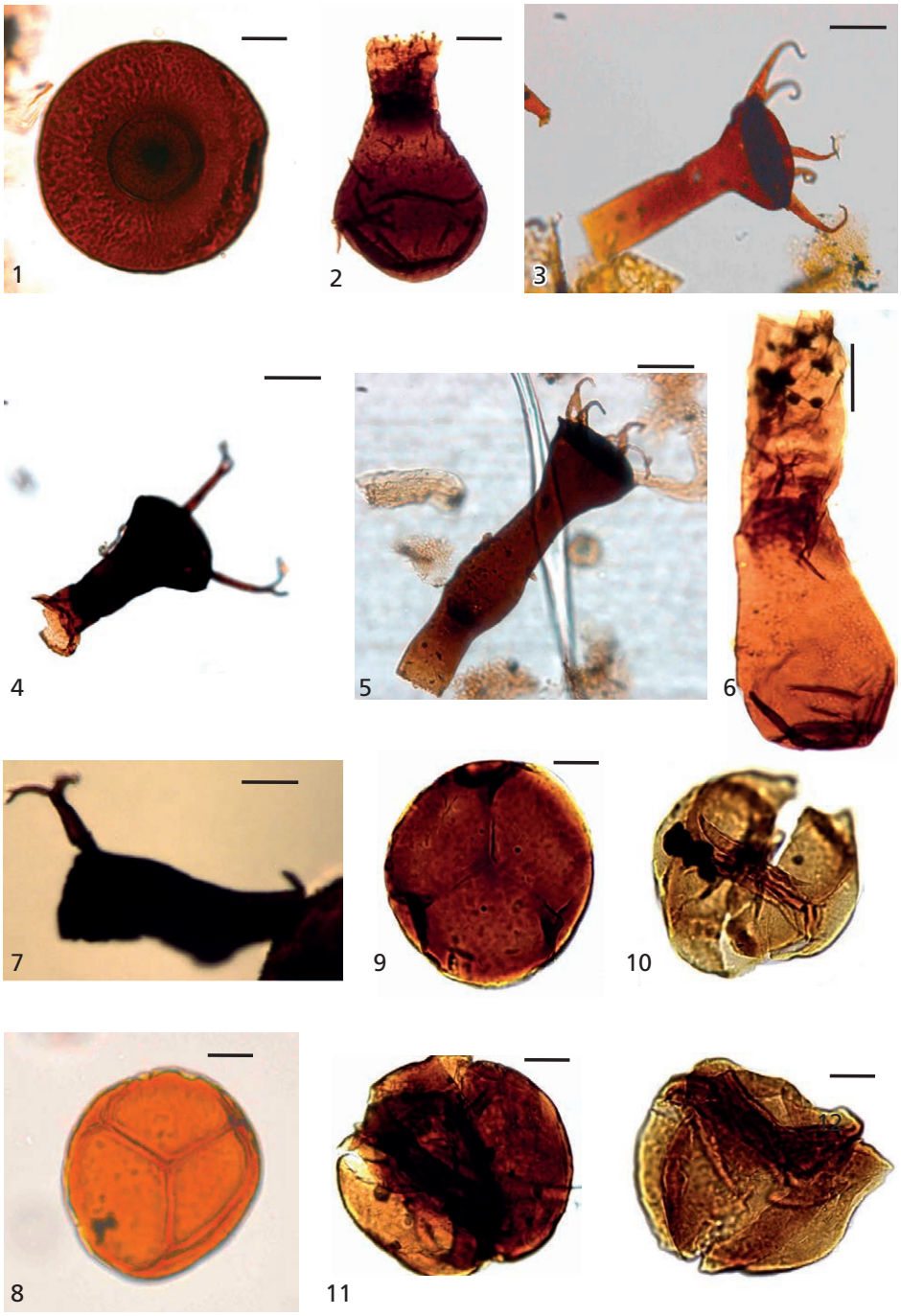

Plate. III. (caption on page 58)

Plate IV. Palynofacies of Silurian sediment (Scale bar μm 10)

Fig.1. *Arthropod cuticle,* possibly Eurypterus (Al-Ameri, 1989) A1-70, 2879 m, 2759 m, slide no. 7A, 2A, and 40X

Fig.2. (a) Sheet of cell of plant cuticle, (b) highly fluorescent cuticle. A1-70, 2759 m, 2730 m, slide no. 2A, 1A. X40.

Fig.3. *Graptolit (zooclasts),* sicula of a graphtolite with metasicula, (Fischer, 1839), A1-70, 3095 m, 3050 m, 3045 m, slide no. 12A, 11B,10A, X40. I3-NC186, 1417 m, 1399 m, 1353 m, 1271 m, slide no. 7A, 6A, 5A, 4B, X40.

Fig.4. *Scolecodonts (zooclasts)* A1-70, 2781 m, 2730 m, slide no. 3A, 1A, X40

Fig.5. Amorphous organic matter (AOM) abundant of well preserved, from the "hot shale" A1-70 borehole, interval 3095 m.

Fig.6. Amorphous (AOM), abundant of well preserved, from the "hot shale" I3-NC186 borehole, interval 1417 m.

Fig.7. (a) Amorphous organic matter (AOM), (b) under fluorescent light excitation, partly well preserved AOM, A1-70 borehole, 3095 m, X10.

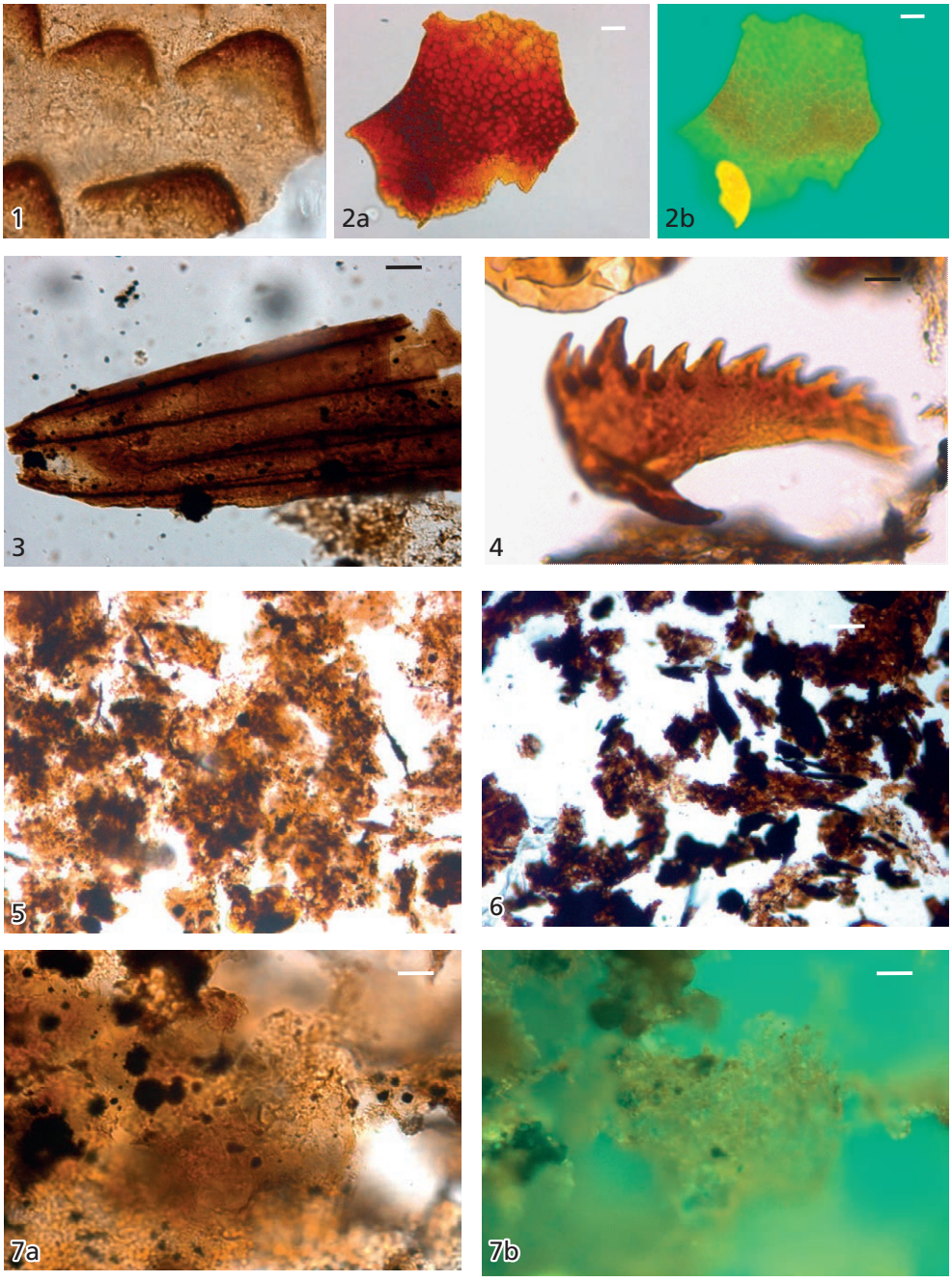

Plate. IV (caption on page 60)

Plate V. Acritarchs taxa from, E1-NC174 borehole (Scale bar 10 μm), and all specimens are X60 magnification except where otherwise stated.

Fig. *1*. *Veryhachium valiente* (Cramer, 1964b), 1844 m, slide no. 1A, B.
Fig. 2 *Beromia rexroadii* (Wood, 1996) 1844 m, 2073 m. slide no. 1A, 11B.
Fig. 3. *Eupoikilofusa cantabrica* (Cramer, 1964), 1935 m. slide no. 5A, B.
Fig. 4. *Eupoikilofusa saetosa* (Le Hérissé, 2000), 2179 m, 1935 m. slide no. 16A, 5B.
Fig. 5. *Geron sp.* (Le Hérissé, 2000), 1951 m, 1966 m. slide no 6A, and 7B.
Fig. 6. *Baiomeniscus camurus*, (Loeblich, 1970), 2073 m.
Fig. 7. *Micrhystridium stellatum*. (Deflandre, 1945), 1844 m.
Fig. 8. *Multiplicisphaeridium rochesterense* (Cramer and Diez 1972b) Eisenack et al., 1973, all the samples.
Fig. 9. *Leiofusa sp. (Eisenack, 1938)2134 m to 1902 m.*
Fig. 10. *Neoveryhachium caminae* (Le Hérissé, 1995), 2195 m to 1844 m.
Fig. 11. *Veryhachium trispinosum*,(Eisenack) Stockmans and Williére, 1962) all the samples.
Fig. 12. *Tylotopalla caelamenictis* (Loeblich, 1970), 2179 m, 2039 m, 2012 m.

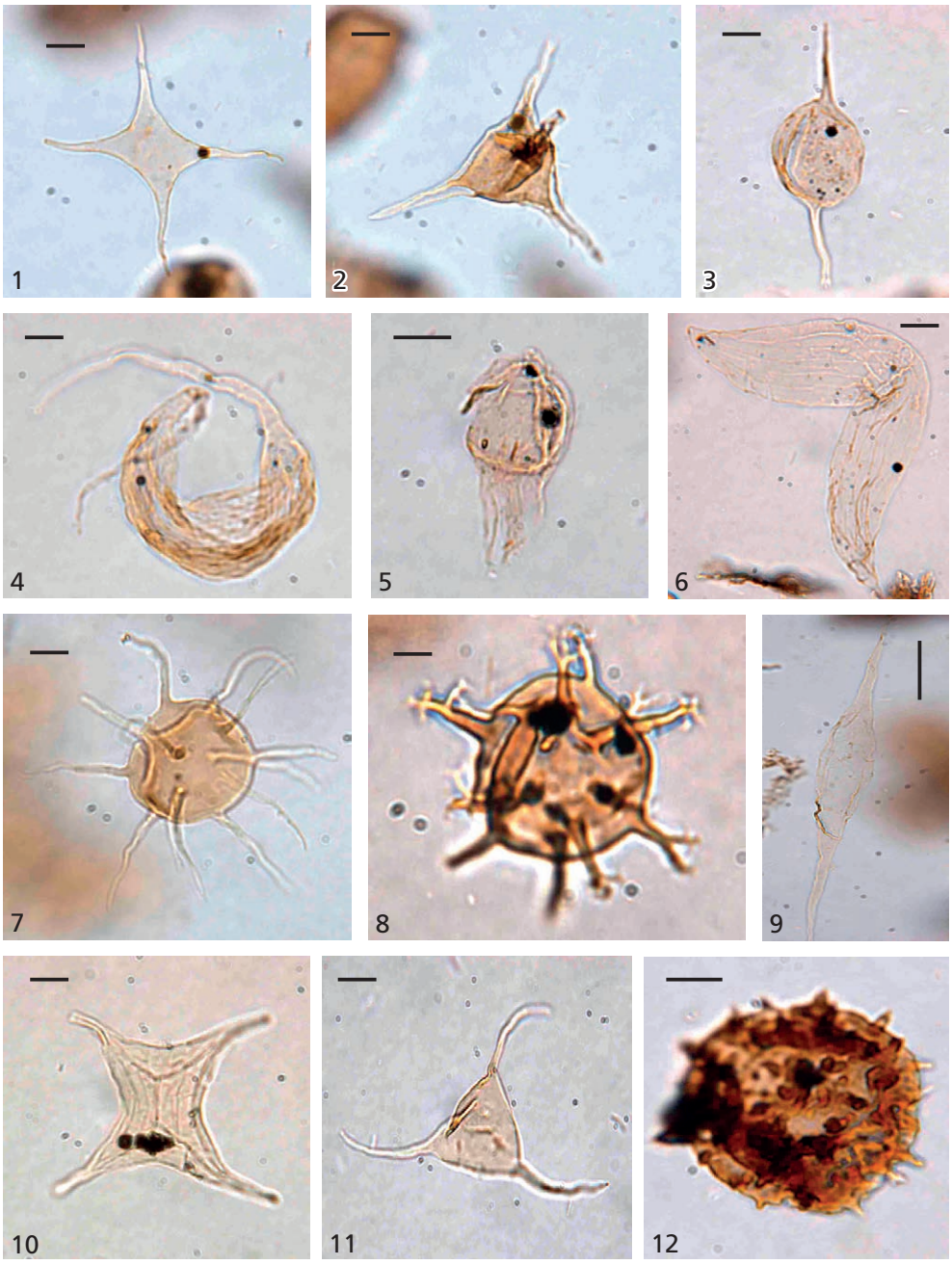

Plate. V. (caption on page 62)

Plate VI. Acritarchs and prasionphytes (Scale bar μm 10)

Fig. 1. *Tunisphaeridium tentaculiferum* (Martin) Deunf and Evitt, 1968. 2073 m, 1935 m, slide no 17B
Fig. 2. *Multiplicisphaeridium* sp. (Eisenack *et al*. 1973).
Fig. 3. *Beromia rexroadii* (Wood, 1996), 2073 m, slide no 2B.
Fig. 4. Diexallophasis *denticulate* (Stockmans and Williere) Loeblich, 1970.
Fig. 5. *Veryhachium sp*. (Eisenack) Stockmans and Williére, 1962). *1417 m.*
Fig. 6. Diexallophasis *sp.* (Stockmans and Williére) Loeblich, 1970, all the samples
Fig. 7. Multiplicisphaeridium fermosum, all samples, slide no. 1A
Fig. 8. Oppilatala sp. 2103 m, 2073 m, 1935 m.
Fig. 9. *Dictyotidium dictyotum (*Eisenack *et al*., 1973) 2221 m, 2195 m.
Fig. 10. *Tasmanites sp.* (Newton, 1875), 2221 m to 1981 m.
Fig. 11. *Leiosphaeridia* sp. *(Johnson, 1985*), 2195 m.
Fig. 12. *Pterospermella* sp. (Cramer, 1964) 2198 m, 2134 m.

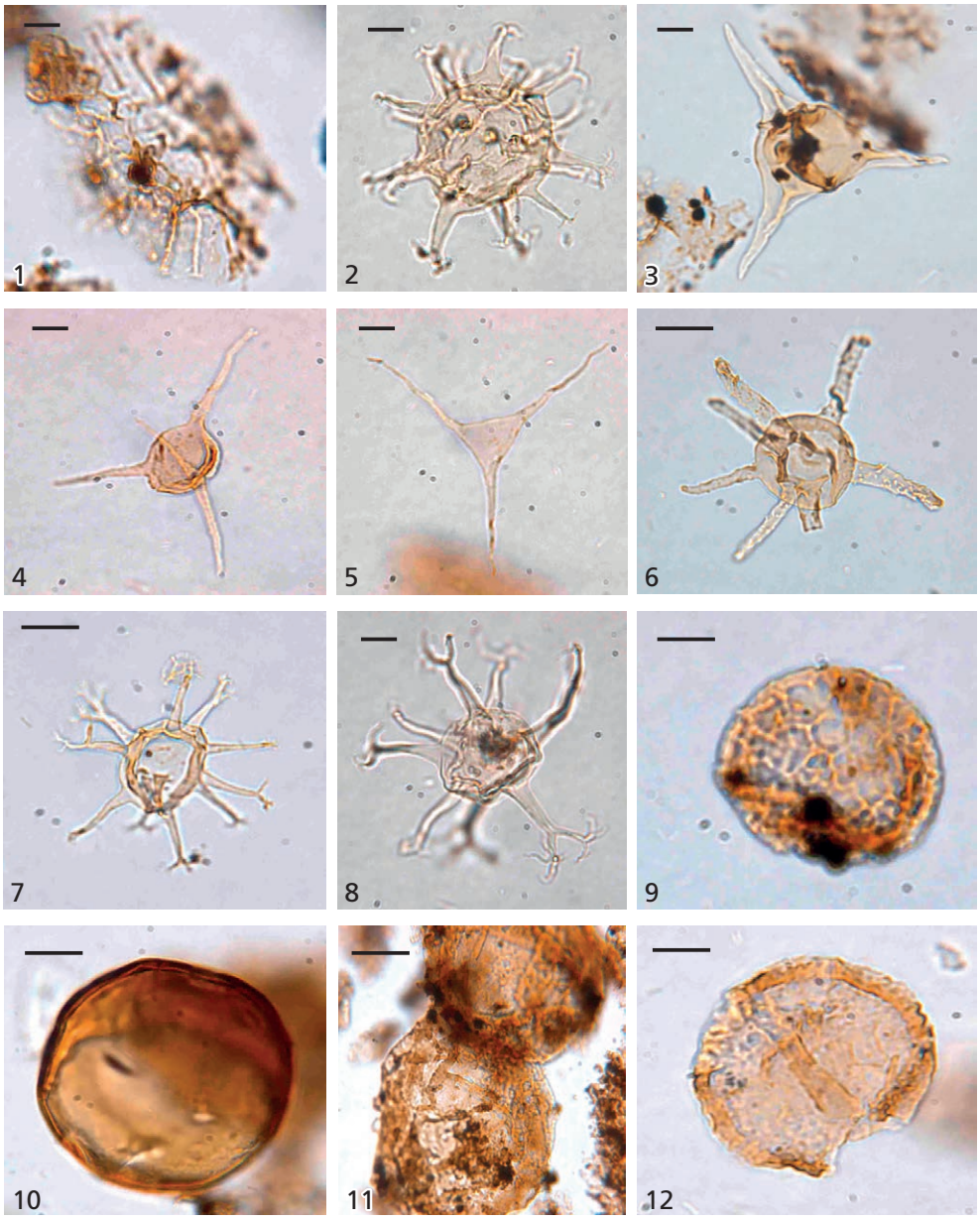

Plate. IV. (caption on page 64)

Plate VII. Chitinozoan, spores and palynofacies of Silurian sediment (Scale bar 40 µm)

Fig. 1. *Ambitisporites avitus,* (Steemans *et al*., 2000) 1951 m
Fig. 2. *Tetrahedraletes medinensis* (Wellman and Richardson 1993) 1981 m.
Fig. 3. *Rimosotetras problematica* (Burgess, 1991; Steemans *et al*., 2007) 1966 m.
Fig. 4. *Euconochitina vitree* (Taugourdeau, 1962; Hill *et al*., 1985; Paris, 1988) 1966 m to 1935 m.
Fig. 5. *Spinachitina fragilis* (Vandenbroucke et al., 2009), 2221 m, 2213 m, 2211 m.
Fig. 6. *Conochitina edjetensis* 1966 m, 1935 m.
Fig. 7. *Ancyochitina laevaensis,* 2221 m to 1935 m.
Fig. 8. *Scolecodonts (zooclasts)* 1902 m, x100
Fig. 9. *Graptolit* (zooclasts), sicula of a graphtolite with metasicula, 2211 m.
Fig. 10 **(a)** *Amorphous organic matter* (AOM), **(b)** under fluorescent light excitation, partly well preserved AOM, 2211 m.

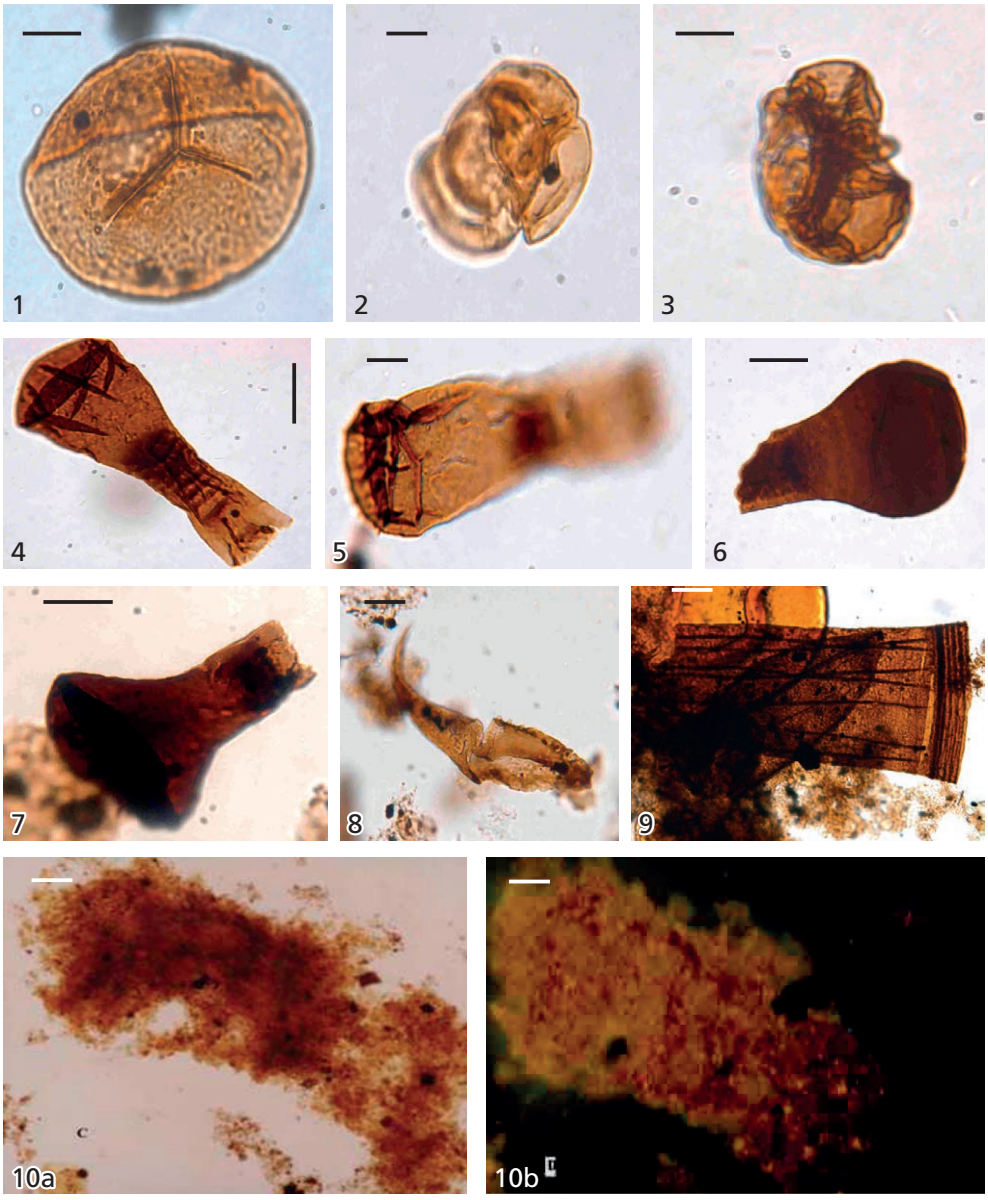

Plate. VII. (caption on page 66)

Plate VIII. Acritarchs and miospores from Silurian-Devonian boundary (Scale bar 40 μm)

Fig. 1. *Stellinium micropolygonate*,(Playford, 1977) 1902 m, slide no.3A,B, X60
Fig. 2. *Stellinium comptum,* (Wicander and Loeblich, 1977), 1902 m, slide no.3A,D
Fig. 3. *Horologinella quadrispina* (Jardiné et al, 1972), 1859 m, slide no. 2B
Fig. 4. *Grandispor protea*. (Moreau-Benoit, 1980) 1902 m, slide no. 3E,D
Fig. 5. *Maranhites mosesii* (Sommer, 1965), Brito, 1967. 1844 m, slide no. 1C
Fig. 6. *Maranhites lobulatus* (Burjack and Oliveira, 1989), 1859 m, slide no.2C,E
Fig. 7. *Indotriradites dolianitii*, (Streel, 1967) 1902 m. slide no. 3C,D
Fig. 8. *Grandispors sp.*(McGregor and Camfield, 1992), 1859 m. slide no. 2B
Fig. 9. *Acinosporites apiculatus* (Playford and Streel, 1999) 1902 m. slide no. 3A,C
Fig.10. *Cordylosporites marciae*, (Playfor and Satterthwait 1985) 1859 m. slide no. 2B
Fig.11. *Grandispora permulta* (Daemon) Loboziak, Streel & Melo, 1999, 1859 m, slide no. 2C
Fig.12. *Samarisporites* sp. (Loboziak and Streel, 1989) 1859 m. Slide no. 2A, C.

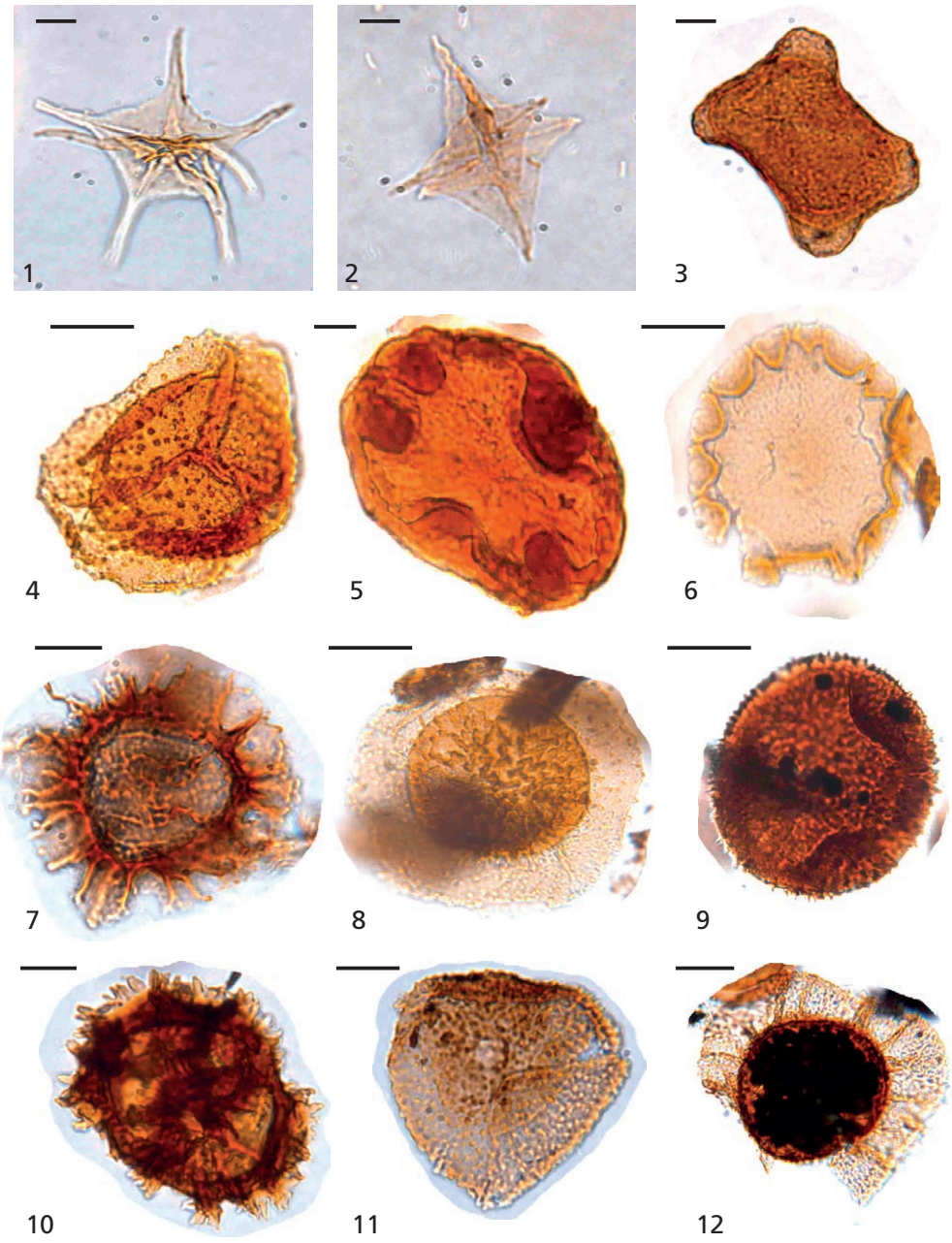

Plate. VIII. (caption on page 68)

3 Carbon isotope chemostratigraphy and palynology of Late Devonian black shales from the eastern Murzuq Basin, Libya

Mohamed M.A. Elkelani[1], Jaap S. Sinninghe Damsté[1,2], Philippe Steemans[3], Gert-Jan Reichart[1,2], Zwier Smeenk[4]

[1] *Utrecht University, Faculty of Geosciences, Department of Earth Sciences, Organic Geochemistry, Budapestlaan 4, 3584 CD Utrecht, The Netherlands.*
[2] *NIOZ Royal Netherlands Institute for Sea Research, P.O. Box 59, 1790 AB, Den Burg, The Netherlands.*
[3] *University of Liège, Paléobiogéologie, Paléopalynologie, Paléobotanique B-18, Sart Tilman, 4000 Liège, Belgium.*
[4] *Utrecht University, Marine Palynology and Paleoceanography, Laboratory of Palaeobotany and Palynology, Faculty of Geosciences, Department of Earth Sciences. Budapestlaan 4, 3584 CD, Utrecht, The Netherlands*

Abstract

In North Africa, several secondary source rocks have been suggested to contribute to known local oil reserves, in addition to the main Silurian age "hot" shale, source rock. It is, however, not clear from what age these potential source rocks would be and whether their contribution would come from appreciable in addition to the well-known major source rocks, which in Libya constitute the Tannezuft formation. One of the formations that was previously suggested to play a potential role in petroleum generation is the Awaynat Wanin formation, which is overlain by the Mrar formation. Therefore, the Awaynat Wanin and Mrar Formations from the eastern part of the Murzuq Basin in Libya were investigated using palynological, carbon isotopic and geochemical approaches. The sediments are from Late Givetian (Middle Devonian), Early Frasnian (Late Devonian) and Early Carboniferous ages. During the Frasnian organic-rich shales were deposited across much of the North African shelf, hence forming a potential secondary hydrocarbon source rock in this region. The high diversity of prasinophytes (e.g *Maranhites*, *Pterospermopsis*), high amount of organic matter and well preserved amorphous organic matter deposited during the early Frasnian strongly support enhanced sea surface productivity and oxygen-depleted bottom water conditions, possibly related to an expanding anoxic zone. Also, biomarker parameters indicate that the organic matter was derived from marine algal inputs and deposited under anoxic (reducing) conditions. Whole-rock carbon isotope analyses through the Awaynat Wanin formation revealed a positive $\delta^{13}C_{TOC}$ excursion, with a small 3‰ positive shift during the deposition of the Early to Middle Frasnian black shales. This excursion appears to be synchronous with a major positive $\delta^{13}C$ excursion previously recognized in northern Gondwana and eastern Laurussia. Increased tectonic activity, increased nutrient flux to the ocean, increased marine bioproductivity, widespread anoxia and related high organic carbon burial and regional relative sea-level rise are all likely factors responsible for the positive $\delta^{13}C_{TOC}$ excursion event. In other areas, this event resulted in the deposition of major amounts of potential source rocks. Although of more limited extent, Rock Eval and maturity data confirm that the early Frasnian black shale at the Late Devonian is potentially an effective source rock containing type II kerogen.

Key words: *Palynology, Carbon isotope, Rock Eval pyrolysis, Biomarker, Devonian, Frasnian black shales.*

1 Introduction

North African black shales form locally important source rocks for both oil and gas. The major source rock in this area, the so-called "hot" shale, was deposited during the Early Silurian (Klitzsh, 1963; Lüning *et al*., 2000; see also Chapter 2). However, other (secondary) source rocks might have contributed to the formation of oil and gas. The marginal setting, with many semi-enclosed basins, probably remained prone to deposition of organic rich sediments for a major part of the geological past. During the Devonian, many of the Early Palaeozoic oceans were closing as Laurasia and Baltica collided into the newly formed continent of Laurussia. The northern African margin was at that

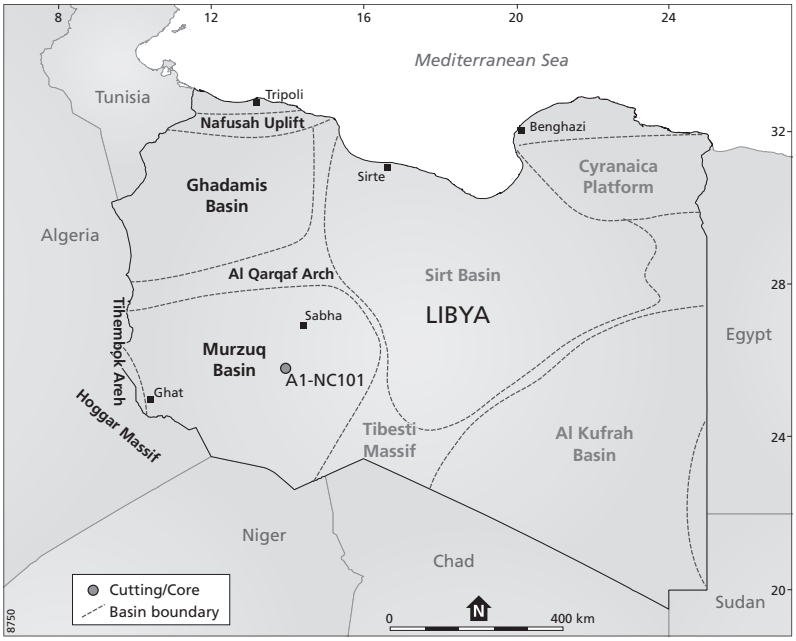

Fig. 1. Map showing the A1-NC101 well and geographic location of the Murzuq Basin.

time bordering the seaway separating Laurussia from the southern supercontinent of Gondwana (Bond *et al*., 2004). The semi-enclosed nature of this seaway indicates that the Devonian was a time characterized by widespread black shale formation.

Particularly during the Frasnian (the early stage of the Late Devonian), black shales were deposited in many parts of North Africa. Thus they potentially form an important hydrocarbon source rock in this region. Time equivalent Frasnian organic-rich deposits in Europe occur, for example, in the Rhenish Massif/Harz Mountains (Germany) and the Montagne Noire (France). The organically richest and thickest Frasnian black shales are, however, deposited in central North Africa (Western Libya and Algeria). These black shales attracted much attention from researchers due to their association with major sea-level change, mass extinctions and their economic importance as a secondary source of hydrocarbons (Luning *et al*., 2004; Wignall, 1991). The most famous of these shales was deposited during the so-called "Kellwasser Event", associated with a distinct transgression at the Frasnian-Famennian (F-F) transition. This event is also characterized by large-scale ocean anoxia and a major mass extinction (Walliser, 1996; Racki *et al*., 2002). Deposits associated with this event have been identified globally in North Africa (Algeria and Morocco), Europe (e.g Germany, Great Britain, Poland, Portugal and Spain) and North America (Johnson *et al*., 1985), although with a different sedimentary lithology. In general, during the Frasnian-Famennian mass extinction, about 15% of families and 50% of genera of marine fauna died out, and reefs almost completely disappeared (Riquier *et al*., 2006). The mass extinction event appears synchronous with the deposition of black shales, which implies that conditions favored organic matter preservation (Joachimski

& Buggisch, 1993; McGhee, 2001). Several studies presenting detailed early and middle Frasnian (early Late Devonian) carbon isotope data from Poland (Racki *et al*., 2004; Pisarzowska *et al*., 2006; Yans *et al*., 2007), Belgium (Yans *et al*.2007), and South China (Ma *et al*., 2008) provide evidence that a major, long-lasting and widespread positive $\delta^{13}C$ isotope excursion occurred during the transition from the early Frasnian to middle Frasnian.

Although regionally potentially important as a secondary hydrocarbon source rock, detailed studies focusing on the Frasnian-Fammenian boundary are missing for the western parts of Libya, and their basin-scale facies distribution is largely unknown (e.g. Loboziak *et al* 1992; Mergl & Massa, 2000). Although many wells have been drilled in the Murzuq Basin studies focusing on the mid to Late Devonian black shale sequence lack age control. The Awaynat Wanin formation is the most likely candidate to be correlated with the "Kellwasser event", but its stratigraphic position remained unclear because of the lack of bio and chemo-stratigraphic data.

Here we present the first stable carbon isotope data for the Middle-Late Devonian black shale sequence from Awaynat Wanin Formation in the Murzuq Basin in western Libya. The $\delta^{13}C_{org}$ record will be discussed in the light of a new biostratigraphic framework and compared with global bio-events. Organic geochemical investigations are used for a better understanding of changes in the depositional environment of this black shale. The source rock potential of this black shale is evaluated using Rock Eval and its molecular composition.

2. Geological setting

The Murzuq Basin is a large intracratonic sag basin situated in the southwestern part of Libya, west of the Tibisti Massif (Fig.1). The basin extends into northern Niger, covering an area of about 330,000 km^2. The basin already formed early during the Paleozoic, acquiring its present shape through a succession of later tectonic activities. The basin is flanked on three sides by anticlines of Paleozoic strata, including the Al Qarqaf Uplift-Atshan Saddle to the north, the Tihemboka Arch in the west and Dor el Gussa-Jebal Mourizdie to the east (Aziz, 2000; Echikh & Sola, 2000).

The basin structure is characterized by normal faulting in an approximately NNW-SSE orientation. This normal faulting is thought to largely follow basement trends and led to the development of a prominent series of troughs and highs, such as the Serdeles trough, Tiririne high and the Ubari trough (Aziz, 2000). The stratigraphic section of the basin is nearly 4000 m thick and is comprised of predominantly marine Paleozoic clastics, with some Mesozoic sediments of mainly continental origin (Belhaj, 1996). The stratigraphic section experienced varying degrees of erosion, mainly during the Caledonian, Hercynian and Alpine orogenies, although magnitude and timing of these events locally remains uncertain (Bellini & Massa, 1980). The Paleozoic section includes several organic-rich shale facies with petroleum source rock potential. These potential source rocks include the early Silurian (Llandoverian to Wenlockian) Tanezzuft Formation (the so-called "hot" shale), the Middle-Upper Devonian Awaynat Wanin, and the Lower Carboniferous Mrar Formations. In contrast to the Tannezzuft formation, the significance of the last two as effective source rocks in the Murzuq Basin has not

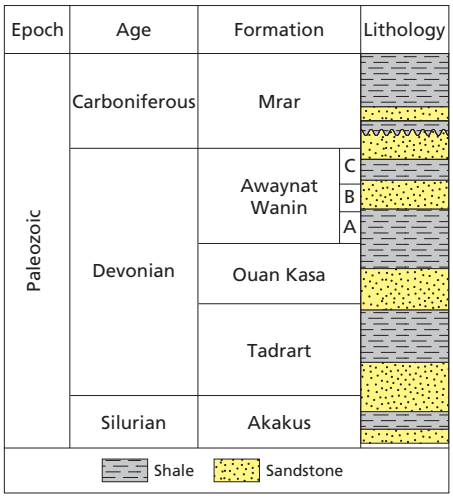

Fig. 2. Generalized stratigraphic column of the Murzuq Basin (modified after NOC, 2002)

been proven. Based on both outcrop and oil exploration wells drilled in the area, the Devonian sedimentary record in Libya has been divided into three formations (Fig. 2): Tadrart Formation, Ouan Kasa Formation, Awaynat Wanin Formation (A, B, and C) (Belhaj, 1996). The name Awaynat Wanin was introduced by Lelubre (1946), based on exposures on the western flanks of the Al Qarqaf Uplift. Such outcrops on the margins of the Murzuq Basin are, however, heavily weathered and oxidized and hence no longer suitable for organic biostratigraphic and organic geochemical studies. For that reason, we here concentrate on records drilled from the sub-surface.

3. Materials and methods

Concession NC101 was awarded to the Bulgarian Oil Company (BOCO) and drilled in 1980 (Fig. 1). The A1-NC101 borehole was positioned on the western flanks of the Traghan High to the south-east of Murzuq Basin (25°48 55 N 13°57 10 E). Repsol Oil Company provided 14 samples from this borehole-10 core samples and 4 cutting samples, together with infill cuttings from intervals between the cored sections. Unfortunately, no well log and gamma ray data are available. Core and cutting samples were retrieved from the interval between 2200 m to 2307.5 m depth, giving a total sampled thickness of 107 m. The samples were selected based on their shale contents, including green, grey and dark black shales (Table 1).

3.1. TOC and stable carbon isotope analysis

Total organic carbon content was determined using an elemental analyzer on decalcified samples. Samples were decalcified using 0.5 g of powdered material, which was allowed to react with 12 ml 1M HCl for 24 h. After decalcification, residues were washed with

demineralized water, centrifuged and decanted three times to remove acid-soluble components. Subsequently Total Organic Carbon (TOC) was determined using an elemental analyzer (Fisons NA 1500 NCS).

Sulfur content was measured on powdered whole rock samples using a LECO C/S SC632 analyzer with high-purity ceramic crucibles that had ultra-low sulfur content, and using standard instrument settings. One whole-rock sample from the most organic -rich rock from the Awaynat Wanin black shale formation from a depth of 2295 m was analyzed at the Royal Netherlands Institute for Sea Research (NIOZ). After complete destruction with an acid mixture of HNO_3, HF and HCl, the residue was taken up in HNO_3, before being measured on a Quadrupole ICP-MS (Thermo iCap) for Fe content.

Stable carbon isotope analysis of TOC was performed on 40-300 µg sub-samples of decalcified crushed rocks using an isotope ratio mass spectrometer (Thermofinnigan Delta Plus) coupled online to an elemental analyzer (Fisons NA 1500 NCS). Graphite Quartzite (GQ) was used as an internal standard and nicotinamide as a control. Results were normalized relative to Vienna Pee Dee Belemnite (VPDB) using international standards.

3.2. Rock-Eval pyrolysis

Pyrolysis analyses were carried out on a Rock Eval 6 pyrolysis instrument (Vinci Technologies SA, France) to evaluate the organic content and kerogen type of the samples. A crucible containing a small amount (100 mg) of crushed whole rock was introduced into a furnace at 300˚C. The free hydrocarbons volatized at this temperature (S1) from the sample were quantified by a flame ionization detector (FID). The furnace temperature was then raised by 35 ˚C/minute to 600 ˚C. Within this temperature range the kerogen in the rock sample "cracks" produced further hydrocarbons (S2) and CO_2 associated with pyrolysis (300-390 ˚C) (S3). Parameters measured include volatile hydrocarbon content (mg HC/g rock, S_1), remaining hydrocarbon generative potential (mg HC/g rock, S_2), carbon dioxide yield (mg CO_2/g rock, S_3) and temperature of maximum pyrolysis yield (T_{max}). Source rock parameters such as Hydrogen Index (HI = S2/TOC*100), Oxygen Index (OI = S3/TOC*100), and Production Index (PI = S1/(S1+S2) were calculated from these measured values. Details on the Rock-Eval method and parameters as well as a summary of interpretive guidelines for Rock-Eval data are available in Espitalié *et al.* (1985).

3.3. Palynological and microscopical analysis

Eleven samples were selected for palynological analysis, with sample intervals varying according to the material available. For each sample ca, 15 g of shale were treated using standard palynological techniques. In short, samples were coarsely crushed with a pestle and mortar to pieces of about 5 mm, and then subjected to a 20% hydrochloric acid (HCl) treatment to dissolve carbonates. The samples were then allowed to stand until any reaction had stopped. After three washes with distilled water the samples were treated with 40% hydrofluoric acid (HF) to remove any silicate material and allowed to stand for at least 24 h, followed again by three washes with distilled water. No oxidation was performed on the organic residue. The size of the palynomorphs ranged from 5 µm

to > 200 µm. A 250 µm mesh sieve was used to remove oversized organic material. Subsequent sieving with a 10 µm mesh allowed the collection of the fraction containing palynomorphs. Because of the large amount of mineral residue still occurring in the samples after sieving, $ZnCl_2$ was applied to separate the lighter organic material from the heavier mineral particles such as pyrite. After that, a small part of the residue was mounted on a slide, embedded with glycerine jelly, covered and sealed with paraffin wax, allowing the palynomorphs to be studied using transmitted light microscopy.

3.4. Extraction and fractionation

A known weight (15-20 g) of powdered rock (core and cuttings; six samples in total), were used to extract lipids in a Soxhlet unit with an azeotropic solvent mixture of 200 ml of DCM/MeOH (9/1: v/v) for 24 h. Extracts were transferred to another round bottom flask to remove the anti-bumping granules and subsequently dried using a rotary evaporator until a few drops of solvent were left. These extracts were then transferred to a pre-weighed small vial and reduced to dryness under a stream of nitrogen. The vial with containing extract was weighed again to allow for quantification. When required elemental sulfur was removed from the extracts using activated copper, again drying the extracts under a stream of nitrogen and recording the weights before and after.

The total extracts were separated into apolar and polar fractions using short column chromatography on activated alumina by eluting with *n*-hexane/DCM (9:1, v/v), and MeOH/DCM (1:1, v/v) as solvents, respectively. The apolar fraction was subsequently separated into a saturated and aromatic fraction using an Ag^+-impregnated silica column, with n-hexane and a *n*-hexane/DCM (9:1) mixture, respectively.

3.5. Gas chromatography and gas chromatography-mass spectrometry (GC-MS)

The aliphatic and aromatic hydrocarbon fractions were analyzed by capillary column gas chromatography. Each fraction was dissolved in hexane to a concentration of about 1mg/ml of sample and 1 µl was injected. The fractions were run on a gas chromatograph (HP6890 series II) equipped with a CP-Sil 5 CB (Agilent) column (length 25 m, diameter 0.32 mm, film thickness 0.12µm), a FID for quantifying organic compounds and a flame photometric detector (FPD) to check for the presence of bound and/or elemental sulfur. Helium was used as a carrier gas, kept at constant pressure (100 kPa). Samples were injected on-column. The oven temperature was programmed from 70 to 130°C at 30 °C/min, from 130 to 320 °C at 4°C/min and kept at 320 °C for 20 min. The data was collected on a Lab Agilent chemstation data acquisition system. Aliphatic and aromatic fractions were analyzed and compounds were identified by GC/MS (Thermo, Trace GC Ultra), set at constant flow, using the same column and temperature programme as used for the GC analyses. Hopane (*m/z* 191) and steranes (*m/z* 217) were identified by comparison of mass spectra with previously published mass spectra. Because of co-elution, the concentration of phenanthrene, dibenzothiophene and methyldibenzothiophenes were determined by CG-MS analyses of the aromatic fractions using the ions mass m/z 178, 184, and 198, respectively.

4. Results

4.1. Biostratigraphy

The Awaynat Wanin Formation is considered to comprise the entire sequence between the top of the middle Devonian Ouan Kasa Formation (e.g. Loboziak *et al*. 1992; Streel *et al*. 1990; Boumendjel *et al*. 1988) and the base of the Carboniferous Mrar Formation (Fig. 2, Klitzsh, 1963). Dark grey to black shale recovered in the A1-NC101 borehole in the Murzuq Basin between 2300 and 2200 m in depth were, initially collected from the section by the national oil company. The assumption was that it represented the Silurian Tanezuft Formation ("hot" shale), which explains the ill-constrained local stratigraphy.

We investigated 11 palynological samples from the core and cutting samples, collected from the grey and dark black shales, because they are usually the most suitable for palynological study. The stratigraphic range of each palynomorphs and miospores taxon encountered in the section, and relative abundance of different palynological groups, are plotted in Fig. 3 and Plates I, II, III, IV, V, VI. Conodonts potentially allow high-resolution biostratigraphic dating of Early Paleozoic sediments. Conodonts, however, are not very frequent in shale-dominated succession, such as in the studied interval of core A1-NC101. Although in outcrops there sometimes still exists enough material to be collected for conodont stratigraphy, identification of the organic-rich intervals in outcrops is complicated, because the organic matter has often been oxidized due to weathering under Saharan arid conditions (Belhaj, 1996; Lüning *et al*., 2004). Since conodont stratigraphy is not possible in the Murzuq basin well, biostratigraphy here is based on miospore and acritrach occurrences.

4.1.1 Miospore assemblages

In most samples, miospores are abundant and well-preserved, which suggests overall a relatively low thermal maturity. Down core occurrences for each miospore taxon encountered, as well as that of other palynological groups, are plotted in Fig. 3. Microscope pictures of typical examples of species are illustrated in Plates I and II. Using the down core occurrences, a time frame is developed based on the published miospore stratigraphy for the Awaynat Wanin formation through the basal Mrar Formation (Streel *et al*., 1988).

The deepest samples between 2307 m and 2304 m contain *Geminospora lemurata, Grandispora protea,* and *Samarisporites eximius*. Based on the sedimentary log, these samples are considered to belong to the lower part of Awaynat Wanin Formation. This implies that the base of this formation is late Givetian to early Frasnian (Playford, 1983; Loboziak & Streel, 1995, 1998; Streel *et al*., 1988, 1990).

The common miospores species recovered from laminated black shales (2297, 2295 and 2290 m) immediately above the lower Awaynat Wanin Formation boundary contain *Ancyrospora pulchra, Auroraspora* sp,. *Geminospora lemurata, Grandispora riegelii, Hystricosporites* sp., *Samarisporites triangulatus,* and *Verrucosisporites premnus,* a species typical of the Early Frasnian (Streel *et al*., 1987; Melo & Loboziak, 2003). In line with the Amazon Basin the earliest representatives of *Samarisporties triangulatus* area also associated with, or immediately succeeded by, spores bearing a tabulate sculpture, such as

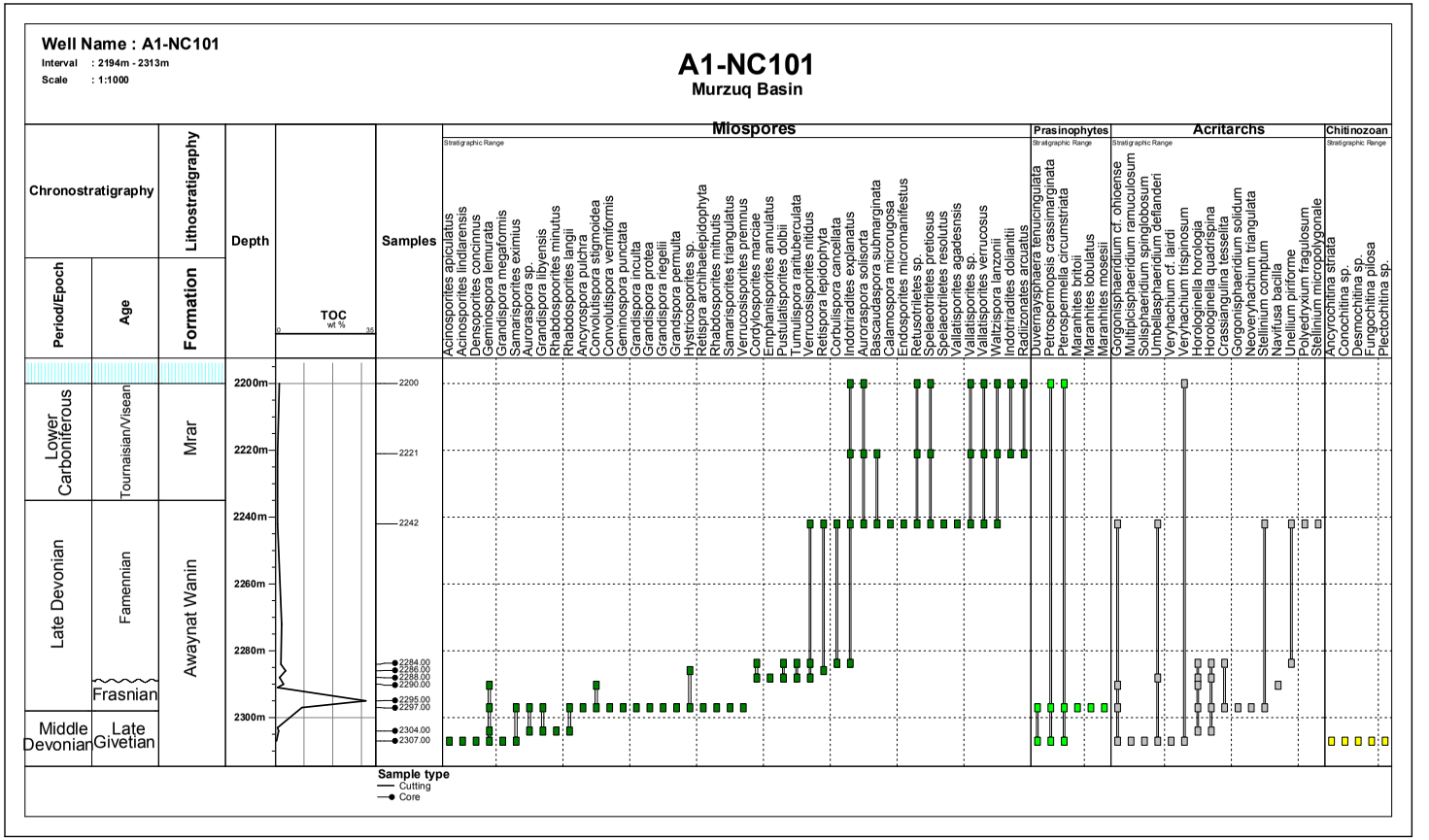

Fig. 3. Stratigraphic occurrence of miospore and palynomorhp range chart recorded samples of A1-NC101 borehole in the Murzuq Basin.

Geminospor, and *Verrucosisporites*. This implies that this section corresponds to Frasnian to late Famennian times.

The next miospore assemblage *Cordylosporites marciae, Indotriradites explanatus, Retispora lepidophyta, Tumulispora rarituberculata* and *Verrucosisporites nitidus,* occurs throughout the upper, less black shale containing, part of the record. This should correspond to the Latest Frasnian to late Famennian (Loboziak & Melo 2000; Melo & Loboziak 2003). In the Amazon Basin latest Famennian miospore assemblages are often characterized by the joint occurrence of *Indotriradites explanatus Retispora lepidophyta* and some *Tumulispora rarituberculata* (Loboziak & Melo, 2000).

Three cutting samples (2242, 2221 and 2200 m) were investigated from this borehole as well (Fig. 3 and Plates I). Caving, however, could induce contamination by rock fragments falling from the borehole walls, as no casing has been used. Still, palynological cutting samples potentially contain *in situ* material from the maximum depth reached by the drilling, mixed with palynomorphs from the open hole. In this case, the Lower Carboniferous assemblage is promptly distinguished from the Latest Devonian ones by an abrupt change in the composition of the palynoflora. This change is evidenced by the appearance of several species such as *Indotriradites explanatus, Spelaeotriletes pretiosus, Vallatisporites verrucosus,* and *Waltzispora lanzonii* of Late-middle to early-late Tournaisian age (Dreesen *et al*., 1993). Visean palynofloras recovered from the investigated samples are generally characterized such as *Indotriradites dolianitii, Radiizonates arcuatus,* which corresponds to an Early Visean age (Loboziak & Streel, 1995; Melo *et al*., 1999). As currently envisaged, our proposed scheme consists of a succession of more than 40 miospore species spanning in age from Middle Devonian to the Lower Carboniferous.

4.1.2. Acritrach and Prasinophyte assemblages

The acritarchs are long-ranging and of little biostratigraphic significance, except that the taxa present here include the marker species *Hologinella horologia, Horologinella quadrispina, Navifusa bacilla, Polyedryxium fragosulum, Stellinium micropolygonate, Stellinium comptum, Unellium piriforme,* and *Umbellasphaeridium deflandrei.*

All samples are characterized by high abundance, and moderately diverse acritarch assemblages. (Fig. 3 and Plates III, IV, V). Highest abundances of prasinophytes (mostly *Pterospermopsis, Maranhites, and Leiosphaeridia*) occur between 2297 and 2295 m depth. Maranhites species (particularly *Maranhites mosesii*, *Maranhites lobulatus and Maranhites britoi*) are common in the Frasnian, together with other characteristic taxa such as *Duvernaysphaera* sp., and *Umbellasphaeridium deflandrei* (Oliveira, 1997). These species were previously recorded in the early Frasnian of northwestern Argentina (Ottone, 1996) and Brazil (Quadros, 1988, 1999). Other important species that have been recorded in Frasnian assemblages also appear within this interval, including *Umbellasphaeridium deflandrei,* which has Frasnian occurrences in Algeria, Ghana, Brazil and Bolivia (Pérez Leyton, 1991).

4.1.3. Chitinozoan assemblages

Chitinozoan assemblages were only observed in the deepest sample, at 2307 m, in the lower part of the Awaynat Wanin Formation. The association at this depth contains

Fungochitina pilosa, Desmochitina sp., *Plectochitina* sp., *Ancyrochitina* sp., *and Conochitina* sp (Fig. 3 and Plate VI), which have been reported from the Middle Devonian of northeast Libya (Streel *et al*., 1988; Hutter., 1979). Hence this is in line with both Miospore and Acritarch stratigraphy.

4.2. Total organic Carbon and Sulfur content

The TOC values range between 0.4 and 38.4% (Fig. 4A, and Table 1). Low TOC values (0.43 and 1.16%) are observed in the Givetian rocks of the lower Awaynat Wanin Formation (Middle Devonian), between 2307 m and 2303 m. An increase is noted corresponding to the lowermost Frasnian of the upper Awaynat Wanin Formation (Upper Devonian), which is characterized by high TOC values (from 9.3 up to 38.4%). Maximum TOC values identify the dark black shale interval (between 2297 and 2295 m in depth). A return to relatively low TOC values is observed during the Upper Famennian (upper Awaynat Wanin Formation) and Lower Carboniferous (Mrar Formation), with green to grey shales (average TOC of about 1.5%), except at 2286 m, where a TOC value up to 3.6% is recorded.

The TOC values are clearly correlated to the S% content. Total sulfur values range between 0.27 to 16.4 wt% (Fig. 4B and Table 1). The maximum sulfur content (16.4%) was observed during the Frasnian black shale (2295 m depth). Combining the data from the ICP-MS analyses for Fe (5.2 %) with the S data from the elemental analyzer (16.4 %), shows that the molar Fe/S ratio is over 5.

4.3. Rock- Eval pyrolysis data

The source rock properties of the Awaynat Wanin shales were investigated using Rock Eval pyrolysis, characterizing organic richness, hydrocarbon potential of the organic matter, kerogen type and thermal maturity (Fig. 5 and Table 1). The samples analyzed between 2286 and 2295 m have S_2 yields in the range of 7.7-181 mg HC/g rock. Frasnian black shale samples have high HI values between 236-472 mg HC/g TOC and low OI values, ranging from 3-31 mg CO_2/g TOC (Fig. 5, Table 1). T_{max} values are fairly uniform throughout the record, ranging from 438 to 442 °C.

4.4. Carbon isotopes

During the lower part of the record, i.e., the Givetian section, $\delta^{13}C_{org}$ values range between -27.0‰ to -26.0‰, which implies a+1‰ positive shift toward the Frasnian. During the Early Frasnian, the carbon isotope record (Fig. 4C Tabe 1) shows an appreciable increase in $\delta^{13}C_{org}$, with maximum values at 2295 m. The values around -24‰ imply a +3‰ positive shift from the base of the record. $\delta^{13}C_{org}$ values return to values of about -25.5‰ during the Late Frasnian, staying constant between 2286 and 2200 m throughout the rest of the record, from Famennian to Tournaisian (Lower Carboniferous).

Table 1. Sample description, total organic carbon, and Rock Eval pyrolysis parameters.

Well name	depth	Sample type	TOC	S%	δ13CTOC	Rock-Eval pyrolysis						
	m		wt %		(‰VPDB)	S1	S2	S3	Tmax	HI	OI	PI
						mgHC/g rock	mgHC/g rock	mgCO2/g rock	˚C	mgHC/g TOC	mgC02/g TOC	–
A1-NC101	**2200**	**Cutting**	1.0	0.8	-25.64	0.10	1.43	0.23	441	142	23	0.06
	2221	**Cutting**	1.0	1.5	-25.66	0.04	0.62	0.08	435	63	8	0.06
	2242	**Cutting**	0.7	0.5	-25.68	0.05	0.37	1.45	438	56	220	0.13
	2272	**Core**	1.2	0.7	-25.90	0.07	0.93	1.85	440	78	154	0.07
	2284	**Core**	1.9	1.4	-25.71							
	2286	**Core**	2.4	2.8	-25.72	0.40	7.73	0.06	439	328	3	0.05
	2288	**Core**	1.4	1.0	-25.80							
	2290	**Core**	3.5	0.1	-25.08	0.92	11.14	0.13	430	316	4	0.08
	2291	**Core**	0.8	0.1	-25.54	0.20	1.98	0	438	236	0	0.09
	2295	**Core**	38.4	16.4	-24.16	17.16	181.38	1.69	442	472	4	0.09
	2297	**Core**	9.3	0.3	-25.97	0.06	0.75	0.11	440	208	31	0.07
	2303	**Core**	0.7	0.3	-25.93							
	2304	**Core**	1.2	1.2	-26.05	0.74	3.98	0.03	442	343	3	0.16
	2307	**Core**	0.4	3.4	-27.03							

TOC= Total Organc Carbon**, S% =** Sulfur content, **Carbon isotope (whole rock), S1**= Free hydrocarbon, **S2** = remaining hydrocarbon generative potential yield, **S3**= carbon dioxide **HI**= Hydrogen index = S2/TOC*100 , **OI**= Oxygen index S3/TOC*100, **Tmax** = Temperature of maximum pyrolysis yield, **PI**= Production index S1/(S1+S2),

Table 2. Aliphatic gas chromatography. ,aturity evaluation and palaeoenviroment data. parameters.

Well name	Depth	Sample type		Gas chromatography data				Maturity and paleoenviroment data			
	m		EOM	Pr/Ph	Pr/*n*-C_{17}	Ph/*n*-C_{18}	CPI	Ts/Ts+Tm	Homohopane index	C_{28}/C_{29}	DBT/P
			mg/g rock					m/z 191	m/z 191	m/z 217	(m/z 184, 178)
A1-NC101	**2200**	**Cutting**	37.3	0.76	0.33	0.50	0.90	0.27	0.10	0.43	
	2242	**Cutting**	31.2	1.00	0.31	0.41	1.01	0.26	0.09	0.41	
	2272	**Core**	46.8	3.94	0.32	0.48	0.87	0.27	0.09	0.43	
	2286	**Core**	37.2	3.46	0.13	0.08	1.02	0.52	0.12	0.48	
	2290	**Core**	54.9	1.31	0.43	0.14	1.12	0.60	0.13	0.70	
	2295	**Core**	129.6	1.61	0.47	0.11	1.15	0.59	0.13	0.79	0.03
	2304	**Core**	43.7	1.02	0.35	0.15	1.12	0.56	0.14	0.57	

EOM= Extractable organic matter, **Pr/Ph ratio** = Pristane/Phytane, **Ts/Ts+Tm** (*m/z* 191), (Ts) = C27 18α(H)-trisnorneohopane, (Tm)= C27 17α(H)-trisnorhopane, (Homohopane index (m/z 191) C35αβ (S+R)/(C31αβ+C32αβ+C33αβ+C34αβ+C35αβ(S+R), C28/C29 (m/z 217) C28αα/C29αα, DBT/P (m/z 184/m/z178), Dibenzothiophenes/Phenanthrene, Carbon preference index (CPI) = $CPI = \frac{1}{2}\left[\frac{C_{25}+C_{27}+C_{29}+C_{31}+C_{33}}{C_{24}+C_{26}+C_{28}+C_{30}+C_{32}} + \frac{C_{25}+C_{27}+C_{29}+C_{31}+C_{33}}{C_{26}+C_{28}+C_{30}+C_{32}+C_{34}}\right]$

4.5. Composition of hydrocarbon biomarkers

A representative gas chromatogram of the saturated hydrocarbon fraction showing the *n*-alkane (*n*-C_{15}+) and acyclic isoprenoid alkane distribution within typical Devonian and Carboniferous samples are displayed in Fig. 6, and values for geochemical parameters based on *n*-alkane and acyclic isoprenoid alkane distribution are given in Table 2. In the upper part of the record, the *n*-alkane distribution shows a high abundance of the short-chain (*n*-C_{15}-*n*-C_{20}) compound. The values of the carbon preference index values (CPI) for the C_{25} to C_{34} *n*-alkanes vary between 1.12 and 1.15 (Table 2). However, in the upper part of the section they are lower, ranging between 0.87 and 1.02.

Acyclic isoprenoids occur in high relative abundances, with pristane/phytane (Pr/Ph) ratios varying between 0.76 and 3.9. At all depths, the *n*-C_{17} is more abundant than pristane and *n*-C_{18} is more abundant than phytane. Distinct changes in the ratio of pristane to *n*-C_{17} and phytane to *n*-C_{18} are observed in the record (Table 2).

The distributions of triterpanes and steranes were studied using GC-MS by monitoring the ions *m/z* 191 and *m/z* 217 (Fig. 7). The tricyclic terpanes were either low or absent. All intervals studied show abundant pentacyclic triterpanes, as evidenced by the m/z 191 mass chromatograms (Fig. 7). The relative abundance of the C_{29} to C_{30} hopane is generally similar throughout the record. C_{27} 17α (H)-trisnorhopane (Tm) is dominant over C_{27} 18α (H) -22,29,30-trisnorneohopane (Ts) at 2200, 2272, 2286 and 2295 m, with Ts/Ts+Tm ratios ranging from 0.3 to 0.6 (Fig. 4D and Table 2). The samples from 2290 and 2304 m depths show Ts being higher than Tm. The homohopane distributions (Seifert and Moldowan, 1978) are dominated by the C_{31} homohopane and show decreasing abundances with increasing carbon numbers. The αβ-hopanes are more prominent than the βα-hopanes, while the 22S-isomers are more dominant than the 22R-isomers among the homohopanes (C_{31}-C_{35}). The observed range of homohopane index values is between 0.09 and 0.14, with the highest values corresponding to the Frasnian black shale (Figs. 4E and Table 2).

The distributions of the regular steranes (C_{27}, C_{28}, and C_{29}) are revealed by the *m/z* 217 mass chromatograms shown in Fig. 7. The distributions of C_{27}: C_{28}: C_{29} regular steranes for the analysed intervals are similar (C_{27} > C_{29} > C_{28}), and diasteranes are absent. The distributions of C_{27}, C_{28}, and C_{29} ααα (20R) and βαα (20R) steranes are similar throughout. The C_{28}/C_{29}-sterane ratio (Schwark & Empt, 2006) was calculated (Table 2) and plotted in Fig. 4F. This ratio shows values between 0.43 and 0.79, with an average of 0.56. No isomerized steranes (e.g. αββ20S) were identified.

Results of the analyses of the aromatic fraction from the Frasnian black shale (2295 m) are presented in Fig. 8A and Table 2. The relative abundances of phenanthrene (P), and dibenzothiophene (DBT), were determined using the trace of the summed mass fragments m/z 178, 184, and 198 (Hughes *et al.*, 1995), (Fig. 8B). The dibenzothiophene/phenanthrene (DBT/P) ratio is low (0.027).

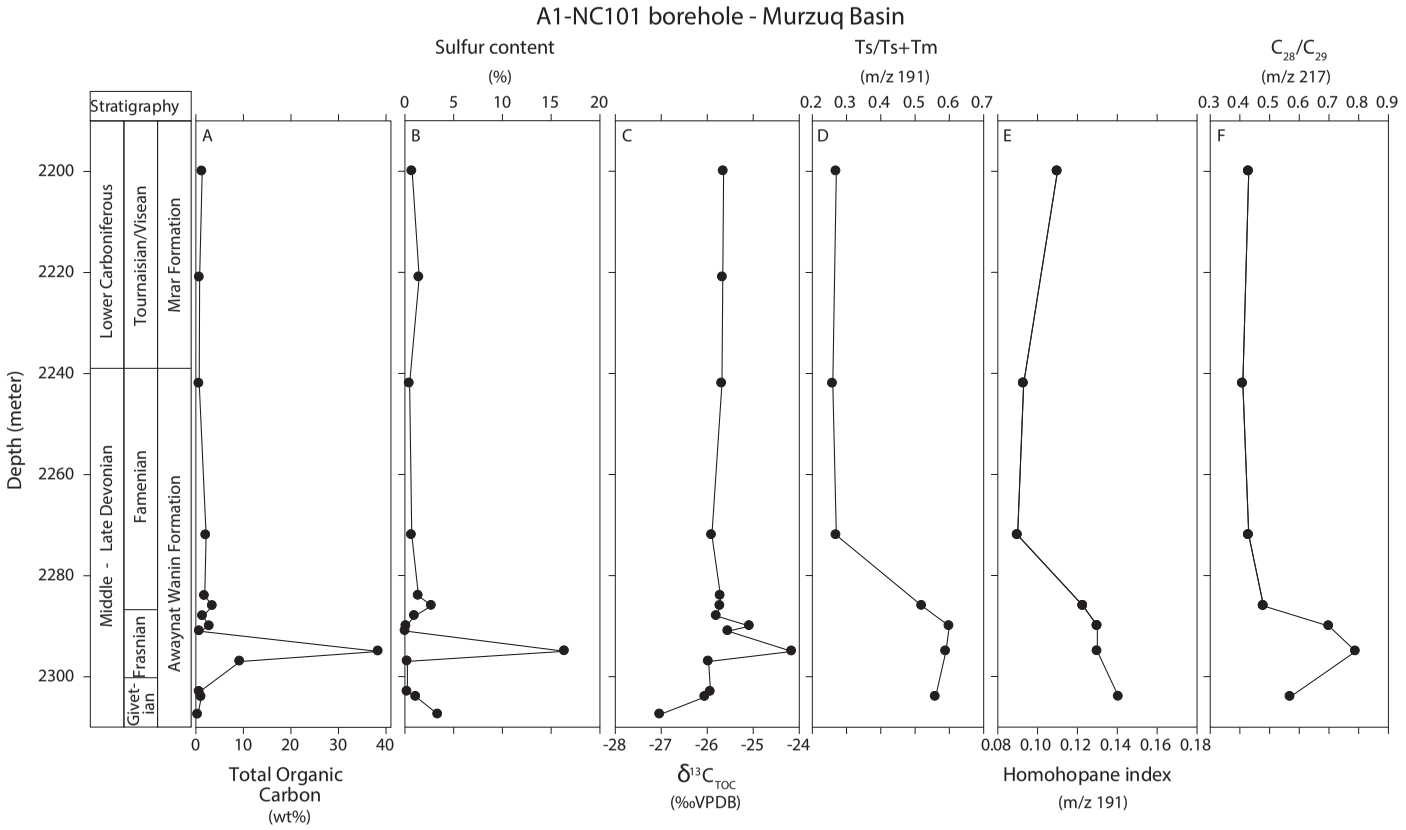

Figure 4. Stratigraphic patterns of biomarker proxies indicative of maturity and depositional environment. (A) total organic carbon (TOC), (B) sulfur content, (C) Ts/Ts+Tm (m/z 19, hopanes), (D) Homohopane index $C_{35}/(C_{31}+C_{35})$ (S+R) (m/z 19, hopanes), (E) C_{28}/C_{29} ααα20R (m/z 217, steranes), (F) Carbon isotope $\delta^{13}C_{TOC}$ from the whole rock

5. Discussion

5.1. Biostratigraphy and age model

The restricted stratigraphic distributions of most species encountered are in close agreement with what is known from other areas globally. The miospore taxa are taxonomically well established and allow for detailed age determination, which we used for establishing the age model. Although the acritarch taxa have much longer ranges, their occurrences are overall in good agreement with the miospore based age model (Fig. 3).

The stratigraphic interval from the Middle Devonian (Late Givetian) from the Murzuq basin yielded a relatively diverse and abundant chitinozoan-acritarch assemblage. Jardine and Yapaudjian (1968) showed similar species for the Middle Devonian (Late Givetian) acritarchs in the Algerian rock record. During the Middle Devonian the most age diagnostic species include *Geminospora lemurata* and *Grandispora libyensis*, a widespread Middle Devonian miospore species (Loboziak & Streel, 1995), which was first described. These form the Libyan Ghadamis Basin.

The Late Devonian assemblage is characterized by the occurrence of miospore species *Geminospora lemurata* and *Grandispora riegelii*, which all indicate an age not younger than Frasnian. Around the black shale interval *Gorgonisphaeridium* sp. is very abundant. The assemblage is dominated by the Praesinophyte species *Maranhites*, which is typical for the late Devonian assemblages in Bolivia, Brazil and Argentina (e.g., Ottone, 1996; Collbath, 1990; Limachi *et al.,* 1996; Le Hérissé & Deunff, 1988). Terrestrial components, such as plant miospores and tracheids, have a similar level or relative abundance throughout the investigated section, albeit being somewhat less abundant from 2297 to 2295 m.

The earliest Carboniferous assemblage is promptly distinguished from the latest Devonian ones by an abrupt change in the composition of the palynoflora. This change is evidenced by the appearance of species such as *Spelaeotriletes pretiosus, Vallatisporites verrucosus,* and *Waltzispora lanzonii,* which occur in the late Famennian to early late Tournaisian age (Dreesen *et al*., 1993). *Indotriradites dolianitii* and *Radiizonates arcuatus,* occur in the Early Visean age (Loboziak and Streel, 1995; Melo *et al*., 1999). The palynoflora also contains various holdovers of the latest Devonian-Tournaisian at the 2242 m interval. According to miospore data for the studied A1-NC101 borehole interval between samples at 2307 m to 2200 m, the timeframe is late Givetian to Lower Carboniferous.

The ratio of C_{28}/C_{29} sterane is considered a reliable age-related parameter for marine settings as it increases from Precambrian to Tertiary due to the relative increases of C_{28} sterane and decrease of C_{29} content through geologic time (Moldowan *et al*., 1985). Therefore, it was possible for Grantham and Wakefield (1988) to distinguish Upper Cretaceous and Tertiary oils from Palaeozoic ones. In our rocks, the majority of the samples have a ratio < 0.7, which might be an indication for a source rock that is probably Palaeozoic in age. The sharp increase of the C_{28}/C_{29} sterane ratio (Fig. 4F) from 0.5 to 0.7 in the Devonian black shale implies a fundamental change in the green algae (e.g. *Pterospermopsis, Maranhites* and *Duvernaysphaera)* assemblage over time (Wignall, 1991; Schwark and Empt, 2006).

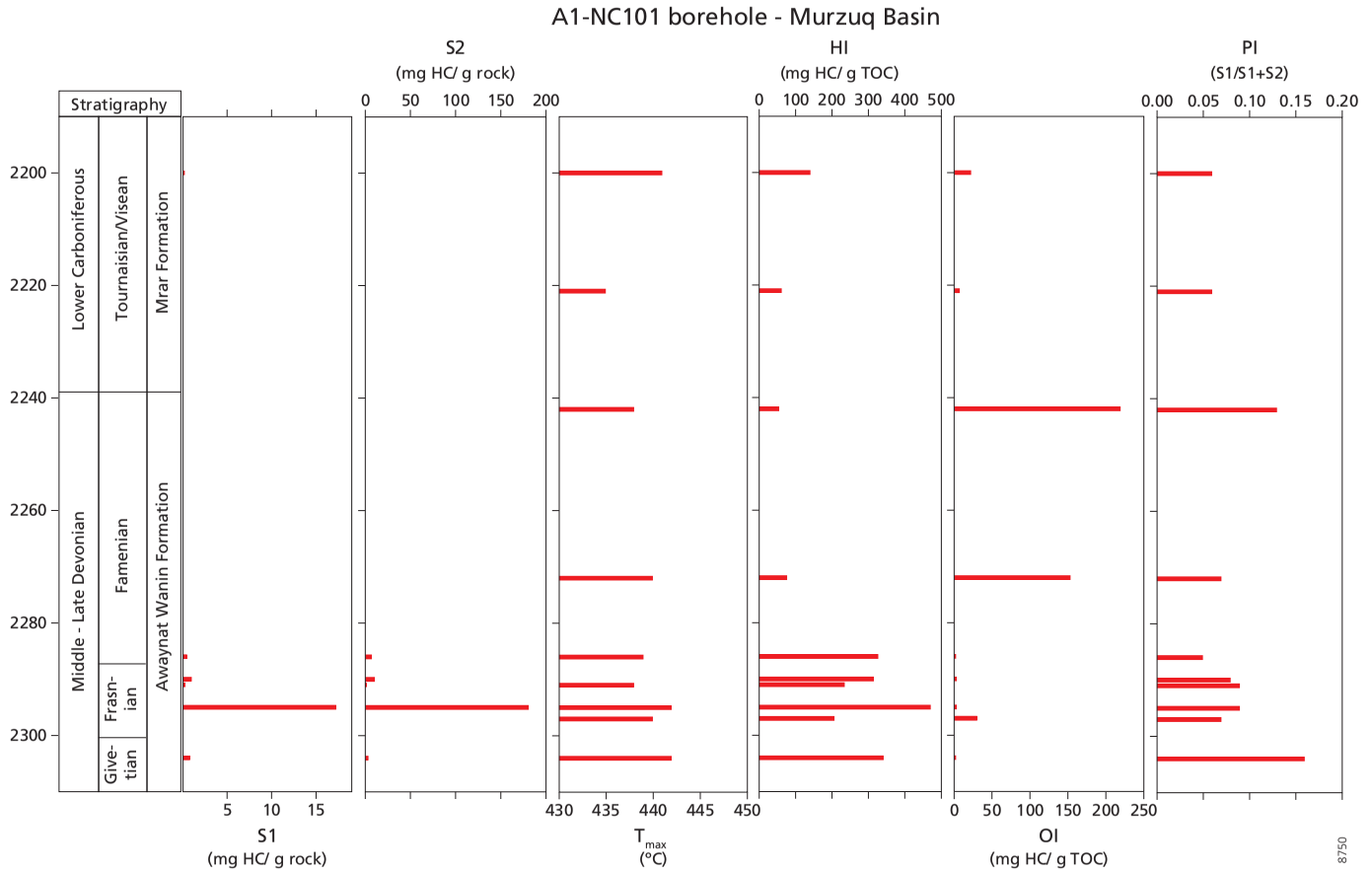

Fig. 5. Geochemical log from Rock Eval pyrolysis data of A1-NC101 borehole of Murzuq Basin

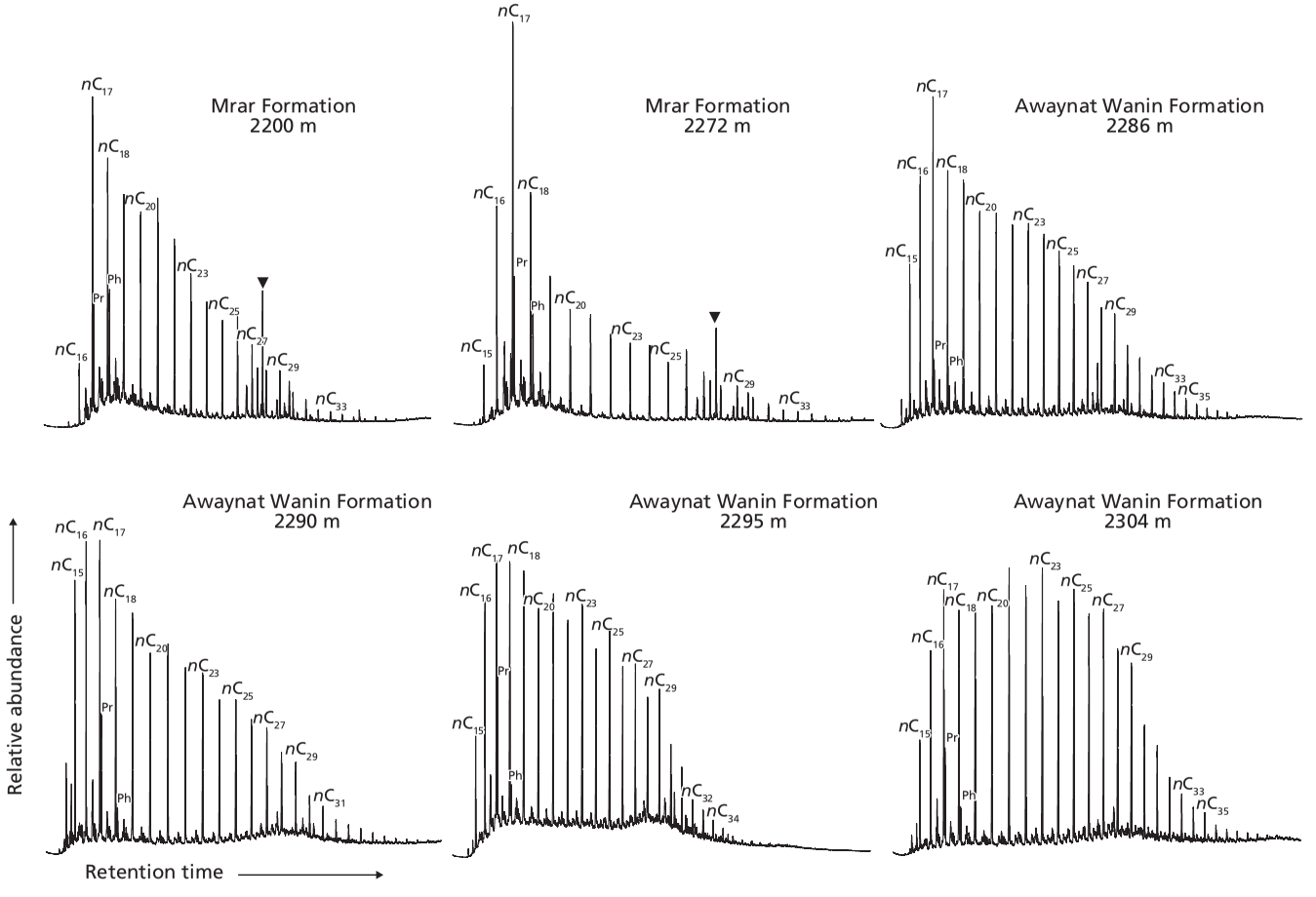

Fig. 6. Gas chromatograms (FID) from six selected aliphatic hydrocarbon fraction from A1-NC101 borehole of the Murzuq Basin. (C_{15}-C_{35} indicates *n*-alkanes, Pr= pristane, Ph=phytane, and (Triangle symbol= $C_{27}\alpha\alpha\alpha$20R sterane).

5.2. Stable carbon isotopic excursion

Our biostratigraphic results indicate that the observed excursion (Fig. 4C) to high $\delta^{13}C_{org}$ values in the Frasnian black shale in Awayant Wanin formation is time-equivalent to the globally observed isotope excursion during the early Frasnian. This excursion shows a maximum amplitude of around +7‰, representing the most prominent $\delta^{13}C$ excursion during the Devonian (Yans *et al.*, 2007). The isotopic excursion recorded in the Murzuq Basin has a smaller amplitude, but was measured on bulk organic carbon. Although compositional differences might have an influence on this $\delta^{13}C_{org}$ record (e.g. Sinninghe Damste & Köster, 1998), the relatively smaller amplitude of the excursion in Murzuq suggests that the complete event has not been captured. This might be due to the limited sample resolution in a relatively condensed sequence.

On a global scale, increased eutrophication and consequent enhanced organic carbon burial during the Early- Middle Frasnian transition has been invoked to explain the major positive carbon excursion (Racki *et al.*, 2004; Pisarzowska *et al.*, 2006). Global scale enhanced deposition of isotopically depleted organic carbon and resulted in an overall shift toward heavy values of the global exogenic carbon pool during the Frasnian. This is confirmed by the ubiquitous presence of Kellwasser black shales globally (e.g. Hangenberg black shale, Morocco, and Changshun Shale of South China), which provides evidence for a worldwide period of intensified accumulation of organic matter (Kump & Arthur, 1999). Also in the Murzuq, recorded elevated levels of OM burial (as judged from the elevated contents of TOC reaching almost 40%) coincide with the carbon isotopic excursion during the earliest Frasnian.

5.3. Conditions responsible for black shale deposition

The Frasnian black shale in the Murzuq Basin is characterized by unusually high TOC content, up to 38 wt % (Fig. 4A). This black shale is, however, relatively thin (~ 2 m). Both below, with organic carbon values during the late Givetian ranging from 0.16 to 0.36%, and above, with TOC values between 0.66 to 1.21% in the Lower Carboniferous, the TOC content is much lower than within the black shale. The black shale also has a high petroleum potential, with an S_2 >5 mg HC/g rock. The early Frasnian black shale interval also shows an interval of generally high HI and low OI values (Table 2). These high HI values, in combination with the high TOC content, suggest anoxic bottom water conditions and enhanced surface water productivity (Combaz, 1966; Revill *et al.*, 1994).

The sulfur content of the black shale is also relatively high, with atomic S/Fe ratios over 5, which implies that, at most, only a limited part of S is present in the form of pyrite. Microscopic observation revealed that some pyrites are present in the shales. Pyrite forms during early diagenesis when H_2S formed due to bacterial sulphate reduction, and reacts with iron(hydr)oxides to form iron monosulfides and ultimately pyrite (Berner, 1970). However, to stoichimetrically transform all formed H_2S to pyrite, enough iron(hydr)oxides are needed. When the water column is already oxygen depleted, the efficient transfer of iron(hydr)oxides is hampered and excess S can build up in the porewater, resulting in high S/Fe ratios. This free S could potentially bind to organic matter or be present as elemental S. The C/S ratio is often used to distinguish ancient euxinic environment, as iron-limited pyrite formation is often accompanied by high- sulfur and low-carbon values (Berner and

Raiswell, 1983), such as observed in the Black Sea. However, although the C/S ratio is rather low at about 2.3, the ratio between dibenzothiophene and phenanthrene (DBT/P), which is used to discriminate the impact of the depositional environment from the potential effect of source rock lithology (Hughes *et al.*, 1995), is 0.03, much lower than typical North Sea oil and Kimmeridge clay source rock showing values between 0.4 and 2.8 (Scotchman *et al.*, 1998). Hence most sulfur, with concentrations up to 16% (Figs. 4B and 8B), is probably present as inorganic sulfur.

The Pristane/Phytane (Pr/Ph) ratio can also be used to determine redox conditions of the sediment during deposition, based on the assumption that both pristane and phytane originate from the phytol side chain of chlorophll (e.g Didyk *et al.*, 1978; Powell, 1985), although the limitations of this approach have also been outlined (Ten Haven *et al.*, 1987). In the record studied here, ratios vary widely, between 0.76 and 3.9. The low values correspond to the Frasnian black shale, which is in line with the expected oxygen-depleted conditions during deposition. The higher values in the upper part of the record confirm reestablishment of oxic bottom water conditions after black shale deposition. Still the Pr/Ph ratio might also be affected by varying input of terrestrial organic matter. Changes therein are suggested by the *n*-alkane distribution, showing a distinct, albeit modest, odd-over-even carbon predominance from 2295 to 2290 m in depth (Fig. 6 and Table 2).

Homohopane distributions are dominated by the C_{31} homohopane, with decreasing relative concentrations with increasing carbon number (Fig. 7). The distribution of the extended hopanes or homohopanes (C_{31} – C_{35}) has also been used to evaluate redox conditions during deposition of source rocks, showing increased relative abundances of the C_{35} homohopane under anoxic conditions (Peters & Moldowan, 1991). Sinninghe Damsté *et al.,* (1995) showed that selective preservation of the C_{35} skeleton by sulfur incorporation is the most likely mechanism for the relative enrichment of the C_{35} homohopane under anoxic conditions. Still, at higher maturity levels the C_{35} homohopane potentially decreases again due to preferential generation of shorter-chain hopanes (Peters & Moldowan, 1991). Relative concentrations of the C_{35} hopane to the summed concentrations of the C_{31} to C_{35} hopanes >0.10 have been interpreted as indicative for deposition under anoxic bottom water conditions (Peters & Moldowan, 1991). This ratio for the samples analyzed here indicates that the Lower Awaynat Wanin Formation, with values ranging between 0.12 and 0.14, was deposited in a continuously anoxic environment. Although anoxic conditions might have extended into the water column, they most likely did not reach the photic zone (Sinninghe Damste *et al.*, 2001) as we did not detect any isorenieratene derivatives (Fig. 8A).

5.4. Thermal maturity assessment

The maturity level of the source rock was estimated by both by Rock Eval derived T_{max} values and by examining the hopane (m/z 191) distribution, specifically the Ts/Ts+Tm ratio. The Rock Eval T_{max} values range between 438 and 442 °C (Table 1). Although the maturation ranges of T_{max} values are known to vary for different types of organic matter (Espitalie *et al.*, 1985; Tissot *et al.*, 1987; Bordenave *et al.*, 1993; Peters, 1986), T_{max} values indicate that the organic matter has just reached the beginning of the oil window.

To distinguish between type and origin of the organic matter present, Rock Eval results can be plotted using a HI-T_{max} diagram (Fig. 9). Most of the Early Frasnian black

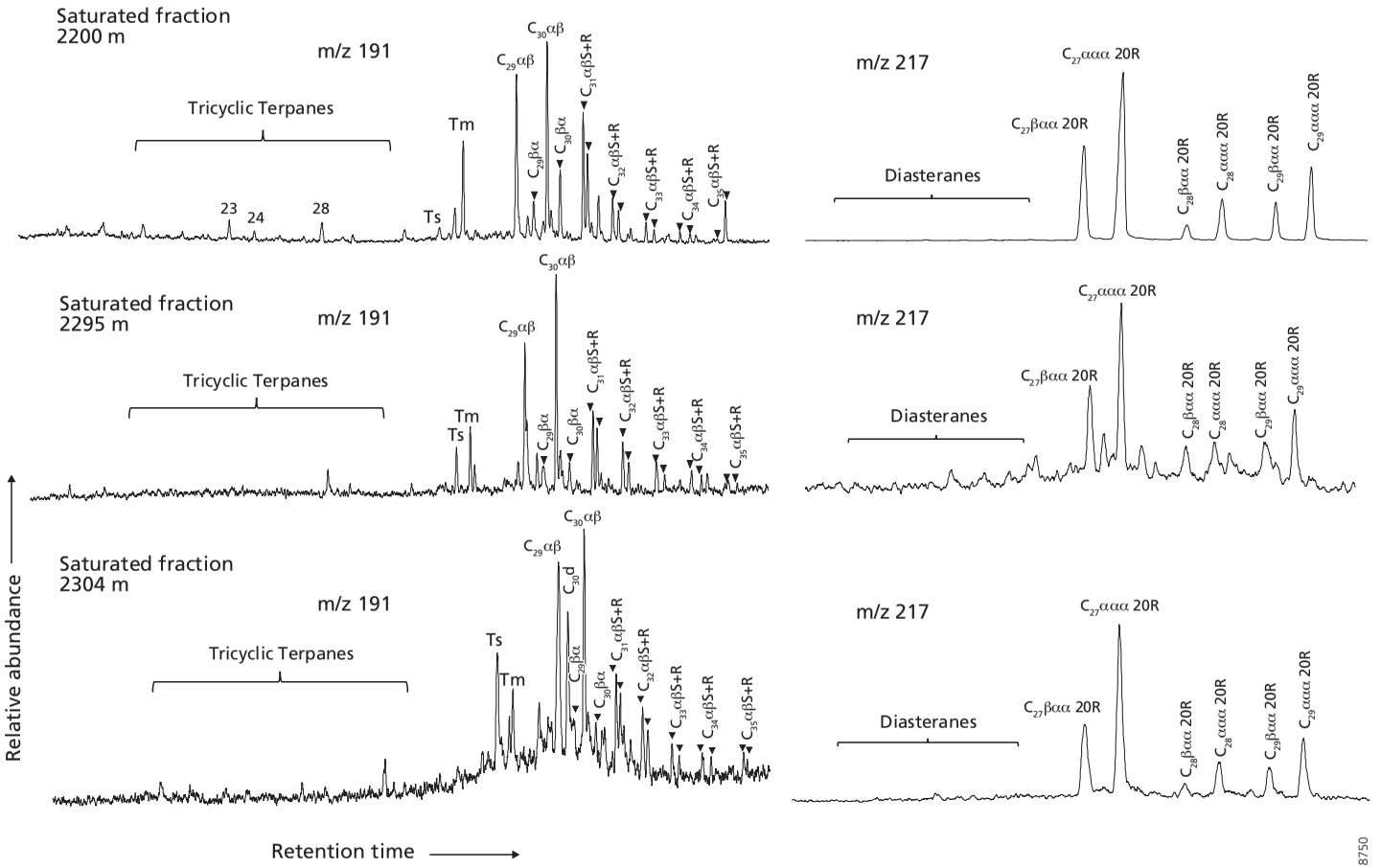

Fig. 7. Mass chromatograms (m/z 191 hopanes and m/z 217 steranes) from three selected aliphatic hydrocarbon fractions from A1-NC101 borehole of Murzuq Basin. (Ts = C_{27} 18α(H)-trisnomeohopane, Tm = C_{27} 17α(H)-trisnomeohopane, Tri =Tricyclic terpanes).

shale of the Awaynat Wanin plots in the Type II organic matter field (oil- and gas-prone), while the Carboniferous Mrar plots in Type III organic matter field (gas-prone) with low HI and S2 values. Similarly, based on hopanes it is also possible to evaluate source rock maturity, using the Ts/Ts+Tm ratio. This ratio is based on different thermal stabilities of these molecules (Seifert & Moldowan, 1978). The Ts/Ts+Tm ratio ranges between 0.59 and 0.60, which suggests that the Early Frasnian black shale attained a level of early maturity, in line with the Rock Eval Tmax data. The dominance of the ααα 20R steranes also indicates that the source rock is relatively immature (Peters *et al.*, 2005).

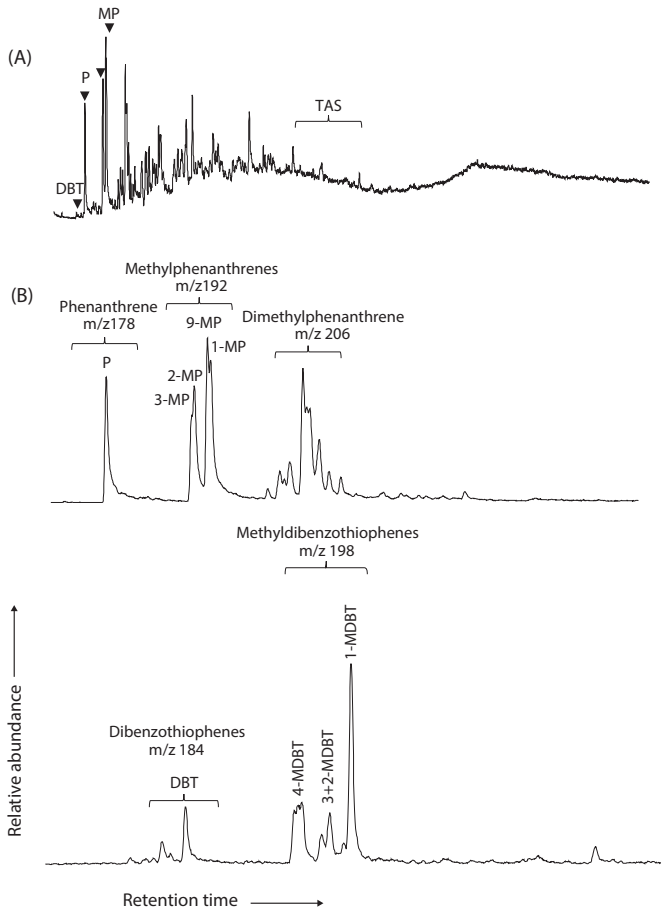

Fig. 8. Mass chromatograms from selected a sample (2295 m), (A) (TIC) of the aromatic hydrocarbon fraction, (B) and summed mass chromatogram of *m/z* 178+192+184+198, from A1-NC101 borehole (Murzuq Basin). Peak identification: P- phenanthrene; MP- methylphenanthrenes; DBT- dibenzothiophenes; MDBT- methyldibenzothiophene; TAS- triaromatic steroids.

5.5. Depositional model

Comparing the distribution of organics between the early Frasnian and the rest of the Devonian section shows that the AOM and *prasinophytes* are well-preserved. Although some supposedly terrestrial particles are present at these depths, the assemblage is overwhelmed by the marine prasinophytes *Pterospermopsis, Maranhites* and *Duvernaysphaera*. Palynofacies rich in AOM are often deposited under anoxic bottom water conditions (Tyson, 1993). At the same time the less diverse small acanthomorph acritarchs species indicate particular conditions at the sea surface. Similar acritarchs assemblages were observed in bituminous shales in the upper part of the Kowala section, in the Dasberg and Hangenberg intervals (Hartkopf-Fröder *et al*., 2007; Marynowski *et al*., 2010). Jardiné *et al*. (1974) studied the Late Devonian acritarchs of the Algeria rock records that showed great similarity to South America acritarch associations from the Frasnian. The paleogeographic setting, however, suggests a link to the Middle to Late Devonian onset of the collision between Laurentia and Gondwana. The relatively narrow nature caused by the gradual closure of the Iapetus Ocean would facilitate restricted conditions.

The Early Devonian in Libya is characterized by four transgressive sequences, which formed a widespread deltaic complex terminated by mid-Devonian uplift and erosion (Aziz, 2000). During the Middle to Late Devonian the gradual closure of the Iapetus

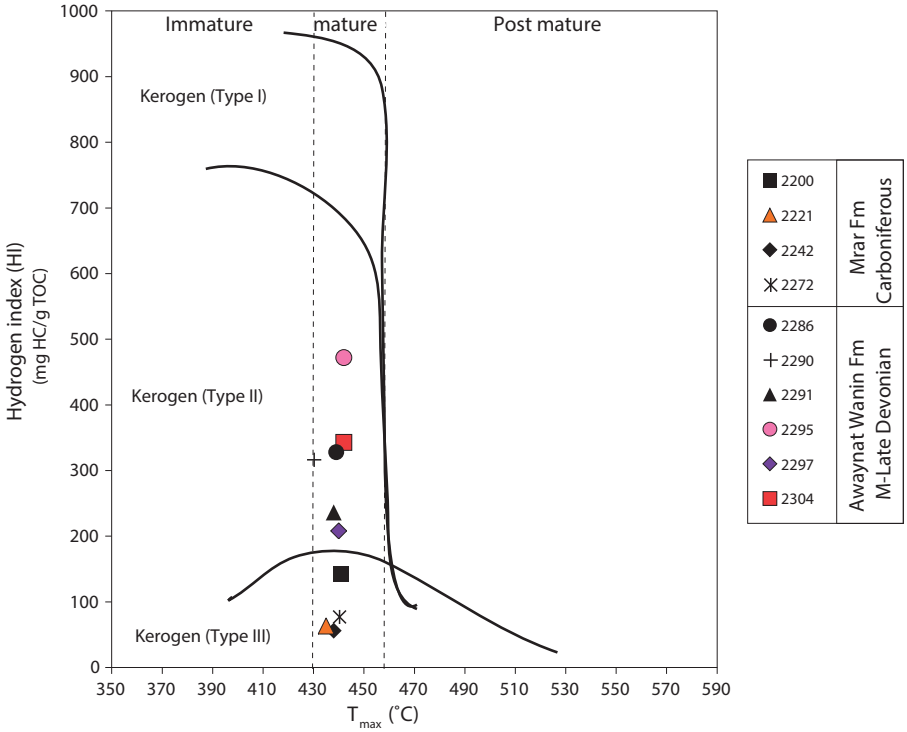

Fig. 9. Rock Eval Hydrogen index (HI) versus Tmax (°C) diagram of A1-NC101 borehole (Murzuq Basin), showing kerogen type and maturity evaluation.

Ocean brought progressive collision between Laurasia and Gondwana marking the onset of the Hercynian orogeny (Kent & Van der Voo, 1990). Initial effects of the closure were confined to Morocco and Algeria, with minor effects in Libya. Still, the basal Frasnian unconformity is caused by extensive erosion of the Al Qarqaf Arch (Boote *et al*., 1998), which borders the Murzuq Basin.

The Frasnian unconformity was succeeded by a significant flooding event, during which organic-rich shales were deposited along the entire north Gondwana Margin (Luning *et al*, 2004). Although Buggisch and Joachimski (2006) and Morrow and Sandberg (2009) previously noted that not all positive excursions are associated with sea-level rise, the positive $\delta^{13}C_{org}$ recorded here appears to be closely timed with the onset of T-R cycle IIc.

The sediment deposited in Algeria and Morocco, however, contains much less organic carbon. While in the Murzuq basin the Frasnian black shale contains up to 38 wt% carbon, the Algerian Frasnian deposits contain up to 9 wt% organic carbon; in the bordering areas, most sediments contain even less organic matter. Clearly, conditions in the Murzuq Basin must have differed considerably. This not only affected preservation and production of organic matter, but also limited dilution with sediment. This is in line with the relatively limited thickness of the Frasnian black shales in Murzuq, which suggests a condensed section.

Uplift of the Al Qarqaf Arch, Tihemboka Arch and Atshan Saddle created ideal restricted depositional conditions in the Murzuq Basin. The highs surrounding the Murzuq Basin were probably still submerged, accumulating a thin Frasnian sedimentary sequence, which was removed during the later Hercynian uplift and erosion phase. More importantly, these uplifted areas effectively cut off the inputs of sediments from the Gondwana continent to the Murzuq Basin. The restricted oceanic conditions, in concert with enhanced weathering and nutrient inputs, set the stage for the deposition of organic rich sediments (Boote *et al*., 1998). The limited input of terrestrial sediment in Murzuq enhanced these effects, explaining the unusual high organic carbon content.

6. Conclusions

Biostratigraphy of the organic-rich black shale of the Awaynat Wanin Formation showed that the recovered organic rich black shale from the eastern Murzuq Basin was deposited during the Early- Middle Frasnian/Late Devonian. This black shale is characterized by high TOC and sulfur contents. The abundant presence of marine amorphous organic matter, together with prasinophytes algae (*e.g. Maranhites, Pterospermopsis*) in this black shale in the Murzuq Basin, is in line with organic geochemical and biostratigraphic evidence for a strongly reducing depositional environment. The diversity of the prasinophycean and high concentration of organic matter also suggest enhanced surface productivity at the time of deposition. The onset of Frasnian black shale sedimentation is probably associated with the earliest Frasnian eustatic sea level rise, concurrent with a major positive $\delta^{13}C_{org}$ carbon isotope excursion of about 3‰. This positive excursion appears to be linked to the coeval deposition organic-rich black shales in Morocco, Algeria, Germany, Poland and South China. Although of limited extent, geochemical evaluation suggest that the Early Frasnian black shale, depending on its maturity, could be a potential secondary source rock for the Murzuq Basin.

Plate description and captions

Plate I. For each figured (miospore) specimen, sampling and slide number are indicated Scale bar is 10μm, except where mentioned otherwise.

1. *Vallatisporites* sp. (new speices), 2200, 2221, 2242 m, slide no. 1A, 2C, and 3A, X100
2. *Radiizonates arcuatus* Loboziak, Playford and Melo, 2000 (2200, 2221 m), slide no. 1A, 2C
3. *Waltzispora lanzonii*, Daemon 1974 (2200, 2221, 2242 m), slides no. 1A, 2C, and 3B, 60X
4. *Indotriradites dolianitii* (Daemon) Loboziak, Melo, Playford and Streel, 1999 (2200 m, 2221 m,), slide no. 1B, 2B.
5. *Spelaeotriletes pretiosus* (Playford) Neves & Belt, 1970 (2200, 2221, 2242 m), slides no. 1B, 2C, 3A
6. *Vallatisporites verrucosus,* Hacquebard, 1957 (2200, 2221, 2242 m), slide no. 1B, 2A and 3B
7. *Tumulispora rarituberculata* (Luber) Potonié, 1966 (2284, 2288 m), slide no. 4B, 5C, X40
8. *Retispora lepidophyta* (Kedo) Playford, 1976 (2284 m, 2288 m), slides no. 4A, 6B
9. *Verrucosisporites nitidus,* Playford, 1964 (2242, 2284, 2288 m), slide no. 3C, 4C, 6C

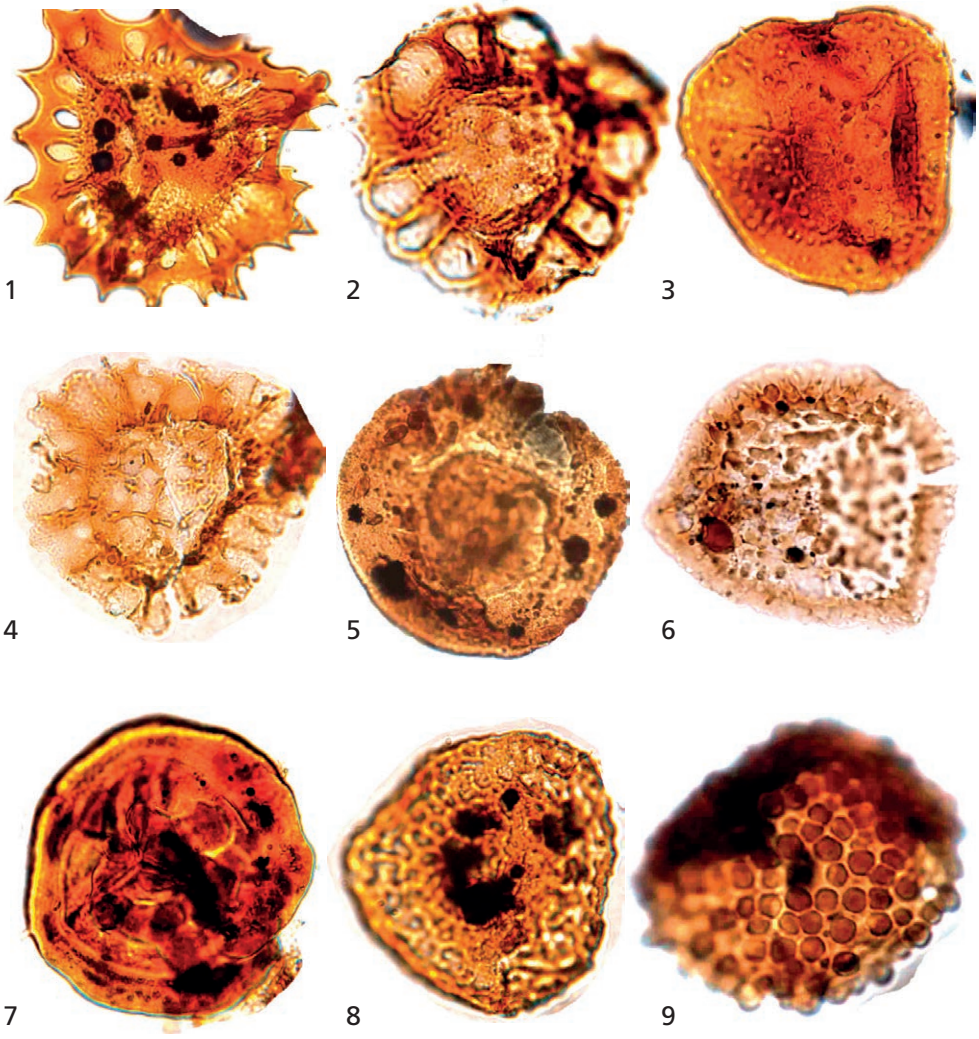

Plate. I (caption on page 96)

Plate II.

1. *Samarisporites triangulatus* Allen, 1965 (2297 m), slides no. 9A.
2. *Geminospora lemurata,* Balme emend Playford, 1983 (2290, 2297, 2304, 2307 m), slide no. 7A, 9C, 10A, 11D.
3. *Ancyrospora pulchra*, Owens, 1971 (2297 m), slide no. 9B.
4. *Samarisporites eximius* (Allen) Loboziak & Camfield, 1982 (2297, 2307 m) slide no. 9A, 11F
5. *Grandispora protea* (Naumova) Moreau-Benoit, 1980 (2297 m), slide no. 9B
6. *Hystricosporites* sp. Owens, 1971 (2286, 2297 m) slide no. 5B, 9A 60X
7. *Verrucosisporites premnus,* Richardson, 1965 (2297 m) slide no. slide no. 9A
8. *Grandspora libyensis,* Moreau-Benoit, 1980 (2297, 2304 m) slide no. 9B, 10B.
9. *Rhabosporites langii* (Eisenack) Richardson, 1960 (2297, 2304 m), slide no. 9C, 10A.
10. *Acinosporites lindlarensis,* Riegel, 1968 (2307 m), slide no. 11C
11. *Densosporites concinnus* (Owens) McGregor & Camfield, 1982 (2307 m) slide no. 11F, 11D

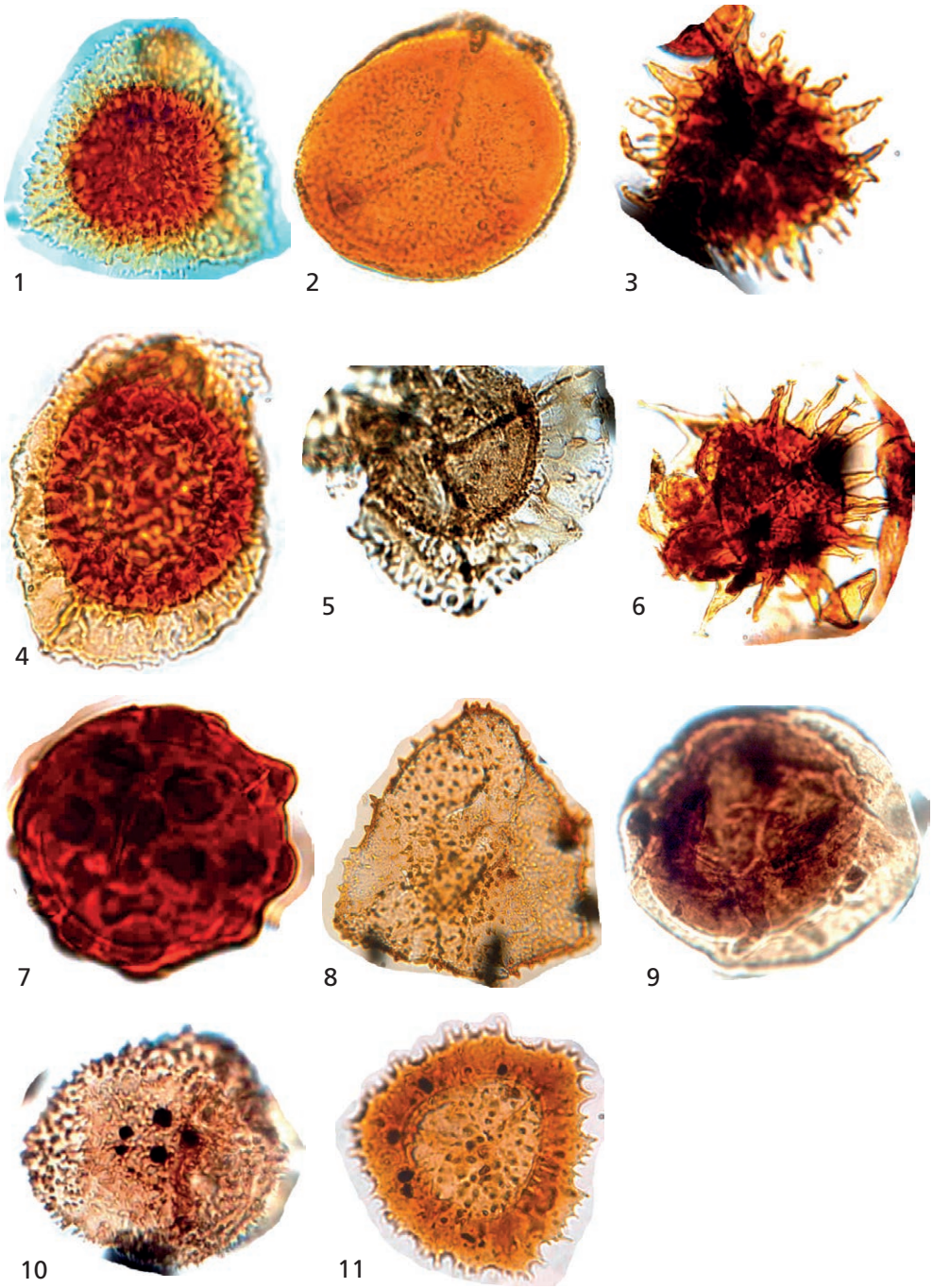

Plate. II (caption on page 98)

Plate III. Acritarchs and Prasinophytes (Scale bar 40µm) X600

1. *Stellinium comptum* Wicander & Loeblich, 1977 (2242, 2297 m), slide no. 3A, 9B.
2. *Stellinium micropolygonale* (Stockmans & Williere) Playford, 1977 (2242 m), slide no. 3C
3. *Horologinella horologia* Jardinė *et al*, 1972 (2284, 2288, 2297, 2290, 2304 m), slide no. 4C, 6B, 7D, 9C, 10C.
4. *Horologinella quadrispina* Jardinė *et al*, 1972 (2304, 2297, 2288, 2284 m), slide no. 10B, 9C, 6A, 4D.
5. *Maranhites lobulatus* Burjack & Oliveira, 1989 (2297 m), slide no. 9C, 9B, 60X
6. *Navifusa bacilla* (Deunff) Playford, 1977 (2290 m), slide no.7C, 7E

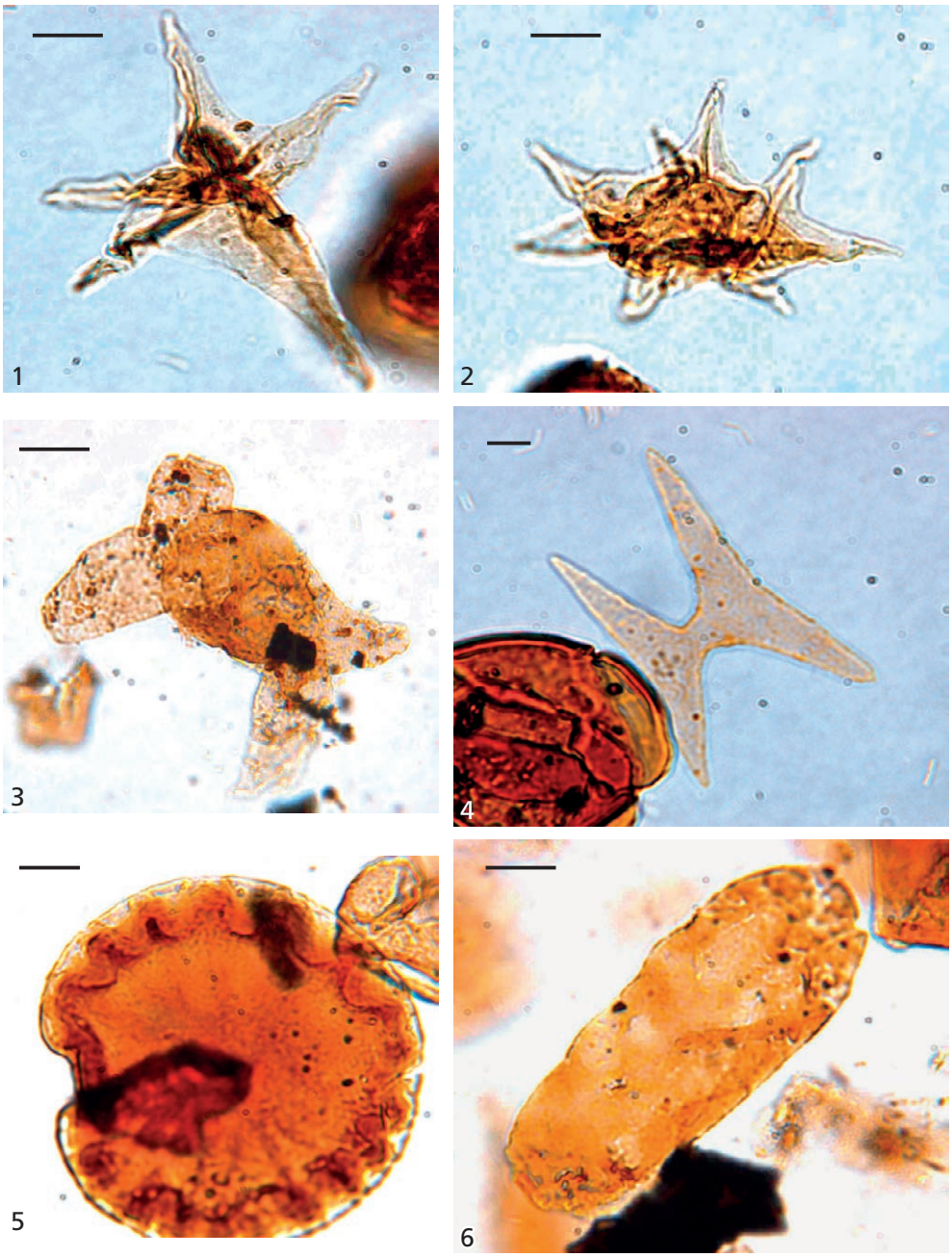

Plate. III (caption on page 100)

Plate IV.

1. *Unellium piriforme* Rauscher, 1969 (2242, 2286 m), slide no. 3A, 5B
2. *Crassiangulina tesselita,* Jardinė *et al*., 1972 (2286 m, 2297 m), slide no. 9A, 5B
3. *Gorgonisphaeridium solidum,* Jardiné *et al*,1974 (2297 m), slide no. 9B
4. *Duvernaysphaera tenuicingulata*, Staplin, 1961 (2307, 2297 m) slide no. 11F, 9C.
5. *Umbellasphaeridium deflanderi* (Moreau-Benoit) Jardine *et al*., 1972. (2307, 2288, 2242 m), slide no. 11C, 6B, 3C.
6. *Maranhites mosesii* (Sommer, 1965), Brito, 1967 (2297 m), slide no. 9C.

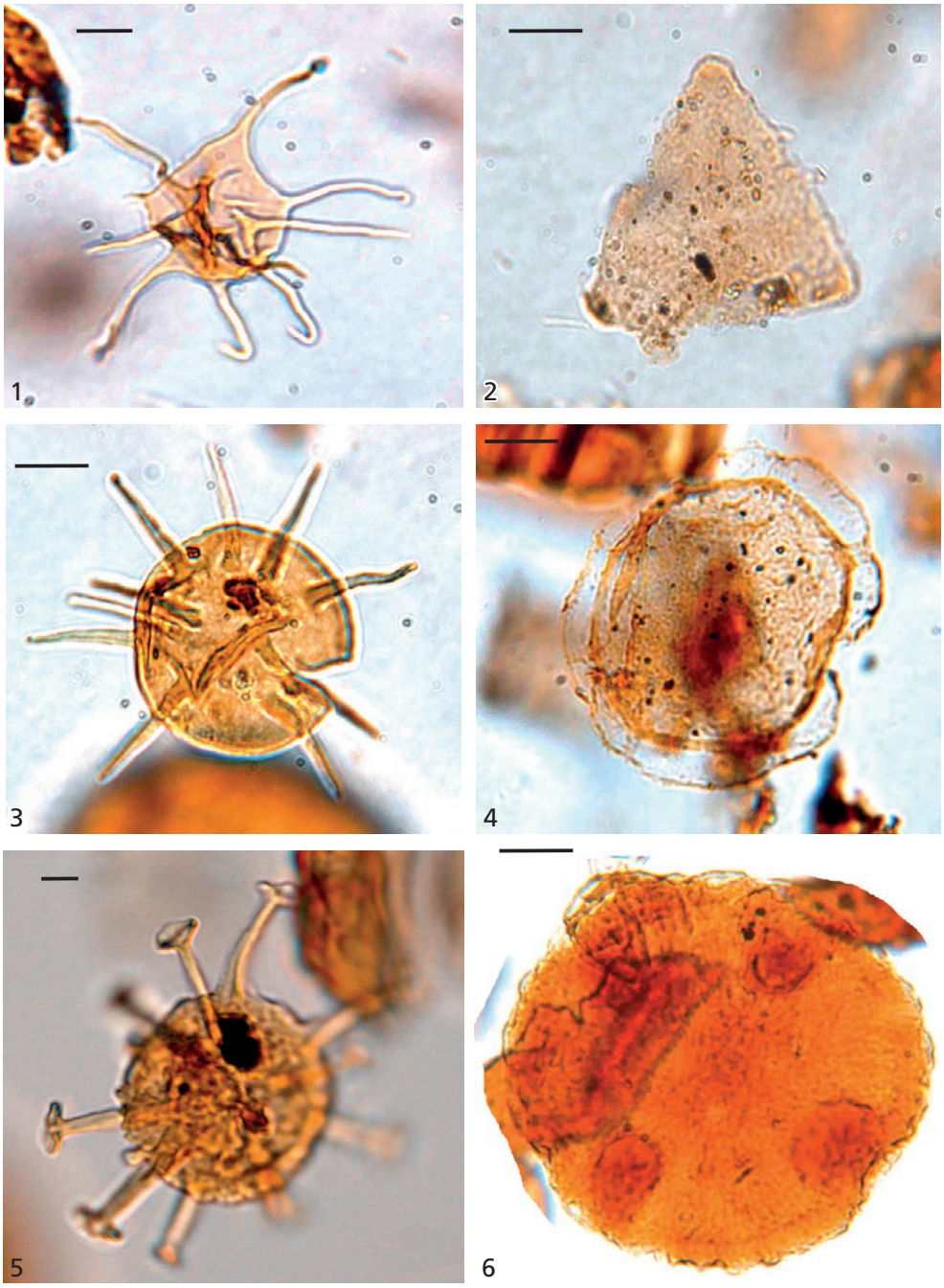

Plate. IV (caption on page 102)

Plate V.

1. *Neoveryhachium triangulate*, Le Hérissé, 1995 (2297m), slide no. 9B
2. *Veryhachium cf.V. lairdi,* Deunff, 1959 (2307 m), slide no. 11F
3. *Pterospermopsis Crassimarginata,* Oliveira, 2007 (2307. 2297, 2200 m), slide no. 1B, 9C and 11C
4. *Polyedryxium fragosulum*, Playford, 1977 (2242 m), slide no. 3B
5. *Gorgonisphaeridium ohioense,* (Winslow) Wicander, 1974 (2242, 2288, 2297, 2304 m), slide no. 3B, 6C, 9B, 10C.
6. *Solisphaeridium spinoglobosum*, (Staplin) Wicander, 1974 (2307 m), slide no. 11F

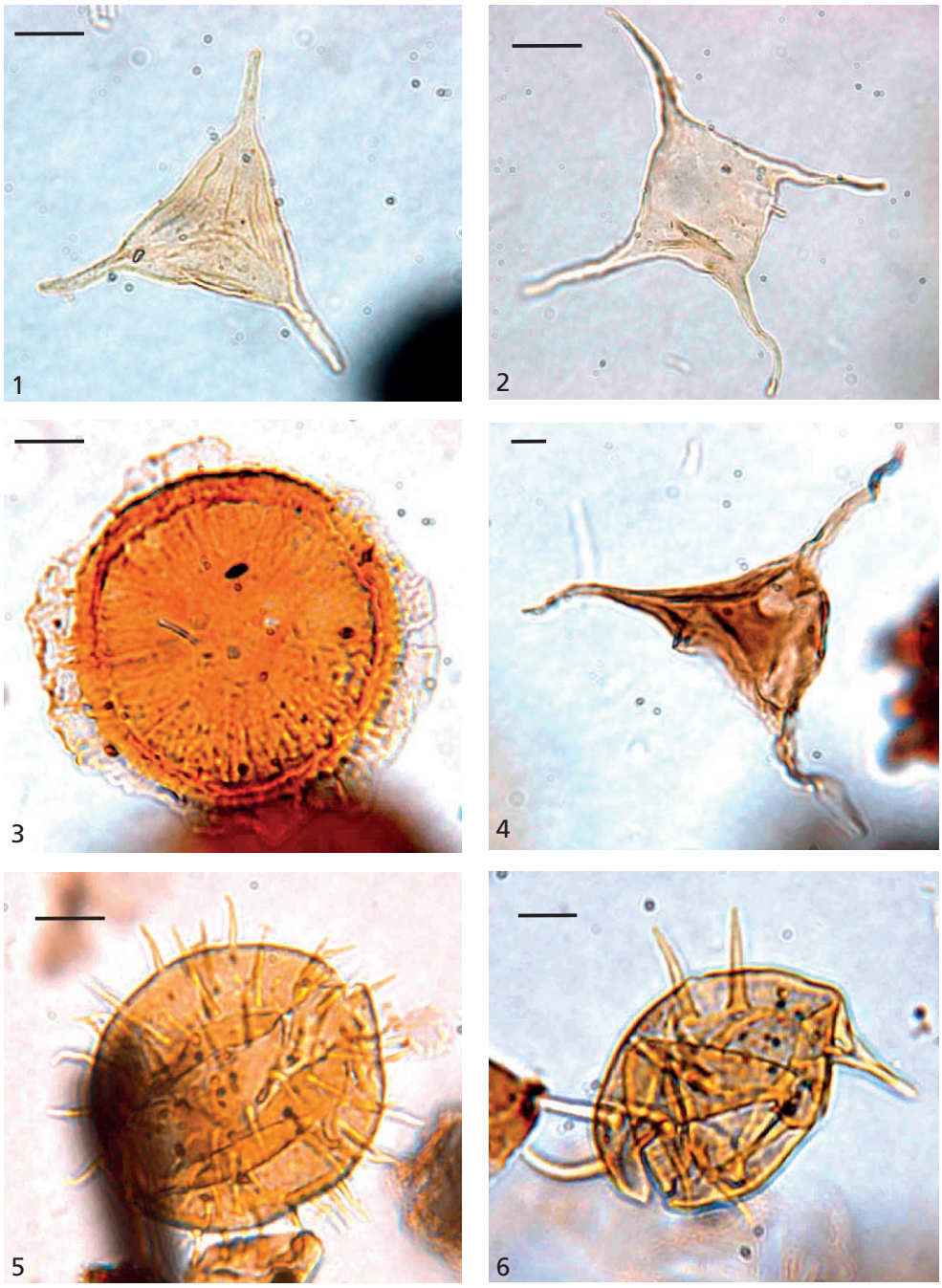

Plate. V (caption on page 104)

Plate VI. Chitinozoans, Amorhouse, Phytoclasts (Scale bar 40µm) X100

1. *Fungochitina fenestrate*, Taugourdeau & Jekhowsky, 1960 (2307 m), slide no. 11B
2. *Fungochitina pilosa* Collinson & Scott, 1958 (2307 m), slide no. 11F
3. *Urochitina* sp. A Jardiné & Yapaudjian 1968 (2307 m), slide no. 11D, 60X
4. *Ancyrochitina striata* Taugourdeau, 1963 (2307 m),slide no. 11B
5. Amorphous organic matter (AOM) (2295 m), slide no. 8A,B,C,D,F
6. Fluorescent light view of structureless, partly fluorescent well preserved AOM from black shale (2295 m).
7. Biostructured phytoclast Tyson, 1995 (2286, 2242 m), slide no. 3B,A, and 5A
8. Opaque biostructured phytoclast Tyson, 1995 (2286, 2242 m), slide no.. 3A, 5B.

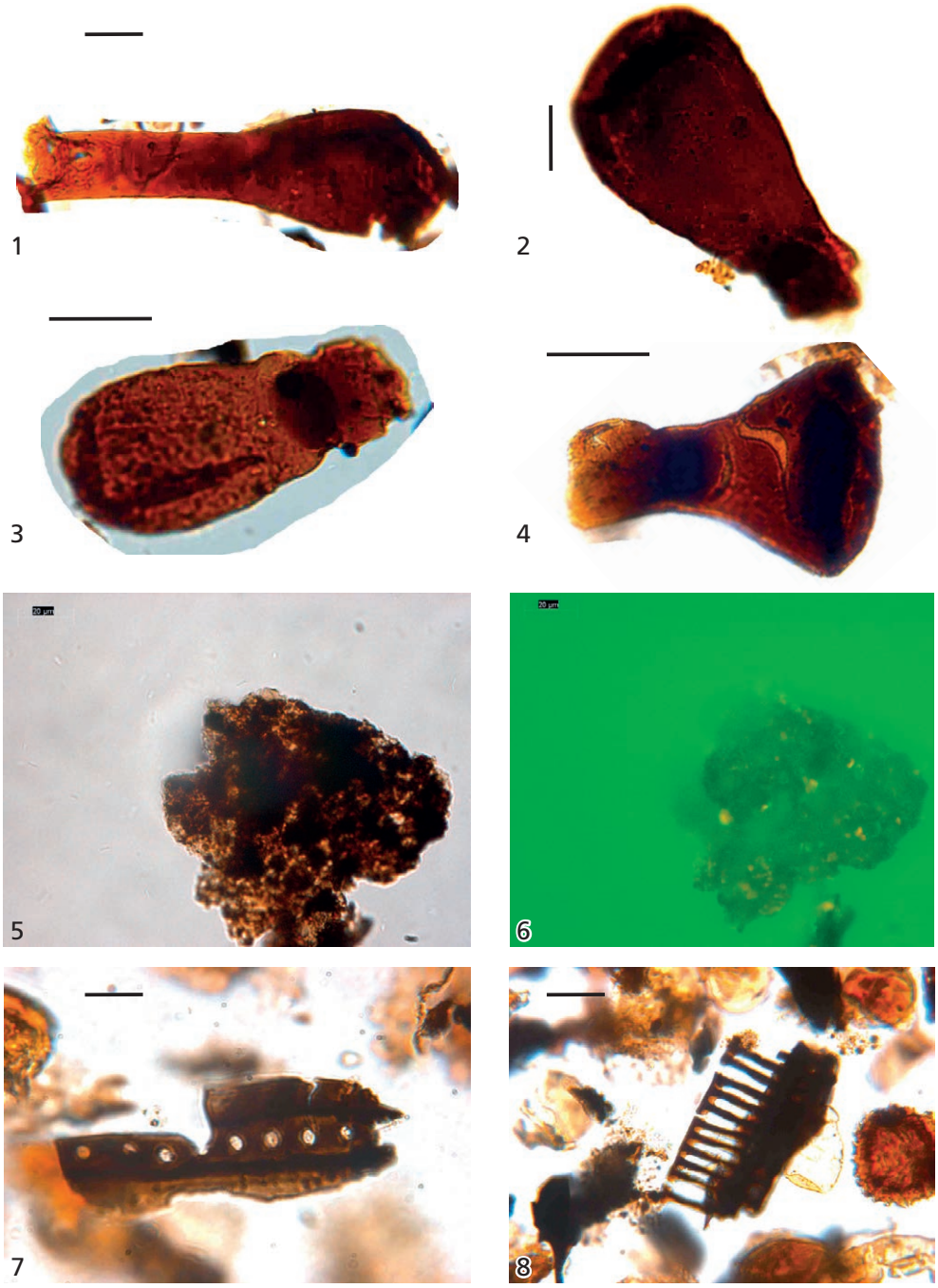

Plate. VI (caption on page 106)

4 Palaeodepositional reconstruction and thermal maturity of the early Silurian Tanezzuft shales in Libya

Mohamed M.A. Elkelani[1], Gert-Jan Reichart[1,2], Jaap S. Sinninghe Damsté [1,2], Klaas G.J. Nierop[1]

[1] *Utrecht University, Faculty of Geosciences, Department of Earth Sciences-Organic Geochemistry, Budapestlaan 4, 3584 CD Utrecht, The Netherlands*
[2] *NIOZ Royal Netherlands Institute for Sea Research Texel, P.O. Box 59, 1790 AB, Den Burg, The Netherlands.*

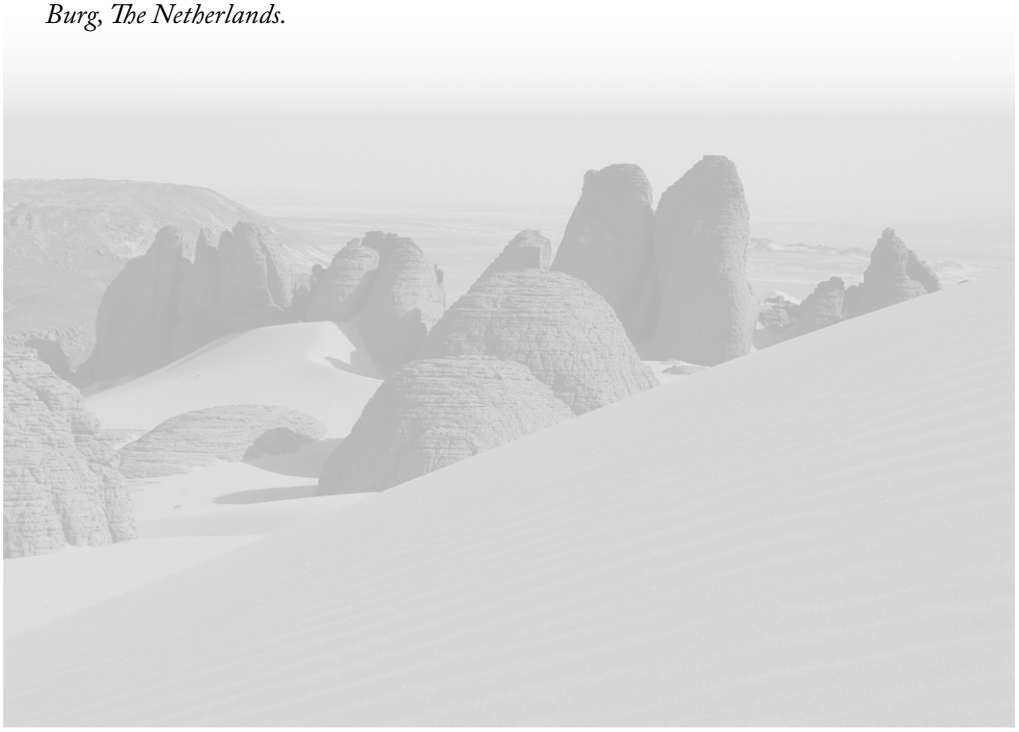

Abstract

The lower Silurian organic-rich "hot" shale is the most important Palaeozoic hydrocarbon source rock in North Africa and Arabia. We studied two oil exploration cores from the Murzuq and Ghadamis basins in Libya. Both cores contain the Silurian Tanezzuft "hot" shale formation, which is characterized by high levels of TOC (up to 23 wt%). The maturity evaluation, based on equivalent vitrinite reflectance and Rock Eval pyrolysis, indicates that the Silurian source rock in the Murzuq basin is thermally more mature than that in the Ghadamis basin. Significant differences in alkylbenzenes distribution patterns were observed between Ghadamis basin kerogen and Murzuq Basin kerogen pyrolysates. The main difference is controlled by maturity and, to some extent, organic facies effects. The extractable hydrocarbon biomarkers provided little information regarding the palaeoenvironmental setting due to some biodegradation and the high thermal maturity of these source rocks in the Ghadamis Basin. Therefore, our study focused on the possibility of reconstructing the palaeoenvironmental setting predominantly based on kerogen and asphaltenes analysis in the Silurian Tanezzuft "hot" shale formation. The presence of the pyrite associated with high organic matter indicated that the source rocks were deposited under anoxic conditions. The degree of anoxia was inferred from the relatively high abundance of the "pyrolytic markers", 1,2,3,4- and 1,2,3,5-tetramethylbenzene and 1-ethyl-3,4,5-trimethylbenzene and 1-ethyl-2,3,6-trimethylbenzene, markers for macromolecularly bound diaromatic cartenoids. Since these carotenoids are derived from green sulfur bacteria, which require both light and sulfide, this demonstrates the occurrence of a photic zone anoxia (PZA). Surprisingly, our data indicate that the occurrence of PZA is not limited to the "hot" shale but also occurred during deposition of shales with a lower TOC content (TOC<0.25 wt%). Our study indicates that Py-GCMS of asphaltenes and kerogens, integrated with other techniques, can be a useful complementary tool for palaeoenvironmantal assessment for thermally mature source rocks.

Keywords- *Hot shale, Silurian, photic zone anoxia, maturity, Rock Eval Pyrolysis, kerogen, asphaltene, Py-GC-MS, Pyrolytic biomarker.*

1. Introduction

The organic-rich shales deposited in many areas of Gondwana during the latest Ordovician-earliest Silurian extend from Iran via Jordan, Syria and Saudi Arabia along the northern African margin into Morocco (Lüning *et al*., 2000). These organic-rich shales are called "hot" shales in the Ghadamis and Murzuq Basins in Libya. The Silurian organic-rich "hot" shale is the most important Palaeozoic hydrocarbon source rock in North Africa and Arabia (Lüning *et al*., 2000, 2006; Belhaj, 1996). In the western part of Libya the organic-rich shales from the Tanezzuft Formation have sourced most of the hydrocarbon reservoirs discovered to date. The time equivalent Qusaiba Member in Saudi Arabia plays a major role in petroleum generation on the Arabian Peninsula (Al-Hajri, 1991). Previous organic geochemical studies of the early Silurian sediments from the

Ghadames and Murzuq Basins focused on source rock characterization and hydrocarbon potential (Belhaj, 1996; Lüning *et al.*, 2000).

The Ghadames and Murzuq Silurian sediments have highly thermally mature, and partially biodegraded source rocks. In such cases, characterization indices based on analyzing extractable hydrocarbon biomarkers are often uninformative. Molecular characterization of asphaltenes and kerogens by pyrolysis-gas chromatography/mass-spectrometry might still be useful at high maturity and/or for severely biodegraded source rocks (e.g. Sarmah *et al.*, 2010; Wanglu *et al.*, 2010; Lis *et al.*, 2008; Koopmans *et al.*, 1996a). Biomarkers may potentially be selectively preserved within the complex structures of kerogen and asphaltenes. Thermal degradation of macromolecules into small fragments with flash pyrolysis offers a powerful method to obtain molecular structural information of complex organic materials (Horsfield, 1989; Hartgers *et al.*, 1992, 1994a, b) and can thus help to identify the selectively preserved biomarkers from kerogen and asphaltenes. Kerogens and asphaltenes represent the bulk of sedimentary organic matter; therefore, they have been the subject of numerous investigations (Van Graas *et al.*, 1981; Larter & Horsfield, 1993: Philp & Gilbert, 1985; Summons and Powell, 1987; Tegelaar *et al.,* 1989a; Pedentchouk *et al.*, 2004; Hartgers *et al.*, 1992, 1994a, 1994b; Hoefs *et al.*, 1995; Sinninghe Damsté *et al.*, 1998). The molecular and microscopic analysis of kerogens and asphaltenes also can provide essential information on the type and origin of organic matter, the thermal history of sedimentary basins, the sedimentary facies, depositional environments, palaeoclimate change, and the presence of specific biota present at the time of deposition (e.g. Hoefs *et al.*, 1995; Hayes et al., 1987).

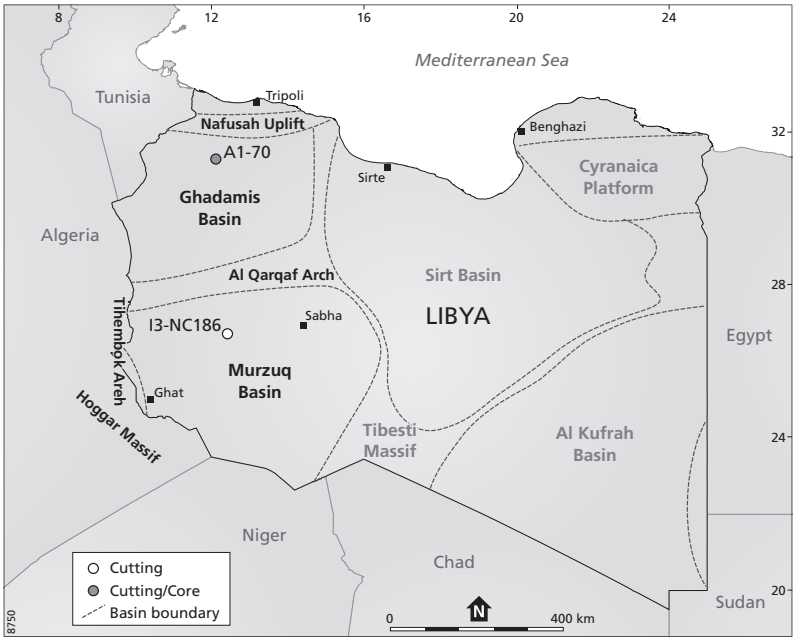

Fig. 1. Map showing the wells and geographic locations of Ghadamis and Murzuq basins (NOC, 2008).

The aim of this study was to further our knowledge about the evolution of the depositional environment of the early Silurian source rocks deposited in the Ghadames and Murzuq Basin (see Chapter 2). We focused on the possibility to reconstruct the palaeoenvironmental setting predominantly based on kerogen and asphaltene analysis of the Silurian Tanezzuft "hot" shale Formation, since, the extractable biomarkers lacked information due to biodegradation and high thermal maturity of these source rocks. Furthermore, the internal consistency and accuracy of molecular maturity parameters was investigated to relate maturity level to source rock composition.

2. Materials and methods

2.1. Sampling and core description

Samples for this study were collected from available core and cutting material from two boreholes A1-70 and I3-NC186 (Fig. 1), they are listed in Table 1 and 2. The cores were described in detail using standard sedimentological log paper during sampling. These sections were previously dated using an arcritarch and chitinozoan stratigraphy (Chapter 2). Cutting samples from the Early Silurian of the Tanezzuft Formation from the I3-NC186 borehole range from depths of 1420 m to 1125 m in the Murzuq Basin. Core samples together with infill cuttings range from lower and upper Silurian from the A1-70 borehole, from depths of 3118 m to 2719 m in the Ghadamis Basin. Shales interbedded in the sandstone were sampled from both cores and cuttings, depending on availability, from the early and late Silurian interval.

The studied core and cutting sections in borehole A1-70 range between 3118 m and 2719 m in depth, spanning the latest Ordovician- late Silurian (Ludlow) stratigraphic interval (Fig. 2). Two samples were collected from the Ordovician interval from the lower part of the section, between 3118 m and 3112 m, which consists of irregular alternations of fine-grained sandstones, and siltstone. Within the section between 3103 m and 3048 m a distinct interval occurs, which mainly consists of organic-rich black to dark grey shale. These so-called "hot" shales (Lüning *et al.*, 2000) are correlated to distinctly elevated gamma ray values in the wireline log (Fig. 2). The interval between 3048 m and 2775 m consists of dark grey silty shales. Finally, the interval between 2775 m and 2719 m consists of an alteration between fine-grained sandstones and siltstones.

Cuttings from the I3-NC186 borehole are from a section ranging between 1420 m and 1125 m, covering only the early Silurian (Llandovery). The interval between 1420 m and 1396 m consists of organic-rich black ("hot" shale). Between 1396 m and 1125 m, the sediment consists of dark gray shale, alternating between siltstone and sandstone.

2.2. Methods

Wireline log data (gamma-ray data) were obtained from the well log of A1-70 borehole by the Arabian Gulf Oil Company and from the I3-NC186 borehole by the Repsol Oil Company. All selected samples were analyzed for total organic carbon (TOC) content. Selected samples were measured using Rock-Eval pyrolysis, microscopic analyses

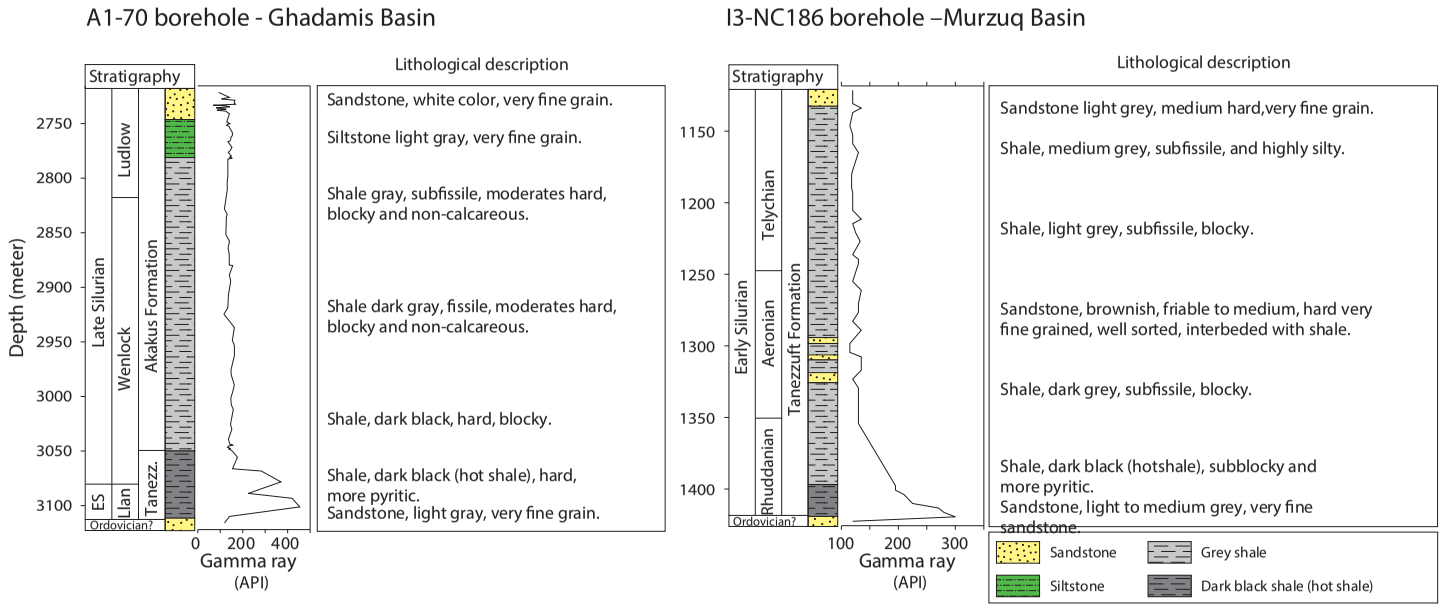

Fig. 2. Lithological description and correlation with Gamma ray data from A1-70 borehole (Ghadamis Basin) and I3-NC186 borehole. Abbreviation **ES** – Early Silurian; **LIan** – Llandovery; **Tanez**- Tanezzuft Formation

of the macerals, extractable hydrocarbon biomarkers, and Curie point pyrolysis-gas chromatography-mass spectrometry of the kerogen and asphaltene fractions.

2.2.1. TOC and Rock-Eval pyrolysis analysis

TOC content was determined using an elemental analyzer on decalcified samples. In short, 0.5 g of powdered material was decalcified with 12 ml 1M HCl for 24 h. After decalcification, residues were washed with demineralized water, centrifuged and decanted several times to remove acid-soluble components. Subsequently samples were freeze-dried and TOC was determined using a Fisons NA 1500 NCS Element Analyzer.

Rock Eval analysis was carried out using a Rock Eval 6 pyrolysis apparatus. A crucible containing a small amount (100 mg) of crushed whole rock sample was introduced into a furnace at 300˚C. The furnace temperature was subsequently raised by 35˚C/minute to 600 ˚C. Free volatile hydrocarbons were quantified by a flame ionization detector (FID) (S1 peak, mg HC/g rock). Within this temperature range kerogens in the rock sample "crack", producing further hydrocarbons (S2 peak, mg HC/g rock) and CO_2 associated with pyrolysis (300-390 ˚C) (S3 peak, mg CO_2/g rock). Parameters also measured the include temperature of maximum pyrolysis yield (T_{max}). Source rock parameters such as HI (Hydrogen index, S2/TOC*100), OI (Oxygen index, S3/TOC*100), and PI (Production index S1/(S1+S2)) were calculated from these measured values. Following Rock-Eval and TOC analyses, samples with high TOC were selected for further geochemical and petrographic studies.

2.2.2. Kerogen isolation and microscopic analyses of macerals

Ten samples were selected for microscopic analyses of the kerogen. Fifteen g of shale from each sample were treated using standard HF-HCl palynological processing (Phipps & Playford, 1984). In short, the samples were disaggregated with a pestle and mortar (to pieces of about 5 mm in diameter) and then subjected to 20% HCl treatment to dissolve carbonates. Samples were then allowed to stand until any reaction had stopped. After three washing with distilled water the samples were treated with 40% HF to remove any silicate material, and were allowed to stand for at least 24 h. An aliquot of the kerogen was kept for further processing and geochemical analyses (see 3.4). No oxidation was performed on organic residues. The size of the organic particles obtained ranged from 5 to > 200 µm. A 250 µm mesh sieve was used to remove oversized organic material. Sieving over 10 µm mesh yielded the fraction containing palynomorphs. After that a small aliquot of the residue was mounted on a slide, embedded with glycerine jelly, covered and sealed with paraffin wax. Slides were studied in transmitted and fluorescent light using a Zeiss microscope. For each sample, a minimum of 200 palynomorphs was counted per sample for standardizing the relative abundance calculations of the different palynomorph groups ;palynomorph, amorphous organic matter (AOM), and phytoclast.

Table 1. Sample description, total organic carbon and Rock Eval pyrolsysis parameters.

Well name	depth (m)	Sample type	TOC (wt%)	S1 (mgHC/g rock)	S2 (mgHC/g rock)	S3 (mgCO2/g rock)	Tmax (°C)	HI (mgHC/g TOC)	OI (mgCO2/g TOC)	PI –
A1-70	**2720**	**Core**	0.3	0.10	0.27	0.24	426	107	95	0.27
	2797	**Core**	1.2	0.22	0.98	3.05	426	82	256	0.18
	2879	**Core**	1.0	0.30	3.30	0.03	436	333	3	0.08
	2995	**Cutting**	1.1	0.53	3.37	0.12	436	296	11	0.14
Hot shale	**3095**	**Core**	18.0	7.52	43.00	0.87	440	240	5	0.15
	3103	**Cutting**	22.3	4.19	26.14	1.92	445	117	9	0.14
I3-NC186	**1137**	**Cutting**	0.5	0.07	0.36	0.36	426	80	80	0.16
	1271	**Cutting**	0.4	0.06	0.23	0.77	427	61	203	0.21
	1353	**Cutting**	0.6	0.04	0.25	0.73	428	42	122	0.14
Hot shale	**1399**	**Cutting**	6.9	1.15	8.37	1.33	438	121	19	0.12
	1408	**Cutting**	8.8	0.93	8.44	5.17	439	96	59	0.10
	1417	**Cutting**	14.8	2.01	19.67	1.98	445	133	13	0.09

TOC= Total Organc Carbon**, S1**= Free hydrocarbon,), **S2** = remaining hydrocarbon generative potentia,l **S3**= carbon dioxide yield,
HI= Hydrogen index = S2/TOC*100 , **OI**= Oxygen index S3/TOC*100, **Tmax** = Temperature of maximum pyrolysis yield,
PI= Production index S1/(S1+S2)

2.2.3. Extraction and fractionation

A known weight (15-20 g) of powdered rock samples (both core and cutting material) was extracted using a Soxhlet apparatus with an azeotropic solvent mixture of 200 ml of DCM/MeOH (9/1: v/v) for 24 h. The extract was dried using a rotary evaporator unit until just a few drops of solvent were left. This was transferred to a pre-weighed small vial and reduced to dryness under a stream of nitrogen. Elemental sulfur was removed from the extracts using activated copper. The solvent of each sample was then removed again under a stream of nitrogen in pre-weighed vials, and the weight of each extract was recorded.

An aliquot of selected extracts (6 samples from I3-NC186 and A1-70 boreholes) was placed in a vial and 12 ml of hexane was added. The asphaltenes precipitated and slowly sank to the bottom of the vial. The process was accelerated by centrifuging the sample and placing the vials overnight in a refridgerator. The deasphaltened extracts were carefully decanted from the top of the vial, after which more hexane was added. The procedure was repeated several times until the hexane remained colorless. After drying under a nitrogen flow the precipitated asphaltenes were subsequently weighed. The asphaltene content was expressed as a weight percentage of the original extract.

The extracts were separated into non-polar and polar fractions using short column chromatography on activated alumina by eluting with *n*-hexane, and MeOH/DCM (1:1, v/v) as solvents, respectively. The non-polar fraction was subsequently separated into a saturated and aromatic fraction using an Ag^{+}-impregnated silica column, with *n*-hexane and an *n*-hexane/DCM (9:1) mixture, respectively.

2.2.4. Gas chromatography and gas chromatography mass-spectrometry (GC-MS)

The aliphatic and aromatic hydrocarbon fractions were analyzed by capillary column gas chromatography. Each fraction was diluted with hexane to a concentration of about 1 mg/ml. The fractions were run on an HP6890 series II gas chromatography equipped with CP-Sil 5 CB column (25 m long, diameter of 0.32mm, film thickness of 0.12μm), using a FID for quantification and a flame photometric detector (FPD) to check for the presence of elemental sulfur and organic sulfur compounds. Helium was used as carrier gas, kept at constant pressure (100 kPa). Samples were injected on-column. The oven temperature was programmed from 70 to 130°C at 20 °C/min, from 130 to 320 °C at 4 °C/min and kept at 320 °C for 20 min. The data was collected on a Lab Agilent Chemstation data acquisition system.

Aliphatic and aromatic fractions were analyzed and identified by GC/MS (Thermo Trace GC Ultra), set at constant flow. A fused silica column (30 m x0.32 mm i.d., film thickness of 0.1μm) coated with CP Sil-5CB was used with helium as a carrier gas. Samples were injected on-column at 70 °C. The temperature program used was identical to that used for GC-FID/FPD analysis. Compounds were identified by comparison of mass spectra to previously published mass spectra. Although most compounds are quantified using the GC-FID, some compounds were quantified using TIC traces.

Table 2. Aliphatic gas chromatography data, maturity evaluation and alkylbenzenes ratios from Ghadamis and Murzuq basins.

Well name	depth			Depositional enviromental				Maturity parameters			Alkylbenzene ratios %			
				Gas chromatography data				Asphaltene fraction (Py-GCMS)						
			Total extract	Pr/Ph	Pr/*n*-C_{17}	Ph/*n*-C_{18}	CPI	2-MN/1-MN	4-MDBT/1-MDBT	RVc	$2C_5$/total C_5		$2C_4$/total C_4	
	(meter)	Sample type	mg/g rock					m/z 142	m/z 198	MPI-1	Kerogen	Asphaltene	Kerogen	Asphaltene
A1-70	**2720**	**Core**	4.4	0.96	0.44	0.39	1.15				16.0		41.1	
	2797	**Core**	4.8	0.57	0.30	0.34	1.04				9.2		31.8	
	2879	**Core**	5.0	1.60	0.35	0.39	1.04	0.89	1.27	0.78	19.1		51.9	47.3
	2995	**Cutting**	35.2	1.36	0.33	0.34	1.02	1.55	1.61	0.80		31.8		57.9
Hot shale	**3095**	**Core**	49.9	1.34	0.32	0.39	1.01	1.70	2.29	0.81	27.5	29.4	56.0	51.9
	3103	**Cutting**	65.3	1.12	0.36	0.31	1.01							
I3-NC186	**1137**	**Cutting**	13.0	0.73	0.36	0.43	1.31							
	1271	**Cutting**	12.0	0.92	0.36	0.35	1.20							
	1353	**Cutting**	16.0	0.90	0.53	0.39	1.20	1.20	1.02	0.68	6.1		32.3	
	1399	**Cutting**	25.0	1.23	0.52	0.34	1.30	1.45	1.26	0.77	16.8	13.6	42.7	33.3
Hot shale	**1408**	**Cutting**	40.2	bd	bd	bd	bd	1.51	1.50	0.81		12.1		39.0
	1417	**Cutting**	44.2	bd	bd	bd	bd	1.60	4.21	0.90	14.1	11.4	34.7	25.2

Pr/Ph ratio = Pristane/Phytane, **2-MN/1-MN** (*m/z* 142) methylnaphthalene, **4-MDBT/1-MDBT** (*m/z* 198) methyldibenzothiophenes,
Methylphenanthrene index (MPI-1) = 1.5(2-MP+3-MP)/(P+1-MP+9-MP) (*m/z* 192+178), Equivalent vitrinite reflectance (RVc) = 0.6+(MPI-1)+0.4,
$2C_5$/total C_5 = (1-ethyl-2,3,6-trimethyl-and-1-ethyl-3,4,5-trimethylbenzenes)/(total C5-benzenes)%, **$2C_4$/totalC_4** = (1,2,3,4- and 1,2,3,5 tetramethylbenzenes)/(total 4-benzenes)%.
bd = biodegraded, **Carbon preference index** $CPI = \frac{1}{2}\left[\frac{C_{25}+C_{27}+C_{29}+C_{31}+C_{33}}{C_{24}+C_{26}+C_{28}+C_{30}+C_{32}} + \frac{C_{25}+C_{27}+C_{29}+C_{31}+C_{33}}{C_{26}+C_{28}+C_{30}+C_{32}+C_{34}}\right]$

2.2.5. Pyrolysis-gas chromatography-mass spectrometry

An aliquot of the kerogen fraction isolated for the maceral quantification was ultrasonically extracted with DCM/MeOH (9/1: v/v) to remove soluble organics (bitumen). This material was subsequently centrifuged and decanted several times until the solvent remained colorless. Both this pre-cleaned kerogen and the precipitated asphaltenes (see above) were analysed by pyrolysis GC-MS, using a Horizon Instruments Curie-point pyrolyser coupled online to a GC-MS. Approximately 100 μg of kerogen and asphaltenes was heated for 5 s at 600°C. The pyrolysis unit was connected to a Carlo Erba GC8060 gas chromatograph and pyrolysis products were separated using a fused silica column (Varian, 25 m, 0.32 mm i.d.) coated with CP-Sil5 (film thickness of 0.40 μm). Helium was used as the carrier gas. The oven was initially kept at 40°C for 1 min; it was subsequently heated at a rate of 7°C/min to 320°C and maintained at that temperature for 15 min. The column was coupled to a Fisons MD800 mass spectrometer (mass range *m/z* 45-650, ionization energy at 70 eV, cycle time of 0.7 s). Identification of the compounds was carried out by comparing their mass spectra with a NIST library or by interpretation of spectra and relative retention time data using literature data (e.g. Hartgers *et al.*, 1992 for alkylbenzene identification).

3. Results

3.1. Microscopic examination

The lower part of the Tanezzuft formation consists of laminated, black dark shale. Throughout the Ghadamis core A1-70, only very limited evidence exists for bioturbation, based on sporadic infills with coarser-grained sediments (silt and sandstone). Such phenomena were observed above the base of the "hot" shale (at depths of 2789 m to 2730 m), but not in any other samples examined.

Microscopic examination of isolated kerogen fractions, particularly those from the "hot" shale of core A1-70 at a depth of 3095 m and core I3-NC186 at a depth 1417 m, revealed a considerable amount of amorphous organic matter (AOM). In both "hot" shales from the Murzuq and Ghadamis basins. appreciable amounts of pyrite were observed (Figs. 3A, B and C). Microscopic examination of the kerogen fractions indicates that the "hot" shale from A1-70 (interval 3103 m to 3095 m) in Ghadamis Basin and I3-NC186 (1417 m to 1399 m) in the Murzuq Basin contains, in addition to AOM, palynomorphs (acritarch, prasinophytes), phytoclasts and graptolite. The AOM itself appeared well aggregated (flaky), yellow-brown and granular textured under white light and yellow fluorescent using ultraviolet light excitation. The preservation of the various types of organic-walled microfossils was variable, ranging from very good-, indicated by light yellow colours of vesicle walls, to medium as indicated by more brownish colours. Still, all palynomorphs had a translucent amber to brown colour and, therefore, are unlikely to have undergone very high levels of thermal maturation. Based on their colour, there were no reworked acritarchs. Prasinophytes, abundant between 3103 m and 3095 m in A1-70 and 1417 m and 1399 m in I3-NC186, are represented by *Leiosphaeridia* (thick-walled spherical bodies), *Tasmanites* (large, thick, walled and produced by marine algae),

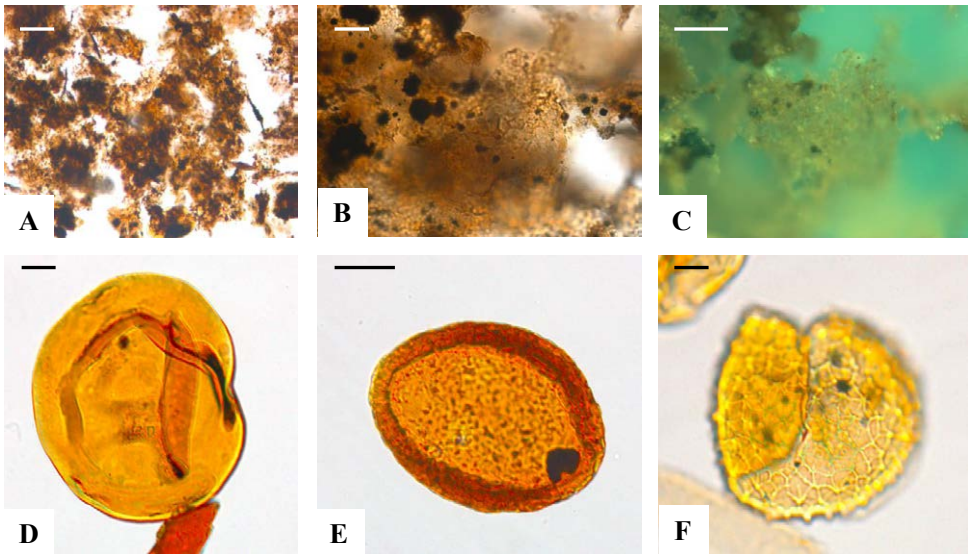

Fig. 3. (A and B) – Amorphous organic matter (AOM) from I3-NC186 borehole, (Murzuq Basin) at interval of 1417 m, (C) AOM under fluorescent light excitation of well preserved AOM from the 'hot" shale interval in borehole A1-70, (D) *Leiosphaeridia* (thick-walled spherical bodies), (E) *Tasmanites* (large, thick, perforate walled), (F) *Cymatiosphaera* sp. (scale bar equals 40µm, X100)

and *Cymatiosphaera sp*. (Fig. 3, D, E, and F). Above the "hot" shale in both boreholes the observed prasinophytes showed a gradual decrease in relative abundance and ultimately are absent from the upper part of the Tanezzuft and Akakus Formations.

3.2. TOC and Rock-Eval pyrolysis

The TOC contents for A1-70 (Ghadamis Basin) and I3-NC186 (Murzuq Basin) are shown in Fig. 4A and 4B, respectively. Within the section studied from the Ghadamis Basin organic carbon ranges from 0.27 to 22.3 wt. % (Table 1), with highest values at the base of the Tanezzuft formation. On gamma-ray logs the "hot" shale shows the well-known typical response, with gamma-ray values increasing at elevated TOC values. The "hot" shale interval, based on the gamma ray log (>150 API), contains between 3.0 to 22.3 wt. % TOC. A return to relatively low TOC values (< 0.99 wt. %) is observed in the Silurian section composed of silty shales (3045 m and 2728 m) (Fig. 4A). The bioturbated shales of the upper part of the Akakus Formation (2804 m and 2728 m) consist of grey shale, siltstone and sandstones, having even lower TOC values (< 0.25 wt. %). In the section studied from the Murzuq Basin the TOC content varies between 0.38 and 15.0 wt. %, with highest values again being observed at the base of the Tanezzuft Formation (Fig. 4B). Also, here this unit is characterized by high radioactivity, albeit somewhat lower compared to that of the Ghadamis Basin (API > 150).

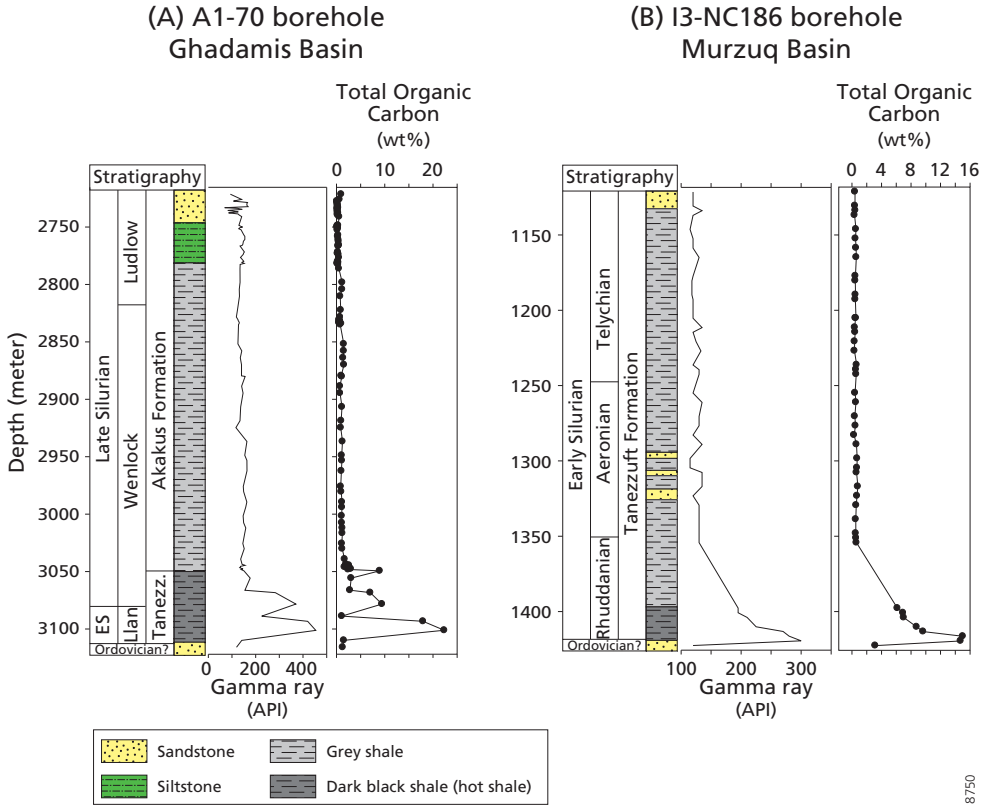

Fig. 4. Gamma ray with correlation TOC content for the A1-70 borehole (Ghadamis Basin) and the I3-NC186 borehole (Murzuq Basin). Abbreviations: ES- Early Silurian; Llan- Llandovery; Tanez- Tanezzuft Formation.

The upper Tanezzuft Formation in Murzuq (1353 m to 1134 m) consists of alternating shales and siltstones with a TOC content of typically <1%.

From the Tanezzuft Formation six shale samples were selected for Rock-Eval pyrolysis; six samples came from the Murzuq Basin (Table 1). In the Ghadamis basin average hydrocarbon potential based on Rock Eval (S2), within the "hot" shale interval (3103 m to 3095 m) ranges between 26.1 and 43.0 mg HC/g rock (Table 1). The hydrogen index (HI) shows values of 117 and 240 mg HC/g TOC, whereas Oxygen index (OI) values are low, at 5 and 9 mg CO_2/g TOC. Accordingly, the calculated production index (PI) values range from 0.14 to 0.15. The pyrolysis temperature indicator (T_{max}) ranges from 440 to 445 °C. In the TOC-lean shale (2995 m to 2730 m) S2 values are much lower, ranging from 0.3 to 3.3 mg HC/g rock (Table 1). The HI values are similar, ranging from 82 to 333 mg HC/g TOC, whereas OI average values are much higher, between 95 and 256 mg CO_2/g TOC. In the TOC-lean shale T_{max} is similar, between 426 and 436 °C. The calculated PI values range from 0.08 to 0.27. In the Murzuq basin within the "hot" shale interval (1417 m and 1399 m) S2 values range from 8.4 to 19.7 mg HC/g rock. In

the same interval HI values range from 96 to 133 mg HC/g TOC and are associated with relatively low OI values ranging from 13 to 59 mg CO_2/g TOC. T_{max} values within the "hot" shale are fairly uniform, between 438 and 445 ˚C. Calculated PI values Murzuq "hot" shale range from 0.09 to 0.12. In contrast, within the lean shale interval (1353 m and 1137 m) S2 values are very low, ranging between 0.3 and 0.4 mg HC/g rock. HI values for the lean shale samples ranged between 42 and 80 mg HC/g TOC. OI values ranged between 80 and 203 mg CO_2/g TOC. T_{max} values of the TOC- lean shales were in the range between 426 and 428 ˚C. The calculated PI for the TOC-lean shales ranged from 0.14 to 0.21.

3.3. Hydrocarbon biomarker analysis

Twelve samples were analyzed for their biomarker contents (Table 2). Distributions of hydrocarbon biomarkers of representative samples are shown in Figs. 5A and B (Ghadamis Basin) and Fig. 6A, B and C (Murzuq Basin). These examples correspond to "hot" versus lean shale from each basin, with one additional sample being added from the top of the "hot" shale in Murzuq Basin to investigate internal consistency.

The gas chromatograms of the saturated hydrocarbon fraction of rocks from the Ghadamis basin (Fig. 5) show smooth *n*-alkane distributions from C_{14} to C_{30} with no odd over even predominance (CPI ≈1.0, Table 2). The pristane/phytane (Pr/Ph) ratio ranged from 0.96 to 1.6, with *n*-C_{17} alkane being more abundant than Pr. The lower Silurian Tanezzuft Formation "hot" shale shows an *n*-alkane distribution dominated generally by short-chain (*n*-C_{14}-C_{19}) over long-chain *n*-alkanes, with a maximum at *n*-C_{16}-C_{17}. For all samples from the Ghadamis Basin the Pr/*n*-C_{17} and Ph/*n*-C_{18} ratios show values ranging from 0.30 to 0.44.

In the rocks from the "hot" shale in the Murzuq Basin the gas chromatograms of the saturated hydrocarbon fraction show signs of some biodegradation (Fig. 6B and C and Table 2). The *n*-alkanes and the isoprenoids Pr and Ph are present in low abundance, whereas an unresolved complex mixture (UCM) has developed. Comparing the upper and lower "hot" shale interval suggests higher amounts of hydrocarbons present at the upper part. The sample from the TOC-lean shale still contains appreciable amounts of *n*-alkane and Pr and Ph, in a distribution that is comparable to the TOC-lean rocks in the Ghadamis Basin (cf. Figs. 5 and 6).

An *m/z* 191 mass chromatogram was used to identify potential differences in the occurrence of hopanes between the lean and "hot" shales in both basins. Except for the two lower intervals in Murzuq Basin hopanes and tricyclic terpanes were identified in all intervals studied, although the relative abundances in the "hot" shales were low. Where hopanes could be identified, they are dominated by the thermally stablest 17α(H), 21β(H)-hopanes ranging from C_{27} to C_{35} with C_{29} and C_{30} dominating the sample at 2879 m (Fig. 5A). The 22S epimers are more abundant than the 22R epimers to the extent that they have reached the thermodynamic equilibrium (Peters *et al.*, 2005). This implies that throughout the sections studied in both basins the organic matter is thermally mature beyond the useful range for applying hopane isomer ratios.

The aromatic fraction of the extracts of the rocks from the Ghadamis Basin contains alkylbenzenes, naphthalene and a limited amount of methylnaphthalenes (Fig. 5). Phenanthrene and methylphenanthrene are superimposed on a pronounced UCM.

Alkylbenzenes were detected in the aromatic fraction extracted from both "hot" and lean shale, monitoring fragment ions at m/z 133+134 (Figs 5A and B). The most abundant compounds were identified as a series of C_{15}-C_{23} aryl isoprenoids with 1-alkyl-2,3,6-trimethylbenzenes (Summons & Powell, 1987) as the most abundant. Minor amount of 1-alkyl-2,3,6-trimethylbenzenes were tentatively identified in rock extracts of the Ghadamis TOC-lean shale (not shown).

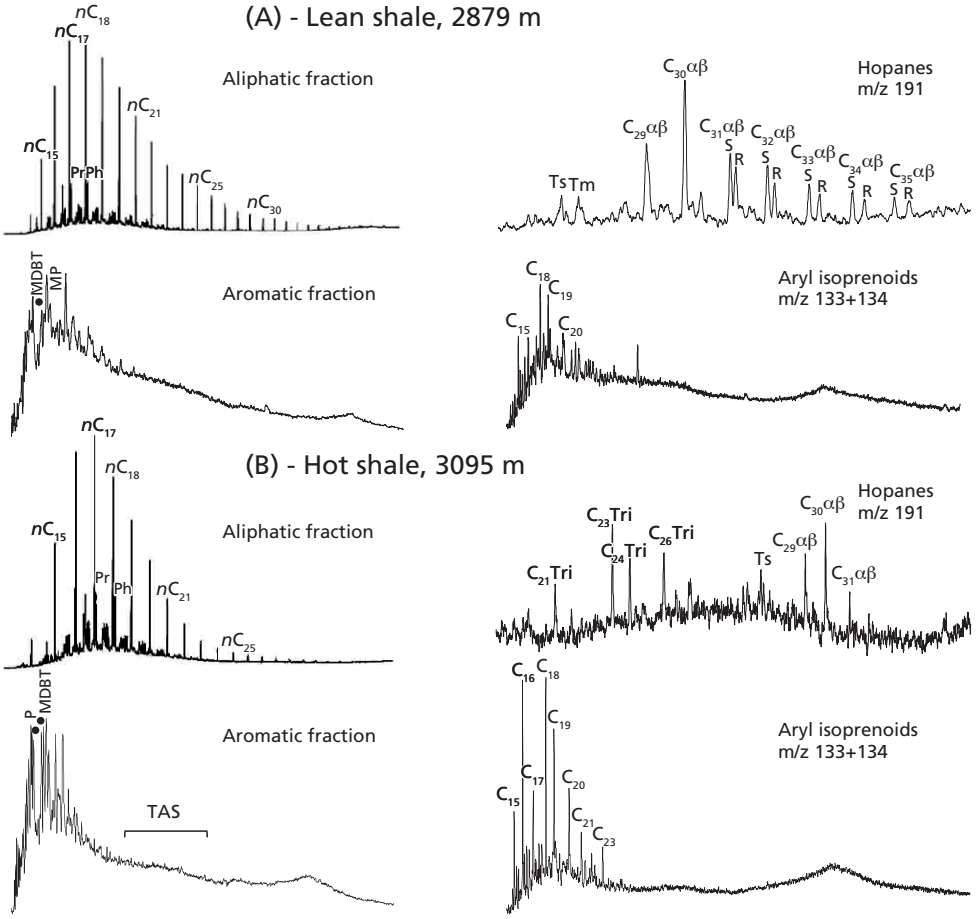

Fig. 5. Gas chromatograms (FID) of the total aliphatic hydrocarbon fraction, mass chromatograms *m/z* 191 of aliphatic fraction showing the hopane distribution, gas chromatograms (TIC) of the total aromatic hydrocarbon fraction, and summed mass chromatogram of *m/z* 133+134, showing the aryl isoprenoid distribution of the 2879 m (A) and 3095 m (B) samples from A1-70 borehole (Ghadamis Basin). Peak identification: Pr- pristane, Ph- phytane, P- phenanthrene, MP- methylphenanthrenes, MDBT- methyldibenzothiophene, TAS- Triaromatic steroids,Ts = C_{27} 18α(H)-trisnomeohopane, Tm = C_{27} 17α(H)-trisnomeohopane, Tri =Tricyclic terpanes.

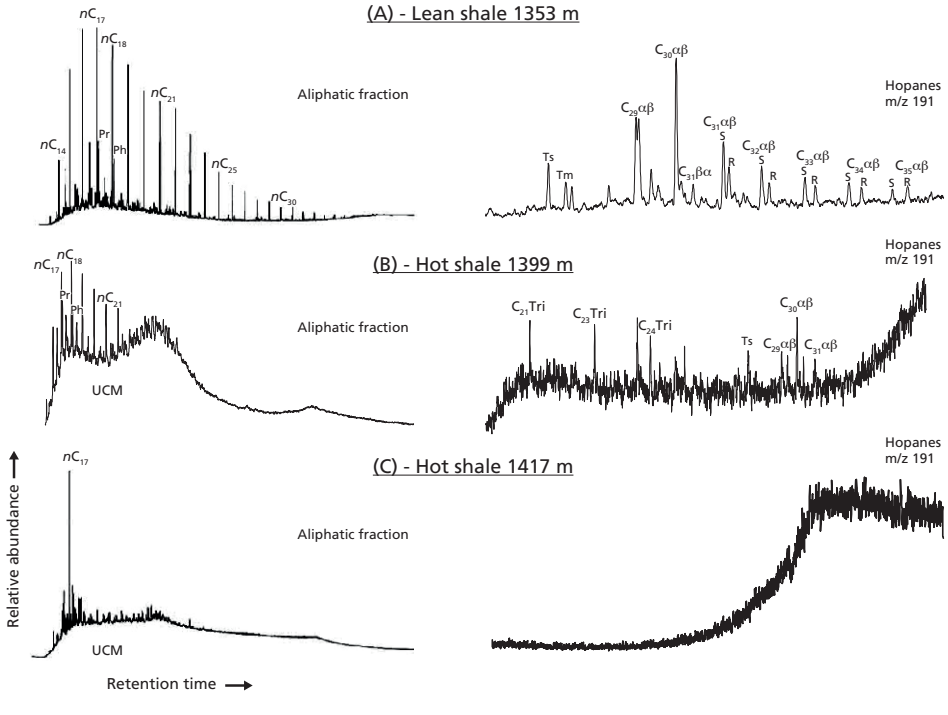

Fig. 6. Gas chromatograms (FID) and mass chromatograms *m/z* 191 of aliphatic fraction showing the hopane distribution of samples 1353 m (A), 1399 m (B) and (C) 1417 m from I3-NC186 borehole, (Murzuq Basin). UCM- Unresolved Complex Mixture. Peak identified refer to Fig.5.

3.4. Pyrolysis-gas chromatography-mass spectrometry

Two isolated kerogens from the "hot" shale (Type II) and two isolated kerogens from the lean shale (Type III) were analyzed by Curie-point pyrolysis gas chromatography-mass spectrometry. All flash pyrolysates were characterized by *n*-alkene/*n*-alkane doublets ranging in carbon number from C_8 to C_{30} (Fig. 7). We noticed the absence of prist-1-ene from all kerogen pyrolysates, which is in agreement with the relatively high level of thermal maturity (Goossens *et al.*, 1988), and a large UCM. In all pyrolysates an important contribution from alkylbenzenes is noted. In the "hot" shale of Ghadamis 1,2,3,4-tetramethylbenzene (TMB) is actually the most abundant compound produced from the kerogen during pyrolysis (Figure 7A).

To explore the relative distribution of alkylbenzenes in more detail we plotted partial summed mass chromatograms (*m/z* 78+91+92+105+106+119+120+133+134+147+148) revealing their distribution (Fig. 8). Substantial differences in the distribution patterns of C_0-C_4 alkylbenzenes in pyrolysates of the Ghadamis and Murzuq basins kerogen

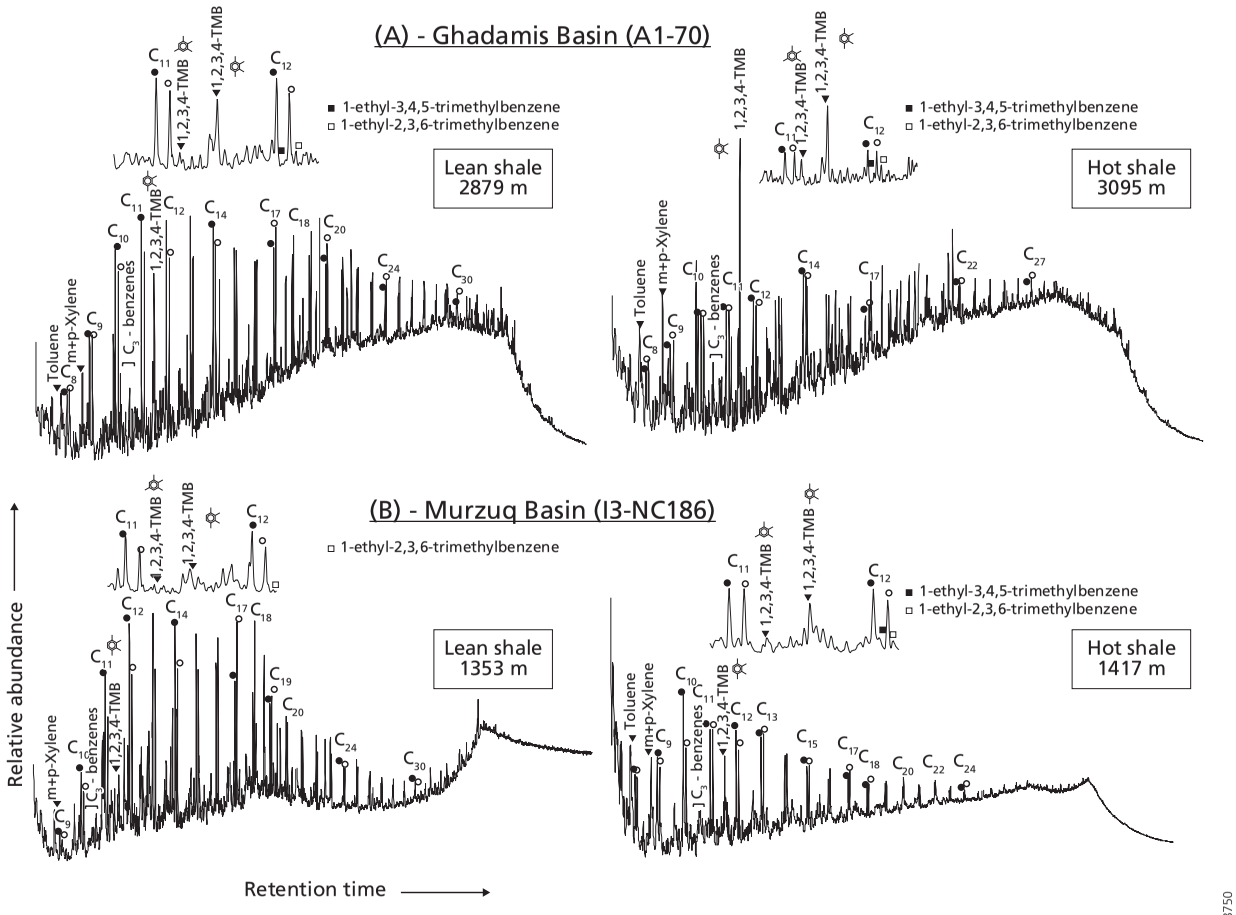

Fig 7. Total ion current (TIC) traces of the flash pyrolysates (Curie temperature 600 °C) of isolated kerogen from source rocks (TOC-lean shale and hot shale) of (A) A1-70 borehole, (Ghadamis basin) and (B) I3-NC186 borehole, (Murzuq basin). Peak identifications: 1,2,3,4-tetramethylbenzene (TMB); (closed circle) *n*-alkene and (open circle) *n*-alkane.

Peak	Compounds
1	Benzene
2	Toluene
3	Ethylbenzene
4+5	1,3 and 1,4-Dimethylbenzene
6	1,2-Dimethylbenzene
7	*n* -Propylbenzene
8	1-Methyl-3-ethylbenzene
9	1,3,5-Trimethylbenzene
10	1-Methyl-2-ethylbenzene
11	1,2,4-Trimethylbenzene
12	1,2,3-Trimethylbenzene
13	Dimethylethylbenzene
14	1,2,3,5-Tetramethylbenzene
15	1,2,3,4-Tetramethylbenzene
16	1-Ethyl-3,4,5-tetramethylbenzene
17	1-Ethyl-2,3,6-tetramethylbenzene

Table 3. Major alkylbenzenes (Fig. 8) identified in the pyrolysates of the kerogen fractions.

are seen (Figs. 8A and B, respectively). The pyrolysate of the Murzuq Basin kerogen (both "hot" and lean shale) is dominated by relatively higher abundances of benzene, toluene, m- and p-xylene (1,3-and 1,4-dimethylbenzene), 1-methyl-3-ethylbenzene, 1,2,4-trimethylbenzene compared to the Ghadamis Basin kerogen pyrolysates. Ghadamis Basin kerogen pyrolysates are characterized by high relative abundances of the C_4-alkylbenzenes TMB and, to a lesser extent, 1,2,3,5-tetramethylbenzene (compounds numbers, 15 and 17, respectively in Fig. 8, table 3). C_5-alkylbenzenes are present in the pyrolysates of all seven kerogens (see insets in Figs. 8A and B) as exemplified by using mass chromatograms of their molecular ion (*m/z* 148; cf. Hartgers et al., 1992). The C_5-alkylbenzenes in the Ghadamis "hot" and lean shale pyrolysates are dominated by 1-ethyl-2,3,6-trimethylbenzene (compound number 17 in Fig. 8A) and, to a lesser extent, 1-ethyl-3,4,5-trimethylbenzene (compound 16). In the C_5-alkylbenzene distribution of the Murzuq Basin kerogen pyrolysates (Fig 8B) these two isomers are less abundant.

Fig. 9 shows the TIC traces from asphaltene pyrolysates. A general feature of the asphaltene pyrolysates was the presence of *n*-alkene/*n*-alkane doublets although they are much less abundant than in the corresponding kerogen pyrolysates (Fig. 7). All asphaltene pyrolysates also showed considerable UCMs. Alkylbenzenes were also important pyrolysis products and, again, the relatively high abundance of TMB in the Ghadamis "hot" shale is notable. The asphaltene pyrolysates from the Murzuq and Ghadamis "hot" shales are also characterized by relatively high abundances of alkylnaphtalenes, although the relative concentrations of alkylnaphthalenes in the Ghadamis asphaltene pyrolysates is much higher compared to those from Murzuq. To reveal the distributions of alkylnaphthalenes, alkylphenanthrenes and alkyldibenzothiophenes for the Ghadamis and Murzuq "hot" shale partial summed mass chromatograms of m/z 128+142+156+170

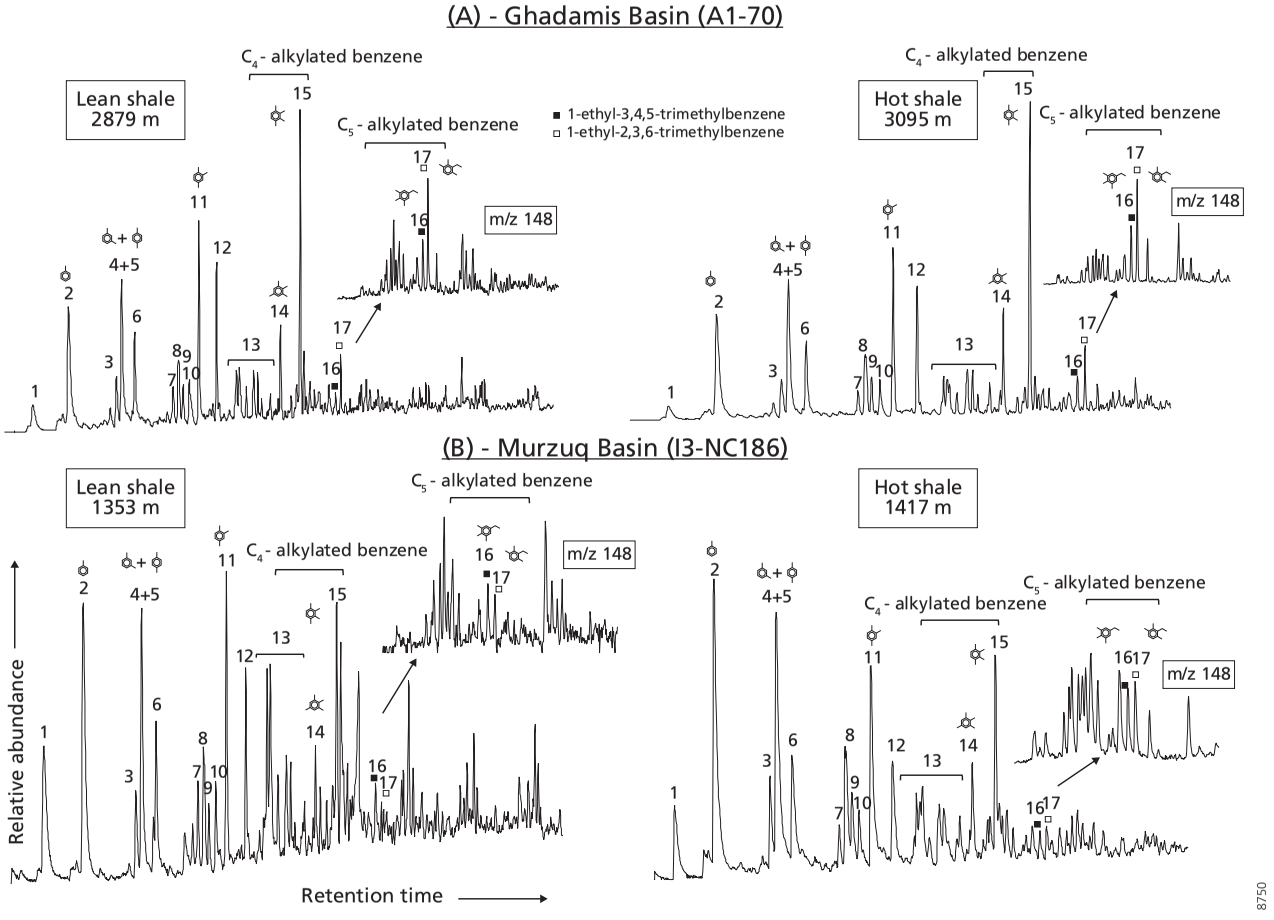

Fig. 8. Mass chromatograms (*m/z* 78+91+92+105+106+119+120+133+134+147+148) of the 600 °C Curie-point pyrolysate of kerogen fractions of (A) A1-70 borehole (Ghadamis Basin) and (B) I3-NC186 borehole (Murzuq Basin), revealing typical distribution of benzene, toluene and C_2-C_5 alkylatedbenzenes. The identification of the number peaks is listed in Table (3).

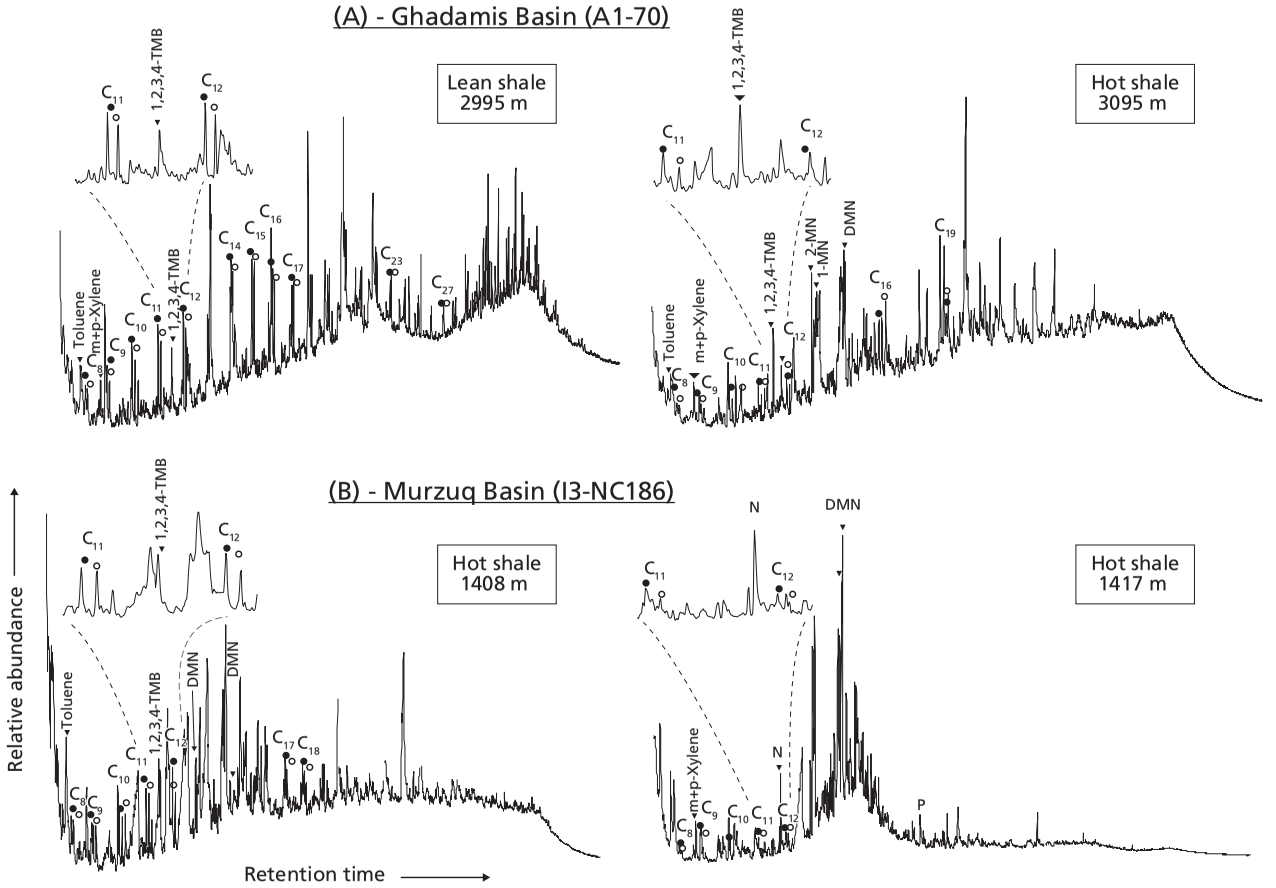

Fig. 9. TIC traces of the flash pyrolysates (Curie temperature 600 °C) of isolated asphaltenes from rock extracts of (A) A1-70 borehole, Ghadamis Basin and (B) I3-NC186 borehole Murzuq Basin. Peak identification; 1,2,3,4-tetramethylbenzene (TMB); N- Naphthalene; MN- Methylnaphthalene; DMN- Dimethylnaphthalene; P- Phenanthrene; (closed circle) *n*-alkene and (open circle) *n*-alkane.

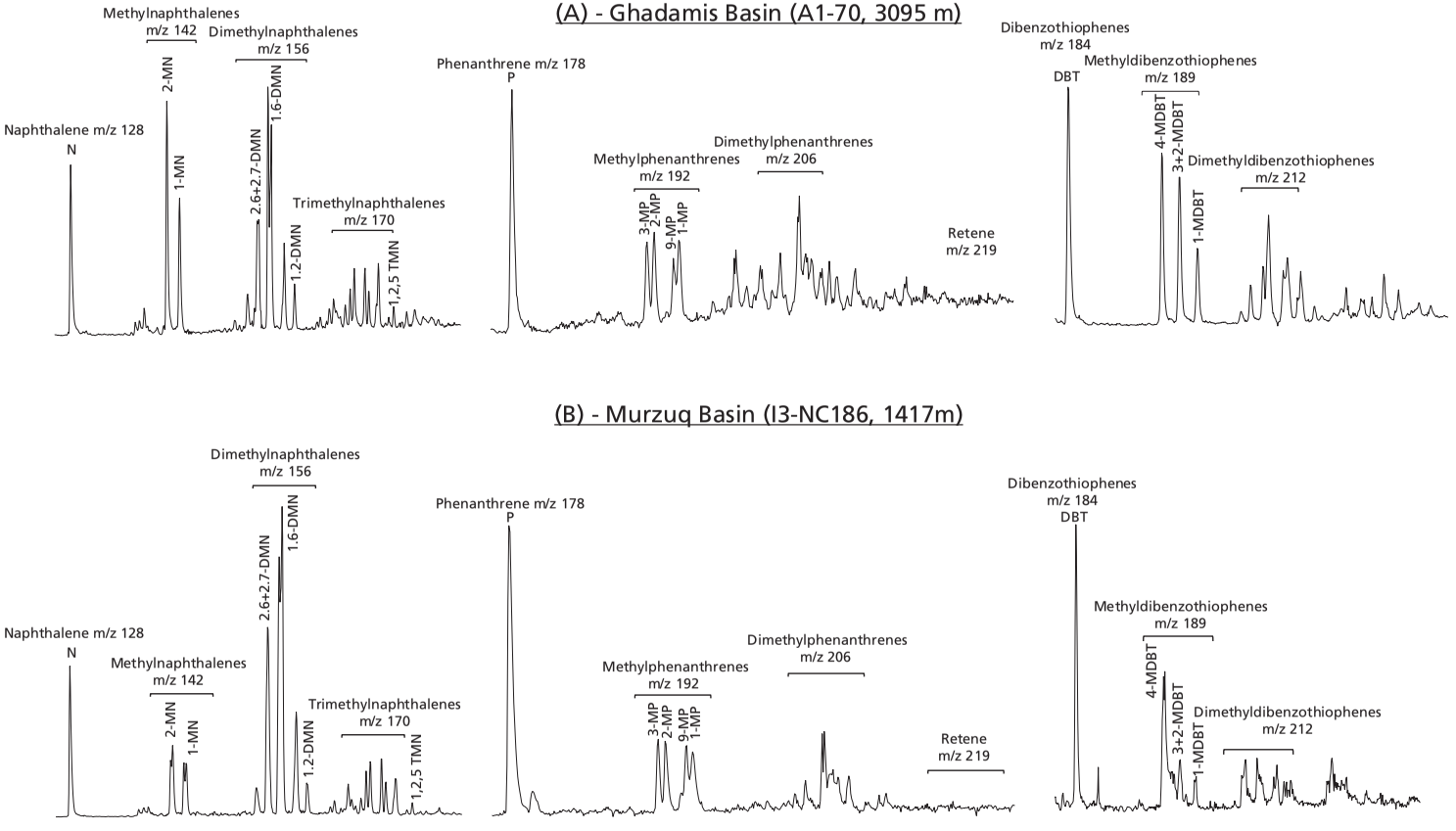

Fig. 10. Mass chromatograms of alkylnaphthalenes (*m/z* 128+142+156+170); alkylphenanthrene (*m/z* 178+192+206+219); and alkyldibenzothiophene (*m/z* 184+198+212) in pyrolysates from asphalthenes of (A) A1-70 borehole, Ghadamis Basin and (B) I3-NC186 borehole Murzuq Basin. Refer to Fig. 9 for peak identification.

(alkylnaphthalenes), m/z 178+192+206+220 (alkylphenanthrenes), and m/z 184+198+212 (alkyldibenzothiophenes) were used (Figs. 10A-B, respectively).

The methylphenanthrene index (MPI-1) was subsequently calculated and translated into vitrinite equivalents (VRc%) (Radke & Welte, 1983). In Table 2, it can be observed that the VRc increases from 0.68 to 0.90 in Murzuq Basin, going from the TOC-lean toward the "hot" shale. In Ghadamis Basin the MPI-1 values are relatively constant at about 0.8. Based on similar components Hughes (1984) proposed a maturity index based on methylnaphthalenes, taking the ratio between 2-MN and 1-MN. This ratio (based on the peak area of the selected fragment ions *m/z* 142) was suggested to increase with increasing maturity. In the Ghadamis Basin values ranged from 0.89 to 1.70, going from the lean shale towards the "hot" shale, whereas in Murzuq Basin ratio varies from 1.20 in the lean shale towards 1.60 in the "hot" shale. A similar ratio has been proposed based on the relative concentrations of methyldibenzothiophenes (MDBT) (m/z 198), using relative abundances of the 2 + 3-MDBT compared to 4-MDBT (Hughes, 1984). We noticed that 4-MDBT was the most abundant compound, whereas 1-MDBT decreased relatively to 2 + 3-MDBT and 4-MDBT. The 4-MDBT/1-MDBT ratio was proposed as maturity parameters to distinguish more detailed changes in maturity within kerogen type II and III source rocks (Radke *et al*., 1986). The 4-MDBT/1-MDBT ratios (based on the integrated peak areas of the selected fragment ion *m/z* 189) increased from 1.27 to 2.29 from the lean toward the "hot" shale in the Ghadamis Basin and from 1.26 to 4.21 in the Murzuq Basin towards the "hot" shale.

4. Discussion

4.1. Assessment of the thermal maturity level

A variety of maturity indicators have been developed to evaluate the thermal maturity level of source rocks (Tissot & Welte, 1984). Here, we use indicators based on the molecular composition of pyrolysates of asphaltenes with the more traditional Rock Eval based maturity index T_{max}. To test the robustness of such indicators, we contrasted the "hot" and lean shales in the Ghadamis and Murzuq basins, which encompass a large range of TOC content. Moreover, whereas the "hot" shale in the Murzuq Basin shows signs of some biodegradation, the Ghadamis "hot" shale does not. Maturity levels were based on T_{max}, methyldibenzohiophene (MDBT-4/MDBT-1), methylnaphthalenes (2-MN/1-MN ratio) and the methylphenanthrene ratio (MPI-1) (Table 2). True vitrinite is not found in rocks of Silurian age; therefore, some authors have, proposed using reflectivity measurements on zooclasts such as graptolites and chitinozoans (Tyson, 1993). Others used organic compound ratios (Radke *et al*., 1986).

The best-established geochemical maturity index is arguably Rock Eval based T_{max} (Peters, 1986). The increase in T_{max} values with depth in both Ghadamis and Murzuq basins (Table 1) suggests that maturity increases with higher temperatures deeper in the sedimentary column. Although no heat flow data is available, this is in line with what is expected. The T_{max} values for the two basins are similar. Since the the Murzuq basin "hot" shale is somewhat biodegraded, this confirms that T_{max} is a robust parameter for maturity in these settings. A plot of HI and OI versus T_{max} can be used to classify the type

of kerogen and maturity (Figs. 11A- B, respectively). This plot shows that the "hot" shale samples contain Type II kerogen, whereas the lean shale is more in line with Type III kerogen.

The production index (PI) is also used as a maturity evaluation tool (Langford & Blanc-Valleron, 1990). In general, T_{max} and PI are positively correlated. In both basins studied here, the PI values in the "hot" shale are relatively low, which suggests that they are mature. The somewhat higher values in the lean shale might be related to the fact that a relative contribution of contaminants (e.g. drilling mud and additives) would be much higher with low TOC content. Still, since we used both cutting and core samples and do not observe an appreciable offset between these two this is probably of minor importance . Overall, the relationship between PI and T_{max} (Fig. 12) indicates that the "hot" shales in both Murzuq and Ghadamis basins are thermally (post)mature (oil window) and hydrocarbons have been generated (Peters, 1986).

Plotting S2 *vs.* TOC (Fig. 13) shows that the HI value for the "hot" shale in Ghadamis and Murzuq basins is relatively limited between 100 and 300 mg HC/g TOC. In both basins the "hot" shale contains Type II kerogen, which is based on the T_{max}-values. Moreover, a cross-plot between OI and HI values (so-called Van Krevelen diagram; Fig. 11B) shows that the kerogen is Type II and III. Still, these parameters do not allow for distinguishing potential effects of biodegradation. Moreover, after hydrocarbons have been produced and expelled from the potential source rock, this results in a drop in HI values.

An alternative index is based on changes in relative concentrations of phenanthrene and the methylphenanthrene complex in response to thermal maturity, which was shown to be relative independent of organic matter type (Radke, 1983). Radke *et al.* (1986) observed an increase in the relative amount of 2- and 3-methylphenanthrenes compared

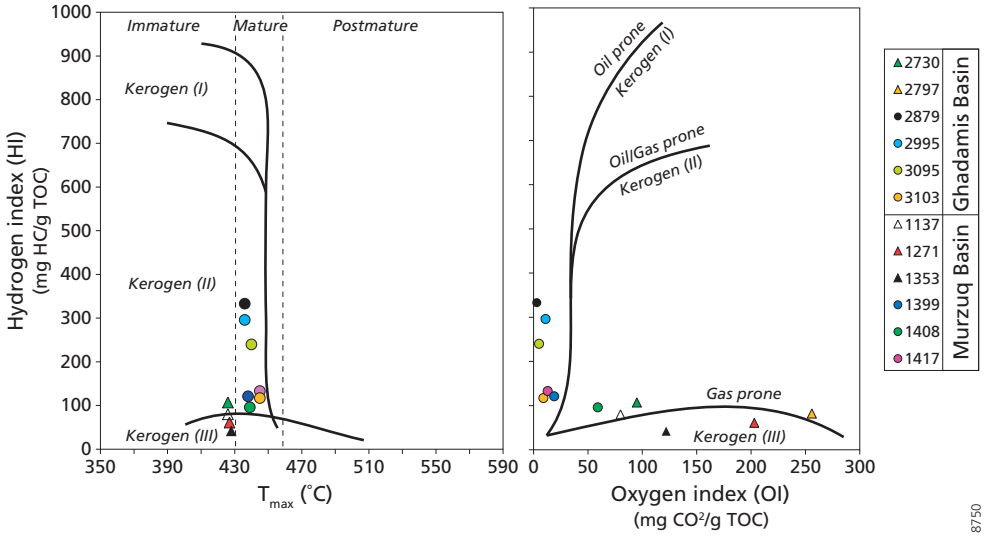

Fig. 11. Plot of (A) HI versus pyrolysis T_{max} and (B) HI versus OI for the analyzed shale samples from boreholes A1-70 (Ghadamis Basin) and I3-NC186 (Murzuq Basin), showing kerogen quality and thermal maturity stages.

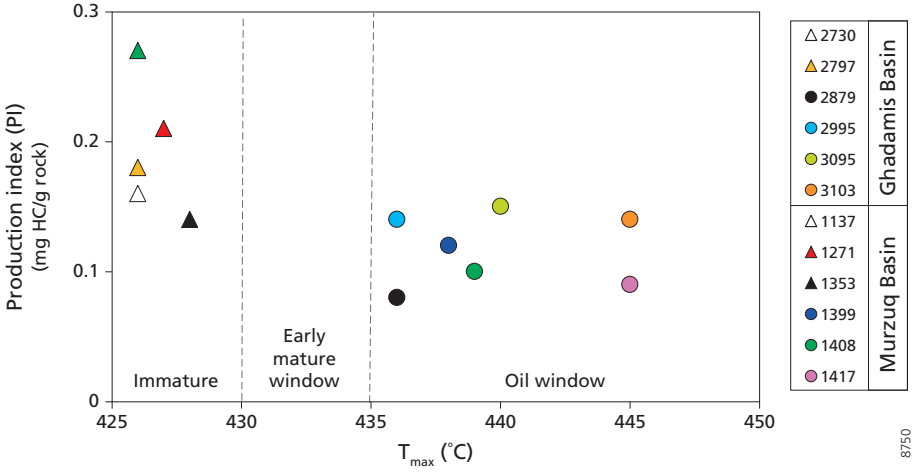

Fig. 12. Plot of T_{max} against PI for rocks from borehole A1-70 (Ghadamis Basin) and I3-NC186 (Murzuq Basin). Triangles are used for TOC-lean shales and circles for the hot shales.

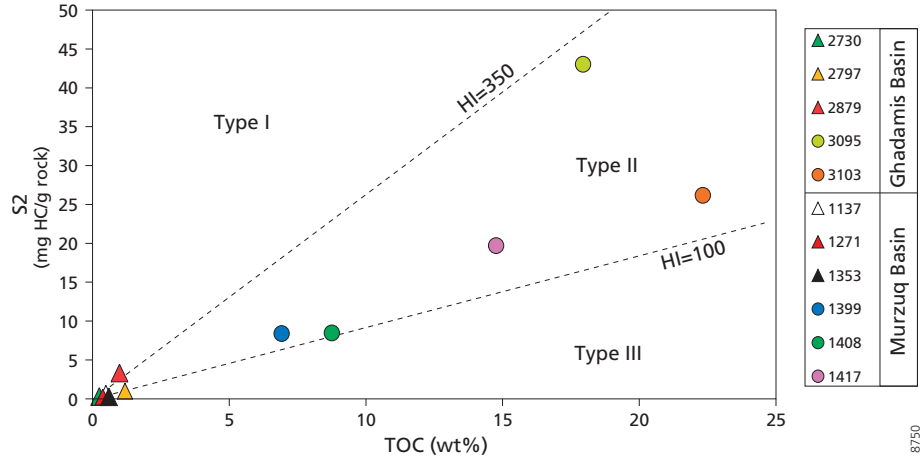

Fig. 13. Cross-plot between S_2 and TOC for A1-70 (Ghadamis Basin) and I3-NC186 (Murzuq Basin). (Langoford and Blanc-Valleron, 1990). The line represents a transition between kerogen types. Triangles are used for TOC-lean shales and circles for the hot shales.

to 1- and 9-methylphenanthrenes with increasing burial depth and temperature. This can be explained in terms of rearrangement of monomethylphenanthrenes, favouring, the thermodynamically more stable 2- and 3-positions at high temperature. The general concept is based on higher thermal stabilities of 2- and 3-methylphenanthrenes compared to 1- and 9-methylphenanthrenes (Alexander *et al.*, 1997) and the production of phenanthrene at higher maturities. Radke *et al.* (1986) previously empirically calibrated the MPI-1 index to equivalent vitrinite reflectance (VRc %) (Table 2). This ratio can also be applied to asphaltene pyrolysates (Sarmah *et al.*, 2010).

Comparing the asphaltene-derived methylphenanthrene index (MPI-1) with T_{max} here shows a clear-cut correlation (R^2=0.92), with maximum index values corresponding to highest T_{max} values (Fig. 14). Overall, both methods indicate that the Silurian source rock in Murzuq Basin is more thermally mature than that of the Ghadamis Basin. The Murzuq Basin "hot" shale shows highest calculated maturity at 0.90 VRc%, compared to 0.81% VRc% for the Ghadamis Basin. This suggests that the potential source rocks in both basins have been well within the window of oil formation. For kerogens it was not possible to calculate these ratios due to scant or no presence of the components involved. Other molecular ratios have also been proposed as indicators of source rock maturity, also based on Curie-point pyrolysis of asphaltenes. Consequently, we investigated the methylnaphthalene ratio (2-MN/1-MN) (Alexander *et al.*, 1997) and the methyldibenzothiophene ratio (4-MDBT/1-MDBT) (Alexander & Suzuki, 1995). Both these ratios show increases with increasing depth, in both basins, with highest maturity being observed for the "hot" shale The similarity in these indicators is also evident when plotting them against T_{max} (Figs. 15 and 16). Whereas the 4-MDBT/1-MDBT ratio shows that the Murzuq Basin "hot" shale has the highest thermal maturity, the 2-MN/1-MN ratio suggests that the "hot" shale in Ghadamis Basin is more mature.

The ratios discussed above were specifically developed to evaluate maturity independently from the source rock composition. Isoprenoids/*n*-alkane ratios, however, are often used to provide information not only on maturation, but also the depositional environment and secondary processes, such as biodegradation (Table 2) (Peters *et al.*, 1999). Both Pr/*n*-C_{17} and Ph/*n*-C_{18} ratios, on the one hand, increase with biodegradation due to the initial loss of *n*-alkanes; on the other hand, they decrease with increasing maturity due to the increasing dominance of these *n*-alkanes. The Ph/*n*-C_{18} and Pr/*n*-C_{17} ratios (both around 0.4) are in line with the high maturities calculated with the other indices discussed above (Hunt, 1996; Peters *et al.*, 1999). For the two deeper samples of the Murzuq Basin "hot" shale these ratios could not be calculated, as both phytane and pristane were below the level of detection due mild biodegradation (Table 1).

4.2. Palaeoenvironmental reconstruction

A relationship between TOC content and gamma ray intensity for Early Silurian shale in North Africa and Middle East is well-documented (Lüning *et al.*, 2000). Shales are defined as "hot" when the gamma-ray values exceed >150 API units, which correlates approximately with a TOC of ≥ 3% (Lüning *et al.*, 2000). The TOC content decreases from graptolitic early Silurian shales to the non-graptolitic shales in the late Silurian in both Ghadamis and Murzuq basins; it also shows a clear correspondence to the gamma ray intensity (Fig. 4A and B). The "hot" shales are characterized by high AOM and

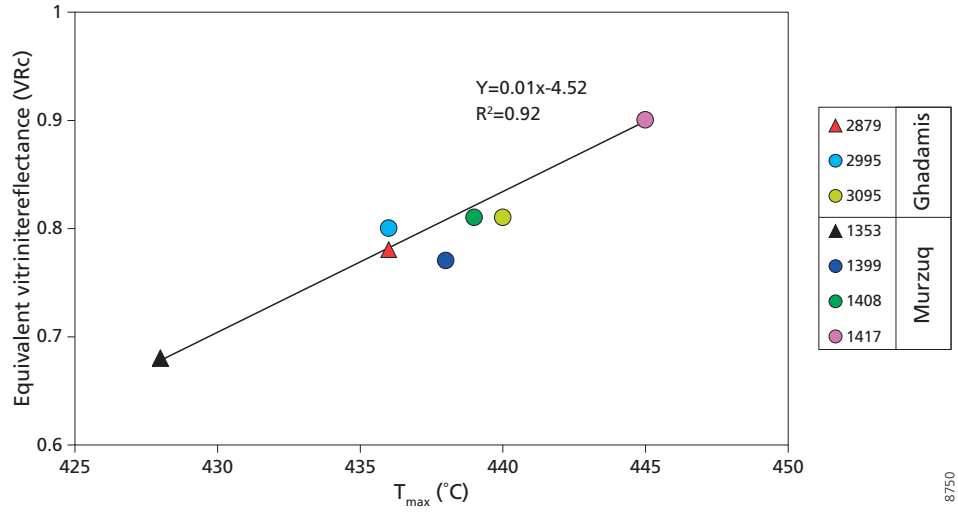

Fig. 14. Cross plot showing correlation between equivalent vitrinite reflectance based on MPI-1 and T_{max} for lean and hot shales in Murzuq and Ghadamis Basins. Triangles are used for TOC-lean shales and circles for the hot shales.

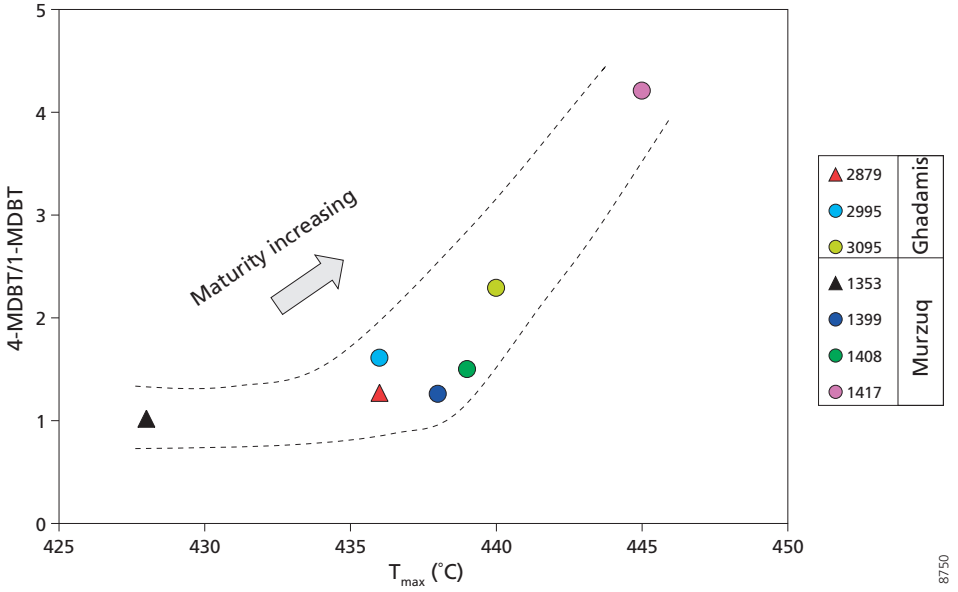

Fig. 15. Cross plot between T_{max} and 4-MDBT/1-MDBT for lean and hot shales in Murzuq and Ghadamis Basin. Triangles are used for TOC-lean shales and circles for the hot shales.

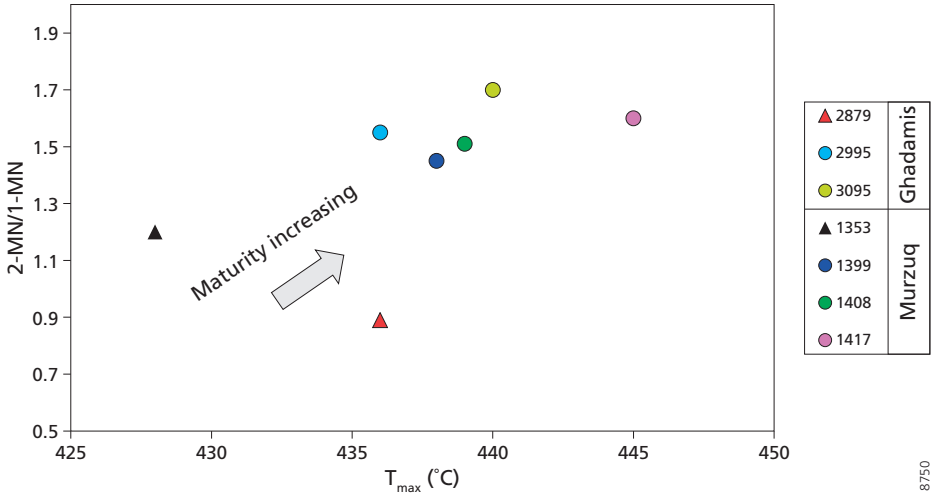

Fig. 16. Cross-plot between T_{max} and 2-MN/1-MN for lean and hot shales in Murzuq and Ghadamis basins. Triangles are used for lean shale and circles for hot shale.

show more elevated fluorescence of isolated macerals compared to other parts of the sequence studied (Fig. 3C). The high TOC contents are mainly due to good preservation of AOM, which is thus considered to be of marine origin (Tyson, 1993). A plot of HI versus T_{max} and OI can be used to classify the type of kerogen and maturity (Figs. 11A and B, respectively). This plot shows that the "hot" shale sample contains Type II kerogen, whereas the lean shale is more in line with kerogen Type III. Although the "hot" shales from the Ghadamis Basin were also affected by thermal maturation, their high TOC content and relatively high HI with low OI also indicate better preservation of AOM, thus suggesting the establishment of anoxic conditions within the sediments. For the Murzuq Basin, the HI index is smaller. The OI index still suggests anoxic conditions along with the hydrocarbons already generated. Also the presence of fine-grained pyrite (Fig. 3C) indicates that the "hot" shales were deposited under anoxic conditions (cf. Lüning *et al.*, 2000). The abundant and well-preserved prasinophytes suggest dysoxic-anoxic conditions (Tyson, 1993). The highest content of thick-walled prasinophytes (Tasmanites type algae), Leiosphaeridia and Cymatiosphaera sp. occurs in the lowermost part of the Tanezzuft in both Ghadamis and Murzuq suggesting enhanced surface water productivity (Combaz, 1966; Revill *et al.*, 1994; Tyson, 1995). High productivity and reduced bottom water oxygenation resulting in extensive black shale deposition was widespread across the entire Sahara Platform during the early Silurian (Lüning *et al.*, 2000, 2006).

The "hot" shales were followed by a return to organically leaner silts and shales in both Ghadamis and Murzuq basins (Fig. 4 and Table 1). Absence of pyrite, lower amounts of prasinophytes and less AOM all suggest a return to suboxic to oxic conditions after "hot" shale deposition. The Rock Eval analyses show a considerable change in OI and HI with depth, evidencing an overall change in kerogen composition. The HI vs. OI plot (Fig. 11B) shows that the "hot" shale kerogen is still relatively rich in hydrogen and has a low oxygen contents compared to the lean shale. Furthermore, the HI values of the "hot"

shale in Ghadamis Basin are higher than in the Murzuq Basin. The higher HI and lower OI values suggest deposition under anoxic conditions (Peters, 1986). Still, interpretations based on OI values require caution as contributions of carbon dioxide produced from unstable carbonates can increase such values (Langford & Blanc-Valleron, 1990). However, since this is often accompanied by much scatter in the data and the sediments here do not contain much carbonate the close correspondence with the other proxies is probably reflecting true changes in the depositional environment.

The ratio of pristane to phytane (Pr/Ph) has been widely used as indicators of the redox conditions at the time of deposition (Didyk *et al.*, 1978). Here these ratios have, however, been affected by both thermal maturity and biodegradation. Although the Pr/Ph ratio < 2.0 (0.57-1.60) is in line with these source rocks being deposited under typically marine anoxic conditions, this could also be coincidental. Since it is know that the Silurian strata were deposited in an open marine environment without an appreciable supply of terrestrial organic matter (pre-land plant evolution), it is expected that thermal maturity resulted in the higher Pr/Ph values (Tissot & Welte, 1984). Similar arguments also hold for the relationship between isoprenoids Pr/*n*-C_{17} and Ph/*n*-C_{18} ratios (Table 2).

In agreement with the Rock Eval data and microscopic examination, the composition of kerogen pyrolysates also suggests that the organic matter is predominantly of marine algae origin, indicated by the highly abundant series of *n*-alk-1-enes and *n*-alkanes in kerogen pyrolysates (Fig. 7A and B). *n*-Alk-1-enes/*n*-alkanes doublets are typical pyrolysis products of algaenan biopolymers, occurring in cell walls of various freshwater and marine microalgae (Horsfield, 1989). The relative abundance of doublets was seen to decrease with increasing carbon number from C_8 to C_{29}, which is typical of marine kerogens (van de Meent *et al.*, 1980).

Significant differences in distribution patterns of C_0-C_4 alkylbenzenes in the kerogen pyrolysates were observed between the Murzuq and Ghadamis basins (Fig. 8A and B). The relatively high abundance of 1,3-dimethylbenzene, 1,4-dimethylbenzene, 1,2,4-trimethylbenzene and 1,2,3,-trimethylbenzene is characteristic of kerogen from the Murzuq Basin (Fig. 8B) and is accompanied by high benzene and toluene relative abundances. Hartgers *et al.* (1994a) demonstrated that the structure of monoaromatic moieties in kerogen is biologically controlled. They proposed that a relatively high abundance of 1,3-dimethylbenzene, 1,4-dimethylbenzene and 1,2,3-trimethylbenzene is indicative of the presence of bound, non-aromatic carotenoids, which have undergone aromatization (Hartgers *et al.*, 1994a). These compounds are potentially derived from certain algae and cyanobacteria (Ratledge & Wilkinson, 1988).

The flash pyrolysates of the Ghadamis "hot" shales are characterized by relatively high abundances of 1,2,3,4-tetramethylbenzene. While being the dominant alkylbenzene in the "hot" shale pyrolysates, the relative abundance of 1,2,3,4-tetramethylbenzene in the pyrolyzates of the lean shales substantially decreased (Fig. 7A). A similar dominance of 1,2,3,4-tetramethylbenzene is observed in the pyrolysates of "hot" shale from Murzuq; the TOC-lean shales showed a much smaller contribution. Hartgers *et al.* (1994a,c) showed that this compound might be derived from macromolecular-bound aromatic carotenoids. The mechanism of incorporation is not fully understood but may involve the reaction of the double bonds with reduced forms of sulfur during early diagenesis (Koopmans *et al.*, 1996a). The aromatic carotenoids of photosynthetic green sulfur bacteria are characterized by various kinds of aromatic substitution patterns. Based on former studies

(see Sinninghe Damsté & Schouten, 2006 for a review) two of them are important for the Silurian era, i.e. isorenenieratene, containing two aromatic rings with the 1-alkyl-2,3,6-trimethylbenzene substitution pattern (Summons & Powell, 1986, 1987), and an orphan diaromatic carotenoid in which one of the aromatic rings of isorenieratene is replaced by an aromatic ring with the 1-alkyl-3,4,5-trimethylbenzene (Hartgers *et al.*, 1993) (Fig. 8). When bound to kerogen, they will produce 1,2,3,4-tetramethylbenzene, and 1,2,3,4-tetramethylbenzene and 1,3,4,5-tetramethylbenzene in a 1:1 ratio, respectively, upon ß-cleavage (Hartgers *et al.*, 1994a,c). Indeed, 1,3,4,5-tetramethylbenzene is also detected as a prominent C_4 alkylated benzene in the kerogen and asphaltene pyrolysates (Fig. 17). Although indicative of a potential presence of bound aromatic carotenoids, another study indicated that an algal origin for tetramethylbenzenes in pyrolyzates is also possible (Hoefs *et al.*, 1995). Furthermore, Koopmans *et al.* (1996b) proposed a mechanism that could explain the formation of aryl isoprenoids and thus occurrence of 1,2,3,4-tetramethylbenzene in pyrolysates, from a source other than isorenieratane. They demonstrated that aromatization of β-carotene may result in the formation of β-isorenieratane, so that diagenetic products of this compound could be an additional source of 1,2,3,4-tetramethylbenzene upon pyrolysis.

Confirmation of the origin of the tetramethylbenzenes from bound aromatic carotenoids in the pyrolyzates can be obtained by carbon isotopic analyses ($\delta^{13}C$ > -15‰ for isorenieratene-derived moieties) (Koopmans *et al.*, 1996a; Sinninghe Damsté *et al.*, 2001), but was not feasible for the produced Curie-point pyrolysates studied on-line here. Alternatively, the distribution of the C5-alkylated benzenes in the pyrolysates can be studied, since they contain potential γ-cleavage products of diaromatic carotenoids

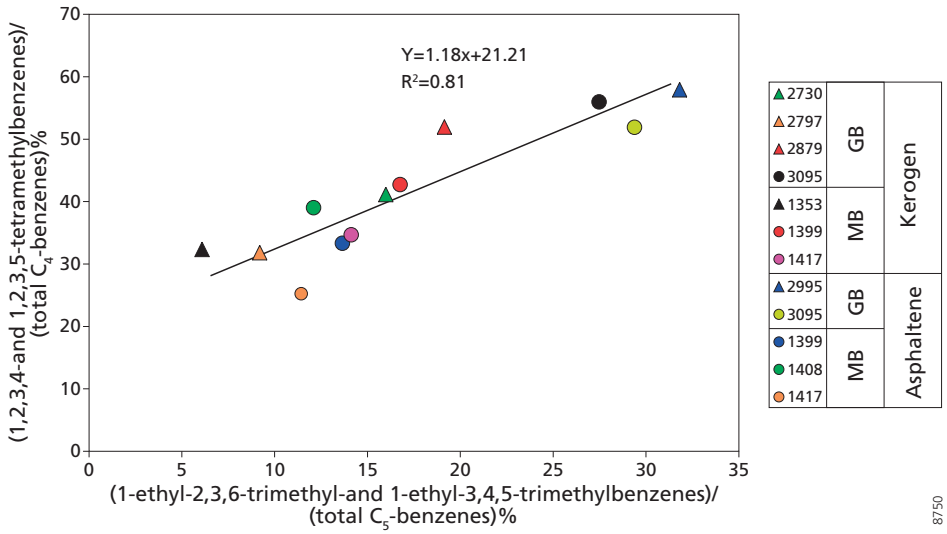

Fig. 17. Cross-plot showing correlation between 1-ethyl-2,3,6-trimethyl- and 1-ethyl-3,4,5-trimethylbenzenes)/(total C_5-benzenes)% and (1,2,3,4- and 1,2,3,5-tetramethylbenzenes)/(total C_4-benzenes)% for the hot (circle) and lean (triangle) shales from Murzuq (MB) and Ghadamis Basins (GB).

(Hartgers *et al*., 1994a). The distributions of C_5-alkylbenzenes in the kerogen and asphaltene prrolyzates of the "hot" shales of both Ghadamis and Murzuq basins show that 1-ethyl-2,3,6-trimethylbenzene and 1-ethyl-3,4,5-trimethylbenzene dominate the C_5-alkylbenzene isomers (Fig. 8), and the relative abundance of the former isomer is higher than that of the latter. This strongly suggests the presence of bound diaromatic carotenoids in the kerogen and asphaltenes. Plotting the ratio of both TMBs to the total of C_4-benzenes versus the relative contribution of 1-ethyl-2,3,6-trimethylbenzene and 1-ethyl-3,4,5-trimethylbenzene to the C_5-benzenes (ETMB ratio) in the pyrolysates of both kerogens and asphaltenes reveals a strong correlation (R^2 = 0.81), suggesting a (partially) similar source for these pyrolysis products (Fig. 17, Table 2). However,

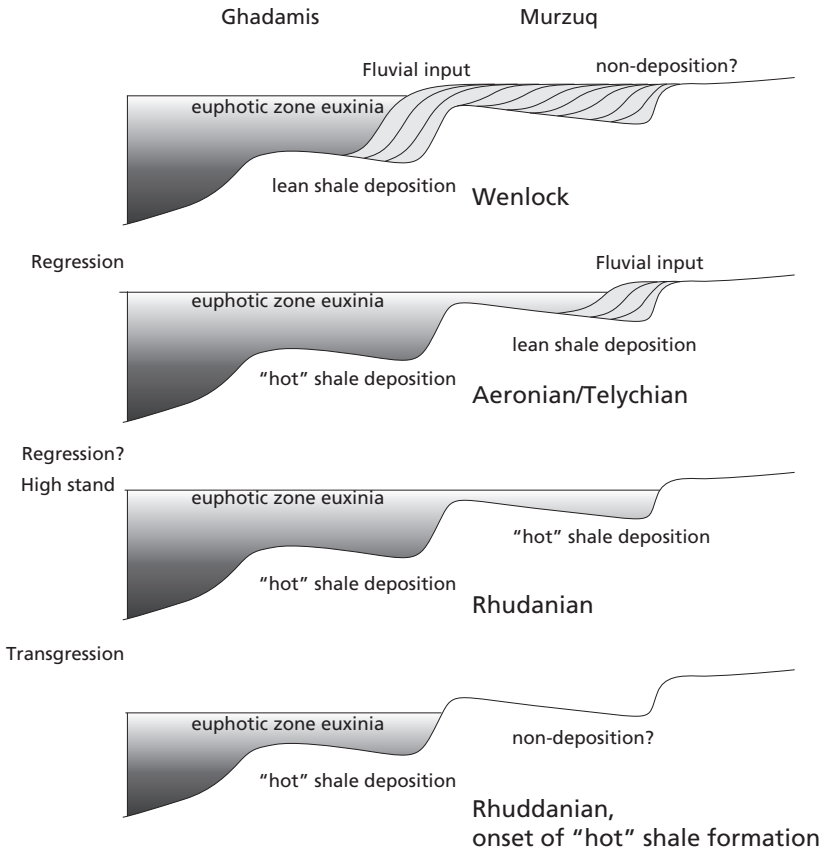

Fig. 18. General depositional model for early Silurian "hot" shale deposition in Ghadamis and Murzuq basins. Melting of the glacial ice cap during the earliest Silurian leads to a significant sea level rise and rapid flooding of wide parts. Organic-rich strata were deposited in palaeodepression during the early to middle initial Rhuddanian transgression. With rising sea level, hot shale began to encroah on the margins of these palaeodepression. During the Wenlock, shelf waters eventually became more oxygenated, resulting in a switch to organically lean shales. In Murzuq Basin, the Wenlock is missing from the subsurface. (Modified after Lüning et al., 2000).

according to this correlation, at TMB/C_4-benzenes ratios of <24% the specific ethyltrimethylbenzenes are no longer present. This most likely reflects the fact that TMBs in the pyrolysates also partially derive from other sources such as algae (Hoefs *et al.*, 1995; Koopmans *et al.*, 1996b). Consequently, the ETMB ratio provides the best indication for a contribution of diaromatic carotenoids to the kerogen and asphaltenes.

Confirmation of the presence of diaromatic carotenoids in the depositional environment comes from the identification of C_{13}-C_{23} aryl isoprenoids with a 2,3,6-trimethyl substitution pattern of the aromatic ring and an isoprenoid chain (C_{13}-C_{23}) in the aromatic fractions of extracts from the Ghadamis Basin, particularly in the "hot" shale (Fig. 5B). These aryl isoprenoids are believed to be derived from thermal breakdown of isorenieratene (Summons & Powell, 1986, 1987; Requejo *et al.*, 1992). In view of the thermal maturity of the rocks no isorenieratene itself or its hydrogenation product, isorenieratane, is expected anymore. Aryl isoprenoids could not be identified in the rock extracts of the Murzuq Basin. We were also unable to identify aryl isoprenoids with the 3,4,5-trimethyl substitution pattern (cf. Hartgers *et al.*, 1994c).

In summary, both evidence from the pryrolysates (ETMB ratio) and biomarkers (aryl isoprenoids) point to the production of diaromatic carotenoids by green sulfur bacteria during deposition of these rocks. Since green sulfur bacteria are phototrophic anaerobes, which require both light and sulfide for growth, this is interpreted to indicate euxinic conditions in the photic zone (see Sinninghe Damste & Schouten, 2006 for a review). Such conditions result in optimal preservation of organic matter and characterize the depositional environment of many petroleum source rocks (Koopmans *et al.*, 1996a). Armstrong *et al.* (2009) examined upper Ordovician-Silurian black shales of the BG-14 core, Jordan, providing evidence for a consistent increase in primary productivity during ice melting. Based on the widespread occurrence of isorenieratene derivatives they concluded that at least part of the photic zone was anoxic during deposition of the "hot" shale, in good agreement with our results. However, our data show that the occurrence of photic zone euxinia continued after deposition of the "hot" shale into the TOC-lean shale based on the elevated ETMB ratios (Fig. 17) although photic-zone euxinia probably occurred more frequently during deposition of the "hot" shales since they typically have the highest ETMB ratios. The results presented here thus imply that photic zone euxinia might have been important, but there must be another reason (higher productivity, decreased inorganic matter influx) for the substantially elevated TOC content of the "hot" shales.

Various depositional models have been proposed for the deposition of these Silurian "hot" shales (Lüning *et al.*, 2000; Armstrong *et al.*, 2009). Organic-rich sediments, were initially deposited in palaeovalleys and depressions only, extending to the higher areas following the Early Silurian transgression (Fig. 18). During the subsequent deposition of the organically lean shales, higher sedimentation rates, related to the input of fluvial sediments resulted in dilution of the still well-preserved organic matter. Our results agree with earlier studies that linked the formation of the North African "hot" shales to productivity and anoxia (Lüning *et al.*, (2000). Still, the conditions resulting in the deposition of the "hot" shale must have lasted several millions of years, which can hence not be explained by salinity stratification due to ice-melting. More likely alternating high and lower productive episodes in a (semi) stratified basin must have resulted in the deposition of these very organic-rich deposits due to the very low sedimentation rates

(Fig. 18). In the Ghadamis Basin 60 meter of "hot" shale was deposited in about 10 million years, i.e., a sedimentation rate of 0.6 cm/kyr. In the Murzuq Basin, 24 meters of "hot" shale was deposited in 5 million years, i.e., a sedimentation rate of 0.5 cm/kyr. Assuming an average whole rock bulk density of about 2.7 g/cm^3, this implies for the organic-richest parts (22% TOC) a carbon burial rate of about 3 g/m^{2}yr. Apparently, low sedimentation rates in combination with enhanced organic matter preservation due to water column anoxia led to organic-rich sediments that are deposited even when productivity would have remained relatively modest. Although there are no present-day analogues for such an environment, this seems to resemble an open ocean setting during Ocean Anoxic Events (OAE), such as OAE-2 at Demerara Rise (Hetzel *et al.*, 2009). Sediment starvation in combination with high organic matter fluxes and preservation resulted in the deposition of very organic-rich sediments.

5. Conclusions

Py-GC-MS has the potential to provide a rapid characterization of bulk kerogen and asphaltene, providing information both on maturity and the depositional environment, when extractable biomarkers lack information due to biodegradation and/or high maturity of the source rocks. Analyzing both kerogen and asphaltenes potentially allows linking source rocks and expelled hydrocarbons.

Extractable fractions from the "hot" shales from the Ghadamis and Murzuq basins could not be used fully to assess paleoenvironmental reconstruction, due to partial biodegradation and high thermal maturity. Several indices for source rock maturity based on the pyrolysates were compared to Rock Eval data, showing a close agreement. In both Murzuq and Ghadamis basins high abundances of 1,2,3,4- and 1,2,3,5-TMB together with appreciable amounts of 1-ethyl-3,4,5-trimethylbenzene and 1-ethyl-2,3,6-trimethylbenzene argue for the presence of macromolecularly-bound diaromatic cartenoids. This is in line with the series of aryl isoprenoids found in the rock extracts from Ghadamis. Hence, pyrolysates of both kerogen and asphaltene fractions from the early Silurian "hot" shale showed that these shales were deposited in a permanently stratified marine basin. Continued photic zone euxinia into the lean shale suggests that other factors controlled organic carbon concentrations in the shale, such as limited admixing of lithogenic material.

5 Application of diamondoids in maturity assessment and oil to source rock correlation in the Libyan Ghadamis Basin

Mohamed M.A. Elkelani[1], Gert-Jan Reichart[1,2], Klaas G.J. Nierop[1], Jaap S. Sinninghe Damsté [1,2], Erik W. Tegelaar[3], Rolande Dekker[3]

[1] *Utrecht University, Faculty of Geosciences, Department of Earth Sciences-Organic Geochemistry, Budapestlaan 4, 3584 CD Utrecht, The Netherlands*
[2] *NIOZ Royal Netherlands Institute for Sea Research Texel, P.O. Box 59, 1790 AB, Den Burg, The Netherlands*
[3] *Shell Global solutions BV, Kesslerpark 1, 2288 GS, Rijswijk, The Netherlands.*

Abstract

Oil and source rock extracts from the Libyan sector of the Ghadamis basin were investigated for their thermal maturity and their potential relationship. The main regional source rocks, the lower Silurian Tanezzuft "Hot" shale-obtained from both the northern and southern part of the basin-and five crude oils from Silurian/Devonian reservoirs from across the Ghadamis basin were studied. Assessment of thermal maturity becomes increasingly difficult at higher levels, as traditionally used biomarker-based indices reach the end of their useful range. This holds true for both source rock extracts and crude oils in the Ghadamis Basin. Therefore, diamondoids, known for their high but differing thermal stabilities, were analyzed and applied as maturity indicators. This approach revealed that the two source rock possess different levels of thermal maturity. Significant differences were also noted for the source rock extracts and the crude oils. While the source rock extracts contain both adamantanes and diamantanes, the latter group is absent in the crude oils. Since the thermal stability of the diamantanes is actually higher than that of the adamantanes, this implies that the crude oils were expulsed before diamantanes formed in the source rock. Considering the distributions of adamantanes in the crude oils and source rock extracts, strong similarities between the northern crude oils and both source rock extracts from the Ghadamis basin were noted. On the other hand the southern crude oils are similar to each other, but considerably differ from both the northern basin crude oils and the source rock extracts. This suggests that the crude oils in the northern part of the basin formed locally from the Tanezzuft "Hot" shale, the southern Ghadamis Basin' s crude oils might have migrated from another (unknown) source.

Keywords: *Rock Eval pyrolysis; Biomarkers; diamondoids; oil maturity; GCxGC-ToFMS*

1. Introduction

The level of thermal maturity is an important parameter for assessing petroleum evolution in sedimentary basins. Apart from the initial composition of the kerogen, the quality of petroleum produced and the relative amounts of gas critically depend on the thermal history during the catagenetic stage. At higher temperatures, during metagenesis, only gas is released. While at low maturity, a large variety of indices are available, assessing maturity at higher values becomes increasingly difficult because reliable indicators are lacking (Peters *et al.*, 2005).

During thermal cracking, diamondoids are thermally more stable than most other hydrocarbons present in petroleum, and therefore, are of particular importance for maturity assessment at high levels of thermal maturity (Dahl *et al.*, 1999). Diamondoids are cage hydrocarbons, naturally occurring in petroleum systems in varying abundances with substituted and unsubstituted homologues. A series of lower diamondoids include adamantane and diamantane (see Appendix for structures), but these compounds have been notoriously difficult to quantify. Recent developments in comprehensive two-dimensional gas chromatography, coupled to a time-of-flight mass spectrometer (GC x GC- ToFMS), now enable their routine analyses (Silva *et al.*, 2011; Zhu *et al.*, 2013). Because of their high but differing thermal stabilities diamondoids have been used for

evaluating source rocks and crude oils with high maturity (Wingert, 1992). The more stable diamondoids generally become increasingly enriched in high maturity oils and even condensates. Moreover, diamondoids are significantly more resistant to microbial degradation than most other petroleum components, e.g. *n*-alkanes (Wingert, 1992). This makes diamondoids excellently suited to study the thermal maturity of the highly mature and biodegraded oil and/or source rocks.

Correlating oils to their source is important, especially in basins with a complex structural history such as the Ghadamis Basin in Libya, as different source rocks may have undergone several phases of oil formation. Oil trapped in different structures, stratigraphical or structural, might be derived from the same or different source rocks. Detailed geochemical analyses of source rock extracts and oils provide potentially valuable tools to correlate oils with each other and also to correlate oils to their source rocks. In the Ghadamis Basin, the hopanes and steranes isomerization ratios and other conventional parameters are at the end of their useful range due to the high maturity and biodegradation (Boote *et al.*, 1998; Hallett, 2002). Diamondoids are, therefore, the ideal tool to reconstruct potential differences in maturity within the Ghadamis Basin.

Here we apply GGxGC-ToFMS to identify diamondoids of typical crude oil samples from the Ghadamis Basin in Libya and compared this to TLE from their source rocks. We compare diamondoid concentrations and ratios with Rock Eval data and conventional biomarker indices for a more refined assessment of maturity and oil to source rock correlation.

2. Geological setting

The Ghadamis Basin is an intracratonic sag basin of Palaeozoic to Cenozoic age, in which a thick sequence of clastic rocks was deposited during the Palaeozoic. The Ghadamis Basin extends between Libya, Algeria, and Tunisia (Fig. 1A), with the depositional center close to the triple junction between the three countries (Boote *et al.*, 1998). It covers an area of 250,000 km^2, with the Al Qarqaf Arch defining the southern edge of this basin and the northeastern margin being the Nafusah Arch. The structural configuration of the Ghadamis Basin is complex due to the presence of several paleo-highs located at its borders, which have been uplifted and tilted from Palaeozoic times to present. A weak northerly trending structural component related to early Palaeozoic arches and basins control a number of hydrocarbon accumulations (Echikh & Sola, 2000). Large ENE-WSW-trending compressional faults and folds have been associated with the early Alpine orogeny, which were later modified with smaller N-S and NW-SE normal faults (Boote *et al.*, 1998). Other tectonic episodes include the Caledonian (Wenlockian, late Early Silurian) and Hercynian (Visean, Early Carboniferous). It is the Caledonian orogeny that may have produced the Al Qarqaf Arch in the south of the basin, and thereby was instrumental in the formation of the Ghadamis Basin as we know it today (Klitzsch, 1981).

The regional Hercynian unconformity (Early Carboniferous) separates Palaeozoic deposits from overlying Mesozoic strata and marks a major shift in depocentre (Fig. 1B). Severe erosion took place during Caledonian and Hercynian times, responsible for major uplifts during the corresponding periods (Fig 1B). The estimated amount of erosion

corresponding with the Hercynian unconformity ranges from 2000 m to 3000 m in the western and northern marginal parts of the basin (Boote *et al.*, 1998; Underdown & Redfern, 2007). These differences in burial uplift and erosion all likely affected the burial history of the underlying strata.

The Silurian sequence is divided lithologically into two major units: Tanezzuft and Akakus. The basal Tanezzuft is generally interpreted as providing the main local source rock in the entire basin; the upper part of Tanezzuft and the Akakus Formation provide reservoir rocks in the Northwest. Several other minor source rocks have also been recognized (Chapter 3). The Tadrart rocks, which are of Devonian age, provide the main reservoir rock in the southeastern part of the Ghadamis Basin. A minor reservoir is formed by the Devonian Awaynat Wanin Formation. The oil and gas fields discovered in the Ghadamis Basin have pure structural traps or complex combined structural-stratigraphic traps. Most of the exploration wells in the Ghadamis Basin show evidence for oil and/or gas.

Deposition of the Tanezzuft source rock has been linked to sustained anoxic bottom water conditions, probably extending into the photic zone (Chapter 4). This organic rich shale typically has a high radioactive signature and thus is known as the "hot" shale. Occurrence of this so-called "hot" shale is determined by the paleotopography and is hence discontinuous (Klitzsch, 1970). The upper Silurian in these basins is represented by sand-rich sediments belonging to the Akakus Formation (Bellini & Massa, 1980; Belhaj, 1996; Lüning *et al.*, 2000).

3. Sampling and methods

The study area is located in the Ghadamis Basin, in the western part of Libya, within concession areas, NC169, NC5, NC8, NC3, NC1, and 70 (Table 1 and 2). The samples analysed for this work consist of five oils from wells A4-NC169, V2-NC8, Z4-NC5, A1-NC3, and A1-NC1 (Fig. 1A). The oils were selected to represent examples of different reservoirs ranging in age from the Silurian and Devonian. Oil samples were collected at the wellhead and any water produced with the oil was quickly removed. Samples were collected in glass containers, carefully sealed and stored until further analyses.

Two source rocks were selected for study, one from the north and one from the south, i.e., from wells A1-70 and A1-NC8 (Table 1 and Fig. 1A and B). Well A1-NC8 was drilled close to the basin margin, whereas A1-70 was drilled closer to the depocenter. We contrast samples from the northern and southern part of the basin, as earlier basin modeling studies suggest a contrasting level of thermal maturity (Underdown & Redfern, 2007). The source rock consisted of ditch cutting samples. No oil samples were available from these wells, but A1-NC8 was drilled from the same concession. Crude oil sample V2-NC8 was included in the analyses.

3.1. Total organic carbon (TOC) and Rock-Eval pyrolysis analyses

The two source rock samples were analyzed for their organic carbon contents and Rock Eval pyrolysis (see Chapter 4). Rock Eval parameters include free volatile hydrocarbon content (in mg HC/g rock, S1), remaining hydrocarbon generative potential (in mg HC/g

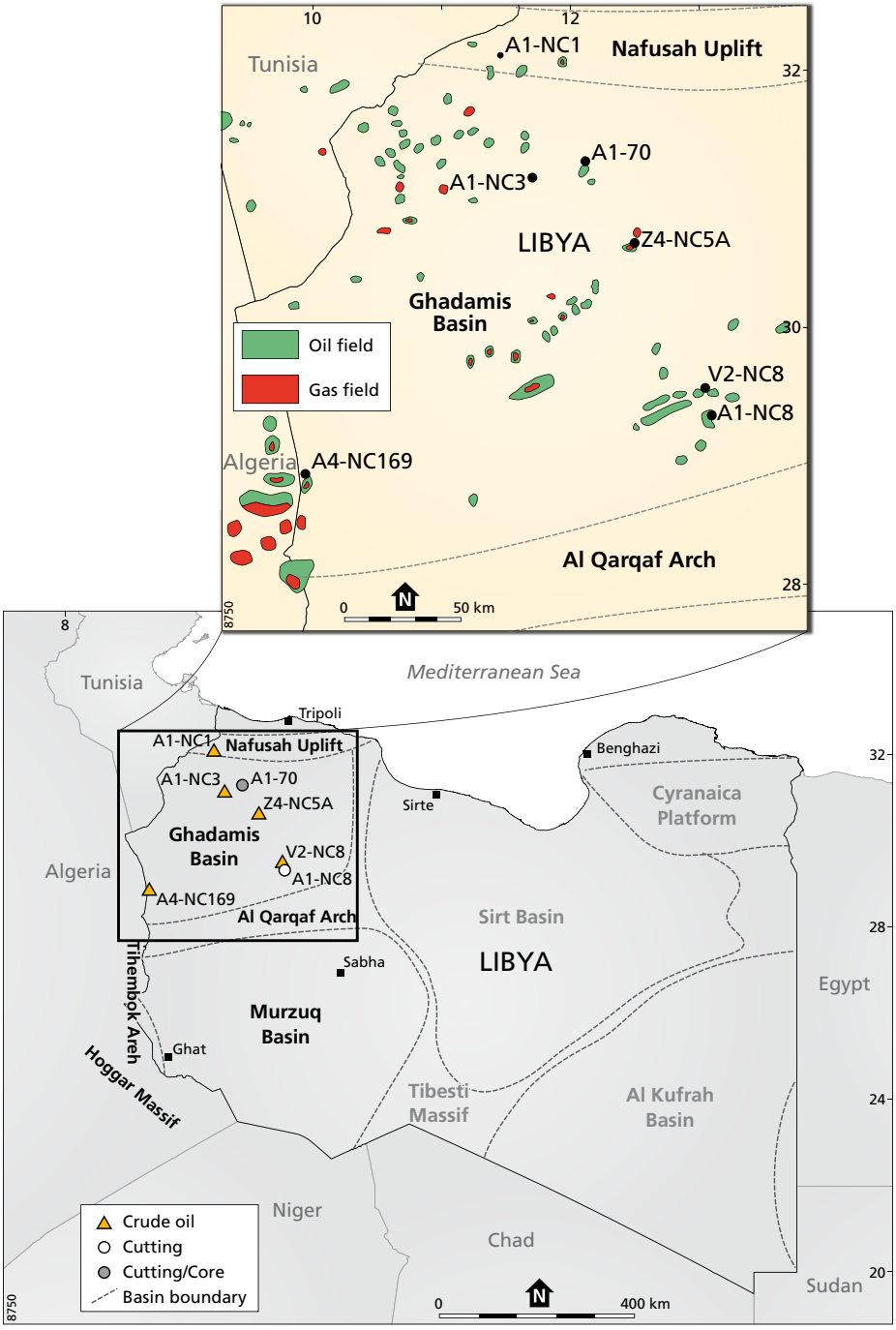

Fig. 1. (A) Location map of the Ghadamis Basin showing the location of the wells from which the analysed oil and source rock samples were obtained.

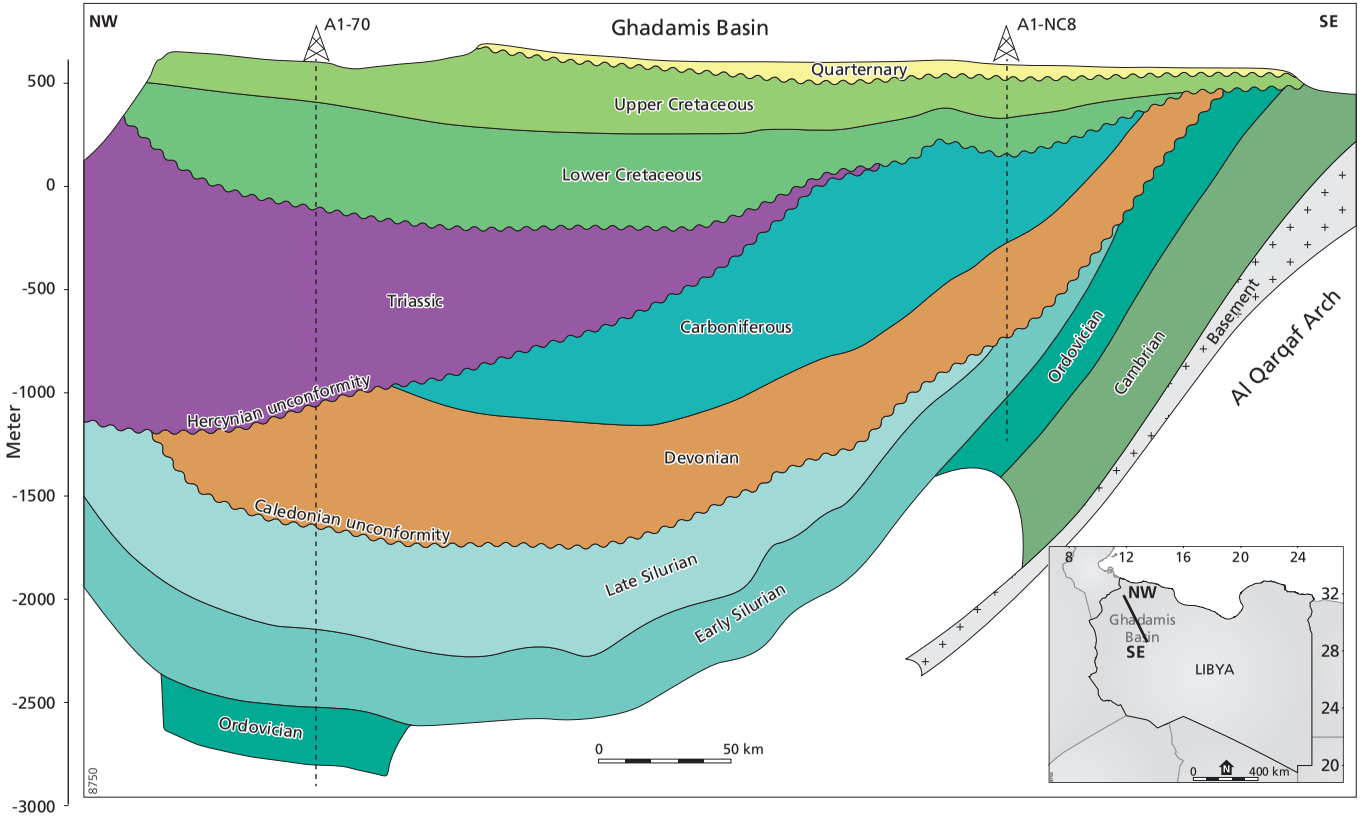

Fig. 1. (B) NW-SE cross-section from the Ghadamis Basin. The section shows the progressive truncation of the Palaeozoic strata by the Hercynian unconformity from south to north. (Modified and redrawing after Boote *et al.*, 1998)

rock, S2), carbon dioxide yield (in mg CO_2/g rock, S3) and temperature of maximum pyrolysis yield (T_{max}). Source rock parameters such as HI (Hydrogen index, S2/TOC*100), OI (Oxygen index, S3/TOC*100), and PI (Production index S1/(S1+S2) were calculated from these measured values.

3.2. Physical properties of crude oils

Physical properties analysis of the API° (American Petroleum Institute) gravity was performed by the different oil companies upon recovery and subsequently verified in the laboratory.

3.3. Solvent extraction and fractionation

Known amounts (15-20 g) of powdered rock sample (cuttings) for the two samples (A1-70 and A1-NC8) were used to extract lipids in a Soxhlet unit with an azeotropic solvent mixture of 200 ml of DCM/MeOH (9/1: v/v) for 24 h. Extracts were transferred to a round bottom flask to remove the anti-bumping granules and subsequently dried using a rotary evaporator until a few drops of solvent were left. These extracts were then transferred to a pre-weighed small vial and reduced to dryness under a stream of nitrogen. Vials with extracts were weighed again to allow quantification. When needed elemental sulfur was removed from the extracts using activated copper, again drying the extracts under a stream of nitrogen and recording the weights before and after. Five crude oil samples were collected from the study area; approximately 2 ml of each sample was subjected to complete removal of asphaltenes using *n*-hexane. The total extracts (maltenes) from source rock extracts and crude oils were separated into non-polar and polar fractions using short column chromatography on activated alumina by eluting with *n*-hexane/DCM (9:1, v/v), and MeOH/DCM (1:1, v/v) as solvents, respectively. The non-polar fraction was subsequently separated into a saturated and aromatic fraction using an Ag^+-impregnated silica column, with *n*-hexane and an *n*-hexane/DCM (1:1) mixture, respectively.

3.4. Gas chromatography and Gas chromatography mass-spectrometry (GC-MS)

The aliphatic and aromatic hydrocarbon fractions from source rock and oil samples were analyzed by capillary column gas chromatography. Each fraction was dissolved in hexane to a concentration of about 1 mg/ml of sample. Ca. 1 µl of the fractions was injected on a gas chromatograph (HP6890 series II) equipped with CP-Sil 5 CB (Agilent) column (length of 30 m, diameter of 0.32 mm, film thickness of 0.12µm), using a flame ionization detector (FID) for quantifying organic compounds and a flame photometric detector (FPD) to check for the presence of bound and/or elemental sulfur. Helium was used as a carrier gas, kept at constant pressure (100 kPa). Samples were injected on-column. The oven temperature was programmed from 70 to 130°C at 30 °C/min, from 130 to 320 °C at 4°C/min and subsequently kept isothermally at 320 °C for 20 min. The data was collected on a Lab Agilent Chemstation data acquisition system. Compounds were identified based on retention times and by using a GC equipped with a mass spectrometer (Thermo, Trace GC Ultra GC-MS). The same column and temperature programme were used for the

GC analyses. However, the He carrier gas was set at constant flow (1.0 ml/min). Hopanes (*m/z* 191) and steranes (*m/z* 217) were identified by comparison of mass spectra with previously published mass spectra.

3.5. (GCxGC) coupled to time of flight mass spectrometry (ToFMs) analysis

Diamondoid analysis was carried out at the Shell Global Solutions laboratory in Rijswijk using a time-of-flight mass spectrometer coupled on line to a gas chromatograph (GCxGC/ToFMS, Agilent 7890 coupled to JOEL AccuTOF). Whole oil and the maltene fraction from the extracts were injected to avoid any possible loss of volatile diamondoids. MassCenter software (version 2.4.5) was used to operate the GC x GC-ToFMs system and for data acquisition. Two columns were used in this study, separating polar and non-polar phases. Each oil and extract was injected in split mode and variable split rates to keep compounds in line air range of the ToF instrument. The inlet temperature was set at 270 °C. The 1st dimension of the analyses was separated by a polar DB-17ms column (25 m x 0.25 mm i.d., 0.25 µm film thickness), held at 40 °C for 2 min and then ramped to 300°C at 2.5 min^{-1}. Compounds eluting from the first dimension column were cryogenically modulated (ZOEX I modulator) onto the second dimension column. The modulator cold jet gas was dry N_2. In the thermal modulator nitrogen was heated to 50 °C above the temperature of the main GC oven. The second dimension separation was performed with an Agilent DB-1ms, 2 m x 0.10 mm i.d., 0.1 µm film thickness) following the same oven temperature program as for the first column. The carrier gas used was He at a constant flow rate of 1.0 ml min^{-1}. The ToFMS detector samples at 10 KHz, summing up 400 spectra to arrive at 25 spectra s^{-1}. The scan range used was from 41 to 600 atomic mass units (amu). The second dimension column was directly inserted in the ion source. Interface temperature was set at 280°C The ToF source temperature was 250 °C and detector was set to 2150 V. The internal standard used for the analysis was fully deuterated napthalene (CAS#1146-65-2). Diamondoids were detected in the samples examined using the following ions: *m/z* 135, 136, 149, 163 (admantanes); *m/z* 187, 188, and 201 (diamantanes), (Chen et al., 1996; Dahl et al., 1999). The structures and nomenclature for adamantane (I) and diamantane (II) are shown in the Appendix. Compound ratios were calculated from integrated peak areas on the characteristic mass chromatograms.

4. Results and Discussion

4.1. Rock-Eval pyrolysis of the source rocks

Organic matter quantity and quality of the source rocks was investigated using TOC and Rock Eval analyses (Peters, 1986). The dark black laminated shales of the lower Tanezzuft Formation (hot shale) have the highest TOC content in well A1-70 is (22.3 wt%), recorded at a depth of 3103 m (Table 1). The TOC content of the Tanezzuft source rock in the A1-NC8 well at a depth of 1542 m is 5.6 wt%. These high organic carbon contents are in line with both rocks having an excellent source rock potential (Peters, 1986).

Rock-Eval S_2 yields for the source rocks in the A1-70 and A1-NC8 wells are 26.1 mg HC/g rock and 21.1 mg HC/g rock, respectively (Table 1). These values are well above 5 mgHC/g, which is generally accepted as the cut-off point for source rocks considered as having excellent source rock potential. Hydrogen and oxygen indices (HI and OI) of the A1-70 and A1-NC8 source rocks are 117 and 379 mg HC/g TOC (HI) and 9 and 34 mgCO_2/g rock (OI), respectively. Although the HI values as such would suggest both source rocks having the potential to produce a mixture of oil and gas (kerogen Type II), the HI is probably strongly affected by thermal maturity. Within a Van Krevelen plot (Tissot & Welte, 1984; Bordenave, 1993) of whole rock HI and OI (Fig. 2) both shales plot as Type II (oil and gas prone).

Table 1. Total organic carbon and Rock Eval pyrolysis data from the studied source rocks of the Tanezzuft Formation (hot shale) in Ghadamis Basin.

Well Name	Depth	TOC	S1	S2	S3	Tmax	HI	OI	PI
	(m)	(wt %)	(mgHC/g rock)	(mgHC/g rock)	(mgCO2/g rock)	(°C)	(mgHC/g TOC)	(mgC02/g TOC)	–
A1-70	3103	22.3	4.2	26.1	1.9	445	117	9.0	0.14
A1-NC8	1542	5.6	2.3	21.1	1.9	435	379	34.0	0.09

TOC= Total Organic Carbon, **S1**= Free hydrocarbon, **S2** = remaining hydrocarbon generative potentia,l **S3**= carbon dioxide yield **HI**= Hydrogen index S2/TOC*100 , **OI**= Oxygen index S3/TOC*100, **PI** = Production index S1/(S1+S2), Tmax = Temperature of maximum pyrolysis yield.

The thermal maturity of organic matter in the source rocks was evaluated based on the T_{max} of the S2 peak (Table 1). The maturation range of T_{max} varies for different types of organic matter (Tissot and Welte, 1984) and T_{max} values generally increase as result of increasing burial depth (i.e., older, more deeply buried rocks have higher T_{max} values). Hence, T_{max} is the most common parameter used to estimate thermal maturity of the organic matter. T_{max} values < 435 °C represent immature organic matter; values between 435-470 °C represent the oil window and T_{max} values > 470 °C represent overmature kerogen (Peters, 1986). The two source rock samples have T_{max} values of 445 and 435°*C*. The maturation window for oil/condensate generation from Type I and II organic matter ranges from 430 °C to 470 °C (Peters, 1986). Hence the Early Silurian hot shales are thermally mature and within the main oil window. The T_{max} value for the southeast well around 435 °C suggests early maturity of the source rock with respect to oil generation, whereas T_{max} values of 445 °C in the northeast well indicate a more mature source rock.

4.2. Bulk properties of the oils

For crude oils several bulk parameters are potentially useful for initial screening and tentative identification of genetically related oils. API gravity is a physical property expressing the density of liquid petroleum and used to classify the crude oils into heavy or light (Tissot & Welte 1984). API gravity values available for the five oils studied here are listed in Table 2. The oil recovered from close to the Algerian border (hence the depocenter; Hallett, 2002) has an API value >45 (51.0), which corresponds to a condensate rather than a crude oil. The other oils have mostly API gravities corresponding to very light oil, (43.2, 42.5 and 41.2), with one oil from the northwestern section of the basin with a lower API gravity (36.0). The asphaltene content of the oils is low ranging

from 0.1 to 2.3% (Table 2). The asphaltene content of extracts of the source rock extracts is low to moderate (3.3 to 5.0%).

Source rock extracts and oils are commonly enriched in saturated hydrocarbons (Mackenzie, 1984). The extracts and oils investigated here are characterized by saturated hydrocarbon contents between 43.4 and 75.4% (Table 2). The aromatic hydrocarbon content of the extract and oils ranges between 17.5% and 42.8%. Hence the ratio of saturates to aromatics is >1 for all extracts and oils.

4.3. *n*-alkane and isoprenoids

These similar distributions are, however, rather inconclusive and do not allow for unraveling the relationships between oils and source rocks studied here.

The composition of the saturated hydrocarbons of crude oils and the extracts of the source rocks shows similar *n*-alkane and isoprenoid hydrocarbon distributions (Fig. 3). All oils reveal gas chromatograms characterized by a clear *n*-alkane distribution, without a notable unresolved complex mixture (UCM). The source rock extracts show slightly more pronounced UCMs, which might suggest biodegradation. However, although biodegraded oils may contain a series of 25-norhopanes (Volkman *et al.*, 1983), these compounds were not detected here. The carbon preference index of the long-chain *n*-alkanes ($CPI_{24\text{-}34}$) shows values close to unity (Table 2). However. the CPI cannot be used for maturation evaluation because land plants were still at the early stages of their evolution in the Silurian and hence do not provide an appreciable contribution to the bulk organic matter.

The oils and source rock extracts contain more saturated and aromatic hydrocarbons than polar components (Table 2), which suggests a lack of biodegradation (Peters *et al.*, 2005). Source rock extracts and oils from the Ghadamis Basin are characterized by low saturated/aromatic hydrocarbon ratios (Saturate/Aromatic = 1.3-3, Table 2), which is typical of marine derived organic matter, deposited in a intermittently anoxic environment (Clayton & Bjoroy, 1994).

4.4. Biomarker-based maturity parameters

Thermal maturity evaluation of oils and source rocks is often based on ratios based on hopanes and steranes (Peters *et al.*, 2005). The distributions of hopanes and steranes are commonly studied using GC-MS by monitoring the fragment ions *m/z* 191, m/z 218 and *m/z* 217, respectively (Peters *et al.*, 2005) (Fig. 4). In the Ghadamis Basin, hopane and sterane concentrations are, however, just below the level of detection, probably due to the high level of thermal maturity. For instance, homohopanes were not present in sufficient quantities to allow quantification in most oils and extracts. Still, other parameters might still be applicable, such as hopane-based ratio Ts/(Ts+Tm) (Moldowan *et al.*, 1985); it could be calculated for all oils and extracts studied, except for the oil from A1-NC1. Similarly, the sterane-based ratios 20R/(20S+20R), (Seifert & Moldowan, 1978) and ββ/(ββ+αα) (Mackenzie, 1984) and the triaromatic steroid based ratio (TAS) (Peters *et al.*, 2005) were calculated for almost all samples (Table 2).

The hopane-based maturity index Ts/(Ts+Tm) uses the relative abundance of C_{27} 18α-trinorneohopane (18α -22, 29, 30-trinorneohopane or Ts) over C_{27}

Table 2. API gravity and biomarker data for source rock extracts and crude oils from Ghadamis Basin.

Well Name	**A1-70**	**A1-NC8**	**A4-NC169**	**V2-NC8**	**Z4-NC5**	**A1-NC3**	**A1-NC1**
Sample type	**Cutting**	**Cutting**	**Oil (*DST*)**	**Oil (*Well head*)**	**Oil (*Well head*)**	**Oil (*DST*)**	**Oil (*DST*)**
Depth (meter)	**3103**	**1542**	**2618-2627***	**1541-1551***	**2912-2920***	**2726-2745***	**1195-1199***
Age	**Early Silurian**	**Early Silurian**	**Devonian**	**Devonian**	**Silurian**	**Silurian**	**Silurian**
Formation/Reservoir	**Tanezzuft**	**Tanezzuft**	**Awaynat Wanin (F3)**	**Tadrart (D1)**	**Upper Tanezzuft**	**Akakus**	**Akakus**
Physical properties							
API gravity			51.0	42.5	43.2	41.2	36.0
Isoprenoid ratios							
Pr/n-C17	0.30	0.42	0.33	0.53	0.46	0.45	0.59
Ph/n-C18	0.60	0.37	0.31	0.40	0.31	0.51	0.50
CPI	1.0	1.0	1.0	1.1	1.0	1.1	1.0
Molecular composition							
Saturate %	69.9	56.2	75.5	55.3	58.1	53.3	43.4
Aromatic %	22.3	40.2	23.3	42.9	40.3	40.2	41.2
Polar %	7.8	3.5	1.2	1.9	1.6	6.5	15.4
Asphaltenes %	5.0	3.3	0.1	0.55	2.3	0.3	0.2
Saturate/Aromatic	3.1	1.4	3.2	1.3	1.4	1.3	1.1
Biomarker							
Ts% (m/z 191)	59.0	50.0	70.0	61.0	60.2	51.0	nd
ββ% (m/z 217)	64.0	46.0	65.0	54.2	63.2	64.0	60.2
20S% (m/z 217)	53.0	53.2	47.0	58.2	56.2	60.0	54.0
TAS% (Triaromatic m/z 231)	nd	nd	94.0	82.0	89.0	88.0	90.0
Diamondoid							
MAI% (Methyl Admantane Index)	57.0	52.0	63.0	61.0	47.0	45.0	51.0
MDI% (Methyl Diamantane Index)	47.0	34.0	nd	nd	nd	nd	nd
EAI% (Ethyl Adamantane Index)	67.0	62.0	68.0	70.0	71.0	74.0	65.0

Pr/*n* -C17 ratio = Pristane/*n* -alkane, **Ph/*n* -C17 ratio** = Phytane/n-alkane, **Ts/Ts+Tm%** (m/z 191)= C27 18α(H)-trisnorneohopane (Ts),C27 17α(H)-trisnorhopane (Tm), **ββ%** =ββ/(ββ+αα) (m/z 217 steranes), **20S%**=20S/(20S+20R)(m/z 217 steranes), Triaromatic steroid **TAS**=(TA20+TA21)/(TA20+TA21+TA26+TA27+TA28), **Methyl Admantane index (MAI)**=1-MA/(1-MA+2-MA), **Methyl Diamantane index (MDI)**= 4-MD/(1-MD+3-MD+4-MD), **Ethyl Adamantane index** (EAI)= 2-Ethyladamantane/(2-Ethyladamantane+1-Ethyladamantane) **Triaromatic steroids** (TASC)=(TA20+TA21)/(TA20+TA21+TA26+TA27+TA28) (m/z 231), **nd**= no data, **DST**= Drill steam test, **F3 and D1** = Reservoir zone, * Reservoir perforation interval, Carbon Preference Index $CPI = \frac{1}{2}\left[\frac{C_{25}+C_{27}+C_{29}+C_{31}+C_{33}}{C_{24}+C_{26}+C_{28}+C_{30}+C_{32}} + \frac{C_{25}+C_{27}+C_{29}+C_{31}+C_{33}}{C_{26}+C_{28}+C_{30}+C_{32}+C_{34}}\right]$

Table 3. Distribution of individual adamantanes and diamantanes in % (based on the total individual compounds) in crude oils and source rock extrcats from Ghadamis Basin.

			Well name	A4-NC169	A1-NC1	A1-NC3	Z4-NC5	V2-NC8	A1-70	A1-NC8
			Sample Type	Oil	Oil	Oil	Oil	Oil	Source rock extract	Source rock extract
Peak no.	Compound	m/z	Abbreviation/Unit	(%)	(%)	(%)	(%)	(%)	(%)	(%)
1	Adamantane	136	A	4.6	3.3	3.6	3.9	3.1	3.0	2.7
2	1-Methyladamantane	135	1-MA	17.8	13.3	11.3	12.3	16.6	10.5	11.0
3	2-Methyladamantane	135	2-MA	10.3	13.1	14.0	13.8	10.5	8.1	10.2
4	1-Ethyladamantane	135	1-EA	5.5	9.0	7.9	7.8	5.8	8.0	12.9
5	2-Ethyladamantane	135	2-EA	12.0	16.8	22.3	19.1	13.4	16.1	21.1
6	1,4-Dimethyladamantane	149	1,4-DMA (cis)	10.5	9.1	9.4	10.3	10.2	7.8	8.9
7	1,4-Dimethyladamantane	149	1,4-DMA (trans)	9.7	11.4	10.7	11.2	10.9	8.1	10.4
8	1,2-Dimethyladamantane	149	1,2-DMA	11.4	11.7	11.1	11.6	10.8	11.0	13.5
9	1,3-Dimethyladamantane	149	1,3-DMA	13.3	9.7	8.2	8.0	13.8	6.9	6.4
10	1,3,5 Trimethyladamantane	163	1,3,5-TMA	4.9	2.5	1.6	1.9	4.9	1.7	1.3
11	1,3,5,7-Tetramethyl Adamantane	177	1,3,5,7-TeTMA	0.8	0.2	0.0	0.0	0.7	0.1	0.0
12	Diamantane	188	D	0.0	0.0	0.0	0.0	0.0	3.3	0.4
13	4-Methyldiamantane	187	4-MD	0.0	0.0	0.0	0.0	0.0	6.2	0.4
14	1-Methyldiamantane	187	1-MD	0.0	0.0	0.0	0.0	0.0	3.1	0.4
15	3-Methyldiamantane	187	3-MD	0.0	0.0	0.0	0.0	0.0	3.9	0.4
16	4,9-Dimethyldiamantane	201	4,9-MD	0.0	0.0	0.0	0.0	0.0	2.2	0.1
	Total			100	100	100	100	100	100	100

17α-trinorhopane (17α -22, 29, 30-trinorhopane or Tm) as a maturity parameter (Seifert & Moldowan, 1978), albeit being influenced as well by source facies (Moldowan *et al.*, 1986). Here the Ts/Ts+Tm ratio varies between 50% and 70% for the oil samples and source rock extracts (Table 2). This indicates approximately middle maturity, within the main oil window (Moldowan *et al.*, 1985).

The sterane-based maturity index 20S/(20S+20R) uses the isomerization at C_{20} in the C_{29} 5α,14α,17α(H)-sterane, which increases from 0 to slightly over 50% (52-55% = equilibrium) with increasing maturity (Seifert & Moldowan, 1978). In the studied oils and source rock extracts, this maturity-related parameter ranges from 47% to 60% (Table 2) indicating that most samples have reached or even exceeded the equilibrium limit for this maturity index (Table 2, Fig. 5)

The sterane-based maturity parameter ββ/(ββ+αα) also uses the isomerization of the C_{29} sterane and is supposed to be independent of organic matter source. In the oil the ββ% ratio ranges from 54% to 65% (Table 2), meaning that it has not yet reached the equilibrium values at about 70% (Peters *et al.*, 2005). The ββ% ratio of the source rock extract from the northern part of the basin was 64%, whereas that from the southeast was 46% only, suggesting a somewhat lower maturity for this part of the basin. Still, all values are quite high and well within the oil window. A crossplot (Fig. 5) between %20S

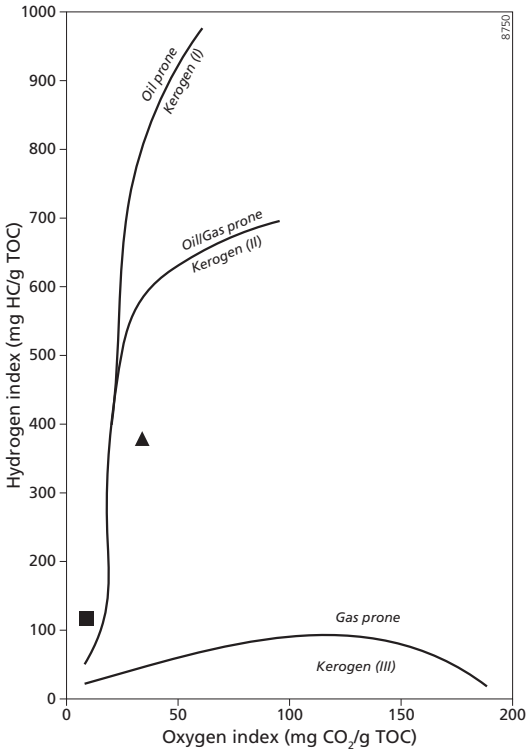

Fig. 2. Hydrogen index versus Oxygen index (Van Krevelen) plot, from Rock Eval pyrolysis data from A1-70 (Square) and A1-NC8 (Triangle) samples in the Ghadamis Basin.

and %ββ shows that both source rock extracts and oils are highly mature and at the end of the useful range for the two indices, i.e. close to equilibrium. Based on these two maturity indices, it is therefore not possible to distinguish oils from different parts of the basin, although the source rock extracts suggest that there might be differences.

Based on relative abundances of triaromatic steroids, the TAS ratio increases from 0 to 100% during thermal maturation (Seifert & Moldowan, 1978; Beach *et al*., 1989). This indicator is based on the relative abundances of the C_{20} and C_{28} 20R triaromatic steroid hydrocarbons. The triaromatic steroid components could not be identified in the source rock extracts (Fig. 4, Table 2), but were detected in five oils studied here (using their characteristic mass fragment *m/z* 231 and relative retention times; Peters *et al*., 2005). For those oils, the TAS shows rather similar values (Table 2) that range from 82% to 94%, which is in line with the presence of mature crude oils (Mackenzie, 1984). The values of the TAS are somewhat higher in the southern part of the basin, suggesting that the oil samples from that part of the basin are more mature. Still, this index is close to the limit of applicability and overall suggests high maturity.

4.5. Diamondoid hydrocarbons

Crude oils and source rock extracts were analyzed for their diamondoid composition using GCxGC ToFMS. These diamondoids include adamantanes, with one cage, and diamantanes, with two cages (Wei *et al*., 2007). The different adamantanes and diamantanes were identified using standards and by comparing their mass spectra with previous publications (Wingert, 1992; Chen *et al*, 1996; Li *et al*., 2000; Grice *et al*., 2000). Characteristic ion fragments used for their identification using GCxGC/ToFMS are *m/z* 135, 136, 149, 163, and 177, for adamantanes, and *m/z* 187, 188, and 201 for diamantanes, respectively. Overall all extracts and crude oils contain substantial amounts of highly alkylated adamantanes, most of which have not yet been identified. Sixteen individual diamondoids (compounds 1 to 16; Table 3) could be identified and quantified. In the source rock extract theses diamondoids consist of both adamantanes and diamantanes, whereas in the crude oils only adamantanes were detected (Figs. 6 and 7; Table 3). In the source rock extracts the principal dominant adamantane hydrocarbons are 1-MA, 1-EA, 1,4-DMA and 1,3-DMA (Table 3). The principal dominating diamantane compounds are 4-MD, and 3-MD, with overall higher concentrations in the northern part of the basin. In the crude oils the dominant individual adamantanes are 1-MA, 1-EA, 1,4-DMA and 1,3-DMA. Either 1-MA or 2-MA is the most abundant homologue in all crude oils (Table 3). Tri- and tetramethyl diamondoids have been identified, albeit with much lower abundances compared to methyl- and dimethyl homologues.

Diamondoids are thermally more stable than most other hydrocarbons (Dahl *et al*., 1999) and during thermal cracking of oil the thermodynamically stable diamondoids become increasingly enriched in the oil or condensate. Diamondoids are also significantly more resistant to microbial degradation than most other petroleum components such as *n*-alkanes (Wingert, 1992). Consequently, most oils that have a low thermal maturity and are not subjected to thermal cracking typically have high concentration of other biomarkers and extremely low concentration of diamondoids (Zhibin *et al*., 2007). Conversely, in highly cracked oils, concentrations of diamondoids are generally high and common biomarkers are extremely low, or in some cases totally absent (Trolio *et al*., 1999).

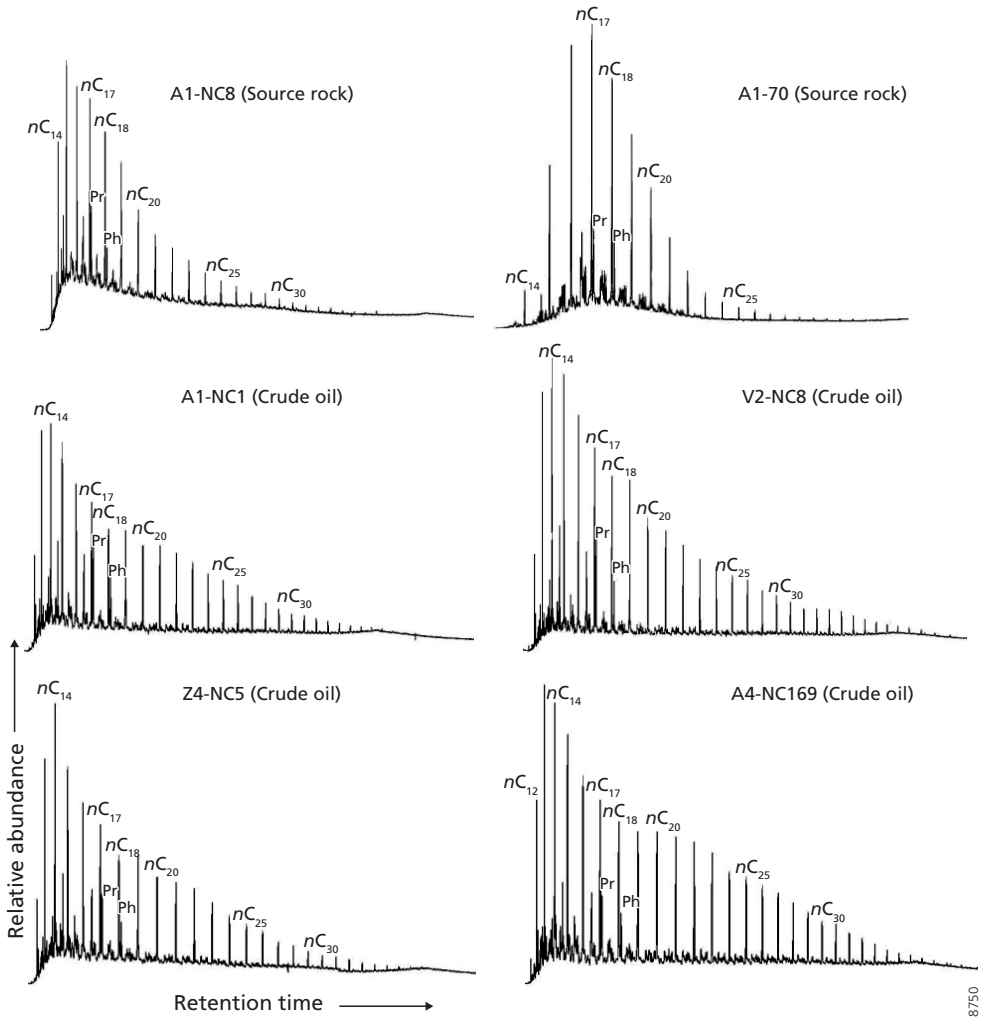

Fig. 3. Gas chromatograms showing distribution of *n*-alkanes and isoprenoids (Pr = Pristane and Ph= Phytane) of the source rock extracts and crude oils from the Ghadamis Basin.

The high diamondoid and low biomarker concentrations of both source rock extracts and crude oils studied here are in agreement with the high maturity inferred earlier. The plot between diamondoids versus API gravity (Fig. 8) showed that the A4-NC169 and V2-NC8 oils had high concentrations of diamondoids and a high API gravity, which indicates that they are mixed uncracked and cracked oils (Dahl *et al*., 1999; Muhammad *et al*., 2011). In the A1-NC3, A1-NC1 and Z4-NC5 oils, the reverse trend was observed less cracking, which resulted in fewer diamondoids and higher API gravity (Zhibin *et al* 2007; Dahl *et al*., 1999).

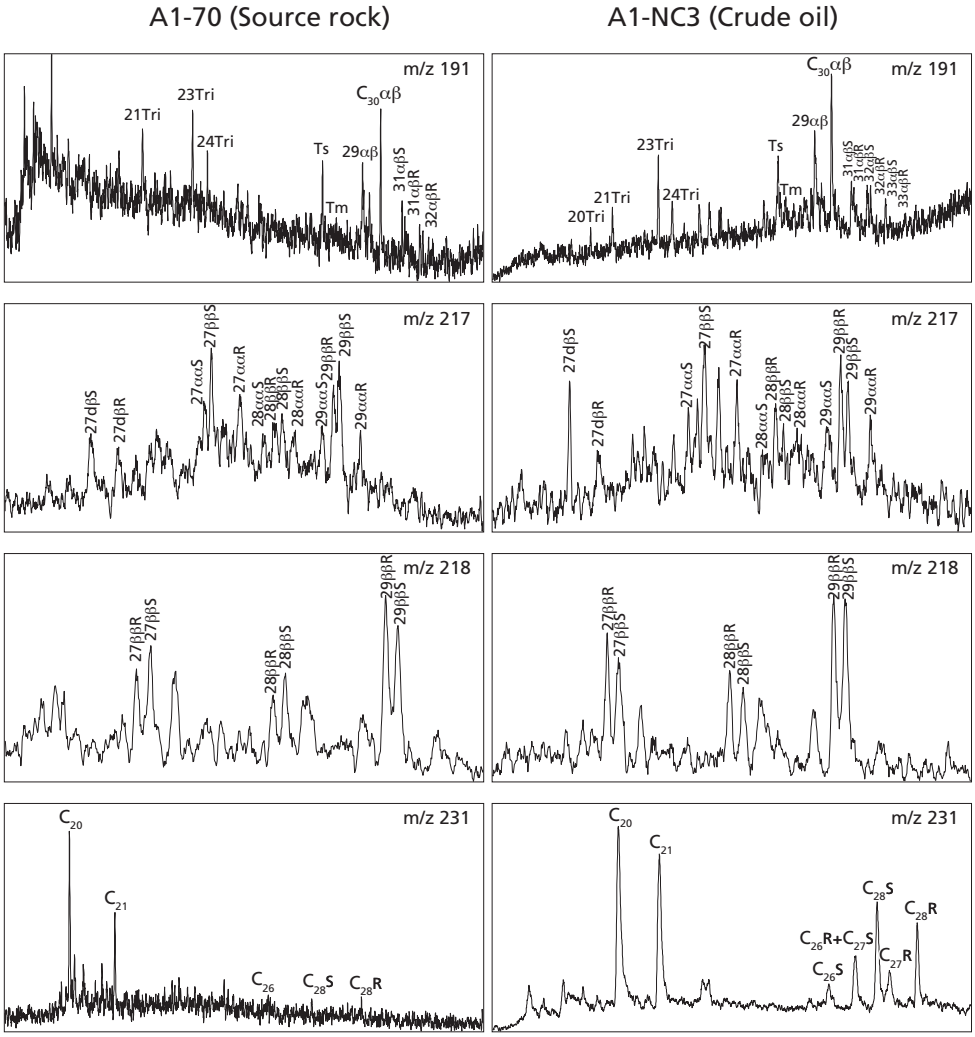

Fig. 4. Mass chromatograms displaying the distribution of hopanes (m/z 191) and steranes (m/z 217 and m/z 218) in aliphatic fractions and triaromatic steroids (m/z 231) of crude oil and a source rock extract from the Ghadamis Basin.

Since there are differences in the thermal stability of methyl-substituted diamondoids, they have been applied as maturity indicators. Certain isomers ratios in crude oils and source rock extracts have been proven useful for especially overmature stages of hydrocarbon generation (Chen *et al.*, 1996). Diamondoid maturity indices are based on the fact that stability differs between diamondoid hydrocarbons. For instance, 1-methyladamantane (1-MA) is more stable than 2-methyladamantane (2-MA) because of the presence of a methyl group at the bridgehead position (Dahl *et al.*, 1999). Similarly 4-methyldiamantane (4-MD) is more stable than 1- or 3-methyldiamantane (1-MD,

3-MD). Therefore, two ratios have been suggested as maturity indicators (Chen et al., 1996): the Methyl Adamatane Index (MAI) = 1-MA/(1-MA+2-MA) and the Methyl

Diamantane Index (MDI) = 4-MD/(4-MD+1-MD+3-MD). High values of these indices have been shown to preferentially coincide with highly mature oils (Chen *et al.*, 1996). In addition, the Ethyl Adamantane Index (EAI) =2-EA/(2-EA+1-EA) has been proposed to distinguish between Type II and Type III organic matter (Schulz *et al.*, 2001), based on the formation of these compounds being dependent on facies of the source rock. Although even more indices have been proposed, these could not be applied here, as not all involved compounds were identified.

The main difference between the source rock extracts and the crude oils is the absence of diamantanes from crude oils (Figs. 7; Table 3). Still, even in the source rock extracts

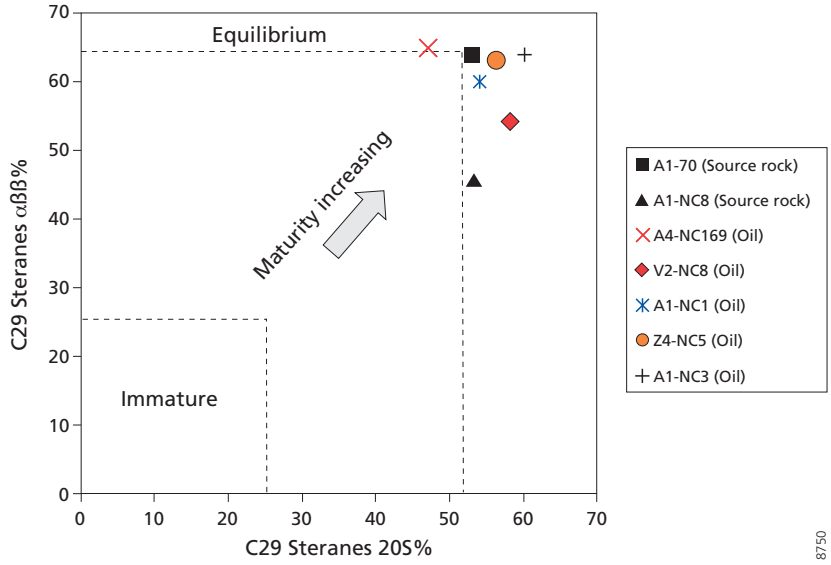

Fig. 5. Cross-plot of the thermal maturity parameters 20S/(20S+20R)% versus ββ/(ββ+αα)- C29 steranes of Silurian source rock and crude oils from the Ghadamis Basin.

the one-cage adamantanes are much more abundant than the two-cage diamantanes. Since diamantane is more stable than adamantine, it is not likely that the diamantane was lost from the oil because of intense or prolonged cracking (Wingert, 1992; Schulz, *et al.*, 2001). Also, a selective loss of diamantane due to evaporation and/or condensation seems highly unlikely, as adamatane has a rather high melting point and already sublimates at room temperature (Yang, *et al.*, 2006). Hence the most likely component to be lost by either process would be adamantane and not diamantane. Also, in other studies (e.g. Wang *et al.*, 2013) diamondoids were found in most, but not all oils. This was attributed to the fact that the higher diamondoids derive from the lower diamondoids in response to very high temperatures (Dahl *et al.*, 2010). In our, case this implies that diamantane must have formed in the source rock after the oil was expelled. Hence the oil never reached the temperature needed for diamantane formation as it already migrated to the reservoir

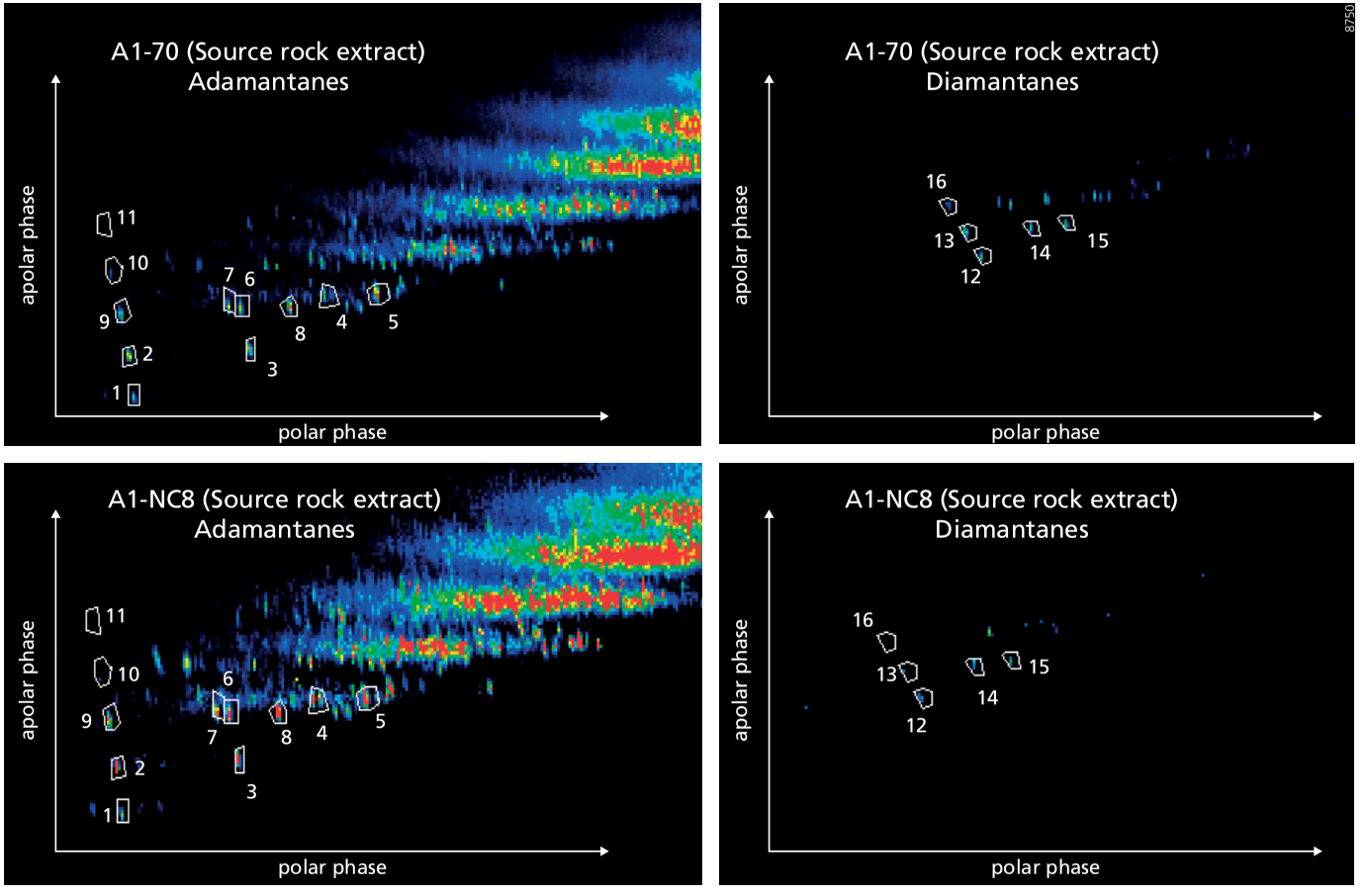

Fig. 6. GCxGC-ToFMS of adamantanes (*m/z* 135+136+149+163+177) and diamantanes (*m/z* 187+188+201) in the source rock extracts from the Ghadamis Basin (A1-NC8 and A1-70 wells). Peak numbers refer to compounds listed in Table 3.

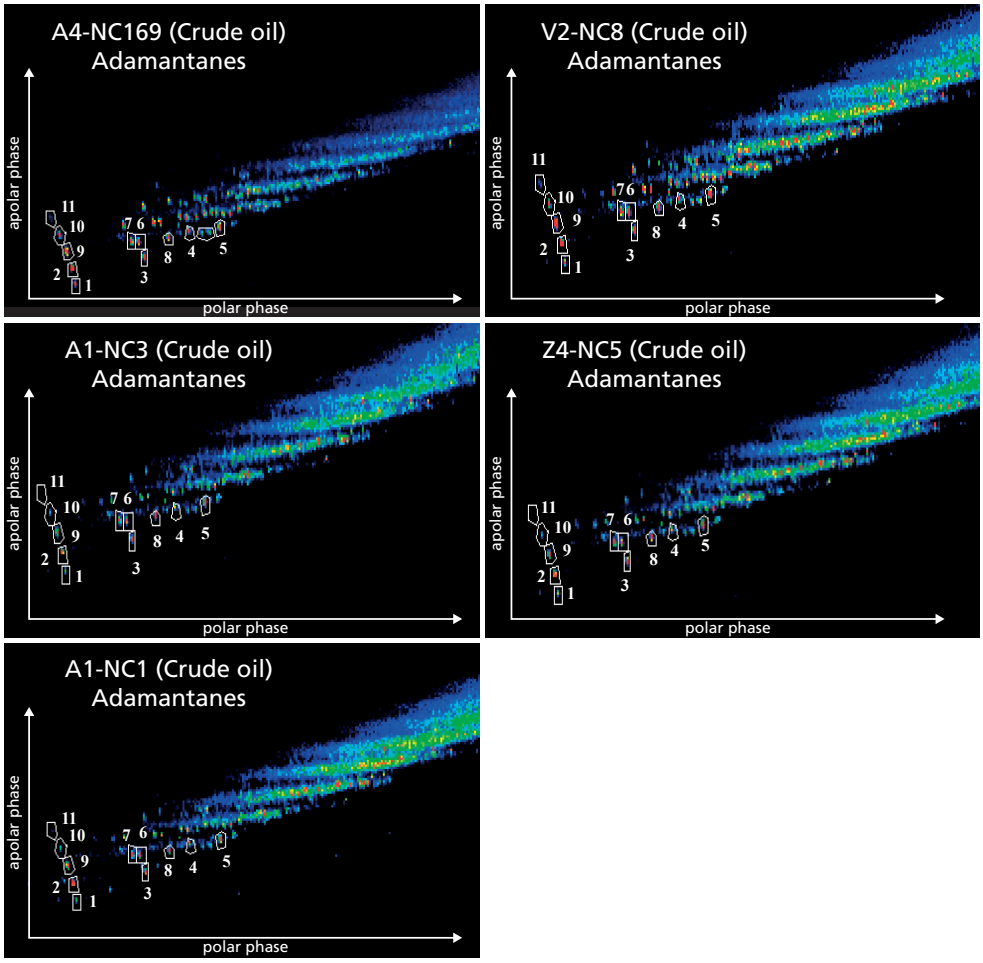

Fig. 7. GCxGC-ToFMS of adamantanes (*m/z* 135+136+149+163+177) from selected crude oil from the A4-NC169, V2-NC8, A1-NC3, A4-NC5 and A1-NC1 wells, Ghadamis Basin. Peak numbers refer to compounds listed in Table 3.

rock higher up in the stratigraphy. In most cases, the maturity of a crude oil depends on the maturity of its source rock at the time of expulsion. The oil must have been expelled between the windows of adamantane and diamantane formation.

The two diamondoid hydrocarbon ratios MAI and MDI values calculated for the source rock extracts (Table 2) are plotted in Fig. 9. Since we only detected diamantane in the source rock extracts and not in the crude oils we cannot compare the MAI and MDI for the oils. As a reference estimated corresponding vitrinite equivalent values have been plotted based on Chen *et al.* (1996). They proposed that samples of vitrinite reflectance (Ro) values of 1.1-1.3% correspond to MAI values between 50 and 70% and MDI values between 30 and 40%. Similarly samples with Ro values of 1.3-1.6% were shown

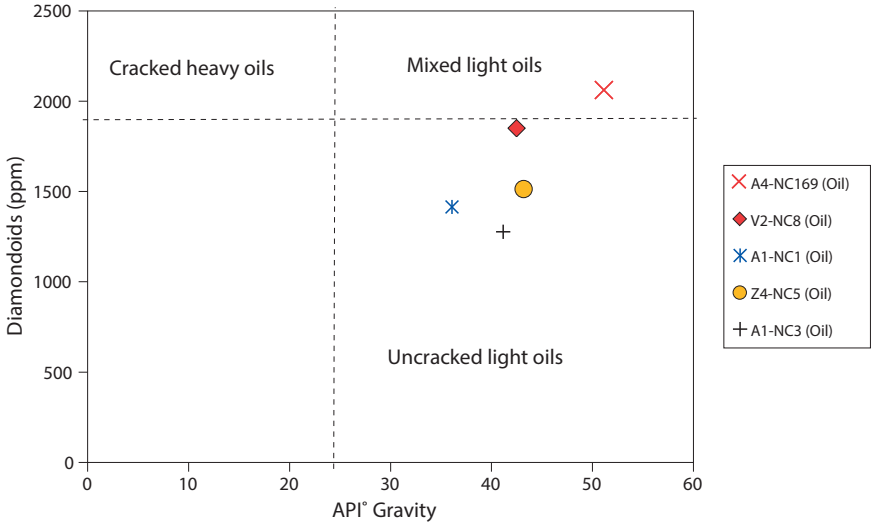

Fig. 8. Plot between API gravity and total diamondoid concentration, showing the effects of cracking and maturity.

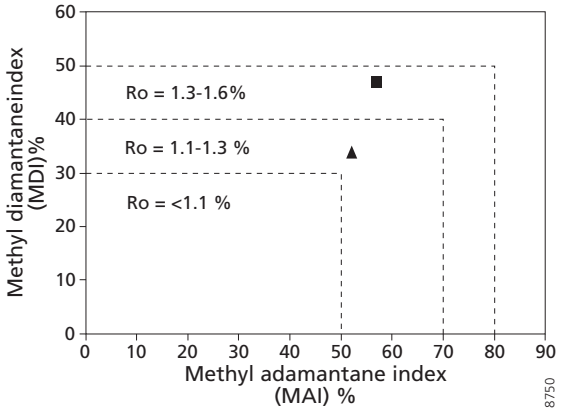

Fig. 9. Cross plot of MAI and MDI of source rock extracts from Ghadamis Basin, showing high thermal maturity corresponding to Ro 1.1-1.3%, A1-NC8 well (Triangle) and Ro 1.3-1.6% for A1-70 well (Square).

to have MAI 70-80% and MDI 40-50%, while those with Ro values of 1.6-1.9% showed MAI 80-90% and MDI 50-60% (Chen *et al.*, 1996). The values for the MAI and MDI suggest that the source rock from the northern part of the basin has a higher thermal maturity compared to the southern part. This is in line with the observed trend in source rock maturity based upon Tmax values from Rock Eval pyrolysis (Table 1). The estimated vitrinite equivalent values are much higher than the values estimated based on biomarker molecules (Chapter 4), which indicated vitrinite equivalent values of ca. 0.8%. This offset

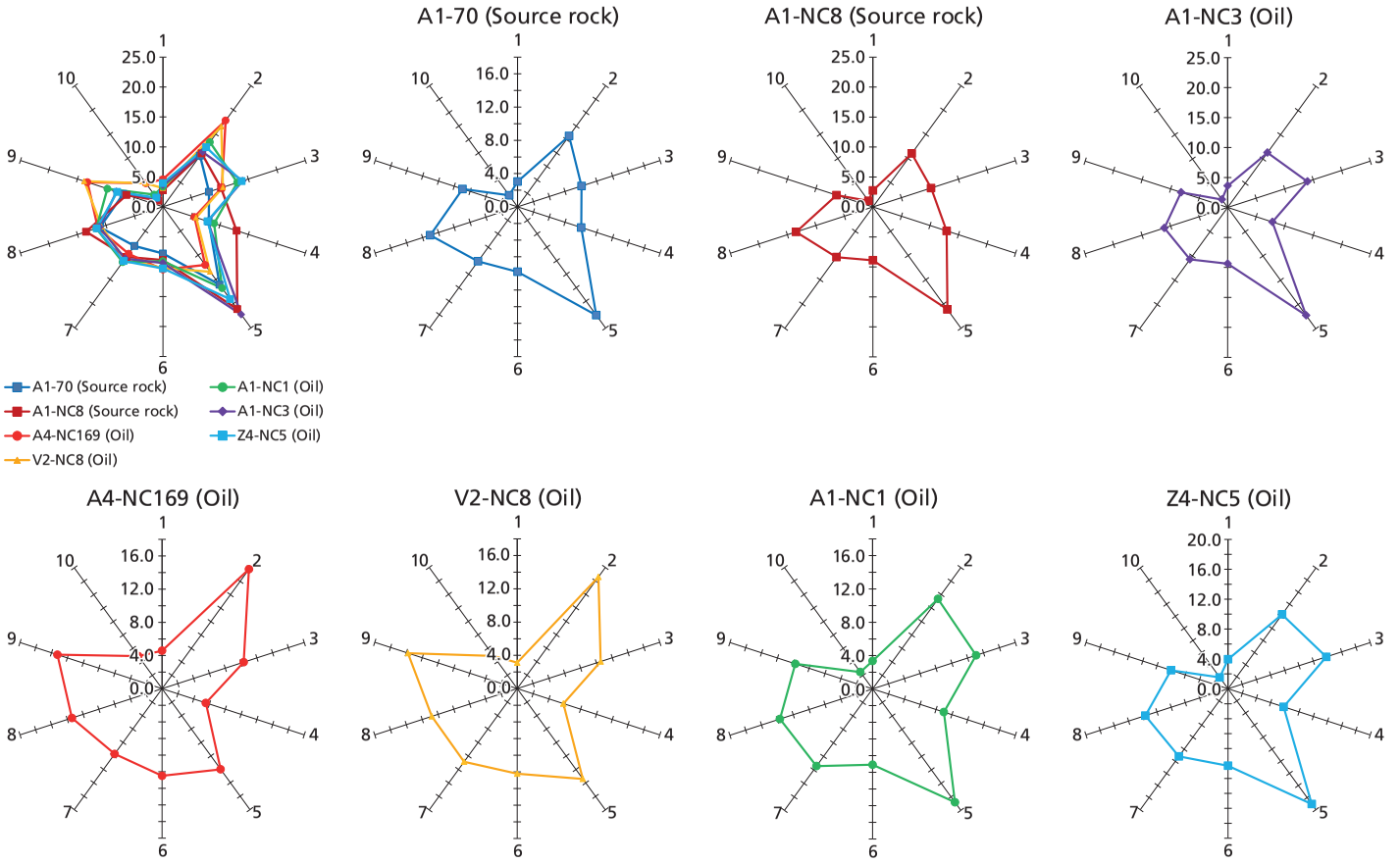

Fig. 10. Source-oil correlation, using star plot of diamondoids (adamantane %) data from source rock extracts and crude oils in the Ghadamis Basin. The numbers refer to compounds listed in Table 3.

may suggest that the biomarkers underestimate the source rock maturity as the higher values based on the diamondoid ratios are difficult to explain without additional cracking.

The crude oils from A4-NC169 and V2-NC8 wells generally have higher MAI values (63 and 61%); thus they have higher maturities than the crude oils from the northern part (47-51%). These values are similar, albeit showing an opposite trend compared to the source rock extracts. The source rock extracts show EAI values in the range previously suggested to indicate marine shale Type II source rocks (Schulz et al., 2001), which is in line with microscopic investigation (Chapter 4). The oils have enhanced EAI values (65 – 74%) in line with a Type II marine source rock (i.e. the Tanezzuft Formation).

4.6. Oil-source rock correlation

Geochemical correlation between source rock extracts and crude oils relies upon establishing similarities in the organic geochemical composition. Comparing the compositions across the basin primarily shows there is overall a strong similarity between all source extracts and crude oils from the Ghadamis Basin. Still, as the oil is distributed across a large geographic area and more than one reservoir horizon, it is potentially generated by separate source kitchens (Chapters 3 and 4). Correlations based on API gravity, biomarker, and aromatic maturity parameters (Table 2) suggest that they are all genetically related. Based on comparing maturity of the source rock extracts and the crude oils, it appears that the Tanezzuft hot shale was the major source of the Ghadamis Basin.

Using the diamondoid composition, it might still be possible to investigate more subtle differences between the oils and source rock extracts. Since diamantanes were only detected in the source rock extract we plotted the adamantanes (%) data in a star diagram (Fig. 10), which suggests some subtle differences. The crude oil appears to be divided into sub-families: (i) sub-family A is represented by the highly mature oils from A4-NC196 and V2-NC8 wells (Southern Ghadamis Basin), whereas (ii) sub-family B includes the somewhat less mature oils from Z4-NC5, A1-NC1 and A1-NC3 wells (North). Overall oils in sub-family A are characterized by higher concentration of diamondoids compared to sub-family B (Fig. 10; Table 3), in line with the higher maturities of these oils that were also indicated by the other indices studied here. The two subfamilies, hence, may represent separate source kitchens and/or different thermal maturity levels and/or different migration pathways.

Based on comparing maturity of the source rock extracts and the crude oils (Fig. 10) and comparing diamondoid distributions, it appears that the two source rocks, although having different maturities, have nearly identical diamondoid distributions (Fig. 10). Both source rock extracts seem to resemble the crude oil sub-family B, from the northern part of the Ghadamis Basin. It can be observed that the southern crude oils (sub-family A) does also not match either source rock extract, not even that from the same concession NC8 (Figs. 1 and 10). This suggests that these crude oils migrated from elsewhere to the southwestern part of Ghadamis Basin.

5. Conclusions

The Ghadamis basin crude oils and source rocks are highly mature and at the end of traditional biomarker indices for estimating maturity. Cross-correlation of these indices with diamondoid-based indicators suggests differences in maturity of the lower Silurian Tanezzuft "hot" shale source rock ranging from early mature in the southern source to late mature in the northern source. The lack of diamantane in the crude oils indicates that crude oils were expelled before diamantane formed in the source rock. Plotting adamantane concentrations shows that there is a strong compositional similarity between the northern crude oils (sub-family B), and that they resemble both Ghadamis Basin source rock extracts. Hence these oils most likely formed locally. The crude oils from the southern part of the basin (sub-family A) differs from both the northern basin crude oils and the local source rock extracts and hence most likely migrated from elsewhere.

Appendix. Structure of admantane (I) and diamantane (II).

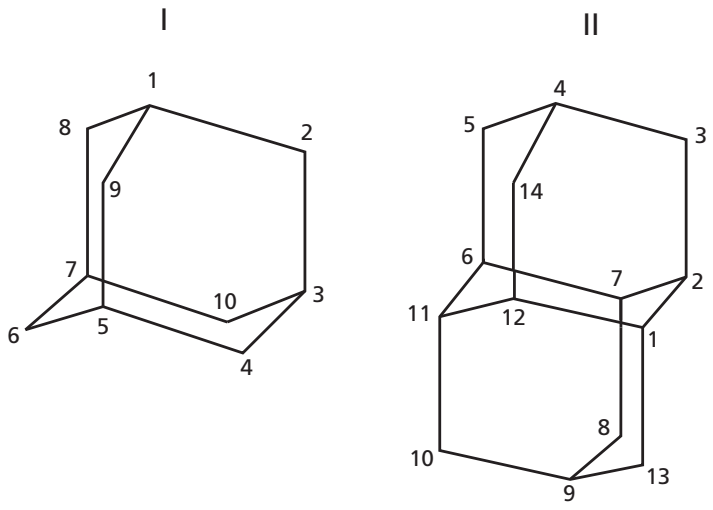

References

Al-Ameri, T.K., 1983. Acid resistant microfossils used in the determination of Palaeozoic palaeoenvironments in Libya. Palaeogeogr. Palaeoclimatol. Palaeoecol. 44, 103 – 116.

Alexander, C., Suzuki, N., 1995. Aromatic sulfur compounds as maturity indicators for petroleums from the Buzuluk depression, Russia. Org. Geochem. 23, 617-625.

Alexander, C., Suzuki, M., Takayama, K., 1997. Distribution of alkylated dibenzothiophenes in petroleum as a tool for maturity assessments. Org.Geochem. 26, 483-490.

Al-Hajri, S., 1991. Systematics and Biostrigraphy of Middle Ordovician to Lower Silurian chitinozoans of the Arabian Peninsula. Master thesis of Geosciences, University of Pennsylvania.

Andrew, A.S., Hamilton, P.J., Mawson, R., Talent, J.A., Whitford, D.J., 1994. Isotopic correlation tools in the mid-Palaeozoic and their relation to extinction events. Aus. Petrol. Explor. Assoc. J. 34, 268 – 277.

Aoudeh, S.M.., Al-Hajri, S.A., 1995. Regional Distribution and Chronostratigraphy of the Qusaiba Member of the Qalibah Formation in the Nafud Basin, Northwestern Saudi Arabia. In: Al-Husseini, M.I. (Ed), GEO, 94; The Middle East Petroleum Geosciences. Gulf Petrolink, Bahrain, v.1, p143-154.

Armstrong, H.A., Turner, B.R., Makhlouf, I.M., Weedon, G.P., Williams, M., Al Smadi, A., Abu Salah, A., 2005. Origin sequence stratigraphy and depositional environment of an upper Ordovician (Hirnantian) deglacial black shale, Jordan. Palaeogeogr. Palaeoclimatol. Palaeoecol. 220, 273-289.

Armstrong, H.A., Abbott, G., Turner, B.R., Makhlouf, M., Muhammad, A.B., Pedentchouk, N., Peters, H., 2009. Black shale deposition in an Upper Ordovician-Silurian Permanently stratified, peri-glacial basin, southern Jordan. Palaeogeogr. Palaeoclimatol. Palaeoecol. 273, 368-377.

Aziz, A., 2000. Stratigraphy and hydrocarbon potential of the Lower Palaeozoic succession of License NC115, Murzuq Basin, SW Libya In: Sola, M.A. and Worsley, D. (Eds.) Geological Exploration in Murzuq Basin, p. 349-368.

Azmy, K., Veizer, J., Bassett, M.G., Copper, P., 1998. Oxygen and carbon isotopic composition of Silurian brachiopods: implications for coeval seawater and glaciations. Geol. Soc. Am. Bul. 110, 1499-1512.

Beach, F., Beakman, T.M., Abbott, G.D., Sleeman, R., Maxwell, J.R., 1989. Laboratory thermal alteration of triaromatic steroid hydrocarbons. Org. Geochem. 14, 109-111.

Belhaj, F. 1996, Palaeozoic and Mesozoic stratigraphy of eastern Ghadamis and western Sirt basins. In: The Geology of Sirt Basin, M.J. Salem, A.J. Mouzughi and O.S. Hammuda (Eds). Elsevier, Amsterdam, 1, 57-96.

Belhaj, F., 2000. Carboniferous and Devonian stratigraphy- the Mrar and Tadrart reservoir, Ghadamis Basin. In: Sola, M.A. and Worsely, D. (Eds). The geological Exploration in Murzuq Basin, Elsevier Science B.V, p. 117-142.

Bellini, E., Massa, D., 1980. A stratigraphic contribution to the Palaeozoic of the southern basins of Libya. In: Salem, M.J., Busrewil, M.T. (Eds). The geology of Libya. Volume 1. Academic Press, London, 348 pp.

Berner, R.A., 1970. Sedimentry pyrite formation. Am. J. Sci. 268, 1-23.

Berner, R.A., Raiswell, R. 1983. Burial of organic carbon and pyrite sulfur in sediments over Phanerozoic time: a new theory. Geochim. Cosmochim. Acta, 47, 855-862.

Berner, R.A., 1994. GEOCARB II: a revised model for atmospheric CO_2 over Phanerozoic time. Am. J. Sci. 294, 56-91.

Berner, R.A., Kothavala, Z., 2001. GEOCARB III: a revised model of atmospheric CO_2 over Phanerozoic time. Am. J. Sci. 301, 182-204.

Bond, D., Wignall, P.B., Racki, G., 2004. Extent and duration of marine anoxia during the Frasnian-Famennian (Late Devonian) mass extinction in Poland, Germany, Austria and France. Geol. Mag, 141, 173-193.

Bond, D., Wignall, P.B., 2005. Evidence for Late Devonian (Kellwasser) anoxic events in the Great Basin, western United States. In: Over, J., Morrow, J., Wignall, P.B (Eds.). Development in Palaeontology and Stratigraphy. Understanding Late Devonian and Permian-Triassic Biotic and Climatic Events, 20. Elsevier, pp. 225-261.

Boote, D.R.D., Clark, L.D.D., Traut, M.W., 1998. Palaeozoic Petroleum System of North Africa In: Macgregor, D.S., Moody, R.T.J., Clark-Lowes, D.D. (Eds.) Petroleum Geology of North Africa. Geological Society, Special Publication 132, 7-68.

Bordenave, M.L., 1993. Applied Petroleum Geochemistry. Paris: Edition Technip.

Bordenave, M.I., Espitalié, L., Leplat, P., Oudin, J.I., Vandenbroucke, M., 1993. Screening techniques for source rock evalution. In: Bordenave, M.I. (Ed.), Applied Petroleum Geochemistry. Editions Technip, Paris, p. 217-278.

Boumendjel, K., Loboziak, S., Paris, F., Steemans, P., Streel, M., 1988. Biostratigraphie des chitinozoaires et des spores du Dévonien dans un sondage du Bassin d'Illizi (Sahara algérien). Géobios 21, 329-357.

Brand, U., Azmy, K., Veizer J., 2006. Evaluation of the Salinic I tectonic, Cancafiari glacial and Irevken biotic events: biogeochemostratigraphy of the Lower Silurian succession in the Niagara Gorge area, Canada and USA. Palaeogeogr. Paleoclimatol. Palaeoecol. 241, 192 – 213.

Brenchley, P.J., Marshall, J.D. Carden, G.A.F., Robertson, D.B.R. Long, D.G.F., Meidla, T., Hints, L., Anderson, T.F., 1994. Bathymetric and isotopic evidence for a short-lived Ordovician glaciation in a greenhouse period. Geology 22, 295-298.

Brinkhuis, H., Munsterman, D.K., Sengers, S., Sluijs, A., Williams, G.L., 2003. Late Eocene-Quaternary Dinoflagellate cysts from ODP site 1168, off western Tasmania plateau. In: Exon et al., Scientific Results ODP leg 189 College station.

Buggisch, W., Joachimski, M.M., 2006. Carbon isotope stratigraphy of the Devonian of central and southern Europe. Palaeogeogr. Paleoclimatol. Palaeoecol. 240, 68-88.

Butcher, A., 2009. Early Lilandovery chitinozoans from Jordan. Palaeontology 52, 593-629.

Butcher, A., 2013. Chitinozoans from the middle Rhuddanian (lower Llandovery, Silurian) "hot" shale in the E1-NC174 core, Murzuq Basin, SW Libya.

Calner, M., Kozłowska, A., Masiak, M., Schmitz, B., 2006. A shoreline to deep basin correlation chart for the middle Silurian coupled extinction-stable isotope event. GFF 128, 79 – 84.

Calvert, S.E., Pederson, T.F., 1992. Productivity, accumulation, and perseveration of organic matter in recent and ancient sediments. Columbia Univ. Press, p. 231-263.

Calvert, S.E., Pederson, T.F., 1993. Geochemistry of recent oxic and anoxic sediments: implication for the geological record. Mar. Geol. 113, 67-88.

Chen, J., Fu, J., Sheng, G., Liu, D., Zhang, J., 1996. The diamondoid hydrocarbon ratios: novel maturity indices for over-mature crude oils. Org. Geochem. 25, 179-190.

Clayton, C.J., Bjoroy, M., 1994. Effect of maturity on 13C/12C ratios of individual compounds in North Sea oils. Org. Geochem. 21, 737-750.

Colbath, G.K., 1990. Palaeobiogeography of Middle Palaeozoic organic-walled phytoplankton. In: McKerrow, W.S., Scotese, C.R. (Eds). Palaeozoic Palaeogeography and Biogeography. Geological Society, London, Memoir, 12, 207-213.

Combaz, A., 1962. Sur un nouveau de microplanctonte cenobial fossil du Gothlandien de Lybia. Deflandrastrum nov. gen C.R. Acad. Sci. paris, Vol. 255, pp. 1977-1979.

Combaz, A., 1966. Remarques sur les niveaux á tasmanacé du Paléozoique saharien. Palaeobot. 15, 29-34.

Cooper, J.D., Keller, M., 2001, Palaeokarst in the Ordovician of the southern Great Basin, USA: Implications for sea-level history: Sedimentology 48, 855 – 873.

Corfield, R.M., Siveter, D.J., Cartlidge, J.E., McKerrow, W.S., 1992. Carbon isotope excursion near the Wenlock – Ludlow (Silurian) boundary in the Anglo-Welsh area. Geology 20, 371-374.

Cramer, F.H., 1966. Palynomorphs from the Siluro-Devonian boundary in NW Spain, Espana, 1st. Geol. Min. Not. Commun 85, 71-82.

Cramer, B.D., Saltzman, M.R., Kleffner, M.A., 2006. Spatial and temporal variability in organic carbon burial during global positive $\delta^{13}C_{carb}$ excursions: new insight from high-resolution $\delta^{13}C_{carb}$ stratigraphy from the type area of the Niagarian (Silurian) Provincial Series. Stratigraphy 2, 327 – 340.

Cramer, B.D., Saltzman, M.R., 2007. Early Silurian paired $\delta^{13}C_{carb}$ and $\delta^{13}C_{org}$ analyses from the Midcontinent of North America: implications for paleoceanography and paleoclimate. Palaeogeogr. Palaeoclim. Palaeoecol. 256, 195 – 203.

Dahl, J.E., Moldowan, J.M., Peters, K.E., Claypool, G.E., Rooney, M.A, Michael, G.E, Mello, M.R., Kohnen, M.L., 1999. Diamondoid hydrocarbons as indicators of natural oil cracking. Nature 399, 54-57.

Dahl, J.E., Moldowan, J.M., Wei, Z. Lipton P.A., Denisevich, P., Gat, R., Shengao, L., Schreiner, P.R., Carlson, R.M.K., 2010. Synthesis of higher diamondoids and implications for their formation in petroleum. Angew. Chem. Int. Ed. 49, 9881-9885.

Didyk, B.M., Simoneit, B.R.T., Brassell, S.C., Eglinton, G., 1978. Organic geochemical indicators of palaeoenviromental conditions of sedimentation. Nature 272, 216-222.

Dreesen, R., Poty, E., Streel, M., Thorez, J., 1993. Late Famennian to Namurian in the eastern Ardenne, Belgium, I.U.G.S., Subcom. Carb. Strat. Guidebook. Liége Uinversity, Liege, 60.

Echikh, K. Sola, M.A., 2000. Geology and Hydrocarbon Occurrences in the Murzuq Basin, SW Libya. In: Sola, M.A., Worsley, D. (Eds.) Geological Exploration in Murzuq Basin, p.175-222.

Edwards, D., Wellman, C.H. 2001. Embryophytes on land: The Ordovician to Lochkovian (Lower Devonian). In: Gensel, P.G., Edwards, D. (Eds.), Plants invade the land: Evolutionary and Environmental Perspectives, 3 – 28. Columbia University Press, New York, New York, USA.

Eglinton, G., Scott, P.M., Besky, T., Burlingame, A.L., Calvin, M., 1964. Hydrocarbons of biological origin from one-billion-year-old sediment. Science 145, 263-264.

Espitalié, J., Deroo, G., Marquis, F., 1985. La Pyrolyse Rock-Eval et ses applications. Oil Gas Sci. Technol. 40, 563-579.

Farrimond, P., Love, G.D., Bishop, A.N., Innes, H.E., Watson, D.F., Snap, C.E., 2003. Evidence for the rapid incorporation of hopanoids into kerogen. Ceochimica Cosmoch. Acta 67, 1383-1394.

Ghienne, J, F., Deynoux, M. 1998. Large-scale channel fill structures in Late Ordovician glacial deposits in Mauritania, western Sahara. Sedim. Geol. 119, 141-159.

Goossens,, H., Due, A., De Leeuw, J.W., van De Graaf, B., Schenck, P.A., 1988. The Pristane Formation index, a new molecular maturity parameter. A simple method to assess maturity by pyroslysis/

evaporation-gas chromatography of unextracted samples. Geochem. Cosmochim Acta 52, 1189-1192.

Gradstein, F.M., Ogg, J.F., Smith, A.G. (Eds.) 2004. Geologic Time Scale 2004. Cambridge University Press, 500 pp.

Grantham, P.J., Wakefield, L.L., 1988. Variations in the sterna carbon number distributions or marine source rock derived crude oils through geological times. Org. Geochem. 12, 61-77.

Grice, K., Alexander, R., Kagi, R.I., 2000. Diamondoid hydrocarbon ratios as indicators of biodegradation in Australian crude oils. Org. Geochem. 31, 67-73.

Hallett, D., 2002. Petroleum Geology of Libya. Elsevier, Amsterdam, pp. 322-333.

Hartgers, W.A., Sinninghe Damsté J.S., De Leeuw, J.W., 1992. Identification of C_2 to C_4 alkylated benzenes in flash pyrolysis of kerogens, coals and asphaltenes. J. Chrom. 606, 211-220.

Hartgers, W.A., Sinninghe Damsté, J.S., Koopmans, M.P., De Leeuw, J.W., 1993. Sedimentary evidence for the occurrence of a diaromatic carotenoid with an unprecedented aromatic substitution pattern. J. Chem. Soc. Chem. Commun. 23, 1715-1716.

Hartgers, W.A., Sinninghe Damsté J.S., De Leeuw J.W., 1994a. Geochemical significance of alkylbenzene distributions in flash pyrolysis of kerogens, coal and asphaltenes. Geochem. Cosmochim. Acta 58, 1759-1775.

Hartgers, W.A., Sinninghe Damsté, J.S., De Leeuw, J.W., Ling, Y., Dyrkacz, G.R., 1994b. Molecular characterization of 2 Carboniferous coals and their constituting maceral fractions. Energy Fuels 8, 1055-1067.

Hartgers, W.A., Sinninghe Damsté, J.S., Requejo, A.G., Allan, J., Hayes, J.M., Ling, Y., Xie, T.M., Primack, J., De Leeuw J.W., 1994c. A molecular and carbon isotopic study towards the origin and diagenetic fate of diaromatic carotenoids. Org. Geochem. 22, 703-725.

Hartkopf-Fröder C., Kloppisch M., Mann U., Neumann-Mahlkau P., Schaefer R.G., Wilkesh H., 2007. The end-Frasnian mass extinction in the Eifel Mountains, Germany: new insights from organic matter composition and preservation. Geol. Soc. London Spec. Publ. 278, 173-196.

Hayes, J.M., Takigiku, R., Ocampo, R., Callot, H.J., Albrecht, P., 1987. Isotopic compositions and probable origin of organic molecules in the Eocene Messel Shale. Nature 329, 48-51.

Hetzel, A., Böttcher, M.E., Wortmann, U.G., Brumsack, H.J., 2009. Paleo-redox conditions during OAE2 relfected in Demerara Rise sediment geochemistry (ODP Leg 207). Palaeogeogr. Palaeoclimatol. Palaeoecol. 273, 302-328.

Hill, P.J., Dorning, K.J., 1984. Appendix 1. Acritarchs. In: Cocks, L.R.M. et al. (Eds.). The Llandovery Series of the Type Area. Bulletin British Museum natural History (Geology) v38, p. 174-176.

Hill, P.J., Paris, F., Richardson, I.B., 1985. Silurian Palynomorphs. In: Thusu, B.G.. Owens, B. (Eds), The Palynostratigraphy of Northeast Libya Micropalaeontology 4, 27-48.

Hill, P. J., Molyneux, S.G., 1988. Biostratigraphy, palynofacies and provincialism of Late Ordovician – Early Silurian acritarch from northeast Libya, in: El-Arnauti A. et al. (Eds) Subsurface Palynostratigraphy of Northeast Libya, Garyounis University, Benghazi, Libya, SPLAJ, pp. 27-43.

Hoefs, M.J.L., Van Heemst, J.D.H., Gelin, F., Koopmans, M.P., Van Kaam-Peters, H.M.E., Schouten, S., De Leeuw, J.W., Sinninghe Damsté, J.S. 1995. Alternative biological source for 1,2,3,4-tetramethylbenzene in flash pyrolysate of kerogen. Org. Geochem. 23, 975-979.

Horsfield, B., 1989. Practical criteria for classifying kerogens: Some observation from pyrolysis-gas chromatography. Geochim. Cosmochim. Acta 53, 891-901.

Hughes, W.B., 1984. The use of thiophenic organosulfur compounds in characterizing crude oils derived from carbonate versus siliciclastic source rocks. In: Petroleum Geochemistry and Source Rock Potential of Carbonate Rocks (ed. J.G. Palacas); AAPG Studies in Geology 18, 181-196.

Hughes, W.B., Holba, A.G., Dzou, L.I.P., 1995. The ratios of dibenzothiophene to phenanthrene and pristane to phytane as indicators of depositional environment and lithology of petroleum source rocks. Org. Geochem. 17, 3581-3598.

Hunt, J.M., 1996. Petroleum Geochemistry and Geology, 2nd edition, W.H. Freeman San Francisco, 743 pp.

Hutter, 1979. Alpenachitina crameri, Anew chitinozoan from the Middle Devonian of Egypt. (Shell company, internal report).

Jardiné, S., Yapaudjian, L., 1968. Lithostratigraphie et palynology du Dévonien-Gothlandien gréseux du Bässin de Polignac (Sahara). Rev.I. Fr. Petr. 23, 439-469.

Jardiné, S., Combaz, A., Magloire, L., Peniguel, G., Vachey, G. 1974. Distribution stratigraphiqué des Acritraches dans le Paléozoique de Sahara Algérien. Review of Palaeobotany and Palynology, 18, 99-129.

Jeppsson, L., 1990. An oceanic model for lithological and faunal changes tested on the Silurian record. J. Geol. Soc. London 147, 663-674.

Jeppsson, L.,1997.. A new latest Telychain Sheinwoodian and Early Homerian (Early Silurian) Standard Conodont Zonation. T.R.S.E. Earth 88, 91-114.

Joachimski, M.M., Buggisch, W., 1993. Anoxic event in the late Frasnian- Causes of the Frasnian-Famennian faunal crisis? Geology 21, 675-678.

Johnson, J.G., Klapper, G., Sandberg, C.A., 1985, Devonian eustatic fluctuations in Euramerica. Geol. Soc. Am. B. 96, 567-587.

Kaljo, D., Boucot, A, J., Corfield, R.M., Le Hérissé, A., Koren, T.N., Kriz, J., Männik, P., Märss. T., Nestor, V., Shaver, R.H., Siveter, D.J., Viira, V., 1995. Silurian bio-events. In: Walliser, O.H. (Ed), Global Events and Events Stratigraphy in the Phanerozoic. Spring, Berlin, pp. 173-223.

Kaljo, D., Kiipli, T., Martma, T., 1997. Carbon isotope event markers through the Wenlock-
Pridoli sequence at Ohesaare (Estonia) and Priekule (Latvia). Palaeogeogr. Palaeoclimatol. Palaeoecol. 132, 211 – 233.

Kaljo, D., Martma, T., 2006. Application of carbon isotope stratigraphy to dating the Baltic Silurian rocks. GFF 128, 123 – 129.

Kenrick, P., Crane, P.R., 1997.The Origin and Early Diversification of Land Plants: A Cladistic Study. Smithsonian Institution Press, Washington.

Kent, D.V., Van der Voo, R. 1990. Palaeozoic palaeogeography from palaeomagnetism of Atlantic-bordering continents. In: Mckerrow, W.S., Scotese, C.R. (Eds.) Palaeozoic Palaeogeography and Biogeography, Geol. Soc. Mem. 12, 49-56.

Klitzsh, E., 1963. Geology of the North-East Flank of the Murzuq Basin (Djebel Ben Ghnema-Dor el Gussa Area) Rev. Inst. Fr. Pt., 18, 1411-1472.

Klitzsch, E., 1968. Outline of the geology of Libya. In: Geology and Archaeology of Northern Cyrenaica, Libya. Petrol. Explor. Soc. Libya, 10th Annu. Field Conf., 71-78.

Klitzsch, E., 1969. Stratigraphic section from the type areas of Silurian and Devonian strata at western Murzuk Basin (Libya). In: Kanes, W.H. (Ed.). Geology, archaeology and prehistory of the southwestern Fezzan, Libya. Petroleum Exploration Society of Libya, Tripoli, p. 83-90.

Klitzsch, E., 1970. Die strukturgeschichte der Zentralsahara. Neue Erkenntnisse zum Bau und zur Paläogeographie eines Tafellandes. Geol. Rundsch. 59, 459-527.

Klitzsch, E., 1981. Lower Palaeozoic rocks of Libya, Egypt and Sudan. In: Holland, C. (Ed.) Lower Palaeozoic of the Middle East, Eastern and Southern Africa and Antarctica. John Wiley & Sons, Chichester, p. 131-163.

Koopmans, M.P., Köster, J., Van Kaam-Peters, H.M.E., Kenig, F., Schouten, S., Hartgers, W.A., De Leeuw, J.W., Sinninghe Damsté, J.S., 1996a. Diagenetic and catagenetic products of isorenieratene: Molecular indicators for photic zone anoxia. Geochim. et Cosmochim. Acta 60, 4467-4496.

Koopmans, M.P., Schouten S., Kohnen M.E.L., Sinninghe Damsté J.S., 1996b. Restricted utility of aryl isoprenoids as indicators of photic zone anoxia. Geochim. Cosmochim. Acta 60, 4873-4876.

Kump, L.R., Arthur, M.A., Patzkowsky, M.E., Gibbs, M.T., Pinkus, D.S., Sheehan, P.M., 1999. A weathering hypothesis for glaciation at high atmospheric pCO_2 during the Late Ordovician. Palaeogeogr. Palaeoclimatol. Palaeoecol. 152, 173 – 187.

Kump, L. R., and M. A. Arthur (1999), Interpreting carbon-isotope excursions: Carbonate and organic matter, Chem. Geol., 161, 181-198.

Langford, F.F., Blanc-Valleron, M.M., 1990. Interpreting Rock-Eval pyrolysis data using graphs of pyrolisable hydrocarbons vs. total organic carbon. Amer. Assoc. Petrol. Geol. Bull. 74, 799-804.

Larter, S.R., Horsfield, B., 1993. Determination of structural components of kerogen by the use of analytical pyrolysis methods. In: Organic Geochemistry, Principle and Application (Eds. M.H. Engel and S.A. Macko), pp. 271-287. Petroleum Press, New York.

Lécuyer, C., Paris, F., 1997. Variability in the δ13C of lower Palaeozoic palynomorphs: implications for the interpretation of ancient marine sediments. Chem. Geol. 138, 161 – 170.

Le Hérissé, A., Deunff, J., 1988. Acritarches et Prasinophycés (Givétien supérieur-Frasnien moyen) de Ferques (Boulonnais-France). Biostratigraphie du Paléozoïque 7, 104-152.

Le Hérissé, A., 2000. Characteristics of the acritarchs recovery in the early Silurian of Saudi Arabia. In: Al-Hajri, S., Owens, B. (Eds.) Stratigraphic palynology of the Palaeozoic of Saudi Arabia. Gulf PetroLink, Bahrain, 57 – 81.

Lelubre, M., 1946. Sur le Paléozoique du Fezzan. C.R. Hebd. Séanc. Acad. Sci. 222, 1403-1404.

Li, Ji., Philp, P., Cul, M., 2000. Methyl diamantine index (MDI) as a maturity parameter for Lower Palaeozoic carbonate rock at high maturity and overmaturity. Org. Geochem. 31, 267-272.

Limachi, R., Goitia, V.H., Sarmiento, D., Arispe, O., Montecinos, R., Diaz Martínez, E., Dalenz Farjat, A., Liachenco, N., Pérez Leyton, M., Aguilera, E., 1996. Estratigrafía, geoquímica, correlaciones, ambientes sedimentarios y bioestratigrafía del Silúrico-Devónico de Bolivia 12th Congreso Geológico de Bolivia Tarija, Memorias 12, 183-197.

Lis, G.P., Mastalerz, M., Schimmelmann, A., 2008. Increasing maturity of kerogen type II reflected by alkylbenzene distribution from pyrolysis-gas chromatography-mass spectrometry. Org. Geochem. 39, 440-449.

Loboziak, S., Steemans, P., Streel, M., Vachard, D., 1992. Biostratigraphie par miospores du Dévonien inférieur à supérieur du sondage MG-1 (Bassin d'Hammadah, Tunisie). Comparaison avec les données des faunes. Rev. Palaeobot. Palynol. 74, 193-205.

Loboziak, S. Streel, M., 1995. West Gondwanan aspect of the Middle and Upper Devonian miospore zonation in the North African and Brazil. Rev. Palaeobot. Palynol. 86, 147-155.

Loboziak, S., Streel, M., 1998. Middle-Upper Devonian miospores from Ghadamis Basin (Tunisia-Libya): systematics and stratigraphy. Rev. Palaeobot. Palynol. 58, 173-196.

Loboziak, S., Melo, J.H.G., 2000. Miospore events from late Early to Late Devonian strata of Western Gondwana. Geobios 33, 399-407.

Loeblich Jr., T.R., 1970. Morphology, ultrastructure and distribution of Paleozoic acritrachs. Proceedings of the North American Paleontological Convention, Chicago 1969, part G, p.705-788.

Loydell, D.K., 2007. Early Silurian positive $\delta^{13}C$ excursions and their relationship to glaciations, sea-level changes, and extinction events. Geol. J. 42, 531 – 546.

Loydell, D.K., Fryda, J., 2007. Carbon isotope stratigraphy of the upper Telychian and lower Sheinwoodian (Llandovery – Wenlock, Silurian) of the Banwy River section,
Wales. Geol. Mag. 144, 1015 – 1019.

Loydell, D.K., Butcher, J., Fryda, J., Lüning, S., Fowler, M., 2009. Lower Silurian "hot shales" in Jordan: Anew depositional Model. J. Petrol. Geol. 32, 261-270.

Loydell, D.K., 2012. Graptolite biostratigraphy of the E1-NC174 core, Rhuddanian (lower Llandovery, Silurian), Murzuq Basin, Libya. B. Geosci. 87, 651-660.

Lüning, S., Craig, J., Loydell, D.K., Storch, P., Fitches, B., 2000. Lower Silurian "hot shales" in North Africa and Arabia: regional distribution and depositional model. Earth. Sci. Rev. 49, 121 – 200.

Lüning, S., Kolonic, S., Loydell, D.K., Craig, J., 2003. Reconstruction of the original organic richness in weathered Silurian shale outcrops (Murzuq and Kufra basins, southern Libya). GeoArabia 8, 299-308.

Lüning, S., Shahin, Y.M., Loydell, D., Al-Rabi, H.T., Masri, A., Tarawneh, B. and Kolonic, S. 2005. Anatomy of a world-class source rock: Distribution and depositional model of Silurian organic-rich shales in Jordan and implications for hydrocarbon potential. Am. Assoc. Petrol. Geol. Bull. 89, 1397-1427.

Lüning, S., Wendt, J., Belka, Z., Kaufmann, B., 2004. Temporal-spatial reconstruction of the early Frasnian (Late Devonian) anoxia in NW Africa: new field data from the Ahnet Basin (Algeria). Sed. Geol. 163, 237-264.

Lüning, S., Loydell, D.K., Storch, P., Shahin, Y., Craig, J., 2006. Origin, sequence stratigraphy and depositional environment of an Upper Ordovician (Hirnantian) deglacial black shale, Jordan: Discussion. Palaeogeogr. Palaeoclimatol. Palaeoecol.230, 352 – 355.

Ma, X. P., Wang, C.Y., Raki, Raka, M., 2008. Facies and geochemistry across the Early-Middle Frasnian transition (Late Devonian) on South China carbonate shelf; comparison with the Polish reference succession. Palaeogeogr. Palaeoclimatol. Palaeoecol. 269, 130-151.

Mackenzie, A.S., 1984. Application of biological markers in petroleum geochemistry. Advances in petroleum geochemistry, Volume 1, 115-214.

Malkowski, K., Racki, G., Drygant., Szaniawski, H., 2009. Carbon isotope stratigraphy across the Silurian-Devonian transition in Podolia, Ukraine: evidence for a global biogeochemical perturbation. Geol. Mag. 146, 674-689.

Martma, T., Brazauskas, A., Kaljo, D., Kaminskas, D. & Musteikis, P., 2005. The Wenlock-Ludlow carbon isotope trend in the Vidukle core, Lithuania, and its relations with oceanic events. Geol. Quarterly 49, 223-234.

Marynowski, L., Filipiak, P., Zatoń, M., 2010. Geochemical and palynological study of the Upper Famennian Dasberg event horizon from the Holy Cross Mountains (central Poland). Geol. Mag. 147, 527-550.

Massa, D., Jaeger, H., 1971. Données stratigraphiques sur le Silurien de l'Ouest de la Libye. Colloque Ordovicien-Silurien, Brest. Mém. S. Geo. F. 73, 313 – 321.

McGhee, G.R., 2001. The multiple impacts hypothesis for mass extinction: a comparison of the Late Devonian and the Late Eocene. Palaeogeogr. Palaeoclimatol. Palaeoecol. 176, 47-58.

Melchin, M.J., Holmden, C., 2006. Carbon isotope chemostratigraphy of the Llandovery in Arctic Canada: implications for global correlation and sea-level change. GFF 128,173-180.

Melo, J.H.G., Loboziak, S., Streel, M., 1999. Latest Devonian to early Late Carboniferous biostratgraphy of northern Brazil: an update. Bull. Cent. Rech. Explor. Prod. Elf-Aquitaine 22, 13-33.

Melo, J.H.G., Loboziak, S., 2003. Devonian-Early Carboniferous miospore biostratigraphy of the Amazon Basin, Northern Brazil. Rev. Palaeobot. Palynol. 124,131-202.

Mergl, M., Massa, D., 2000. A Palaeontological Review of the Devonian and Carboniferous Succession of the Murzuq Basin and the Djado Sub-Basin, in: Sola, M.A., Worsley, D. (Eds.), Geological Exploration in Murzuq Basin. Amsterdam: Elsevier Science B.V., p. 41-88.

Moldowan, J.M., Seifert, W.K., and Gallegos, E.J. 1985. Relationship between petroleum composition and depositional environment of petroleum source rocks. Am. Assoc. Petrol. Geol. Bull., 69, 1255-1268.

Moldowan, J.M., Sundararaman, P., Schoell, M., 1986. Sensitivity of biomarker properties to depositional environment and/or source input in the Lower Toarcian of SW-Germany. Org. Geochem. 10, 915-926.

Morrow, J.R., Sandberg, C.A,. 2009. Carbon isotope chemostratigraphy and precise dating of middle Frasnian (lower Upper Devonian) Alamo Breccia, Nevada, USA. Palaeogeogr. Palaeoclimatol. Palaeoecol. 282, 105-118.

Muhammad, I.J., Thomas, B.S., Sassen, R., Fazeelat, T., 2011. Diamondoids and biomarkers: as a tool better define the effects of thermal cracking and microbial oxidation on oils/condenates from reservoirs of the Upper Indus Basin, Pakistan. Carbonate Evaporite 26,155-165.

Munnecke, A., Samtleben, C., Bickert, T., 2003. The Ireviken Event in the lower Silurian of Gotland, Sweden – relation to similar Palaeozoic and Proterozoic events. Palaeogeography, Palaeoclimatology, Palaeoecology 195, 99 – 124.

Oliveira, S.F., 1997. Palinologia da sequência devoniana da Bacia do Paraná no Brasil Paraguaie Uruguai: implicações biocronoestratigráficas, paleoambientais e paleogeográficas. Docotoral Thesis. São Paulo, Universidad de São Paulo.

Ottone, E.G., 1996. Devonian palynomorphs from the Los Monos formation, Tarija basin, Argentina. Palynol. 20, 105-155.

Page, A., Williams, M., Zalasiewicz, J., 2006. Were transgressive black shales a negative feedpack mechanism modulating glacio-eustatic cycles in the Early Palaeozoic Icehouse? Geophysical Research Abstract 8, 09210.

Paris, F., Al-Hajri, S., 1995. New chitinozoan specie from the Llandovery of Saudi Arabia. Rev. Micropaleontol. 38, 311-328.

Paris, F., Elaouad-Debbaj, Z., Jaglin, J.C., Massa, D., Oulebsir, L., 1995. Chitinozoans and Late Ordovician glacial events on Gondwana. In: Cooper, J.D., Droser, M.L., Finney, S.C. (Eds.), Ordovician odyssey: short papers for the Seventh International Symposium on the Ordovician System. The Pacific Section for Sedimentary Geology (SEPM), Fullerton, California, pp. 171 – 176.

Pedentchouk, N., Freeman, K.H., Harris, N.B., Clifford, D.J., Grice, K., 2004. Source of alkylbenzene in Lower Cretaceous lacustrine source rocks, West Africa rift basins. Org. Geochem. 35, 33-45.

Pérez Leyton, M., 1991. Miospores du Devonien Moyen et Superieur de la Coup de Bermejo – La Angostura (Sud- Est de la Bolivie). Ann. Soc. Geo. Bel. 113, 373-389.

Peters, K.E., 1986. Guidelines for evaluating petroleum source rock using programmed pyrolysis: AAPG B. 70, 318-329.

Peters, K.E., Moldowan, J.M., 1991. Effects of source, thermal maturity and biodegradation on the distribution and isomerization of homohopanes in petroleum Org. Geochem. 17, 47-61.

Peters, K.E., Fraser, T.H., Amris, W., Rustanto, B., Hermanto, E., 1999. Geochemistry of crude oils from eastern Indonesia. Am. Assoc. Petrol. Geol. B. 83, 1927-1942.

Peters, K., Walters, C. C., Moldowan, J.M., 2005. The biomarker Guide, Vol, 2. Cambridge University Press, p. 1155-1160.

Philp, R.P., Gilbert, T.D., 1985. Source rock and asphaltene biomarker characterization by pyrolysis-gas chromatography-mass spectrometry-multiple ion detection. Geochim. Cosmochim. Acta 49, 1421-1432.

Phipps, D., Playford, G., 1984. Laboratory techniques for extraction and concentration of palynomorphs from sediments. Pap. Dep. Geol. Univ. Qd, 11, 1-23.

Pisarzowska, A., Sobstel, M., Racki, G., 2006. Conodont-based event stratigraphy of the Early-Middle Frasnian transition on South Polish carbonate shelf. Acta Palaeontol. Pol. 51, 609-646.

Playford, G., 1983. The Devonian miospore genus Geminospora Balme 1962: a reappraisal based upon topotypic G. lemurata (type species). Mem. Assoc. Australas. Palaeontol. 1, 311-325.

Powell, T.G., 1985. Paleogeographic implication for the distribution of upper Jurassic source beds: Offshore Eastern Canada. B.. Can. Pet. Geol. 33, 116-119.

Quadros, L.P., 1988. Zoneamento biostratigráfico do Paleozóico inferior e medio (seçáo marinha) da Bacia do Solimórs. Bol. Geociênc. Petrobras, Rio de Janeiro 2, 95-109.

Quadros, L.P., 1999. Silurian-Devonian acritrach assemblages from Paraná Basin: an update and correlation with Northern Brazilian basin. In: Rodrigues, M.A.C., Pereira, E. (eds). Ordovician-Devonian palynostratigraphy in Western Gondwana: update, problems and perspectives. Faculdade de Geologia da Universidade Estatal do Rio de Janeiro, Resumos expandidos, p. 105-145.

Racki, G., Racka, M., Matyja, H., Devleeschouwer, X., 2002. The Frasnian/Famennian boundary interval in the South Polish-Moravian shelf basin: integrated event stratigraphical approach. Palaeogeogr. Palaeoclimatol. Palaeoecol. 181, 251-297.

Racki, G., Piechota, A., Bond, D., Wignall, P.B., 2004. Geochemical and ecological aspects of lower Frasnian pyrite-ammonoid level at Kostomloty (Holy Cross Mountains, Poland). Geol. Q. 48, 267-282.

Radke, M., Welte, D.H., 1983. The methylphenanthrene index (MPI): a maturity parameter based on aromatic hydrocarbons. In: Advances in Organic Geochemistry 1981 (Eds. Bjorøy, M. et al.,). Wiley, Chichester, pp. 504 – 512.

Radke, M., Welte, D.H., Willsch, H., 1986. Maturity parameters based on aromatic hydrocarbons: influence of the organic matter type. Org. Geochem. 10, 51-63.

Ratledge C. and Wilkinson S. G. 1988. Terpenoid lipids. In Microbial Lipids (ed. C. Ratledge and S. G. Wilkinson), vol. 1, Chap. 3 Academic Press.

Requejo, A.G., Allan, J., Creany, S., Gray, N.R., Cole, K.S., 1992. Aryl isoprenoids and diaromatic carotenoids in Paleozoic source rocks and oils from the Western Canada and Willistone Basins. Org. Geochem. 19, 145-164.

Revill, A.T., Volkman, J.K., ÒLeary, T., Summons, R.E., Boreham, C,J., Banks, M.R., Denwer, K., 1994. Hydrocarbon biomarker, thermal maturity, and depositional setting of tasmanite oil shales from Tasmania, Australia. Geochim. Cosmochim. Acta 58, 3803-3822.

Richardson, J.B., 1988. Late Ordovician and Early Silurian cryptospores and miospores from northeast Libya. In: El-Arnauti. A. et al. (Eds), Subsurface Palynostratigraphy of Northeast Libya, Garyounis University, Benghazi, Libya, SPLAJ, p. 89-110.

Richoz, S., Van de Schootbrugge, B., Pross, J., Püttmann, W., Quan, T.M., Lindström, S., Heunisch, C., Fiebig, J., Maquil, R., Schouten, S., Hauzenberger, C.A., Wignall, P.B., 2012. Hydrogen sulphide poisoning of shallow seas following the end-Triassic extinction. *Nature Geoscience* 5, 662-667.

Riquier, L., Tribovillard, N., Averbuch, O., Devleeschouwer, X., Riboulleau, A., 2006. The Late Frasnian Kellwasser horizons of the HARZ Mountains (Germany): two oxygen-deficient periods resulting from different mechanisms. Chem. Geol. 233, 137-155.

Saltzman, M.R., 2001. Silurian $\delta^{13}C$ stratigraphy: a view from North America. Geology 29, 671 – 674.

Saltzman, M.R., 2002. Carbon isotope ($\delta^{13}C$) stratigraphy across the Silurian-Devonian transition in North America: evidence for a perturbation of the global carbon cycle. Palaeogeogr. Palaeoclim. Palaeoecol 187, 83-100.

Samtleben, C., Munnecke, A., Bickert, T., Pätzold, J., 1996. The Silurian of Gotland (Sweden): facies interpretation based on stable isotopes in brachiopod shells. Geol. Rundsch. 85, 278 – 292.

Samtleben, C., Munnecke, A., Bickert, T., 2000. Development of facies and C/O-isotopes in transects through the Ludlow of Gotland: evidence for global and local influences on a shallow-marine environment. Facies 43, 1 – 38.

Sarmah, M.K., Borthakur, A., Dutta, A., 2010. Pyrolysis of petroleum asphaltenes from different geological origins and use of methylnaphthalenes and methylphenanthrenes as maturity indicators for asphaltenes. Bull. Mater. Sci. 33, 509-515.

Schouten, S., Klein Breter, W.C.M., Blokker, P., Schogt, N., Rijpstra, W. I.C., Grice, K., Bas, M., Sinninghe Damsté, J. S. 1998. Biosynthetic effects on the stable carbon isotopic composition of algal lipids: Implication for deciphering the carbon isotopic biomarker record. Geochim. et. Cosmochm. Acta 62, 1397-1406.

Schulz, L.K., Wilhems A., Rein, E., Steen, A.S., 2001. Application of diamondoids to distinguish source rock facies. Org. Geochem. 32, 365-375.

Schwark, L., Empt, P., 2006. Sterane biomarkers as indicators of palaeozoic algal evolution and extinction events. Palaeogeogr. Palaeoclimatol. Palaeoecol. 240, 225-236.

Scotchman, I. C., Griffith, C.E., Holmes, A.J., Jones, D.M., 1998. The Jurassic petroleum system north and west of Britain: a geochemical oil-source correlation study. Org. Geochem. 29, 671-700.

Scotese, C.R., Mckerrow, W.S., 1991. Ordovician plate tectonic reconstructions. In: Ordovician Geology (Eds. By C.R. Barnes and S.H. Williams) Geol. Surv. Can. Pap 90-9, 271-282.

Seifert, W.K., Moldowan, J.M.,1978. Application of steranes, terpanes and monoaromatic to the maturation, migration and source of crude oils. Geochim. Cosmochim. Acta 42, 77-95.

Selley, R.C., 1997. The sedimentary basins of Northwest Africa. Stratigraphy and sedimentation. In: Selley, R.C. (Ed.) African Basins, vol 3, p 3-16. Amsterdam. Elsevier Sedimentary Basins of the World.

Silva, R.S.F., Aguiar, H.G.M., Rangel, M.D., Azevedo, D.A., Aquino Neto, R. 2011. Comprehensive two-dimensional gas chromatography with time of flight mass spectrometry applied to biomarker analysis of oils from Colombia. Fuel, 90, 2694-2699

Sinninghe Damsté, J.S., Van Duin, A.C., Hollander, D., Kohnen, M.E.I., De Leeuw, J.W., 1995 Early diagenesis of bacteriohopanepolols derivates: formation of fossil homohopanoids. Geochim. Cosmochim. Acta 59, 5141-5157.

Sinninghe Damsté, J.S., Kohnen, M.E.L., Horsfield, B., 1998. Origin of low-molecular-weight alkylthiophenes in pyrolysates of sulfur-rich kerogen as revealed by micro-scale sealed vessel pyrolysis. Org. Geochem. 29, 1891-1903.

Sinninghe Damsté, J.S., Köster, J., 1998. A euxinic southern North Atlantic Ocean during the Cenomanian-Turonian oceanic anoxic event. Earth and Planetary Science Letters 158-165.

Sinninghe Damsté, J.S., Schouten, S., van Duin, A.C.T., 2001. Isorenieratene derivatives in sediments: possible controls on their distribution. Geochim. Cosmochim. Acta 65, 1557-1571.

Sinninghe Damsté, J.S., Schouten S., 2006. Biological markers for anoxia in the photic zone of the water column. In: Marine Organic Matter: Biomarkers, Isotopes and DNA (Ed. J.K. Volkman), The Handbook of Environmental Chemistry 2N, Springer, Heidelberg, pp. 127-163.

Stanley, S.M., 2010. Relation of Phanerozoic stable isotope excursion to climate, bacterial metabolism and major extinctions. PNAS 107, 19185-19189.

Steemans, P., Le Hérissé A., Bozdogan, N., 1996. Ordovician and Silurian cryptospores and miospores from Southeastern Turkey. Rev. Palaeobot. Palynol. 93, 35-76.

Steemans, P., Higgs, K.T., Welliman, C.H., 2000. Cryptospores and trilete spores from the Llandovery, Nuayyim-2 Borehole, and Saudi Arabia. In: Al Hajri, S., Owens, B. (Eds.) Stratigraphic palynology of the Palaeozoic of Saudi Arabia. GeoArabia, Bahrain, p. 92-115.

Streel, M., Higgs, K., Loboziak, S., Riegel, W., Steemans, P., 1987. Spore stratigraphy and correlation with faunas and floras in the type marine Devonian of the Ardenne-Rhenish regions. Rev. Palaeobot. Playnol. 50, 211-229.

Streel, M., Paris, F., Riegel, W., Vanguestaine, M., 1988. Acritarch, chitinozoan and spore stratigraphy from the Middle and Upper Devonian subsurface of Northeast Libya. In: El-Arnauti, A., Owens, B., Thusu, B. (Eds.) Subsurface Palynostratigraphy of Northeast Libya, Benghazi-Libya Garyounis Univ. Publ., p. 111-128.

Streel, M., Fairon-Demaret, M., Gerrienne, P., Loboziak, S., Steemans, P., 1990. Lower and Middle Devonian miospore-based stratigraphy in Libya and its relation to the megafloras and faunas. Rev. Palaeobot. Palynol. 66, 229-242.

Summons, R.E., Powell, T.G., 1986. Chlorobiaceae in Palaeozoic seas revealed by biological markers, isotopes and geology. Nature 319, 763-765.

Summons, R.E., Powell, T.G., 1987, Chlorobiaceae in Palaeozoic seas revealed by biological markers, isotopes and geology. Nature 319, 763-765.

Tappan, H., 1980, The Paleobiology of Plant Protists. W.H. Freeman and Company, San Francisco, 1028 pp. 60-62

Tegelaar, E.W., De Leeuw, J.W., Derenne, S., Largeau, C., 1989a. A reappraisal of kerogen formation. Geochim. Cosmochim. Acta 53, 3103-3106.

Ten Haven H.L., de Leeuw J.W., Rullkötter J. and Sinninghe Damsté J.S., 1987. Restricted utility of the pristane/phytane ratio as a palaeoenvironmental indicator. Nature, 330(6149), 641-643.

Tissot, B.P., Pelet, R., Ungerer, P., 1987. Thermal history of sedimentary basins, maturation indices, and kinetics of oil and gas generation. Am. Assoc. Petrol. Geol. B. 71, 1445-1466.

Tissot, B.P., Welte D.H., 1984. Petroleum Formation and Occurrence, 2nd edition. Springer, Heidelberg, pp 356-359.

Trolio, R., Grice, K., Fisher, S.J., Alexander, R., Kagi, R.I., 1999. Alkylbiphenyls and alkylphenylmethane as indicators of petroleum biodegradation. Org. Geochem. 30, 1241-1253.

Tyson, R.V., 1993. Palynofacies analysis. In: Jenkins, D.G. (Ed.). Applied Micropaleontology Kluwer Academic Publisher, p. 153-191.

Tyson, R.V., 1995. Sedimentary organic matter. Chapman & Hall, London. 616 pp.

Underdown, R., and Redfern, J., 2007. The important of constraining regional exhumation in basin modelling: a hydrocarbon maturation history of the Ghadamis Basin, North Africa 13, 253-270.

Van de Meent, D., Brown, S. C. and Philps, R.P. 1980. Pyrolysis-high resolution gas chromatography and pyrolysis gas chromatography-mass spectrometry of kerogens and kerogen precursors. Geochem. Cosmochim. Acta 44, 999-1013.

Van de Schootbrugge, B., Tremolada, F., Rosenthal, Y., Bailey, T.R., Feist-Burkhardt, S., Brinkhuis, H., Pross, J., Kent, D.V., Falkowski, P.G. 2007. End-Triassic calcification crisis and blooms of organic-walled 'disaster species'. *Palaeogeogr. Palaeoclimatol. Palaeoecol.* 244, 126-141.

Van de Schootbrugge, B., Bachan, A., Suan, G., Richoz, S., Payne, J.L. 2013. *Microbes, mud, and methane: Cause and consequence of recurrent Early Jurassic anoxia following the end-Triassic mass-extinction.* Palaeontology, 56, 685-709.

Van der Voo, R. 1988. Paleozoic paleogeography of North America, Gondwana, and intervening displaced terranes: comparsions of paleomagnetism with paleoclimatogy and biogeographical patterns, Geol. Soc. Am. Bull. 100, 311-324.

Van der Weijden, C.H., Reichart, G.J., Visser, H.J., 1999. Enhanced preservation of organic matter in sediment deposited within the oxygen minimum zone in the Northeastern Arabian Sea Deep. Sea Res. 146, 807-830.

Van Dongen, B., Schouten, S., Sinninghe Damsté, J.S., 2002. Carbon isotope variability in monosaccharides and lipids of aquatic algae and terrestrial plants. Mar. Ecol. Prog. Lett. 232, 83-92.

Van Graas G., De Leeuw J. W., Schenck P.A., Haverkamp, J., 1981. Kerogen of Toarcian shales of the Paris Basin. A study of its maturation by flash pyrolysis techniques. Geochim. Cosmochim. Acta 45, 2465-2474.

Vecoli, M., Riboulleau, A., Versteegh, G.J.M., 2009. Palynology organic geochemistry and carbon isotope analysis of a latest Ordovician through Silurian clastic succession from borehole Tt1, Ghadamis Basin, southern Tunisia, North Africa: Palaenvironmental interpretation. Palaeogeogr. Palaeoclimatol. Palaeoecol. 273, 378-394.

Verniers, J., Nestor, V., Paris, F., Dufka, P., Sutherland, S., Van Grootel, G.,1995. A global Chitinozoa biozonation for the Silurian. Geol. Mag. 132, 651 – 66.

Volkman, J.K., Alexander, R., Kagi, R.I., and Woodhouse, G.W. 1983. Demethylated hopanes in crude oils and their application in petroleum geochemistry. Geochim. Et Cosmochim. Acta, 47, 785-794.

Walliser, O.H. (Ed.), 1996. Global Events and Event Stratigraphy in the Phanerozoic. Springer Verlag, Heidelberg. 4

Wang, G., Shi, S., Wang, P., Wang T.G., 2013. Analysis of diamondoids in crude oils using comprehensive two-dimensional gas chromatography/time-of-flight mass spectrometry. Fuel, 107, 706-714.

Wanglu, J, Xiao, Z., Yu, C., Peng, P., 2010. Molecular and isotopic compositions of bitumens in Silurian tar sands from the Tarim Basin, NW China: Characterizing biodegradation and hydrocarbon charging in an old composite basin. Mar. Petrol. Geol. 27, 13-25.

Wauthoz, B., 2005. Correlation of the 83W421 Kortrijk (Sint-Antonius) and 83W44Kortrijk (Lust) Boreholes with Acriatrchs (Late Aeronian-Early Telychian, Silurian, Belgium. Geol. Belg. 8, 176-184.

Wei, Z.B., Moldowan, J.M., Zhang, S.C., Hill, R., Jarvie, D.M., Wang, H.T., Song F.Q., Fago, F., 2007. Diamondoid hydrocrabons as a molecular proxy for thermal maturity and oil cracking geochemical models from hydrous pyrolysis. Org. Geochem. 38, 227-249.

Wignall, P.B., 1991. Model for transgressive black shale. Geology 19, 167-170.

Wingert, W.S., 1992. GC-MS analysis of diamondoid hydrocarbons in Smackover petroleum. Fuel 71, 37-43.

Wood, L., 1996. Biostratigraphic, paleoecologic and biologic significance of the Silurian (Llandovery) acritarch *Beromia rexroadii* gen. emend. et sp. Nov., mid-contintent and Eastern United States. Palynol. 20, 177-189.

Yang, C., Wang, Z.D., Hollebone, B.P, Peng, X., Fingas, M., Landriault, M., 2006. GC/MS Quantitation of diamondoid compounds in crude oils and petroleum products. Environ. Forensics 7, 377-390.

Yans, J., Corfield, R.M., Racki, G., Préat, A., 2007. Evidence for perturbation of the carbon cycle in the Middle Frasnian punctate Zone (Late Devonian). Geol. Mag. 144, 263-270.

Zachos, J., Pagani, M., Sloan, L.,Thomas, E., Billups, K., 2001. Trends rhytms and aberrations in global climate 65 Ma to Present. Science 292, 686-693.

Zhibin, W., Moldowan J.M., Peters, K.E., Wang, Y., Xiang, W., 2007. The abundance and distribution of diamondoids in biodegraded oils from the San Joaquin Valley: implications for biodegradation of diamondoids in petroleum reservoir. Org. Geochem. 38, 1910-1926.

Zhu, G., Wang, H., Weng, N., Huang, H., Liang, H., Ma, Shunping. 2013. Use of comprehensive two-dimensional gas chromatography for the characterization of ultra-deep condensate from the Bohai Bay Basin, China. Organ Geochem, 63, 8-17.

Summary

The Early Silurian "hot" shales and Late Devonian black shales are major regional oil and gas source rocks in North Africa. Moreover their deposition probably played a major role in global carbon cycling and biogeochemical cycles in general because of the large oceanic areas affected. The large amounts of carbon stored are also reflected by the major shifts in carbon isotopes globally. Comparing the Libyan $\delta^{13}C$ record with records from other areas enables us to examine local effects from larger-scale processes during these intervals. Silurian and Devonian formations in the western part of Libya are generally poorly studied, and their basin-scale facies distribution is largely unknown. The main goal of this thesis is to reconstruct the depositional environment on the North Africa margin during the deposition of the Silurian and Devonian black shales in the western part of Libya.

Because of their oil and gas potential many wells have been drilled in the Ghadamis and Murzuq basins. Studies focusing on the Early Silurian "hot" shale to Late Devonian black shale source rocks are, however, lacking; such studies critically depend on accurate age control. The stratigraphic position of the "hot" shale, close to the Ordovician-Silurian boundary, is an important question for hydrocarbon exploration in the northern Gondwana regions as this horizon is a synchronous across the North African margin.

The Tanezzuft and Awaynat Wanin formations are exposed on the western flanks of the Al Qarqaf Uplift. Such outcrops on the margins of the Murzuq Basin are, however, heavily weathered and oxidized. These deposits are therefore no longer suited for organic biostratigraphic and organic geochemical studies. Hence, this thesis concentrates on records drilled from the sub-surface. A biostratigraphic framework was established for four cores from Murzuq and Ghadamis basins along the African continental margin, correlating the Lower Silurian and Late Devonian of Libya to the global record. The bulk and compound specific $\delta^{13}C_{TOC}$ records have been analyzed for both biostratigraphy and paleoenvironmental indicators. Using compound specific $\delta^{13}C$ analyses, which allow us to interpret local and global isotopic signals, the true amplitude of the different carbon isotopic excursions was established in this thesis. The depositional environment at the North African margin during the Silurian was reconstructed and its potential role for preservation of sedimentary organic matter was revealed. Subsequently, differences in organic matter deposition through time and between the different sub-basins were assessed. An attempt was made to develop the stratigraphy for the Silurian and Devonian based on palynomorphs-particularly acritarchs, chitinzoas and miospores. In addition, the maturity of the Silurian and Devonian black shales was assessed.

The Silurian carbon isotopic signal ($\delta^{13}C_{TOC}$) from the west of Libya shows several events correlating with events observed earlier in isotopic curves from other areas. Positive $\delta^{13}C_{TOC}$ excursions occur close to important bioevents and three of these events are correlated to the global carbon isotopic curve. These positive $\delta^{13}C_{TOC}$ excursions are in line with the observed enhanced productivity and organic matter burial, mostly coinciding with rising sea levels.

Also, the Devonian is characterized by widespread formation of black shales; Late Devonian organic-rich sediments have attracted special attention as they coincide with

mass-extinction and evidence for global scale marine euxinia. The Devonian formations in the western part of Libya are poorly studied and their facies distribution is largely unknown. One of the formations previously suggested to play a potential role in petroleum generation is the Awaynat Wanin formation in the western part of Libya. This formation was investigated using a combined palynological, carbon isotopic and organic geochemical approach. During the Frasnian organic-rich shales were deposited across much of the North African margin, forming a potential secondary hydrocarbon source rock in the western part of Libya. The abundant and high diversity of prasinophytes, high TOC content and well-preserved amorphous organic matter deposited during the Early Frasnian strongly supports a scenario of enhanced sea surface productivity and oxygen depleted bottom water conditions. The onset of Frasnian black shale sedimentation is probably associated with eustatic sea level rise during the earliest Frasnian, coinciding with a major positive $\delta^{13}C_{TOC}$ carbon isotope excursion.

Palaeoenvironmetal reconstructions and assessment of thermal maturity of the early Silurian based on kerogen and asphaltene analysis of the Tanezzuft "hot" shale Formation from Murzuq and Ghadamis basins showed that these shales were deposited in a permanently stratified marine basin. In both Murzuq and Ghadamis basins high abundance of the flash pyrolysis products 1,2,3,4- and 1,2,3,5-tetramethylbenzenes together with appreciable amounts of 1-ethyl-3,4,5-trimethylbenzene and 1-ethyl-2,3,6-trimethylbenzene argue for the presence of macromolecularly-bound diaromatic carotenoids derived from phototrophic anaerobes. Continued photic zone euxinia into the lean shale suggests that other factors than enhanced preservation controlled TOC contents in this shale, such as changes in admixing of lithogenic material. Direct assessment of the thermal maturity of the Lower Palaeozoic rocks by vitrinite reflectance was not feasible because terrestrial plants were not present in the Silurian and pre-Silurian rocks. The maturity evaluations, based on equivalent vitrinite reflectance and Rock Eval pyrolysis, indicates that the Silurian source rock in Murzuq Basin is thermally more mature than that in the Ghadamis Basin. Significant differences in alkylbenzene distribution patterns were observed between kerogen pyrolysates in the two basins. This study indicates that pyrolysis gas chromatography-mass spectrometry (Py-GCMS) of asphaltenes and kerogens, integrated with other techniques, can be a useful complementary tool for the palaeoenvironmental assessment of thermal mature source rocks.

Assessment of thermal maturity becomes increasingly difficult at higher maturity levels as traditional biomarker-based indices reach the end of their useful range. This holds true for both source rock extracts and crude oils in the Ghadamis Basin. Two-dimensional gas chromatography, coupled to time of flight mass spectrometry (GCxGC-ToFMS) was applied to identify diamondoids in source rock extracts and crude oils from the western part of Libya. This approach revealed different levels of thermal maturity within the basin. Also, significant differences were noted between source rock extracts and the crude oils. Whereas the source rock extracts contain both adamantanes and diamantanes, the latter group is absent from the crude oils. The lack of diamantanes in the crude oils probably indicates that crude oils were expelled before diamantanes formed in the source rock. Comparing the relative distribution of adamantanes in the crude oils showed compositional differences between crude oils from the northern and southern part of the basin. The source rock extracts showed a strong similarity with the crude oils from the

northern part of the basin, whereas the relative diamondoid distribution in crude oils from the south suggests that these oils might have migrated from another (unknown) source.

Samenvatting

Organisch rijke schalies uit het vroeg Siluur en laat Devoon zijn de belangrijkste regionale olie- en gasbronnen in Noord Afrika. De wereldwijde afzetting van organisch rijke sedimenten in deze periode speelde waarschijnlijk een belangrijke rol in de globale biogeochemische cycli waaronder de koolstofcyclus. De grote hoeveelheid opgeslagen organisch koolstof wordt weerspiegeld door wereldwijde veranderingen in de koolstofisotoopsamenstelling van zowel sedimentair organisch en anorganisch koolstof. Door de Libische $\delta^{13}C$ curves met die in andere gebieden te vergelijken kunnen lokale effecten van wereldwijde verschuivingen in het koolstofbudget binnen deze geologische tijdvakken worden onderscheiden. De tijdens het Siluur en Devoon afgezette formaties in het westelijke deel van Libië zijn tot op heden nauwelijks bestudeerd en hun facies zijn grotendeels onbekend. Het belangrijkste doel van dit proefschrift is om het afzettingsmilieu van de organisch rijke schalies uit het Siluur en Devoon in het westelijke deel van Libië op de Noord Afrikaanse marge te reconstrueren.

Vanwege de grote olie- en gasvoorraden zijn er veel putten geboord in de Ghadamis en Murzuq Bekkens in Libië. De organisch rijke schalies van de Tannezzuft en Awaynat Wanin formaties die waarschijnlijk de bron vormden voor deze olie- en gasvoorraden worden gekenmerkt door een hoog niveau van natuurlijke straling als gevolg van de verrijking in uranium en worden daarom ook wel "hot shales" genoemd. Onderzoek gericht op deze schalies uit het vroege Siluur en de wat dunnere zwarte schalie gesteenten uit het late Devoon, en dan met name de laterale variabiliteit, is afhankelijk van precieze dateringen.

De Tanezzuft en Awaynat Wanin formaties liggen op de westelijke flanken van de Al Qarqaf opheffing. De bekende ontsluitingen zijn echter verregaand verweerd en geoxideerd. Deze sedimenten zijn daarom niet geschikt voor organisch geochemisch onderzoek. Om deze reden is het onderzoek beschreven in dit proefschrift gericht op monsters afkomstig van boorkernen diep uit de ondergrond. Een biostratigrafische correlatie is gemaakt tussen vier boorkernen uit de Murzuq en Ghadamis Bekkens langs de Afrikaanse marge. Met behulp van palynomorfen, en dan met name acritarchen, chitinzoën en miosporen, is inzicht verkregen in de lokale stratigrafische opeenvolging binnen zowel het Siluur als het Devoon. Hiermee kunnen laterale verschillen in de afzettingscondities tijdens het vroege Siluur en het Late Devoon onderling en met andere gebieden vergeleken worden. De bulk organische en component-specifieke $\delta^{13}C$ profielen zijn onderzocht voor zowel biostratigrafische als paleomilieu-reconstructie doeleinden. Met behulp van component-specifieke $\delta^{13}C$ analyses konden afwijkingen in koolstofisotopen, onafhankelijk van effecten door verschillen in samenstelling, worden vastgesteld. Het afzettingsmilieu van de Noord Afrikaanse marge tijdens het Siluur is gereconstrueerd en daarmee ook de rol van dit milieu in de preservatie van organische materiaal in sedimenten. Vervolgens kon een inschatting gemaakt worden van de verschillen in de afzetting van organische materiaal binnen de formaties tussen de verschillende deelbekkens. Daarnaast zijn omzettingen van het organisch materiaal van de schalies onderzocht.

Het Silurische koolstofisotopen signaal van het organisch materiaal ($\delta^{13}C_{TOC}$) uit het westen van Libië weerspiegelt verschillende gebeurtenissen die overeenkomen met gebeurtenissen die eerder in andere gebieden zijn vastgesteld. De gemeten positieve $^{13}C_{TOC}$ excursies correleren goed met bekende veranderingen en drie ervan kunnen aan globale koolstofisotoop excursies gekoppeld worden. Deze positieve $\delta^{13}C_{TOC}$ excursies duiden op een toegenomen opslag van organische koolstof, mogelijk ten gevolge van verhoogde biologische productiviteit, veelal samenvallend met mondiale zeespiegelstijgingen.

Het Devoon werd gekenmerkt door uitgebreide afzetting van organisch rijke schalies waarbij het Laat Devoon interessant is doordat dit samenviel met het massaal uitsterven van soorten in een grotendeels zuurstofarme en zwavelrijke oceaan. Ook de formaties van het Devoon uit het westen van Libië zijn nog nauwelijks bestudeerd en de verdeling van facies is onbekend. Één van de formaties waarvan eerder gesuggereerd werd dat deze een belangrijke rol speelde voor het lokale voorkomen van olie is de Awaynat Wanin formatie in west Libië. Deze formatie is onderzocht aan de hand van palynologische, stabiele koolstofisotopen en organische geochemische methoden. Tijdens het Frasnien werden organisch rijke schalies afgezet op de meeste plaatsen langs Noord Afrikaanse marge, en deze schalies vormen mogelijk een secundaire bron voor aardolie in het westen van Libië. De abundante en in grote diversiteit aanwezige prasinophyten, de hoge organische koolstof gehaltes en de goede preservatie van het organisch materiaal tijdens het Frasnien wijzen sterk op toegenomen biologische productiviteit in de fotische zone in combinatie met een afzettingsmilieu gekenmerkt door zuurstofarm bodemwater leidend tot een verhoogde preservatie van het organisch materiaal.

Reconstructie van het palaeomilieu en vaststelling van de omzettingen van organisch materiaal uit het vroeg Siluur aan de hand van kerogeen en asfalteen fracties geïsoleerd uit de organisch rijke afzettingen van de Tanezzuft formatie uit de Murzuq en Ghadamis bekkens geven aan dat deze zijn afgezet toen de waterkolom permanent gestratificeerd was. Pyrolysaten van deze fracties voor zowel Murzuq als Ghadamis Bekens bevatten een grote hoeveelheid aan 1,2,3,4- en 1,2,3,5-tetramethylbenzenen samen met aanzienlijke hoeveelheden 1-ethyl-3,4,5-trimethylbenzenen en 1-ethyl-2,3,6-trimethylbenzenen, wat wijst op de aanwezigheid van macromoleculair-gebonden diaromatische carotenoïden afkomstig van fototrofe, anaërobe zwavelbacteriën en dus op een overlap van de fotische en de euxinische zone van de waterkolom. Opvallend genoeg heersten deze condities ook na de afzetting van de organisch rijke schalies op de continentale marge. Dit suggereert dat er ook andere factoren bepalend zijn geweest voor de hoge organische koolstof gehaltes in de schalies, zoals bijvoorbeeld verschillen in verdunning met lithogeen materiaal. Dit onderzoek geeft aan dat pyrolyse-gas chromatografie-massa spectrometrie toegepast op asfaltenen en kerogenen, indien mogelijk gecombineerd met andere technieken, een toegevoegde waarde heeft om de milieuafzettingsomstandigheden van thermisch gematureerde gesteenten vast te stellen.

Directe bepaling van de thermische veroudering van de Laat Palaeozoische gesteenten door middel van vitrinietreflectie is niet mogelijk doordat landplanten nog niet bestonden ten tijde van het Siluur en eerder. Omzetting van organisch materiaal gemeten met Rock Eval pyrolyse en vertaald naar de mate van vitrinietreflectie laat zien dat de Silurische gesteenten in het Murzuq Bekken meer thermisch gematureerd zijn dan die uit het Ghadamis Bekken. Het bepalen van de mate van thermische maturatie

wordt steeds lastiger wanneer de maturatiegraad toeneemt omdat dan de traditioneel toegepaste indices op basis van biomarkers aan het einde van hun bereik komen. Dit geldt voor zowel extracten uit de gesteenten als de ruwe olies afkomstig uit het Ghadamis bekken. Tweedimenionale gas chromatografie gekoppeld aan "Time-of-Flight" massaspectrometrie, zijn toegepast om diamondoïden in extracten uit gesteenten en ruwe olies afkomstig uit west Libië te identificeren. Deze aanpak liet zien dat er verschillen bestaan in de thermische maturatiegraad binnen het bekken. Verder werden er duidelijke verschillen gevonden tussen extracten uit gesteenten en de ruwe olies. Terwijl in de extracten zowel adamantanen als diamantanen werden gevonden ontbrak deze laatste groep in de olies. De afwezigheid van diamantanen in aardolie wijst er op dat de olie waarschijnlijk al gemigreerd is uit het aardoliemoedergesteente voordat er diamantanen gevormd konden worden. De onderlinge verhouding van de verschillende adamantanen in de ruwe olies vertoonden verschillen aan tussen de olies afkomstig uit het noordelijke en het zuidelijk deel van het bekken. De extracten uit de gesteentes leken vooral op de aardolie uit het noordelijk deel van het bekken terwijl de verhouding van diamondoïden in de aardolie afkomstig uit het zuidelijke deel erop wijst dat deze wellicht ergens andersvandaan zijn gemigreerd en dus een andere oorsprong hebben.

Acknowledgements

Many people have contributed to the research in this thesis, and to the writing process. Without their help, this thesis could not have been realized. First and most importantly, I wish to thank my supervisors, I consider myself lucky to have worked under their supervision.

This piece of work could not have been possible without the inspiring, devoted and kind supervision of my promoter Prof. Gert-Jan Reichart. Heartiest gratitude to Gert-Jan for everything, clear guidance, critical vision, motivation, kindness and strong support to the different stages of the research and I have learned much from you. Thank you for your continuous encouragement.

I would like to express my appreciation to my other promoter, Prof. Jaap Sinninghe Damsté, who gave great support to this study. I thank him for his time to read through my thesis and his constructive criticism ensured the quality of this dissertation. I gained a lot from him while working under his supervision.

Special thanks go to my co-promoter Dr. Klaas Nierop for many comments and suggestions that helped improving this thesis. Klaas, I appreciate your efforts and the time spent on my research work.

I greatly appreciated the help offered by Alain Le Herisse from the University of Brest, who provided critical comments on the taxonomy and ages for Silurian acritarchs in Chapter 2 and 3. Also Prof. Maurice Streel and Dr. Philippe Steemans from the University of Liège provided critical comments on the dating and helped with the taxonomy of Devonian/Carboniferous miospores in Chapter 3. Jan de Leeuw is acknowledged for helpful discussions and commenting on an earlier version of Chapter 4.

I would like to thank the members of the reading committee Prof. Jack Middelburg, Prof. Henk Brinkhuis, Prof. Appy Sluijs, Prof. Thomas Wagner and Dr. Erik Tegelaar.

I am grateful to Shell Exploration & Production Libya GmbH, Libyan, Libyan Petroleum Institute (LPI), and National Oil Corporation authorities for providing the funding for this research and for their financial support during this study. I would like to express my gratitude to Dr. Ibrahim Al Baggar, Dr. Bourima Belgasem and Dr. Mansour Amtir. I would like to thank Arabian Gulf, Repsol, Sirte and Bulgarian Oil Companies for providing me cutting, core and crude oil samples and gamma ray log data.

Special thanks go to staff members of Shell in Libya and in Rijswijk: in particular Ahmed Aoun, Bashir Elmejrab, Peter Nederlof, Erik Tegelaar, Sander van den Boorn, Rolande Dekker, and Jos Pureveen for their discussion and technical support.

I would like to thank all friends and colleagues who supported me over the last four years. I had the pleasure of working in a group of very nice colleagues of organic geochemistry and received great scientific help; special thanks go to Marieke Lammers, Iuliana Vasiliev, Jiefei Mao, Jorien Vonk, Francien Peterse, Els van Soelen, Johan Weijers, Jos Wit, Julia van Winden, Lennart de Nooijer, Loes van Bree, Laura Buckles, Eveline Speelman, Cornelia Blaga, Angela Scharfbillig, Frédérique Kirkels, Eveline Mezger and Pien van Minnen. Many thanks go to Anita van Leeuwen, Dominika Kasjaniuk, Arnold van Dijk, Helen de Waard, Tom Bosma, Jan van Tongeren, Natasja Welters and Jan Kubiak for their technical support.

Thanks also to colleagues and friends from the Pal&Pal group on the third floor: Niels van Helmond, Zwier Smeenk, Bas van de Schootbrugge, Marjolein Mullen and everyone else. Special thanks go to Harry Veld (Deltares), Roel Verreussel (TNO) and Rader Abdul Fattah (TNO) for their help, discussion and technical support to use Rock Eval pyrolysis and stratabugs software.

I would like to thank other faculty staff in our Earth Sciences department and HR/ advisors: Jan-Willem de Blok, Hans Sonius, Tamara van Mildert and Patricia de Jongh for all kinds of administrative work.

I would like to express my heartfelt thanks to my family, father, mother, sisters and brothers in Libya, who suffered from my years of absence, for their understanding, patience, encouragement and endless support.

Finally, I would like to express my deep gratitude to my wife Sawsan and my daughters Raihan, Ragad, Raneem and my son Anas for their encouragement, support and understanding during all these years of my study and love through all days of my life.

Curriculum Vitea

Mohamed was born on the 10th of December 1965 in Tripoli, Libya. After he completed his secondary school education in 1984, he studied Geology at the University of Tripoli in Libya. He wrote his bachelor thesis on Sirte shales, the main source rock in Sirt Basin in the central part of Libya. In 1989 he started to work at the Petroleum Research Centre, Tripoli, Libya as a geologist in the Exploration department. His areas of interest include petroleum geochemistry, reservoir geochemistry and basin modeling. In 1998, he undertook a long training course on reservoir geochemistry at Robertson International Research, LIandudno, Wales, UK, under supervision of Dr. Patrick Bernard and Steve Thomson. At the end of 2004 he conducted his master studies at the University of Newcastle-upon-Tyne, UK. During this time, Mohamed worked on geochemical characterization of crude oils from Southeastern Ghadamis Basin, Libya, sponsored by Libyan Petroleum Institute and finished his master thesis at the end of 2005. At the beginning of 2006, he began to work as Petroleum Geochemist at Libyan Petroleum Institute in the Exploration department. In 2009 he started as a PhD student of organic geochemistry at Utrecht University. His PhD thesis focuses on the Silurian and Devonian source rocks and crude oils from the western part of Libya, under supervision of Prof. Gert-Jan Reichart and Prof. Jaap Sinninghe Damsté which resulted in this thesis.